

Ice surface temperature, albedo, and surface elevation change of glaciers and ice caps of the
Queen Elizabeth Islands, Nunavut, Canada, 1995-2015.

by

Colleen Adel Mortimer

A thesis submitted in partial fulfillment of the requirements for the degree of

Doctor of Philosophy

Department of Earth and Atmospheric Sciences
University of Alberta

© Colleen Adel Mortimer, 2017

Abstract

Inter-annual variability in glacier and ice cap surface mass balance in the Queen Elizabeth Islands (QEI), Arctic Canada, is driven primarily by variability in summer melt. Mean summer (June-August) QEI glacier surface temperatures (LSTs) and shortwave broadband black-sky surface albedo (BSA) are determined from NASA's Moderate Resolution Spectroradiometer (MODIS) for the period 2000(01)-2015 and provide the first near-complete picture of LST and BSA change for all glacier covered surfaces in the QEI. Between 2000 and 2015, mean summer LSTs increased at an average rate of 0.06 ± 0.04 °C yr⁻¹, for a total increase of nearly 1°C. Most of this surface warming occurred between 2007 and 2012 when mean summer near-surface (2 m) and upper-air (700 hPa) temperatures were 1.0-1.2°C higher than the 1948-2015 mean. Over a similar period (2001-2015), the mean summer BSA for glaciated surfaces south of 80°N decreased by 0.057. Overall the 15-year record of mean summer BSA is negatively correlated ($r = -0.71$, $p < 0.2$) with the 15 year record of mean summer LST, although local clusters of positive correlations were observed at high elevations in eastern Ellesmere Island. The observed positive ice-albedo feedback accelerates rates of melt and mass loss, and repeat airborne laser altimetry measurements show widespread thinning (surface lowering) across glaciated surfaces in the QEI since 1995. Rates of thinning, averaged for 50 m elevation bins, were more than three times larger from 2005/06 to 2012/14 than during the previous two pentads. Comparisons of dh/dt with MODIS-derived mean summer LST and BSA measurements and surface longitudinal strain rates, computed from RADARSAT- and LANDSAT -derived surface velocities for the period 2000-2012/14, indicate that QEI surface elevation changes were driven primarily by changes in climate except along most fast-flowing outlet glaciers where ice dynamics appear to have been a dominant forcing on observed dh/dt .

Acknowledgements

First and foremost, I would like to thank my PhD supervisor, Dr. Martin Sharp for his guidance and support throughout my PhD program. Thank you for your patience and dedication over the years, and for continuously challenging me to improve in every situation. Thank you to committee member Dr. Benoit Rivard for your support and advice during difficult times. I also thank Dr. Jeff Kavanaugh for serving on my supervisory committee.

To all members of the University of Alberta's Arctic and Alpine Research Group past and present, your knowledge and expertise have greatly enhanced this thesis. Additionally, I thank B. Wouters for insight and helpful reviews of Chapter 2, S. Williamson for initial guidance in MODIS data processing, and W. van Wyhcen for providing velocity data for this thesis. I would also like to acknowledge the excellent support provided by Amy at the National Snow and Ice Centre in resolving inconsistencies with the IDHDT4 data product in a timely manner.

I gratefully acknowledge financial funding in support of this project from the following organizations: Natural Sciences and Engineering Research Council of Canada –Vanier Canada Graduate Scholarship and Discovery Grants; University of Alberta - Dean's Excellence Award; UAlberta North - Northern Research Award; Natural Resources Canada – the Polar Continental Shelf Program; Polar Knowledge Canada – Northern Scientific Training Program and the Roger Hobson Award for Northern Research.

Table of Contents

Chapter 1: Introduction.....	1
1.1 Background and motivation.....	1
1.2 Thesis structure.....	5
1.3 References.....	10
Chapter 2: Glacier surface temperatures in the Canadian high Arctic, 2000-2015.....	15
2.0 Abstract.....	15
2.1 Introduction.....	15
2.2 Data and Methods.....	18
2.2.1 MODIS Land surface temperature.....	18
2.2.2 MOD11A2 data processing.....	20
2.3 Results.....	22
2.3.1 Mean summer glacier LST.....	22
2.3.1.1 Glacier LST anomalies 2000-2015.....	24
2.3.2 LST change 2000-2015.....	25
2.3.3 Summer air temperatures.....	28
2.4. Discussion.....	30
2.5. Conclusions.....	34
2.6 Chapter 2 Supplemental material.....	44
2.6.1: Analysis of clear-sky observations within each 8-day period.....	44
2.6.2: Occurrence of melt.....	48
2.6.3: Additional supporting material.....	51
2.6 References.....	53
Chapter 3: Glacier albedo change in the Canadian High Arctic (2001-2015) and its relationship to recent climate warming.....	59
3.0 Abstract.....	59
3.1 Introduction.....	59
3.2 Data and Methods.....	62
3.2.1 MODIS albedo (MCD43A3).....	62
3.2.1.1 MODIS sensor degradation.....	64
3.2.1.2 MCD43A3 data processing.....	66

3.2.2 MODIS LST (MOD11A2).....	68
3.2.3 Mean summer BSA and LST.....	69
3.2.4 Minimum summer BSA.....	70
3.2.5 Climate model data.....	71
3.3 Results.....	73
3.3.1. Mean summer glacier albedo: 2001 to 2015.....	73
3.3.2 BSA anomalies: 2001 to 2015.....	74
3.3.3 BSA change: 2001 to 2015.....	75
3.3.4 Minimum summer BSA.....	78
3.4 Comparison of glacier surface albedo and temperature changes.....	82
3.4.1 Mean summer land surface temperatures: 2001 to 2015.....	82
3.4.2 Spatial patterns of relationship between BSA and LST.....	83
3.4.3 Discussion of spatial patterns in the relationship between BSA and LST.....	84
3.5 Summary and conclusions.....	87
3.6 Chapter 3 Supplemental material.....	97
3.6.1 Introduction.....	97
3.7 References.....	103
Chapter 4: Influence of recent warming and ice dynamics on glacier surface elevations in the Canadian High Arctic, 1995-2014.....	111
4.0 Abstract.....	111
4.1 Introduction.....	112
4.2. Data and methods.....	114
4.2.1 Repeat airborne altimetry measurements.....	115
4.2.2 MODIS data.....	118
4.2.2.1 MOD11A2 LST.....	118
4.2.2.2 MCD43A3 albedo.....	120
4.2.2.2.1 MODIS sensor degradation.....	121
4.2.2.3 Mean summer LST and BSA.....	122
4.2.3 Comparison of dh/dt with LST, BSA, and du/dx	122
4.2.3.1 Mass balance.....	123
4.2.3.2 Ice dynamics.....	124

4.3 Results.....	126
4.3.1 dh/dt by epoch.....	128
4.3.2 dh/dt anomalies.....	130
4.4 Comparison of dh/dt with LST, BSA, and ice dynamics for 2000-2012/14.....	132
4.4.1 Low longitudinal strain rates.....	134
4.4.2 Large longitudinal strain rates.....	137
4.5 Discussion and conclusions.....	140
4.5.1 Discussion.....	140
4.5.2 Conclusion.....	143
4.6 Chapter 4 Supplemental material.....	150
4.7 References.....	158
Chapter 5: Conclusions.....	166
5.1 Summary.....	166
5.2.1 LST change.....	167
5.2.1.1 Summary.....	167
5.2.1.2 Limitations.....	168
5.2.2 BSA change.....	169
5.2.1.1 Summary.....	169
5.2.1.2 Limitations.....	170
5.2.3 Surface elevation change.....	173
5.2.1.1 Summary.....	173
5.2.1.2 Limitations.....	174
5.2 Discussion of LST, BSA, and dh/dt	175
5.2.1 Large-scale spatial patterns and climate.....	175
5.2.2 Small scale features and precipitation.....	177
5.2.3 Feedbacks: LST, BSA, elevation change and climate in the eastern QEI.....	178
5.3 Concluding remarks.....	179
5.4 References.....	180
Chapter 6: Thesis References.....	184

List of Tables

Table 2-1: Clear-sky mean summer land surface temperature (°C) for glaciated regions of the Queen Elizabeth Islands; ± 1 standard deviation.....36

Table 2-2: 16-year average (2000-2015) clear-sky mean summer land surface temperature (°C) for glaciated regions of the Queen Elizabeth Islands by elevation zone (Section 2.2) ± 1 standard deviation.....36

Table 2-3: Clear-sky mean summer land surface temperature anomaly (°C) with respect to the 2000-2015 mean for glaciated regions of the Queen Elizabeth Islands; ± 1 standard deviation.....37

Table 2-4: 16-year linear rate of change (2000-2015) of clear-sky mean summer land surface temperature (°C yr⁻¹) for glaciated regions of the Queen Elizabeth Islands by elevation zone (Section 2.2) ± 1 standard deviation38

Table 2-5: Pearson correlation coefficient, r, of the mean summer LST versus the mean summer 700 hPa air temperature for the period 2000-2015 for the seven major ice masses in the QEI (Figure 2-1c).....38

Table 3-1. Clear-sky BSA and LST for glaciated regions of the QEI south of 80°N; ± 1 standard deviation. Anomalies are with respect to the 2001-2015 mean.....88

Table 3-2. Clear-sky mean summer BSA for glaciated regions of the QEI south of 80°N; ± 1 standard deviation.89

Table 3-3. Clear-sky mean summer BSA anomaly (with respect to 2001-2015 mean) for glaciated regions of the QEI south of 80°N; ± 1 standard deviation..... 90

Table 3-4. 2001-2015 BSA and LST change for glaciated regions of the QEI south of 80°N; ± 1 standard deviation.....90

List of Supplemental Tables

Table 2-S2: Mean QEI-wide clear-sky days (mean \pm 1SD) within each 8 day period between 1-2 June and 28-29 August for 2000-2015.....45

Table 2-S6: Percentage of observations with a value $\geq 0^{\circ}\text{C}$. Data have not been filtered to removed pixels with LST error $> 2^{\circ}\text{C}$. The number of available observations varies for each date.....50

Table 2-S9: Location of site used to calculate summer (June-August) 700 hPa air temperature for 2000-2015 from the NCEP/NCAR R1 Reanalysis. See *Sharp et al.* [2011] (Section 2.3.3).....53

Table 2-S10: Difference between 2005-2009 and 2000-2004 average mean summer LST calculated in this study using all QEI glaciated pixels and by *Sharp et al.* [2011] using 23 km x 23 km cell blocks (Section 2.4)53

Table 3-S1: Percentage of all possible pixels having at least 7 or a possible 12 clear-sky shortwave broadband black-sky albedo observations during each summer (days 153-241).....97

Table 3-S2: Comparison of Empirical Orthogonal Functions (EOFs) for the First Principal Component, QEI-wide mean summer BSA, and LST.....98

Table 3-S3: Clear-sky mean summer land surface temperature ($^{\circ}\text{C}$) for glaciated regions of the Queen Elizabeth Islands south of 80°N ; ± 1 standard deviation.....98

Table 3-S4: Clear-sky mean summer land surface temperature anomaly ($^{\circ}\text{C}$) relative to the 2001-2015 mean for glaciated regions of the Queen Elizabeth Islands south of 80°N ; ± 1 standard deviation.....99

Table 3-S5: 2001-2009 change in mean summer temperature, short- and longwave radiation, precipitation, and albedo for selected glaciated regions south of 80°N100

Table 3-S6: Eight year average (2001-2009) mean summer temperature, short- and longwave radiation, precipitation, and albedo for selected glaciated regions south of 80°N100

Table 4-S1: sign of change in LST, BSA, and dh/dt for the period 2000-2012, QEI south of 80°N150

Table 4-S2: comparison of dh/dt , du/dx , and surface velocities along QEI outlet glaciers.....151

List of Figures

- Figure 2-1** Linear rate of change in mean summer clear-sky land surface temperature ($^{\circ}\text{C yr}^{-1}$) for 2000-2015 for the Queen Elizabeth Islands. Rate of change is computed only for pixels with annual summer mean clear-sky LST for all 16 years of observation. Black dots with white outline indicate location of Environment Canada weather stations at Eureka and Resolute Bay. Base image: Moderate Resolution Spectroradiometer, 4 July 2011. Left panel: (a) Red box indicates location of study site. (b) Elevation zones: < 1000 m a.s.l. (pink), 1000-1400 m a.s.l. (yellow), > 1400 m a.s.l. (grey). (c) QEI glacial regions used in this study: Northwest Ellesmere Island (orange), Agassiz Ice Cap (purple), Prince of Wales Icefield (blue), Manson Icefield (yellow), Sydkap Ice Cap (blue-green), Devon Island and Coburg Island (navy), Axel Heiberg Island (green), and Meighen Ice Cap (red).....39
- Figure 2-2** Mean summer clear-sky land surface temperature ($^{\circ}\text{C}$) for the Queen Elizabeth Islands.....40
- Figure 2-3** Mean summer clear-sky land surface temperature anomaly ($^{\circ}\text{C}$) relative to the 2000-2015 mean for the Queen Elizabeth Islands.....41
- Figure 2-4** Empirical orthogonal function (EOF) for the first Principal Component of the LST time series for 2000-2015 (left-hand axis, solid black line segments). The mean summer (June – August) LST anomaly relative to the 200-2015 mean ($^{\circ}\text{C}$) (black star) and the mean JJA NAO index for 2000-2015 (dashed curve) are plotted on the right-hand axis.....42
- Figure 2-5** Component scores for the first two Principal Components of the mean summer clear-sky land surface temperature (Figure 2-2) for the Queen Elizabeth Islands.....42
- Figure 2-6** Annual anomalies (relative to the 1948-2015 mean) in (a) mean summer (June-August) near-surface air temperature at Eureka and Resolute; (b) mean summer 700 hPa air temperature for sites centered on the interior of each of the major glaciated regions in the QEI (all regions in Figure 2-1c except for the Meighen Ice Cap) from the NCEP/NCAR R1 Reanalysis. Black box indicates period of MODIS satellite record.....43
- Figure 3-1** Glaciated regions of the Queen Elizabeth Islands, Arctic Canada. Only ice south of 80°N (see inset, right) are used in our analysis. Blue boxes indicate approximate area of the seven different regions used in our analysis.....91

Figure 3-2 Annual summer mean clear-sky shortwave broadband black-sky albedo over the Queen Elizabeth Islands glaciers and ice caps south of 80°N for the period 2001-2015. White areas within glaciated terrain indicate no data.....92

Figure 3-3 Annual summer mean clear-sky shortwave broadband black-sky albedo anomaly relative to the 2001-2015 mean over the Queen Elizabeth Islands glaciers and ice caps south of 80°N for the period 2001-2015. White areas within glaciated terrain indicate no data.....93

Figure 3-4 (a) Linear rate of change in mean summer clear-sky shortwave broadband black-sky albedo (yr^{-1}) and (b) mean summer clear-sky land surface temperature ($^{\circ}\text{C yr}^{-1}$) for 2000 to 2015 for the Queen Elizabeth Islands south of 80°N for pixels having 11 or more mean summer observations. (c) Component loadings for the first Principal Component of the 15-year mean summer clear-sky shortwave broadband black-sky albedo record, (d) Pearson Correlation Coefficient of the 15 year mean summer clear-sky shortwave broadband black-sky albedo (Figure 3-2) and mean summer clear-sky land surface temperature (Figure 3-S1) records for 2001 to 2015 for pixels with annual mean summer LST and BSA for all 15 years of observation. Black box shows location of Cadogan Inlet (Section 3.4.3). White areas within glaciated terrain indicate no data.....94

Figure 3-5 Mean summer BSA (solid line) and JJA NAO index (dashed line), Empirical Orthogonal Functions (EOFs) for the First Principal Component of the 15 year mean summer BSA record (dotted line) for 2001 to 2015.....95

Figure 3-6 (a) Minimum summer clear-sky shortwave broadband black-sky albedo change for 2001 to 2015, averaged by 50 meter elevation bins. Right-hand axis: average 15-year minimum summer clear-sky shortwave broadband black-sky albedo (stars) and surface area (bar graph) for each elevation bin. (b) Minimum summer clear-sky shortwave broadband black-sky albedo change for 2001 to 2015, averaged by 0.025 BSA bins from 0.1 to 0.6 according to the 15-year average minimum summer BSA. Right-hand axis: ‘X’ indicates average elevation (m a.s.l.) and area (bar graph) for each minimum BSA bin. (c) Minimum summer BSA for bare-ice (circles), intermediate (diamonds), and firn (squares) categories described in Section 3.2.4 for 2001-2015.....96

Figure 4-1: Mean dh/dt for 50 m elevation bins for glaciated regions in the QEI between 1995 and 2012/14.....144

Figure 4-2: Rate of surface elevation change (m yr^{-1}) over glaciated regions in the QEI between 1995 and 2012/14 from repeat airborne altimetry data (IDHDT4), elevation contours from CDED DEM 1:50k.145

Figure 4-3: dh/dt anomalies ($m\ yr^{-1}$) relative to the 1995-2012/14 mean for the 1995-2000, 2000-2005/06, and 2005/06-2012/14 periods.....146

Figure 4-4: comparison of surface elevation change, longitudinal strain rates, temperature and albedo change for the 2000-2012/14 period. a) dh/dt ($m\ yr^{-1}$) for 2000-2012/14, b) mean du/dx (yr^{-1}) from available velocity data between 2000 and 2015, c) comparison of dh/dt with mean summer LST change, d) comparison of dh/dt with mean summer LST and BSA change for areas south of $80^{\circ}N$147

Figure 4-5: Comparison of dh/dt and du/dx for specific glaciers identified as having large longitudinal strain rates and large and highly variable dh/dt in Figure 4-4. Right-hand axis: mean du/dx (yr^{-1} , solid grey) computed from available annual and velocity data between 1999/2000 and 2015 (italic text). Black line indicates rate of surface elevation change (dh/dt $m\ yr^{-1}$, solid text) for 2000-2012/14 (2005-2012 for Southeast 1). Left-hand axis: pink and blue bar graphs indicate rate of LST ($^{\circ}C\ yr^{-1}$) and BSA (yr^{-1}) change. For glaciers where both LST and BSA data are available, rate of LST change is indicated on the upper left-hand axis and BSA change on the lower left-hand axis.....148

Figure 4-6: dh/dt ($m\ yr^{-1}$) versus surface elevation (ellipsoid height, $m\ a.s.l.$) over glaciated regions in the QEI between 1995 and 2012/14 shown in Figure 4-2. a) northern Ellesmere Island, Otto Glacier shown in light blue, b) Agassiz Ice Cap, Antoinette Glacier centerline shown in light orange. c) Devon Ice Cap, data from Belcher and East 6 Glaciers shown in light green. d) Prince of Wales Icefield divided into eastern (blue) and western (red) portions, data for Taggart Lake Glacier indicated by red crosses.....149

List of Supplemental Figures

Figure 2-S1: Mean QEI-wide (area-averaged) number of clear-sky observations within individual 8 day periods for 2000-2015.....44

Figure 2-S3: Mean number of clear-sky observations during each 8 day period for 2000-2015.....46

Figure 2-S4: Standard deviation of the number of clear-sky observations during each 8 day period for 2000-2015.....47

Figure 2-S5: Percentage of observations with $LST \geq 0^{\circ}C$ for each 8 day observation period from day 113 – 281 for 2000 to 2015. Percentage is calculated with respect to total number of pixels with LST observations for each date. The dotted lines delineate the study period (June-

August) which spans day 153 – 241.....	49
Figure 2-S7: 16-year average clear-sky mean summer land surface temperature (°C) for glaciated regions of the Queen Elizabeth Islands for the period 2000-2015.....	51
Figure 2-S8: Standard deviation of the mean summer clear-sky land surface temperature (°C) for the Queen Elizabeth Islands.....	52
Figure 3-S1: Clear-sky mean summer land surface temperature anomaly (°C) relative to the 2001-2015 mean for glaciated regions of the Queen Elizabeth Islands south of 80°N.....	101
Figure 3-S2: Linear rate of change in (a) mean summer clear-sky shortwave broadband black-sky albedo (yr ⁻¹) and (b) mean summer clear-sky land surface temperature (°C yr ⁻¹) for 2001-2009 for the Queen Elizabeth Islands south of 80°N for pixels having seven or more mean summer (JJA) observations.....	102
Figure 3-S3: p-value for linear regression of the 15 year BSA (a) and LST (b) records shown in Figures 4-4a and 4-4b.....	102
Figure 4-S3: Rate of surface elevation change (m yr ⁻¹) over glaciated regions in the QEI between 1995 and 2000 from repeat airborne altimetry data (IDHDT4), surface elevations from CDED DEM 1:50k. Similar data are presented in <i>Abdalati et al.</i> [2004].....	155
Figure 4-S4: Rate of surface elevation change (m yr ⁻¹) over glaciated regions in the QEI between 2000 and 2005/06 from repeat airborne altimetry data (IDHDT4), surface elevations from CDED DEM 1:50k.....	156
Figure 4-S5: Rate of surface elevation change (m yr ⁻¹) over glaciated regions in the QEI between 2005/06 and 2012/14 from repeat airborne altimetry data (IDHDT4), surface elevations from CDED DEM 1:50k.....	157

Chapter 1

Introduction

1.1 Background and motivation

Canada's Queen Elizabeth Islands (QEI: 74.5-83.5°N, 61-121°W) contain ~14% of the global glacier and ice cap area. Glaciers and ice caps in this region, which covered an area of ~104,000 km² in 2000 [Arendt *et al.*, 2012], have been losing mass since field measurements began in the mid-20th century [Koerner, 2005; Sharp *et al.*, 2011]. Ice core records from the Devon [Koerner, 1977] and Agassiz [Koerner and Fisher, 1990] Ice Caps suggest mildly negative glacier mass balances since the mid to late 1800s, with increasingly negative mass balances since the mid-1900s. Near-continuous field measurements of glacier surface mass balance from White Glacier (Axel Heiberg Island), Meighen and Melville Ice Caps, and the Sverdrup Glacier (Devon Ice Cap) beginning in the late 1950s to early 1960s show a weak negative trend towards increasingly negative surface mass balances from 1960 to 2009, with particularly strong negative mass balances beginning in the late 1990s [Koerner, 2005; Sharp *et al.*, 2011]. These negative glacier mass balances have continued to present day [Sharp *et al.*, 2015] and the rate of QEI glacier mass loss, inferred from in situ and remote sensing measurements, nearly tripled between 2004-2006 and 2007-2009 [Gardner *et al.*, 2011, 2013].

The recent (~2000 onward) acceleration in the rate of QEI glacier and ice cap mass loss has largely been inferred from broad, regional-scale studies. For the period 2003-2009, glacier mass budget estimates for the QEI ice cover as a whole derived from Ice, Cloud, and land Elevation Satellite (ICESat) surface elevation retrievals, and from regional mass anomalies from the Gravity Recovery and Climate Experiment (GRACE) were -37 ± 7 Gt yr⁻¹ and -29 ± 7 Gt yr⁻¹, respectively

[Gardner *et al.*, 2013]. Over a similar time period, surface mass budget [Gardner *et al.*, 2011] and climate modelling [Lenaerts *et al.*, 2013] studies yielded rates of QEI-wide mass loss between $-34 \pm 13 \text{ Gt yr}^{-1}$ (2004-2009, Gardner *et al.*, [2011]) and $-37 \pm 10 \text{ Gt a}^{-1}$ (2003-2012, Lenaerts *et al.* [2013]). Although there is consensus that the QEI glaciers and ice caps as a whole have been losing glacier mass, and that the rate of mass loss has been increasing in recent years, the spatial and temporal variability of glacier and ice cap mass change within the QEI are not well known.

For a glacier in steady-state, the climatic mass balance of a section of a glacier (the sum of the surface and internal mass balances) is balanced by the flux divergence (the difference between the vertically integrated mass fluxes into and out of the section) [Cuffey and Paterson, 2010]. In recent years, the climatic mass balance has been the dominant control of glacier mass change in the QEI [Millan *et al.*, 2017]. The climatic mass balance is the sum of surface and internal accumulation (solid precipitation, wind redistribution, avalanching, firn densification and growth of ice bodies within the firn) and ablation (melt, runoff, sublimation). Although the internal mass balance is typically small relative to the surface mass balance [Cuffey and Paterson, 2010], increased rates of firn densification [Zdanowicz *et al.*, 2012; Bezeau *et al.*, 2013] and the growth of ice bodies within the firn [Gascon *et al.*, 2013a], observed across the Canadian Arctic in recent years, suggest that internal accumulation is an important component of the QEI climatic mass balance.

In the QEI, annual precipitation is extremely low (between ~ 100 and $\sim 300 \text{ mm yr}^{-1}$) and it varies little from one year to the next [Braithwaite, 2005]. In contrast, the annual temperature range is large ($>40^\circ\text{C}$). Inter-annual variations in QEI annual glacier mass balance are therefore dominated by changes in summer temperatures and melt rates [Koerner, 2005]. Near surface (2 m) and upper air (700 hPa) air temperatures over the QEI's major glaciated regions were 0.8°C to 2.2°C warmer from 2005-2009 than during the previous pentad [Sharp *et al.*, 2011], and summer mean air

temperatures from long-running (1948-present) climate stations at Eureka and Resolute Bay were highest between 2010 and 2012 (<http://climate.weather.gc.ca>). QEI summer mean air temperatures and the annual positive degree day index are well correlated with the duration and intensity of summer melt [*Wang et al.*, 2005; *Sharp et al.*, 2011]. Between 2005 and 2009, the melt season duration over seven of the QEI's major ice masses (derived from QuikSCAT data) was between 4.7d and 11.9d longer than during the period 2000-2004 [*Sharp et al.*, 2011, updated from *Wolken et al.*, 2009].

Extreme mass balance years in the QEI have been associated with changes in the strength and geometry of the July circumpolar vortex, which alters the distribution and intensity of regions of high and low pressure across the QEI [*Alt*, 1987; *Gardner and Sharp*, 2007]. A higher incidence of persistent positive mean 500 hPa geopotential height anomalies over the Canadian Arctic and western Greenland between 2007 and 2012 was linked with extreme warm summers and negative glacier mass balances [*Bezeau et al.*, 2013; *Rajewicz and Marshall*, 2014]. These clear-sky conditions allow for an increase in the proportion of incoming solar radiation received at the surface. Net shortwave radiation is the largest source of melt energy in the QEI during June and July [*Gascon et al.*, 2013b]. Variability in net shortwave radiation is, in turn, strongly modulated by the surface albedo [*van den Broeke et al.*, 2011; *Tedesco et al.*, 2016] –the ratio of reflected to incoming solar radiation.

The high albedo of fresh snow (~0.6-0.8; *Cuffey and Paterson* [2010] Table 5.2) declines naturally over time through settling and grain growth [*Wiscombe and Warren*, 1980; *Warren*, 1982]. This initial decrease in albedo raises the shortwave energy absorption, leading to warming and/or melt. Increases in air and surface temperatures promote grain growth, which lowers the surface albedo, while the rate of snow/ice grain metamorphism increases with temperature and in the presence of

liquid water [Warren and Wiscombe, 1980; Colbeck, 1982]. In addition, atmospheric warming and increased melt can lead to an earlier and more widespread removal of the previous winter's snowpack, exposing underlying glacier ice with a low-albedo ($\sim 0.2-0.35$; Cuffey and Paterson [2010] Table 5.2). Albedo declines can also result from increased aerosol deposition [Clarke and Noone, 1985] and enhanced biological activity on the glacier surface [Fountain et al., 2004]. Higher melt rates result in a more rapid release of impurities contained in the snow and ice which become concentrated on the snow/ice surface [Conway et al., 1996; Doherty et al., 2013], further reducing the surface albedo. This positive snow/ice albedo feedback, whereby higher surface temperatures drive albedo declines which enhance surface warming and/or melt, leading to additional reductions in the surface albedo, has been linked to accelerated high-latitude warming. It is increasingly recognised as an important factor in explaining recent increases in rates of mass loss from the Greenland Ice Sheet, immediately adjacent to the QEI [Box et al., 2012; Tedesco et al., 2016].

A reduction in glacier mass results in changes in glacier size. Observed increases in air and surface temperatures [Sharp et al., 2011] and associated enhanced rates of glacier mass loss [Gardner et al., 2013] are therefore expected to have resulted in a reduction in glacier area and/or thickness, depending upon how the evolving ice dynamics adjust to changes in mass. Changes in the elevation of a glacier surface are controlled by the basal-climatic mass balance of the glacier (the sum of the climatic and basal mass balances) and by ice dynamics. Changes in ice dynamics alter the mass transferred into and/or out of a region, resulting in localized thinning or thickening. The basal mass balance is generally small relative to the climatic mass balance, which, as discussed previously, is mainly controlled by changes in summer air temperatures, solar radiation, and melt. In the accumulation zone, warmer air and surface temperatures increase both the amount of melt and the

depth of meltwater percolation into the firn layer. The near-surface ice/firn temperature is raised by latent heat released when the water refreezes, and refreezing increases the rate of firn densification [Pfeffer and Humphrey, 1998; Zdanowicz *et al.*, 2012; Bezeau *et al.*, 2013], resulting in a lowering of the glacier's surface elevation. In the ablation area, where bare glacier ice is exposed at the surface during the summer, and warmer air temperatures result in increased melting, mass loss, and thinning (surface lowering).

Repeat airborne laser altimetry measurements made over QEI ice caps in 1995 and 2000 identified overall thinning (generally $<0.5 \text{ m yr}^{-1}$) during this 5-year period [Abdalati *et al.*, 2004]. Thinning (surface lowering) was strongest at lower elevations while thickening or no change in surface elevation were observed at higher elevations in the interior of most ice masses. It is not known, however, whether this pattern of glacier and ice cap surface elevation change has persisted to present day. Elevation differencing of repeat measurements from ICESat retrievals between 2003 and 2009 identified QEI-wide lowering of ice cap surfaces (average dh/dt : $-0.38 \pm 0.04 \text{ m yr}^{-1}$; Gardner *et al.* [2013]), but the relative contributions of changes in climatic mass balance and ice dynamics to the rate of elevation change (dh/dt) were not investigated. Furthermore, the spatial variability in changes of glacier and ice cap surface elevation within the QEI was not examined.

1.2 Thesis structure

This thesis examines the spatial and temporal variability of recent (2000-2015) changes in glacier and ice cap surface temperature and albedo, and their relationships to changes in glacier and ice cap surface elevation within the QEI. Specifically, this thesis presents the following:

- 1) An assessment of the spatial and temporal variability in land surface temperatures (LSTs) for all glaciated surfaces in the QEI for the period 2000-2015.

- 2) An assessment of the spatial and temporal variability in surface albedo, and its relationship to LSTs, for all glaciated surfaces in the QEI south of 80°N for the period 2001-2015.
- 3) An assessment of spatial and temporal patterns in rates of glacier surface elevation change (dh/dt) in the QEI for the period 1995-2014, and an investigation of the relative influences on dh/dt of changes in the climatic mass balance and ice dynamics.

Remote sensing methods allow us to map spatial patterns in ice cap LST and albedo and to monitor changes in these patterns over time at the scales of both individual ice caps and the regional ice cover. Data from the Moderate Resolution Spectroradiometer (MODIS) sensors are used to present the first near-complete picture of summer LST and albedo changes on the QEI ice cover for the period 2000/01-2015. Observed spatial patterns of changes in LST and albedo, as well as the relationship between the 15 year LST and albedo records, are used to infer spatial patterns in the glacier mass balance, and to identify locations where positive (negative) correlations between LST and albedo may indicate local thickening (or enhanced thinning) of the ice cover. Repeat airborne laser altimetry surveys are then used to investigate spatial and temporal patterns in QEI glacier and ice cap surface elevation change, and to investigate whether areas of positive (negative) correlations between LST and albedo coincide with regions of thickening (thinning).

Changes in LST provide evidence of changing melt conditions over glaciers and ice caps [Hall *et al.*, 2006; Sharp *et al.*, 2011]. The annual and summer melt season mean LSTs, derived from satellite data, have been studied extensively on the Greenland Ice Sheet, immediately adjacent to the QEI [Hall *et al.*, 2008, 2013; Shuman *et al.*, 2014, and references therein], where the probability of melt occurring at a given location in a given summer (during the period 2000-2005) increased with both the summer mean LST and the length of the summer melt season [Hall *et al.*, 2006]. MODIS-derived mean summer (June-August) LSTs have been used as a proxy for the

mean summer ice temperature and for the summer melt duration and/or intensity [Hall *et al.*, 2006; Sharp *et al.*, 2011], and allow for the analysis of spatial and temporal patterns in LST across all glaciated surfaces in the QEI. Sharp *et al.* [2011] analysed glacier surface temperature (LST) trends for 23 km x 23 km boxes centered on the higher elevations of the QEI's seven major ice masses and identified stronger warming in the north and west of the QEI. This trend was, however, inferred for single high elevation grid cell blocks, and it is not known whether the pattern of stronger warming in the north and west of the QEI is characteristic of all elevations on the region's ice caps; nor is it known whether this spatial pattern has been sustained to the present-day.

Chapter 2 presents a near-complete picture of LST changes on QEI glaciers and ice caps for the period 2000-2015. A 16-year record of mean summer LSTs from MODIS data (MOD11A2, 1 km spatial resolution) is used to assess the spatial and temporal variability of LST and to quantify change in the intensity and duration of summer melt across the entire QEI ice cover. Near-surface (2 m) air temperatures from Eureka and Resolute Bay, and upper air (700 hPa) temperatures for locations centered over seven of the QEI's major ice masses derived from the NCEP/NCAR R1 Reanalysis [Kalnay *et al.*, 1996] for the period 1948-2015, are used to place the 16 year LST record into the context of these last 68 years. This chapter, which has been published in the *Journal of Glaciology*, is co-authored. I performed all analyses and wrote the manuscript. B. Wouters provided GRACE data and edited the manuscript; M. Sharp edited the manuscript.

Citation: Mortimer, C. A., M. Sharp, and B. Wouters (2016), Glacier surface temperatures in the Canadian high arctic, 2000-2015, *J. Glaciol.*, 62(235), 963-975, doi: 10.1017/jog.2016.80.

Chapter 2 identifies strong warming (mean summer LST change: $+0.06 \pm 0.04^{\circ}\text{C yr}^{-1}$) across the QEI during the 2000-2015 period. Measured increases in air and surface summer temperatures

were greatest in the north and west of the region. Since rising surface temperatures can accelerate albedo declines via the negative ice-albedo feedback, we anticipate the spatial pattern of albedo decline to be similar to the pattern of LST increase, unless warming is also accompanied by an increase in solid precipitation that is large enough to raise the surface albedo. Previous work on the Greenland Ice Sheet identified decadal-scale albedo declines ($\sim 0.02 \text{ decade}^{-1}$) using remote sensing methods and regional climate models validated by in situ data [e.g. *Stroeve et al.*, 2005, 2013; *Box et al.*, 2012; *Alexander et al.*, 2014; *Tedesco et al.*, 2016]. No similar studies have been conducted over glaciated surfaces in the QEI.

Chapter 3 uses measurements of surface albedo from the MODIS sensors to assess spatial and temporal variations in the summer surface albedo of QEI glaciers and ice caps south of 80°N over the 2001-2015 period, and to quantify the rate of change of surface albedo across the QEI during this 15 year period. The 15-year record of mean summer black-sky shortwave broadband albedo (BSA) (MCD43A3, 500 m spatial resolution) is compared with the record of mean summer LST for 2001-2015 to investigate the relationship between surface temperature and albedo change, and to explore its spatial and temporal variability. This chapter, which is in review for the *Journal of Geophysical Research – Earth Surface*, is co-authored. I completed all analysis and wrote the manuscript, M. Sharp edited the manuscript.

Citation: Mortimer, C. A., and M. Sharp, Glacier albedo change in the Canadian High Arctic (2001-2015) and its relationship to recent climate warming, in review for *J. Geophys. Res.: Earth Surface*.

Chapter 3 identified local clusters of positive correlation between LST and BSA at high elevations in eastern Ellesmere Island that may indicate a negative ice-albedo feedback, whereby, increased

solid precipitation during warm summers [Koerner, 1979] both raises the albedo and results in thickening. In most regions, however, LST and BSA were negatively correlated. This positive ice-albedo feedback is expected to have enhanced melt rates and glacier thinning, unless there was a compensating reduction in ice flow. Rapid changes in surface velocity in the eastern QEI between 1999 and 2015 were linked to changes in glacier thickness [van Wychen *et al.*, 2016]; however, such comparisons were limited to the Dobbin, Parrish, and Trinity Glaciers, and the extent to which recent changes in QEI ice dynamics are tied to glacier surface elevation changes is not well known.

Chapter 4 uses measurements of surface elevation change from repeat surveys with NASA's Airborne Topographic Mapper (ATM), conducted between 1995 and 2014 [Krabill, 2014, updated 2016] to investigate spatial and temporal patterns in rates of glacier surface elevation change (dh/dt). It builds upon previous work by Abdalati *et al.* [2004], which identified slight thinning over QEI glaciers and ice caps between 1995 and 2000 from repeat airborne altimetry. Changes in remotely-sensed LST, BSA, and surface longitudinal strain rates are compared with measured changes in dh/dt to qualitatively assess the relative influences of the climatic mass balance and changing ice dynamics on glacier and ice cap surface elevation changes between 2000 and 2014. This chapter is co-authored. I completed all analysis and wrote the manuscript. W. van Wychen provided surface velocity data, M. Sharp edited the manuscript.

Citation: Mortimer, C. A., M. Sharp, and W. van Wychen. Influence of recent warming and ice dynamics on glacier surface elevation in the Canadian High Arctic, 1995-2014. Submitted to *Journal of Glaciology*.

1.3 References

- Abdalati, W., W. Krabill, E. Frederick, S. Manizade, C. Martin, J. Sonntag, R. Swift, R. Thomas, J. Yungel, and R. Koerner (2004), Elevation changes of ice caps in the Canadian Arctic Archipelago, *J. Geophys. Res.*, 109(F04007), doi: 10.1029/2003JF000045.
- Alexander, P. M., M. Tedesco, X. Fettweis, R. S. W. van de Wal, C. J. P. P. Smeets, and M. R. van den Broeke (2014), Assessing spatiotemporal variability and trends in modeled and measured Greenland Ice Sheet albedo (2000-2013), *The Cryosphere*, 8(6), 2293-2312, doi: 10.5194/tc-8-2293-2014.
- Alt, B. T. (1987), Developing synoptic analogs for extreme mass balance conditions on Queen Elizabeth Island ice caps, *Journal of Applied Climate*, 26(12), 1605-1623, doi: 10.1175/1520-0450(1987)026<1605:DSAFEM>2.0.CO;2.
- Arendt, A., et al. (2012), Randolph Glacier Inventory Vers. 3.0: a dataset of Global Glacier Outlines. Global Land Ice Measurements from Space, Boulder, CO. Digital media: http://www.glims.org/RGI/rgi32_dl.html.
- Bezeau, P., M. Sharp, D. Burgess, and G. Gascon (2013), Firn profile changes in response to extreme 21st-century melting at Devon Ice Cap, Nunavut, Canada, *J. Glaciol.*, 59(217), 981-991, doi:10.3189/2013JoG12J208.
- Box, J. E., X. Fettweis, J. C. Stroeve, M. Tedesco, D.K. Hall, and K. Steffen (2012), Greenland ice sheet albedo feedback: thermodynamics and atmospheric drivers, *Cryosphere*, 6(4), 821-839, doi: 10.5194/tc-6-821-2012.
- Braithwaite, R. J. (2005), Mass balance characteristics of arctic glaciers, *Ann. Glaciol.*, 42, 225-229, doi: 10.3189/17275640578182899.
- Clarke, A. D., and K. J. Noone (1985), Soot in the Arctic snowpack: a cause for perturbations in radiative transfer, *Atmospheric Environment*, 19(12), 2045-2053, doi: 10.1016/0004-6981(85)90113-1.
- Cogley, J. G., R. Hock, L. A. Rasmussen, A. A. Arendt, A. Bauder, R. J. Braithwaite, P. Jansson, G. Kaser, M. Möller, L. Nicholson, and M. Zemp (2011), Glossary of Glacier Mass Balance and

Related Terms, IHP-VII Technical Documents in Hydrology No. 86, IACS Contribution No. 2, UNESCO-IHP, Paris.

Colbeck, S. C. (1982), An overview of seasonal snow metamorphism, *Rev. Geophys.*, 20(1), 45-61, doi: 10.1029/RG020i001p00045.

Conway, H., A. Gades, and C.F. Raymond (1996), Albedo of dirty snow during conditions of melt, *Water Resour. Res.*, 32(6), 1716-1718, doi: 10.1029/96WR00712.

Cuffey, K. M. and W. Paterson (2010), *The physics of glaciers*, 4th edn. Butterworth-Heinemann, Oxford.

Doherty, S. J., T. C. Grenfell, S. Forsstrom, D. L. Hegg, R. E. Brandt, and S. G. Warren (2013), Observed vertical redistribution of black carbon and other insoluble light-absorbing particles in melting snow, *J. Geophys. Res.-Atmos.*, 118(11), 5553-5569, doi: 10.1002/jgrd.50235.

Fountain, A.G., M. Tranter, T. H. Nylén, and D. R. Müller (2004), Evolution of cryoconite holes and their contribution to meltwater runoff from glaciers in the McMurdo Dry Valleys, Antarctica, *J. Glaciol.*, 50(168), 35-45, doi: 10.3189/172756504781830312.

Gardner, A. S., and M. Sharp (2007), Influence of the Arctic circumpolar vortex on the mass balance of Canadian high Arctic glaciers, *J. Climate*, 20(18), 4586-4598, doi: 10.1175/JCLI4268.1.

Gardner, A. S., G. Moholdt, B. Wouters, G. J. Wolken, D. O. Burgess, M. J. Sharp, J. G. Cogley, C. Braun, and C. Labine (2011), Sharply increased mass loss from glaciers and ice caps in the Canadian Arctic Archipelago, *Nature*, 473(7347), 357-360, doi:10.1038/nature10089.

Gardner, A. S., et al. (2013), A reconciled estimate of glacier contributions to sea level rise: 2003 to 2009, *Science*, 340(6134), 852-857, doi:10.1126/science.1234532.

Gascon, G., M. Sharp, and A. Bush (2013a), Changes in melt season characteristics on Devon Ice Cap, Canada, and their association with the Arctic atmospheric circulation, *Ann. Glaciol.*, 54, 101–110, doi:10.3189/2013AoG63A601.

Gascon, G., Sharp M., Burgess D., Bezeau P. and A. B. G. Bush (2013b), Changes in accumulation-area firn stratigraphy and meltwater flow during a period of climate warming: Devon

Ice Cap, Nunavut, Canada, *J. Geophys. Res. Earth Surf.*, 118(4), 2380-2391, doi:10.1002/2013JF002838.

Hall D. K., R. S. Williams Jr, K. A. Casey, N. E. DiGirolamo, and Z. Wan (2006), Satellite-derived, melt-season surface temperature of the Greenland Ice Sheet (2000–2005) and its relationship to mass balance, *Geophys. Res. Lett.*, 33(11), L11501, doi:10.1029/2006GL026444.

Hall, D. K., R. S. Williams, S. B. Luthcke, and N. E. DiGirolamo (2008), Greenland ice sheet surface temperature, melt and mass loss: 2000–2006, *J. Glaciol.*, 54(184), 81–93, doi:10.3189/002214308784409170.

Hall, D. K., J. C. Comiso, N. E. DiGirolamo, C. A. Shuman, J. E. Box and L. S. Koenig (2013), Variability in the surface temperature and melt extent of the Greenland ice sheet from MODIS, *Geophys. Res. Lett.*, 40(10), 2114-2120, (doi:10.1002/grl.50240).

Kalnay, E., et al. (1996), The NCEP/NCAR 40 year reanalysis project, *Bull. Am. Meteorol. Soc.*, 77(3), 437–471, doi:10.1175/1520-0477(1996)077<0437:TNYRP>2.0.CO;2.

Koerner, R. M. (1977), Devon Island ice cap: core stratigraphy and paleoclimate, *Science*, 196(4285), 15-18, doi: 10.1126/science.196.4285.15.

Koerner, R. M. (1979), Accumulation, ablation, and oxygen isotope variations on the Queen Elizabeth Islands ice caps, Canada, *J. Glaciol.*, 22(86), 25-41.

Koerner, R. M. (2005), Mass balance of glaciers in the Queen Elizabeth Islands, Nunavut, Canada, *Ann. Glaciol.*, 42, 417–423, doi:10.3189/172756405781813122.

Koerner, R. M., and D. A. Fisher (1990), A record of Holocene summer climate from a Canadian high-Arctic ice core, *Nature*, 343(6259), 630-631, doi: 10.1038/343630a0.

Lenaerts, J. T. M., J. H. van Angelen, M. R. van den Broeke, A. S. Gardner, B. Wouters, and E. van Meijgaard (2013), Irreversible mass loss of Canadian Arctic Archipelago glaciers, *Geophys. Res. Lett.*, 40(5), 870–874, doi:10.1002/grl.50214.

Millan, R., J. Mougnot, and E. Rignot (2017), Mass budget of the glaciers and ice caps of the Queen Elizabeth Islands, Canada, from 1991 to 2015, *Environ. Res. Lett.*, 12(02), 1-8, doi: 10.1088/1748-9326/aa5b04.

Pfeffer, W. T., and N. F. Humphrey (1998) Formation of ice layers by infiltration and refreezing of meltwater, *Ann. Glaciol.*, 26, 83-91.

Sharp, M., D. O. Burgess, J. G. Cogley, M. Ecclestone, C. Labine, and G. J. Wolken (2011), Extreme melt on Canada's Arctic ice caps in the 21st century, *Geophys. Res. Lett.*, 38(11), L11501, doi:10.1029/2011GL047381.

Sharp, M., et al. (2015) [Arctic] Glaciers and ice caps (outside Greenland [in "State of the Climate 2014"], *Bull. Am. Meteorol. Soc.*, 96(7), 135-137.

Shuman C. A., D. K. Hall, N. E. DiGirolamo, T. K. Mefford, and M. J. Schnaubelt (2014), Comparison of near-surface air temperatures and MODIS ice-surface temperatures at Summit, Greenland (2008-13), *J. Appl. Meteor. Climatol.*, 53(9), 2171 – 2180, doi:10.1175/JAMC-D-14-0023.1.

Stroeve, J. C., J. Box, F. Gao, S. Liang, A. Nolin, and C. Schaaf (2005), Accuracy assessment of the MODIS 16-day albedo product for snow: Comparison with Greenland in situ measurements, *Remote Sens. Environ.*, 94(1), 46-60, doi: 10.1016/j.rse.2004.09.001.

Stroeve, J., J. E. Box, Z. Wang, C. Schaaf, and A. Barret (2013), Re-evaluation of MODIS MCD43 Greenland albedo accuracy and trends, *Remote Sens. Environ.*, 138, 199-214, doi: 10.1016/j.rse.2013.07.023.

Tedesco M., S. Doherty, X. Fettweis, P. Alexander, J. Jeyaratnam, and J. Stroeve (2016), The darkening of the Greenland ice sheet: trends, drivers, and projections (1981-2100), *The Cryosphere*, 10, 477-496, doi: 10.5194/tc-10-477-2016.

van den Broeke, M. R., C. J. P. P. Smeets, and R. S. W. van de Wal (2011), The seasonal cycle and interannual variability of surface energy balance and melt in the ablation zone of the west Greenland ice sheet, *The Cryosphere*, 5(2), 377-390, doi: 10.5194/tc-5-377-2011.

van Wychen, W., J. Davis, D. O. Burgess, L. Copland, L. Gray, M. Sharp, and C. Mortimer (2016), Characterizing interannual variability of glacier dynamics and dynamic discharge (1999-2015) for the ice masses of Ellesmere and Axel Heiberg Islands, Nunavut, Canada, *J. Geophys. Res.- Earth Surf.*, 121, 39-63, doi:10.1002/2015JF003708.

Wang L., M. Sharp, B. Rivard, S. Marshall, and D. Burgess (2005), Melt season duration on Canadian Arctic ice caps, 2000-2004, *Geophys. Res. Lett.*, 32(19), L19502, doi: 10.1029/2005GL023962.

Warren, S. G. (1982), Optical properties of snow, *Reviews of Geophysics*, 20(1), 67-89, doi: 10.1029/RG020i001p00067.

Warren, S. G., and W. J. Wiscombe (1980), A model for the spectral albedo of snow. II Snow containing atmospheric aerosols, *J. Atmos. Sci.*, 37(12), 2734-2745, doi: 10.1175/1520-0469(1980)037<2734:AMFTSA>2.0.CO;2.

Wiscombe, W. J., and S. G. Warren (1980), A model for the spectral albedo of snow. I: Pure snow, *J. Atmos. Sci.*, 37(12), 2712-2732, doi: 10.1175.1520-0469(1980)037<2712:AMFTSA>2.0.CO;2.

Wolken G. J., M. Sharp, and L. Wang (2009), Snow and ice facies variability and ice layer formation on Canadian Arctic ice caps, 1999– 2005, *J. Geophys. Res.*, 114(F3), F03011, doi:10.1029/2008JF001173.

Zdanowicz, C., A. Smetny-Sowa, D. Fisher, N. Schaffer, L. Copland, J. Eley, and F. Dupont (2012), Summer melt rates on Penny Ice Cap, Baffin Island: Past and recent trends and implications for regional climate, *J. Geophys. Res.*, 117(F2), F02006, doi:10.1029/2011JF002248.

Chapter 2

Glacier surface temperatures in the Canadian high Arctic, 2000-2015

2.0 Abstract

Canada's Queen Elizabeth Islands (QEI) contain ~14% of the world's glacier and ice cap area. Sparse in-situ measurements indicate that inter-annual variability in glacier surface mass balance in this region is driven primarily by variations in summer melt, and that the annual surface mass balance of four index glaciers has become increasingly negative since 2007. Here, we use a 16-year record of satellite-derived mean summer (June-August) land surface temperatures (LST) from NASA's Moderate Resolution Imaging Spectroradiometer to investigate large scale spatial and temporal variability in the duration and intensity of summer melt across glaciated surfaces in the QEI from 2000-2015. During this period, QEI mean summer glacier surface temperatures increased at an average rate of 0.06 ± 0.04 °C yr⁻¹, for a total of nearly 1°C. Most of this increase occurred between 2005 and 2012, when mean summer near-surface (2 m) and upper-air (700 hPa) temperatures were 1.0°C to 1.2°C higher than the 1948-2015 mean. There is a strong correlation between the glacier LST and 700 hPa air temperature records ($r > 0.8$). The period 2005-2012, when mean summer LSTs were anomalously high, was likely the warmest period in the region since at least 1948.

2.1 Introduction

Globally, 2011-2015 was the warmest 5-year period on record. Global mean annual air temperatures from 2006-2010 and 2011-2015 were respectively 0.51°C and 0.57°C above the 1961-1990 mean (WMO Provisional Statement, 25 November 2015). Global air temperature

increases are enhanced at high latitudes. In the Canadian Arctic, near-surface summer air temperatures from long-running (1948-present) climate stations at Resolute Bay and Eureka were highest between 2010 and 2012 (<http://climate.weather.gc.ca>). In situ and remote sensing measurements, combined with modeling of the mass balance of glaciers in Canada's Queen Elizabeth Islands (QEI; 74.5-83.5°N, 61-121°W), a region that contains ~14% of the global glacier area, show that the rate of mass loss from these glaciers nearly tripled between 2004-2006 and 2007-2009 [*Gardner et al.*, 2011]. Other modeling studies indicate rates of glacier mass loss from the QEI of between $46 \pm 5 \text{ Gt yr}^{-1}$ and $37 \pm 10 \text{ Gt yr}^{-1}$ from 2003 to 2011 [*Lenaerts et al.*, 2013]. As a result of 21st century warming and accelerated mass wastage, glaciers in the Canadian Arctic have become the largest regional contributor to the eustatic component of global sea level rise outside the major ice sheets [*Gardner et al.*, 2013; *Radić et al.*, 2014].

Annual precipitation in the QEI is extremely low ($<400 \text{ mm yr}^{-1}$) [*Braithwaite*, 2005] and both inter-annual variations and longer-term trends in annual glacier mass balance are dominated by changes in summer melt [*Koerner*, 2005]. Mean summer (June to August) land surface temperatures (LST), an index of melt season intensity and/or duration [e.g. *Hall et al.*, 2006], over selected high elevation regions of major ice caps in the QEI were between 0.8°C and 2.2°C higher from 2005-2009 than in the previous 5-year period (2000-2004) [*Sharp et al.*, 2011]. Summer-melt duration and intensity are highly correlated with QEI summer air temperatures [*Sharp et al.*, 2011], so it is likely that glacier surface melt has also increased over the past decade. QEI-wide annual melt season duration was monitored during the period 2000 to 2009 using active microwave data from the QuikSCAT satellite [*Wang et al.*, 2005; *Wolken et al.*, 2009; *Sharp et al.*, 2011], but a complete assessment of QEI-wide summer LST patterns and their variability from satellite data has yet to be conducted. In contrast, annual and summer melt season mean LSTs of

the Greenland Ice Sheet, which lies immediately to the east of the QEI, have been studied extensively using satellite data [e.g. *Hall et al.*, 2013; *Shuman et al.*, 2014; references therein].

Extreme mass balance years in the QEI have been associated with changes in the geometry and strength of the July circumpolar vortex [*Alt*, 1987; *Gardner and Sharp*, 2007] that alter the distribution and intensity of regions of high and low pressure across the QEI. Between 2000 and 2009, increases in both summer mean air temperature and LST over QEI glaciers and ice caps were greatest in the north and west of the region [*Sharp et al.*, 2011]. This spatial pattern was inferred from LST trends calculated using data from the Moderate Resolution Imaging Spectroradiometer (MODIS) sensors for single 23 km x 23 km grid cell blocks centered on the interior regions of each of the seven major ice masses in the QEI. LST data from high elevation regions were used because they are more likely to vary continuously with air temperature than are temperatures at lower elevations, where melting may be continuous for long periods in summer causing the surface temperature to become insensitive to changing air temperature. As a result, however, it is not known whether the pattern of stronger warming in the north and west of the QEI is characteristic of all elevations on the region's ice caps; nor is it known whether this pattern has been sustained to the present-day.

Remote sensing methods are needed to map spatial patterns in ice cap LST and to monitor changes in these patterns over time at the scales of both individual ice caps and the regional ice cover. Here, we use MODIS LST observations to present the first complete picture of LST changes on QEI glaciers and ice caps over the period 2000-2015. This 16-year record of mean summer LST is used to assess the spatial and temporal variability of LST, and to quantify the rates of change in the intensity and duration of summer melt across the entire QEI ice cover. Near-surface temperature records from Eureka and Resolute Bay, and upper-air temperatures (1948-2015) over each of the

seven major ice masses in the QEI are used to place the LST observations into the context of the 68-year period for which in situ observations of air temperature and results from Climate Reanalysis exist.

2.2 Data and Methods

2.2.1 MODIS Land surface temperature

Changes in LST provide evidence of changing melt conditions over glaciers and ice caps. The probability of melt occurring at a given location in a given summer increases with both the summer mean LST and the length of the summer melt season [Hall *et al.*, 2006]. The MODIS sensors aboard the Terra and Aqua satellites image the Earth in 36 spectral bands every 1 or 2 days, and more frequently in the Polar Regions (<http://modis-land.gsfc.nasa.gov/>). We use the 8-Day L3 Global Land Surface Temperature and Emissivity product (MOD11A2) Version 05 to monitor the spatial and temporal evolution of mean summer LST on glaciers and ice caps in the QEI, which we take to be a proxy for the duration and/or intensity of summer melting. For consistency with previous work in this region [e.g. Sharp *et al.*, 2011] we only evaluate “daytime” LST data generated with the day/night algorithm of Wan and Li [1997]. Because the temperature of pure ice and snow cannot exceed 0°C, we assume that melt occurs if the temperature of the ice/snow-covered surface reaches 0°C. We also assume that the probability that melt is occurring during a given 8 day period increases as the 8 day mean daytime clear-sky LST approaches 0°C. Specifically, these assumptions imply (1) that as the 8 day mean LST approaches zero the number of days on which the surface temperature reached 0°C likely increases and (2) that melting is more prolonged and/or more intense in regions/periods with higher 8 day mean LSTs. Under these

conditions, the summer mean LST is likely correlated with the annual glacier surface mass balance [Sharp *et al.*, 2011]. Annual specific glacier mass balances of White Glacier, Axel Heiberg Island, Meighen Ice Cap and the northwest quadrant of the Devon Ice Cap for 2000/2001-2013/2014 (derived from in-situ measurements; c.f. Sharp *et al.* [2015]; <http://wgms.ch>) are negatively correlated with the MODIS mean summer LST ($r = -0.68$ to -0.85 ; $p > 0.01$).

MOD11A2 LST is computed from MODIS channels 31 (11 μm) and 32 (12 μm) using a split-window technique and all available daytime clear-sky scenes from the Terra satellite for sequential 8 day periods, and 1 km x 1 km pixels set in a sinusoidal projection [Wan *et al.*, 2002]. A cloud mask is used to ensure that only cloud-free observations are used in the calculation [Ackerman *et al.*, 1998]. Nominal product accuracy, estimated from comparison with in situ data, is $\pm 1^\circ\text{C}$ [Wan *et al.*, 2008]; but can be as low as $\pm 2^\circ\text{C}$ over high latitude snow/ice surfaces [Hall *et al.*, 2008a; Koenig and Hall, 2010]. The principal uncertainties in the LST product arise from the effects of cloud contamination [Box *et al.*, 2012; Hall *et al.*, 2012; references therein]. Similarity in the spectral signatures of snow, ice and thin cloud makes it difficult to discriminate between these surface types [Strabala *et al.*, 1994; King *et al.*, 2004]. The MODIS cloud mask is extremely conservative and tends to detect more cloud than is actually present over ice and snow [Hall *et al.*, 2008b]. Cloudy conditions over QEI ice caps tend to be associated with lower air temperatures in June and July but with higher air temperatures in August [Gascon *et al.*, 2013a]. Removal of observations from periods when clouds are detected can thus result in either an over- or under-estimation of the mean surface LST compared with the actual mean surface temperature. Furthermore, variability in cloud cover, both within individual 8 day periods and from one year to the next may introduce variability in the LST record that is not representative of true changes in the surface temperature [Hall *et al.*, 2006].

MODIS MOD11A2 values are produced when a minimum of one clear-sky day is available within a given 8 day period. Consequently, variability in the number of clear-sky days within each 8 day period may result in a higher variability in the mean summer MODIS-derived LST than actually exists in the true surface temperature. For the 2000-2015 period, there were, on average, 4-5 clear sky observations within each 8 day period (Section 2.6.1, Figures 2-S1 to 2-S4). A comparison of the summer LST record with both 700 hPa air temperatures and in situ air temperature measurements from glaciers in the Canadian Arctic, Svalbard, and Greenland between 2000 and 2008 found summer glacier LST to be highly correlated with summer air temperatures in continental climates. However, the relationship was often very weak in cloudy maritime regions situated near storm tracks (due to the bias induced by the lack of LST data during cloudy periods; M-L Geai, pers. comm., 2013). For the period 2000-2009, QEI summer mean glacier LST was highly correlated ($r > 0.82$) with both in situ summer near-surface air temperature measurements from on-ice AWS and summer mean air temperature anomalies at 700 hPa geopotential height derived from the NCEP/NCAR R1 Reanalysis [Sharp *et al.*, 2011]. Close coupling between variability in the mean summer LST and air temperature suggests that the LST record from ice caps in the QEI is a reasonable proxy for both the mean summer surface temperature and the summer melt intensity.

2.2.2 MOD11A2 data processing

Together, MODIS tiles h16v00, h17v00, h16v01 and 15v01 provide complete coverage of glaciated surfaces in the QEI. MODIS MOD11A2 Version 05 summer data (days 153 - 241) for these tiles were downloaded from the USGS Land Processes Distributed Active Archive Center (<http://lpdaac.usgs.gov/>) for the period 2000-2015. Daytime clear-sky LST and accompanying quality assessment information were extracted from the hierarchical data format files and re-

projected from the standard MODIS sinusoidal projection to a North America Albers Equal Area projection, WGS84 datum, 1 km resolution, using the MODIS re-projection tool version 4.1 (https://lpdaac.usgs.gov/tools/modis_reprojection_tool). Pixels for which the average LST error (QC_Day LST error flag) exceeded 2°C were removed from the analysis. Any remaining pixels with a temperature > 0°C were assigned a temperature of 0°C [e.g. *Hall et al.*, 2008b]. Rocks, dust, impurities and ponded water can exist on the snow/ice surface and their temperatures can exceed 0°C. The presence of such targets within a 1 km x 1 km pixel can result in a LST that exceeds 0°C. Pixels having an LST > 0°C were usually located near the ice cap margins and along narrow outlet glaciers, and likely contained a mixture of exposed rock, ice, and meltwater during the melt season.

Since inter-annual variability in QEI annual mass balance is dominated by changes in the summer mass balance [*Koerner*, 2005], we evaluated spatial and temporal patterns in LST for the summer months (June-August). Mean summer LST was computed from all 8 day daytime MODIS LST observations between 1-2 June (day 153) and 28-29 August (day 241). If a pixel has an 8 day mean LST of 0°C or greater we assume that melt occurred during the 8 day period. This approach is conservative because melt can still occur in periods when the 8 day mean LST is < 0°C. Investigation of all 8 day observations from 2000-2015 reveals that, although melt is largely confined to the June to August period, it does sometimes occur at other times (Section 2.6.2 Figures 2-S5 and Table 2-S6). Melt was observed as early as 1 May (2003; 0.004% of pixels) and as late as 7 October (2008; 0.02% of pixels). On average, only ~0.2% of pixels experience melt outside the JJA period, with a maximum of 1.1% (spring 2008) and a minimum of 0.001 % (in 7 different years). For each year, mean summer LST was calculated for cells having at least 7 of a possible 12 summer LST observations. To ensure that only data for glaciated surfaces were retained, the

output was clipped to the Randolph Glacier Inventory v3.2 region 32 Arctic Canada North reference polygons [Arendt *et al.*, 2012; Pfeffer *et al.*, 2014].

Changes in mean summer LST with respect to elevation were evaluated using three broad elevation zones (Figure 2-1b). The high and low elevation zones extend above 1400 and below 1000 m a.s.l. respectively, and are separated by an intermediate zone (1000 – 1400 m a.s.l.), which is centered on the regional mean upper limit of the superimposed ice zone (~1200 m a.s.l.) [Gardner *et al.*, 2011]. Much of the upper zone is likely to be snow-covered year round, while ice will almost always be exposed in summer in the lower zone. The extent and longevity of summer snow cover in the intermediate zone are likely to vary substantially between years with variations in the mean summer air temperature. Surface elevations were obtained from the Canadian Digital Elevation Dataset (CDED) edition 3.0, scale 1:50 k, resampled to a 1 km resolution.

2.3 Results

2.3.1 Mean summer glacier LST

Mean summer clear-sky LST data for all glacier-covered surfaces in the QEI for each year of the period 2000 to 2015 are presented in Figure 2-2. The QEI-wide mean summer glacier LST, averaged over all 16 years (Figure 2-2), was $-3.3 \pm 1.8^{\circ}\text{C}$ (mean \pm 1 SD; Table 2-1; Section 2.6.3 Figure 2-S7). The highest QEI-wide mean summer glacier LST ($-2.3 \pm 1.6^{\circ}\text{C}$) was recorded in 2007 while the lowest ($-5.4 \pm 2.2^{\circ}\text{C}$) was recorded in 2013. The mean summer glacier LST for each of the eight regions shown in Figure 2-1c was computed by averaging the mean summer LSTs (Figure 2-2) for all glaciated pixels within each region. The lowest mean summer glacier LST occurred in 2013 in all regions, with the exception of the Meighen Ice Cap for which it occurred

in 2001. The highest mean summer glacier LST was recorded in 2007 on Meighen Ice Cap and Axel Heiberg Island in the western QEI, and on the Agassiz Ice Cap and Prince of Wales Icefield in eastern Ellesmere Island. The highest mean summer glacier LST for a region in the southeast that includes the ice masses on Devon and Coburg Islands and the Sydkap Ice Cap and Manson Icefield on Ellesmere Island occurred in 2010. The highest regionally-averaged mean summer glacier LST on Northwest Ellesmere Island occurred in 2012. High mean summer glacier LSTs for the period 2007-2012 are consistent with the observed higher incidence of persistent positive mean 500 hPa geopotential height anomalies over the Canadian Arctic and western Greenland between 2007 and 2012 [*Rajewicz and Marshall, 2014; Bezeau et al., 2015*]. Such synoptic conditions have previously been linked with extreme warm summers and negative glacier mass balances in the QEI [*Alt, 1978, 1987; Gascon et al., 2013a*]. The 500 hPa geopotential height anomalies for 2000-2015 from NCEP/NCAR Reanalysis R1 data [*Kalnay et al., 1996*] display a ridge (trough) centered over the north and west of the QEI during warm (cold) summers.

We observe a decrease in mean summer glacier LST (Figure 2-2) and an increase in the standard deviation of the mean summer glacier LST (Section 2.6.3 Figure 2-S8) with increasing latitude and elevation. In general, LST is highest across the southern regions of the QEI (Devon Ice Cap and Coburg Island, Sydkap Ice Cap, Manson Icefield, and the southern part of Prince of Wales Icefield) and lowest on ice masses located further to the north and west (Axel Heiberg Island, Northwest Ellesmere Island, Agassiz Ice Cap and the northern part of the Prince of Wales Icefield). In any given year, mean summer glacier LST is, as expected, higher at low elevations around the margins of the ice masses than in higher elevation interior regions. The QEI-wide 16-year mean summer glacier LST was 3.8°C higher for areas below 1000 m a.s.l. than for areas above 1400 m a.s.l., indicating a longer and/or more intense melt season at lower elevations (Table 2-2). The 8

day mean LST reached 0°C at least once during the study period in 99.9% of all glacier-covered pixels, confirming that melt very likely occurred over the entire ice cover of the QEI at least once during the study period.

2.3.1.1 Glacier LST anomalies 2000-2015

Annual summer QEI-wide and regional glacier LST anomalies were computed relative to the 2000-2015 mean. For consistency with the LST regression analysis (Section 2.3.2), anomalies were only calculated for pixels that had mean summer LST observations for all 16 years, which amounted to 91% of all possible pixels. Positive (negative) LST anomalies indicate melt seasons that are longer (shorter) and/or warmer (cooler) than the 2000-2015 mean. The interval 2000-2015 is characterized by a 5-year period (2000-2004) of negative glacier LST anomalies (between $-0.35 \pm 0.65^{\circ}\text{C}$ and $-0.93 \pm 0.70^{\circ}\text{C}$) and a 6-year period (2007-2012) of positive LST anomalies (between $0.54 \pm 0.43^{\circ}\text{C}$ and $1.08 \pm 0.45^{\circ}\text{C}$), separated by two intermediate years: one of positive LST anomalies (2005; $0.76 \pm 0.40^{\circ}\text{C}$) and one of negative LST anomalies (2006; $-0.87 \pm 0.79^{\circ}\text{C}$) (Figure 2-3; Table 2-3). The largest QEI-wide negative glacier LST anomaly ($-2.06 \pm 0.84^{\circ}\text{C}$) was recorded in 2013. With the exception of Meighen Ice Cap (2001), the largest negative anomaly in each region also occurred in 2013. In 2014, regional glacier LST anomalies were positive in the northwest but negative in the south and east, and the QEI-wide glacier LST anomaly was mildly negative ($-0.10 \pm 0.49^{\circ}\text{C}$). 2015 saw a return to positive LST anomalies ($0.46 \pm 0.45^{\circ}\text{C}$) across the QEI. There is no year in which LST anomalies for all glaciated pixels in the QEI were either entirely positive or entirely negative. However, in 2007 (the year with the highest mean summer LST) and 2013 (the year with the lowest mean summer LST), only 1% and 0.05% of pixels respectively, had negative and positive summer glacier LST anomalies.

The sign of the LST anomaly also varies within each region. From Figure 2-3, we note that glacier LST anomalies were positive along the northwest coast of Ellesmere Island in 2002, 2003 and 2014, but were negative at higher elevations inland during those same years. With the exception of extreme warm or cold years, LST anomalies on the summit of the Devon Ice Cap tended to be of opposite sign to those observed at lower elevations. Another area where summer LST anomalies were often of opposite sign to those in the rest of the region includes the northern part of Manson Icefield and the extreme southeast portion of the Prince of Wales Icefield. This area borders Baffin Bay and is downwind of the North Water (NOW) Polynya (Figure 2-1); this open water source may play a role in moderating the climate in this region by increasing cloud cover and summer snowfall in years when the polynya is relatively large. Baffin Bay is the primary moisture source for maritime-facing slopes in the southeast of the QEI [Koerner, 1979] and warm summers, inferred from ice core data, were well correlated with the maximum open water extent in the QEI's inter-island channels for the 1961-1974 period [Koerner, 1977].

2.3.2 LST change 2000-2015

To determine whether there was a measurable change in mean summer glacier LST over the study period, we performed a linear regression analysis. Regressions were computed on a pixel-by-pixel basis for all pixels having mean summer LST observations in all 16 years (Figure 2-1). Between 2000 and 2015, QEI-wide mean summer glacier LST increased at a rate of 0.06 ± 0.04 °C yr⁻¹ (Table 2-4), for a total increase of 0.96°C over the 16-year study period. There is a general trend towards higher mean summer LSTs across most of the QEI (93% of pixels measured experienced an increase in LST), suggesting an increase in melt season duration and/or intensity in most regions. The measured increase in LST is markedly greater in the north and west of the QEI. The measured rates of change in LST on Meighen Ice Cap, Axel Heiberg Island and Northwest

Ellesmere Island were two to four times higher than those observed in the southeast of the QEI. This spatial pattern of enhanced summer surface warming in the northwest of the QEI is consistent with that reported previously by *Sharp et al.* [2011]. An apparent decrease in mean summer LST is observed for coastal regions of southeast Devon Ice Cap, as well as for Manson Icefield and the southeast coastal region of Prince of Wales Icefield below ~500 m a.s.l.. This might indicate a trend towards a shorter and/or less intense melt season in these regions. The proximity of this region to open water sources in Baffin Bay and Nares Strait (including the NOW polynya; Figure 2-1) may assist in maintaining these low-lying ice masses. During warm summers, when polynya extent is relatively large, we expect an increase in the frequency of storm systems that bring moist air masses from the east, causing snowfall and surface riming. Rime and fresh snow temporarily raise the surface albedo, decreasing the amount of solar energy absorbed at the surface and reducing the surface temperature. Such sudden increases in albedo, especially during the warm summer months, could partly explain the lower rates of LST increase along the southeast coasts of Devon and Ellesmere Islands.

The QEI-wide rate of change in the mean summer LST over the 16 year period for regions above 1400 m a.s.l. ($0.09 \pm 0.03^\circ\text{C yr}^{-1}$) was more than double that for regions below 1000 m a.s.l. ($0.04 \pm 0.03^\circ\text{C yr}^{-1}$) (Table 2-4). The northwest-southeast spatial gradient in LST change is magnified at higher elevations. On both Axel Heiberg and northwest Ellesmere Islands, mean summer LST above 1400 m a.s.l. increased by more than $0.09^\circ\text{C yr}^{-1}$. Between 1000 and 1400 m a.s.l., the rate was between 0.08 and $0.09^\circ\text{C yr}^{-1}$. In contrast, the mean summer LSTs of the high and mid-elevation regions of the Devon Ice Cap increased by only $0.05 \pm 0.02^\circ\text{C yr}^{-1}$ and $0.02 \pm 0.02^\circ\text{C yr}^{-1}$, respectively. This enhanced surface warming at higher elevations is not unexpected, because there is more potential for warming in these regions where the mean summer LST is lower. It is

also possible that, as the incidence of surface melting increases at higher elevations, increased percolation of meltwater into cold snow and firn contributes to surface warming by the release of latent heat during refreezing.

To explore whether there are any additional spatial patterns in the LST data that differ from the long-term (linear) LST trend, we performed a Principal Components Analysis on the 16-year mean summer LST record. Only the first two Principal Components had eigenvalues greater than one. The first Principal Component, which explains 79% of the variance in the LST record, closely follows the pattern of annual summer LST anomalies (Figure 2-4). This component's scores are largest in the northwest and at higher elevations, consistent with the pattern of LST change described previously (Figure 2-5). In addition, the departure from zero is much larger for the minimum scores than for the maximum scores, suggesting that positive and negative LST anomalies have the same pattern and are most likely caused by the same (atmospheric) forcing. Investigating potential atmospheric forcings, we find the Empirical Orthogonal Functions (EOF) of PC1 to be well-correlated (-0.79 , $p < 0.001$) with the mean summer North Atlantic Oscillation (NAO) index, derived by averaging the June-August monthly mean NAO indices, for 2000-2015 (<http://www.cpc.ncep.noaa.gov>). The JJA NAO index displays a similar trend to the EOFs of PC1 for 2007-2015 but the extreme warm and cold years in 2005 and 2006 are not explained by this teleconnection. The second Principal Component, which explains 6% of the variance in the LST record, yields very negative component scores on the Devon Ice Cap and very positive component scores along the northwest coast of Ellesmere Island. The largest positive and negative EOFs for this Principal Component occurred in 2001 and 2002 respectively (Figure 2-4). This suggests localized LST anomalies in these regions in 2001 and 2002 that were out of phase with the rest of the QEI. Large positive LST anomalies were observed on the Devon Ice Cap in 2001 (when

anomalies were negative elsewhere). In the following year, positive LST anomalies were observed along the northwest coast of Ellesmere Island.

There is a clear increase in mean summer glacier LST in all regions of the QEI over the 2000-2015 period. Positive glacier LST anomalies from 2007-2012 suggest that the bulk of this increase occurred over the second half of the study period. The years 2010-2012 produced three of the four highest QEI-wide mean summer glacier LSTs. Although the summer mean LST in 2013 was 1.4 to 2.9°C lower than the period mean, this extreme negative anomaly did not result in a decrease in mean LST during the 2011-2015 pentad. A previous study identified extreme summer warming and enhanced melt over the QEI for a period ending in 2009 [Sharp *et al.*, 2011]. We find that even stronger summer warming occurred after the conclusion of that study.

2.3.3 Summer air temperatures

Mean summer near-surface and upper-air temperatures over glaciated surfaces in the QEI, are highly correlated with mean summer glacier LSTs [Sharp *et al.*, 2011]. Since variability in mean summer glacier LST and mean summer air temperature are strongly coupled, past air temperature changes can be used to infer past changes in glacier LST. The record of air temperature measurements is considerably longer (1948-present) than the MODIS satellite record (2000-present). To place our 16-year LST record in the context of the past 68 years we extend the record of 700 hPa geopotential height air temperatures and 2 m air temperatures presented by Sharp *et al.* [2011] to 2015.

Mean summer air temperatures at 700 hPa geopotential height were obtained from the NCEP/NCAR R1 Reanalysis [Kalnay *et al.*, 1996] for the seven locations used by Sharp *et al.* [2011] (Section 2.6.3 Table 2-S9). These locations correspond to high elevation sites on the

seven major ice masses used in the current study. The Meighen Ice Cap contains only ~0.09% of the QEI glacier area and was not included in the analysis. Mean summer 700 hPa air temperatures (2005-2015) were 1.0-1.2°C higher than the 1948-2015 mean in all regions (Figure 2-6b). Six of the seven warmest years on record occurred between 2005 and 2015, except on the Devon Ice Cap where four of the seven warmest years occurred during this period. 2010 and 2011 were the two warmest years in all regions; 2005, 2007, 2008, 2010, 2011 and 2012 were among the eleven warmest years. 2013 was among the ten coldest years in all regions except for Manson Icefield and Devon Ice Cap (17th and 21st coldest respectively). Mean summer 2000-2015 700 hPa temperatures were highly correlated with the regional mean summer LSTs (Manson Icefield $r > 0.78$, all other regions $r \geq 0.86$; Table 2-5).

Near-surface (2 m) air temperatures from Environment Canada's weather stations at Eureka and Resolute Bay are available for 1948-present (<http://climate.weather.gc.ca>). June-August mean air temperatures at these stations were calculated from monthly mean temperatures derived from daily averages. Daily averages were computed by averaging the daily maximum and minimum hourly temperatures. These stations are located at a distance from the glaciated regions studied and are not situated on ice. In the absence of long-term on-ice recording stations in the Canadian Arctic, these records provide a useful indication of long-term temperature trends in the region. Previous work found good agreement ($r > 0.79$) between the near-surface air temperature records at Eureka and Resolute Bay and on-ice near-surface air temperature measurements from the Agassiz Ice Cap (1988-2010) and the Devon Ice Cap (1997-2010) [Sharp *et al.*, 2011].

Eureka and Resolute Bay summer 2005-2015 air temperatures were 1.2°C higher than the 1948-2015 mean (Figure 2-6a). 2005-2009 and 2010-2014 were the warmest pentads on record at both stations. 2009, 2011 and 2012 were among the four warmest of the last 68 summers at Eureka.

2012, 2011, and 2007 were the three warmest summers recorded at Resolute Bay. 2013 was the coldest summer recorded at Eureka and the 11th coldest at Resolute Bay. The presence of a single extreme cold year (2013) did not significantly alter the upward trend in 21st century summer air temperatures: 2010-2014 was the second warmest pentad at both locations (0.8 to 1.5°C warmer than the next warmest pentad), suggesting that 2013 was more likely a single extreme (cold) year than the beginning of a more prolonged period of lower temperatures.

The near-surface and upper air temperature records display similar patterns of summer temperature anomalies for 1948-2015 (Figure 2-6). Positive anomalies occurred from the mid-1950s until the early-1960s and were followed by a period of relatively lower temperatures lasting until the early to mid-1990s. Although positive summer air temperature anomalies were observed between the mid-1960s and mid-1990s, they did not persist for more than a few years and never exceeded 1°C. A sustained warm period began in the late 1990s and has continued until present, with a few exceptions: temperature anomalies were slightly negative in the early 2000s, and 2013 was one of the coldest years in all records. There is good agreement ($r > 0.79$) between the near-surface and upper-air temperature records for 1948-2015 and we have shown that the upper-air temperatures are highly correlated ($r > 0.78$) with the summer mean glacier LST for 2000-2015. The close coupling between air temperatures and LST suggests that the most recent period of anomalously high QEI summer mean glacier LST (2007-2012) was not just high with respect to the 16-year satellite record; it was likely one of the warmest periods since at least 1948.

2.4 Discussion

I have presented the first picture of mean summer LST and its variability over all glaciated surfaces in the QEI. The only previous study to monitor QEI summer glacier LST using MODIS observations [*Sharp et al.*, 2011] calculated summer LST for individual 23 km x 23 km boxes centered on interior regions of seven large ice masses. Boxes were chosen to avoid areas where the summer LST regularly reached 0°C. Given the significant differences in LST change observed for high and low elevation regions (Section 2.3.2), we would expect the magnitude of LST change calculated from select high-elevation boxes to be larger than that computed using all glaciated surfaces. For comparison, we computed mean summer LST anomalies relative to the 2000-2009 mean for all QEI glaciated surfaces for the 2000-2009 period. The difference in mean summer glacier LST between 2000-2004 and 2005-2009 was 0.2-0.5°C less than reported by *Sharp et al.* [2011] for all regions except Northwest Ellesmere Island where the difference was 0.3°C greater (Section 2.6.3 Table 2-S10). There is good general agreement between the 2000-2009 LST records from the two studies, suggesting that, under current climatic conditions, a spatially-distributed sample of high-elevation locations may be sufficient to determine the sign and approximate magnitude of LST changes and to identify broad spatial patterns. However, the point-based method does not permit evaluation of the complete spatial structure of LST change. For example, the inclusion of all glaciated surfaces has allowed the identification of areas for which the sign of the annual LST anomalies was often opposite to that in the rest of the region (Section 2.3.1.1).

High elevation (>1400 m a.s.l.) LST change was more than double that at low elevations (< 1000 m a.s.l.) and the rate of LST increase was less at lower latitudes. LSTs in southern and low elevation regions regularly reached the pressure melting point during the summer. Differences in the rate of LST change may be attributed, in part, to the fact that the potential for surface warming is greatest in regions where the initial mean LST is lower. Importantly, a smaller increase in mean

summer LST does not necessarily imply a lower rate of glacier mass loss since an increase in atmospheric temperatures over a surface that is at the melting point will result in melting, runoff, and mass loss, rather than surface warming. Unfortunately, sparse in situ measurements and the coarse spatial resolution of the Reanalysis data prohibit determination of whether atmospheric warming was actually greater at higher elevations.

The occurrence of melt at all elevations and locations in the QEI could have important implications for the future distribution of melt, percolation, and runoff on the region's ice caps and glaciers. Meltwater percolation into the firn is expected to increase as melt becomes more frequent at all elevations. Enhanced meltwater percolation and subsequent re-freezing in the firn releases latent heat, which in turn, raises the temperature of the firn. Ultimately, if the firn temperature reaches the melting point, runoff from the firn may occur [Pfeffer and Humphrey, 1998]. Increased rates of firn densification [Zdanowicz *et al.*, 2012; Bezeau *et al.*, 2013] and the growth of large ice bodies within the firn [Gascon *et al.*, 2013b] have been observed across the Canadian Arctic in recent years. Gascon *et al.* [2013b] speculate that this buildup of ice bodies could prevent deep penetration of meltwater into the firn and promote horizontal runoff, thereby increasing the percentage of snowmelt that runs off from higher elevation regions of ice caps. This buildup of ice bodies could also result in a spread of supra-glacial lakes to higher elevations if a perched water table forms above these ice bodies and could also occur without the firn as a whole reaching the melting point [Bezeau *et al.*, 2013; Machguth *et al.*, 2016]. It could also result in more widespread slush flows that cause rapid ablation by failure and downslope transport of water saturated snow/firn.

Increases in summer LST can influence QEI glacier mass balance through the ice-albedo feedback. Absorption of solar radiation at the surface is governed by the surface albedo – the ratio of reflected

to incoming solar radiation. Increases in LST promote grain growth, which lowers the surface albedo, while the rate of snow/ice grain metamorphism increases with temperature and in the presence of liquid water [Wiscombe and Warren, 1980; Colbeck, 1982]. Atmospheric warming and higher LSTs result in a more rapid and/or earlier removal of the previous year's snowpack. Since the albedo of bare ice ($\sim 0.2 - 0.35$) is lower than that of fresh snow ($0.6 - 0.8$) [Cuffey and Paterson, 2010], earlier exposure of bare ice by snowpack removal increases energy absorption, leading to enhanced surface warming and/or melt. Increased melt can also lead to a more rapid release of impurities contained in snow and ice. These impurities become concentrated on the snow/ice surface, further reducing the surface albedo, leading to increased surface temperatures and/or melt [Flanner and others, 2007 and references therein]. Thus, higher LSTs and atmospheric temperatures can lead to a reduction in the surface albedo, which increases solar energy absorption and promotes further surface warming and/or melt. This positive feedback mechanism is expected to result in more negative glacier mass balances in the QEI, unless there is a compensating increase in precipitation and fresh snowfall, which would temporarily increase the surface albedo [e.g. Box *et al.*, 2012].

Ice masses in the QEI contain a total of 86.3 to 138.1 mm of sea level equivalent [Radić *et al.*, 2014]. A higher mean summer glacier LST implies a longer and/or more intense melt season, while higher air temperatures imply an increase in energy available for melt. Since inter-annual variability in QEI glacier surface mass balance is governed by changes in summer melt and runoff (which may be further enhanced through ice-albedo feedbacks), the observed increases in LST and air temperature should be reflected in the mass balance record. In-situ mass balance observations extend up until 2013/2014 and indicate that 2007 was the most negative mass balance year in the QEI since the 1960s (<http://wgms.ch/latest-glacier-mass-balance-data/>). Regional climate and

mass balance modelling, and remote sensing measurements, also indicate strongly negative Canadian Arctic glacier mass balances between 2003 and 2014 [*Gardner et al.*, 2013; *Lenaerts et al.*, 2013; *Sharp et al.*, 2015].

Annual estimates of glacier mass change in the QEI as a whole over the period 2002-2015 were derived by differencing successive annual summer minima in the time series of regional mass anomalies measured by the Gravity Recovery and Climate Experiment (GRACE; update from *Gardner et al.* [2011]). The GRACE mass change data are consistent with the mean summer LST record for 2003/2004-2014/2015. 2013 had the lowest QEI-wide mean summer LST and the least negative QEI-wide mass change. 2007, 2011 and 2012 had the three highest QEI-wide mean summer LSTs and the three most negative annual mass changes. The QEI annual mass change and QEI mean summer LST are strongly correlated ($r = -0.82$; $p < 0.01$), confirming that variations in annual mass balance in this region are strongly influenced by variations in summer air temperature.

2.5 Conclusions

This study provides the first complete picture of summer mean LST variations over all glaciated surfaces of the QEI from 2000-2015. QEI mean summer glacier surface temperature increased by 0.06 ± 0.04 °C yr⁻¹, for a total change of 0.96°C over the 16-year period. More than 90% of the QEI's glaciated area experienced an increase in LST. Nearly all glaciated pixels recorded at least one LST observation of 0°C, suggesting that melt occurred at all elevations and all locations in the region. The LST change was greatest in the northwest, which is consistent with the findings of a previous study [*Sharp et al.*, 2011] that covered a shorter time period with less complete spatial coverage. 2007 had the highest mean summer glacier LST, followed by 2011 and 2012. Summer

700 hPa and near-surface air temperatures from 2010-2012 were among the warmest on record. The strong correlation between summer LST and 700 hPa air temperatures suggests that recent summers were not only anomalously warm relative to the 16-year satellite record but were likely some of the warmest since at least 1948. Increases in LST have important implications for glacier surface mass balance. Longer and/or more intense melt seasons will likely result in more negative glacier mass balances and higher rates of glacier mass loss in a region that is already one of the largest non-ice sheet contributors to the eustatic component of global sea level rise.

Table 2-1: Clear-sky mean summer land surface temperature (°C) for glaciated regions of the Queen Elizabeth Islands; ± 1 standard deviation.

Year	QEI	Agassiz IC	Axel Heiberg I	Devon I & Coburg I	Manson IF	Meighen IC	Northwest Ellesmere I	Prince of Wales IF	Sydkap IC
2000	-4.1 \pm 2.0	-5.3 \pm 1.9	-4.0 \pm 1.4	-2.7 \pm 1.4	-1.9 \pm 0.8	-3.6 \pm 0.8	-5.4 \pm 1.6	-3.6 \pm 1.6	-3.0 \pm 1.0
2001	-3.9 \pm 1.9	-4.7 \pm 1.9	-4.0 \pm 1.6	-2.5 \pm 1.0	-2.1 \pm 1.0	-5.3 \pm 0.7	-5.4 \pm 1.7	-3.4 \pm 1.5	-3.0 \pm 1.1
2002	-3.7 \pm 2.1	-4.7 \pm 2.4	-3.9 \pm 1.9	-3.2 \pm 1.8	-1.9 \pm 1.2	-3.5 \pm 0.8	-4.4 \pm 2.1	-3.3 \pm 1.9	-2.9 \pm 1.4
2003	-3.9 \pm 1.8	-4.9 \pm 2.0	-4.0 \pm 1.6	-3.2 \pm 1.3	-2.1 \pm 1.0	-3.5 \pm 0.6	-4.5 \pm 1.7	-3.7 \pm 1.6	-3.2 \pm 1.0
2004	-4.2 \pm 2.3	-5.2 \pm 2.3	-4.2 \pm 2.3	-3.3 \pm 1.7	-2.3 \pm 1.2	-3.4 \pm 0.3	-5.5 \pm 2.1	-3.9 \pm 2.1	-3.1 \pm 1.3
2005	-2.6 \pm 1.7	-3.6 \pm 1.9	-2.3 \pm 1.5	-2.0 \pm 1.2	-1.2 \pm 0.7	-2.0 \pm 0.3	-3.2 \pm 1.8	-2.4 \pm 1.4	-1.6 \pm 0.8
2006	-4.2 \pm 2.3	-5.4 \pm 2.2	-4.0 \pm 1.9	-2.7 \pm 1.4	-1.9 \pm 1.0	-3.7 \pm 0.4	-5.9 \pm 2.1	-3.5 \pm 1.9	-2.5 \pm 1.1
2007	-2.2 \pm 1.6	-3.0 \pm 1.8	-1.8 \pm 1.2	-1.8 \pm 1.0	-1.0 \pm 0.7	-1.7 \pm 0.3	-3.1 \pm 1.6	-1.9 \pm 1.3	-1.3 \pm 0.7
2008	-2.7 \pm 1.4	-3.5 \pm 1.4	-2.5 \pm 1.3	-2.4 \pm 1.2	-1.3 \pm 0.8	-3.1 \pm 0.7	-3.4 \pm 1.3	-2.4 \pm 1.3	-1.9 \pm 1.0
2009	-2.8 \pm 1.7	-3.9 \pm 1.9	-2.3 \pm 1.3	-2.3 \pm 1.4	-1.3 \pm 0.8	-2.4 \pm 0.2	-3.3 \pm 1.6	-2.7 \pm 1.6	-2.1 \pm 1.1
2010	-2.5 \pm 1.7	-3.3 \pm 1.9	-2.1 \pm 1.4	-1.6 \pm 0.9	-0.9 \pm 0.6	-2.3 \pm 0.3	-3.7 \pm 1.7	-2.0 \pm 1.2	-1.2 \pm 0.7
2011	-2.3 \pm 1.3	-3.1 \pm 1.4	-1.8 \pm 1.1	-1.8 \pm 0.9	-1.4 \pm 0.7	-1.4 \pm 0.3	-3.1 \pm 1.3	-2.1 \pm 1.0	-1.4 \pm 0.7
2012	-2.4 \pm 1.4	-3.0 \pm 1.4	-2.3 \pm 1.2	-1.9 \pm 1.1	-1.1 \pm 0.8	-1.7 \pm 0.8	-2.9 \pm 1.4	-2.4 \pm 1.3	-1.6 \pm 0.9
2013	-5.4 \pm 2.2	-6.3 \pm 2.2	-5.5 \pm 1.8	-3.9 \pm 1.4	-3.1 \pm 1.1	-5.0 \pm 0.6	-7.2 \pm 1.8	-4.5 \pm 1.8	-4.3 \pm 1.3
2014	-3.4 \pm 1.8	-4.3 \pm 2.0	-2.8 \pm 1.6	-3.0 \pm 1.4	-2.1 \pm 1.0	-2.7 \pm 0.2	-4.1 \pm 1.9	-3.4 \pm 1.6	-2.7 \pm 1.1
2015	-2.8 \pm 1.7	-3.8 \pm 1.9	-2.5 \pm 1.5	-2.4 \pm 1.3	-1.4 \pm 0.9	-1.9 \pm 0.3	-3.3 \pm 1.7	-2.8 \pm 1.5	-2.2 \pm 1.1
2000-2015	-3.3 \pm 1.7	-4.2 \pm 1.9	-3.1 \pm 1.5	-2.5 \pm 1.2	-1.7 \pm 0.8	-3.1 \pm 0.4	-4.2 \pm 1.6	-2.9 \pm 1.5	-2.4 \pm 1.0

Table 2-2: 16-year average (2000-2015) clear-sky mean summer land surface temperature (°C) for glaciated regions of the Queen Elizabeth Islands by elevation zone (Section 2.2) ± 1 standard deviation.

Elevation m a.s.l.	QEI	Agassiz IC	Axel Heiberg I	Devon & Coburg I	Manson IF	Meighen IC	Northwest Ellesmere I	Prince of Wales IF	Sydkap IC
< 1000	-2.0 \pm 0.9	-2.0 \pm 0.9	-2.0 \pm 0.9	-1.7 \pm 0.6	-1.5 \pm 0.7	-3.1 \pm 0.4	-2.7 \pm 0.9	-1.8 \pm 0.8	-1.9 \pm 0.8
1000 - 1400	-3.7 \pm 1.0	-3.8 \pm 1.0	-3.5 \pm 1.0	-3.1 \pm 0.5	-2.8 \pm 0.7	N/A	-4.1 \pm 1.0	-3.8 \pm 0.9	-3.4 \pm 0.5
>1400	-5.8 \pm 1.2	-6.1 \pm 1.1	-5.1 \pm 1.3	-4.7 \pm 0.7	N/A	N/A	-6.1 \pm 1.2	-5.1 \pm 0.9	N/A
All elevations	-3.3 \pm 1.7	-4.2 \pm 1.9	-3.1 \pm 1.5	-2.5 \pm 1.2	-1.7 \pm 0.8	-3.1 \pm 0.4	-4.2 \pm 1.6	-2.9 \pm 1.5	-2.4 \pm 1.0

Table 2-3: Clear-sky mean summer land surface temperature anomaly (°C) with respect to the 2000-2015 mean for glaciated regions of the Queen Elizabeth Islands; ± 1 standard deviation

Year	QEI	Agassiz IC	Axel Heiberg I	Devon I & Coburg I	Manson IF	Meighen IC	Northwest Ellesmere I	Prince of Wales IF	Sydkap IC
2000	-0.82 \pm 0.64	-1.10 \pm 0.51	-0.91 \pm 0.58	-0.21 \pm 0.33	-0.21 \pm 0.28	-0.65 \pm 0.67	-1.22 \pm 0.65	-0.61 \pm 0.46	-0.62 \pm 0.42
2001	-0.56 \pm 0.62	-0.45 \pm 0.40	-0.86 \pm 0.54	0.09 \pm 0.54	-0.38 \pm 0.37	-2.48 \pm 0.61	-1.11 \pm 0.56	-0.37 \pm 0.32	-0.61 \pm 0.48
2002	-0.35 \pm 0.65	-0.44 \pm 0.64	-0.79 \pm 0.64	-0.61 \pm 0.64	-0.18 \pm 0.46	-0.39 \pm 0.37	-0.09 \pm 0.65	-0.29 \pm 0.52	-0.51 \pm 0.58
2003	-0.57 \pm 0.49	-0.68 \pm 0.44	-0.91 \pm 0.47	-0.60 \pm 0.43	-0.42 \pm 0.33	-0.48 \pm 0.30	-0.24 \pm 0.45	-0.69 \pm 0.37	-0.85 \pm 0.44
2004	-0.93 \pm 0.70	-0.93 \pm 0.62	-1.11 \pm 0.96	-0.75 \pm 0.59	-0.60 \pm 0.48	-0.52 \pm 0.25	-1.18 \pm 0.67	-0.93 \pm 0.69	-0.73 \pm 0.51
2005	0.76 \pm 0.40	0.65 \pm 0.33	0.89 \pm 0.36	0.58 \pm 0.31	0.51 \pm 0.33	0.92 \pm 0.25	1.07 \pm 0.38	0.61 \pm 0.30	0.76 \pm 0.36
2006	-0.87 \pm 0.79	-1.17 \pm 0.56	-0.91 \pm 0.57	-0.20 \pm 0.37	-0.17 \pm 0.34	-0.80 \pm 0.36	-1.65 \pm 0.71	-0.47 \pm 0.48	-0.08 \pm 0.29
2007	1.08 \pm 0.45	1.27 \pm 0.37	1.39 \pm 0.45	0.72 \pm 0.38	0.69 \pm 0.29	1.28 \pm 0.25	1.16 \pm 0.42	1.08 \pm 0.32	1.08 \pm 0.35
2008	0.63 \pm 0.52	0.79 \pm 0.59	0.70 \pm 0.40	0.14 \pm 0.32	0.34 \pm 0.27	-0.06 \pm 0.32	0.91 \pm 0.51	0.62 \pm 0.37	0.50 \pm 0.36
2009	0.54 \pm 0.43	0.38 \pm 0.27	0.82 \pm 0.38	0.22 \pm 0.26	0.38 \pm 0.22	0.55 \pm 0.24	1.00 \pm 0.33	0.27 \pm 0.29	0.28 \pm 0.33
2010	0.86 \pm 0.49	0.99 \pm 0.39	1.01 \pm 0.42	0.95 \pm 0.48	0.77 \pm 0.46	0.71 \pm 0.21	0.55 \pm 0.42	0.98 \pm 0.54	1.18 \pm 0.43
2011	0.99 \pm 0.62	1.15 \pm 0.59	1.34 \pm 0.55	0.75 \pm 0.57	0.26 \pm 0.45	1.50 \pm 0.25	1.19 \pm 0.59	0.90 \pm 0.55	0.95 \pm 0.51
2012	0.96 \pm 0.64	1.25 \pm 0.69	0.87 \pm 0.63	0.60 \pm 0.39	0.59 \pm 0.30	1.35 \pm 0.44	1.43 \pm 0.59	0.64 \pm 0.38	0.75 \pm 0.45
2013	-2.06 \pm 0.84	-2.09 \pm 0.59	-2.38 \pm 0.69	-1.39 \pm 0.57	-1.40 \pm 0.53	-2.15 \pm 0.60	-2.93 \pm 0.60	-1.52 \pm 0.54	-1.87 \pm 0.62
2014	-0.10 \pm 0.49	-0.01 \pm 0.34	0.30 \pm 0.37	-0.44 \pm 0.48	-0.40 \pm 0.38	0.21 \pm 0.23	0.16 \pm 0.44	-0.41 \pm 0.37	-0.29 \pm 0.38
2015	0.46 \pm 0.45	0.40 \pm 0.31	0.55 \pm 0.32	0.14 \pm 0.28	0.22 \pm 0.20	1.00 \pm 0.23	0.94 \pm 0.41	0.18 \pm 0.27	0.06 \pm 0.31

Table 2-4: 16-year linear rate of change (2000-2015) of clear-sky mean summer land surface temperature ($^{\circ}\text{C yr}^{-1}$) for glaciated regions of the Queen Elizabeth Islands by elevation zone (Section 2.2) ± 1 standard deviation.

Elevation m a.s.l.	QEI	Agassiz IC	Axel Heiberg I	Devon & Coburg I	Manson IF	Meighen IC	Northwest Ellesmere I	Prince of Wales IF	Sydkap IC
< 1000	0.04 \pm 0.03	0.05 \pm 0.03	0.07 \pm 0.03	0.01 \pm 0.02	0.01 \pm 0.02	0.11 \pm 0.03	0.06 \pm 0.03	0.02 \pm 0.02	0.02 \pm 0.03
1000 - 1400	0.06 \pm 0.03	0.07 \pm 0.03	0.09 \pm 0.03	0.02 \pm 0.02	0.03 \pm 0.02	N/A	0.08 \pm 0.03	0.05 \pm 0.02	0.04 \pm 0.03
>1400	0.09 \pm 0.03	0.09 \pm 0.02	0.11 \pm 0.02	0.05 \pm 0.02	N/A	N/A	0.09 \pm 0.02	0.07 \pm 0.02	N/A
All elevations	0.06 \pm 0.04	0.07 \pm 0.00	0.09 \pm 0.03	0.02 \pm 0.03	0.02 \pm 0.02	0.11 \pm 0.03	0.08 \pm 0.03	0.04 \pm 0.03	0.04 \pm 0.02

Table 2-5: Pearson correlation coefficient, r , of the mean summer LST versus the mean summer 700 hPa air temperature for the period 2000-2015 for the seven major ice masses in the QEI (Figure 2-1c).

Agassiz IC	Axel Heiberg I	Devon & Coburg I	Manson IF	Northwest Ellesmere I	Prince of Wales IF	Sydkap IC
0.95	0.94	0.86	0.78	0.95	0.93	0.89

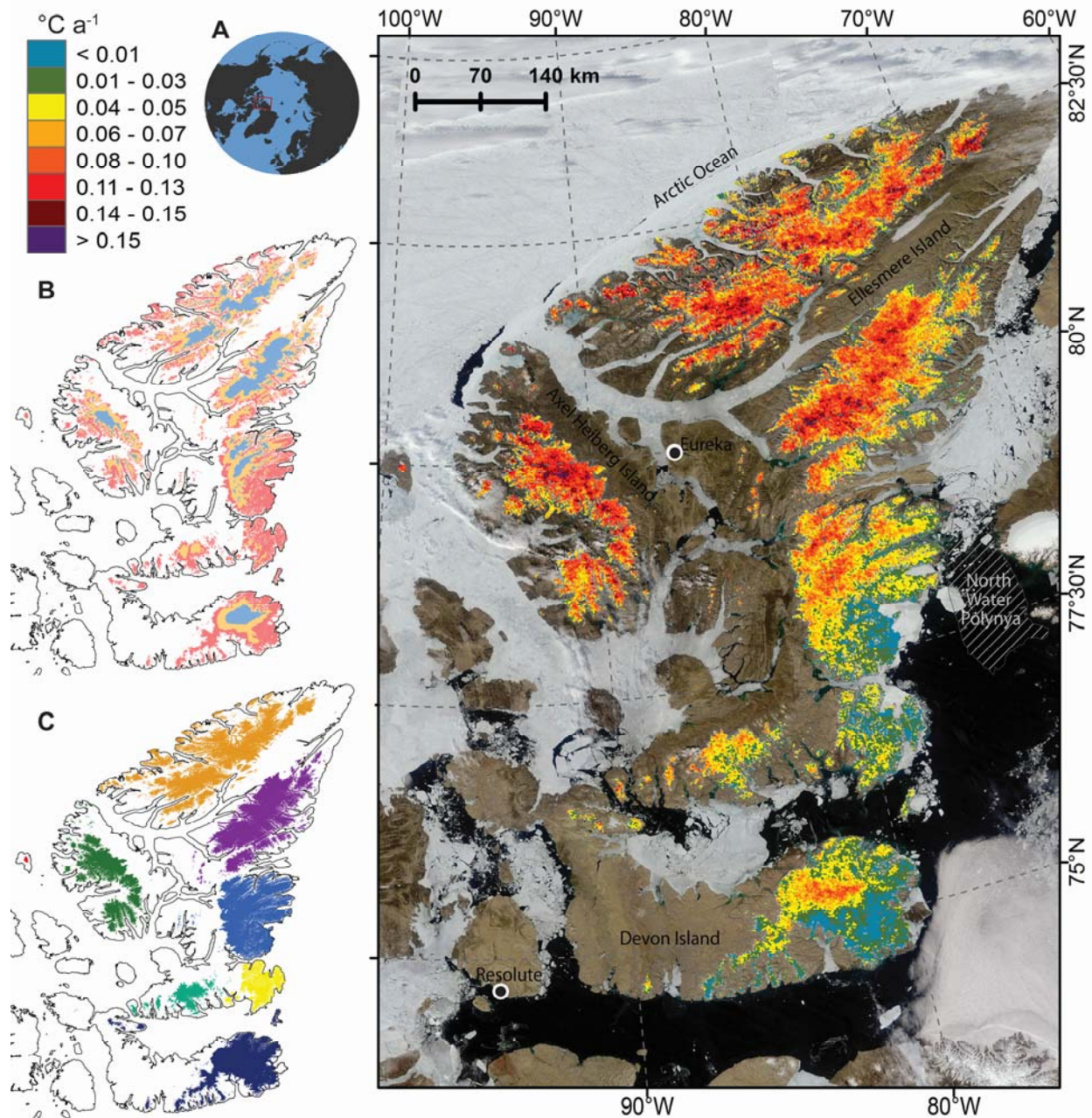


Figure 2-1 Linear rate of change in mean summer clear-sky land surface temperature ($^{\circ}\text{C yr}^{-1}$) for 2000-2015 for the Queen Elizabeth Islands. Rate of change is computed only for pixels with annual summer mean clear-sky LST for all 16 years of observation. Black dots with white outline indicate location of Environment Canada weather stations at Eureka and Resolute Bay. Base image: Moderate Resolution Spectroradiometer, 4 July 2011. Left panel: (a) Red box indicates location of study site. (b) Elevation zones: < 1000 m a.s.l. (pink), $1000\text{-}1400$ m a.s.l. (yellow), > 1400 m a.s.l. (grey). (c) QEI glacial regions used in this study: Northwest Ellesmere Island (orange), Agassiz Ice Cap (purple), Prince of Wales Icefield (blue), Manson Icefield (yellow), Sydkap Ice Cap (blue-green), Devon Island and Coburg Island (navy), Axel Heiberg Island (green), and Meighen Ice Cap (red).

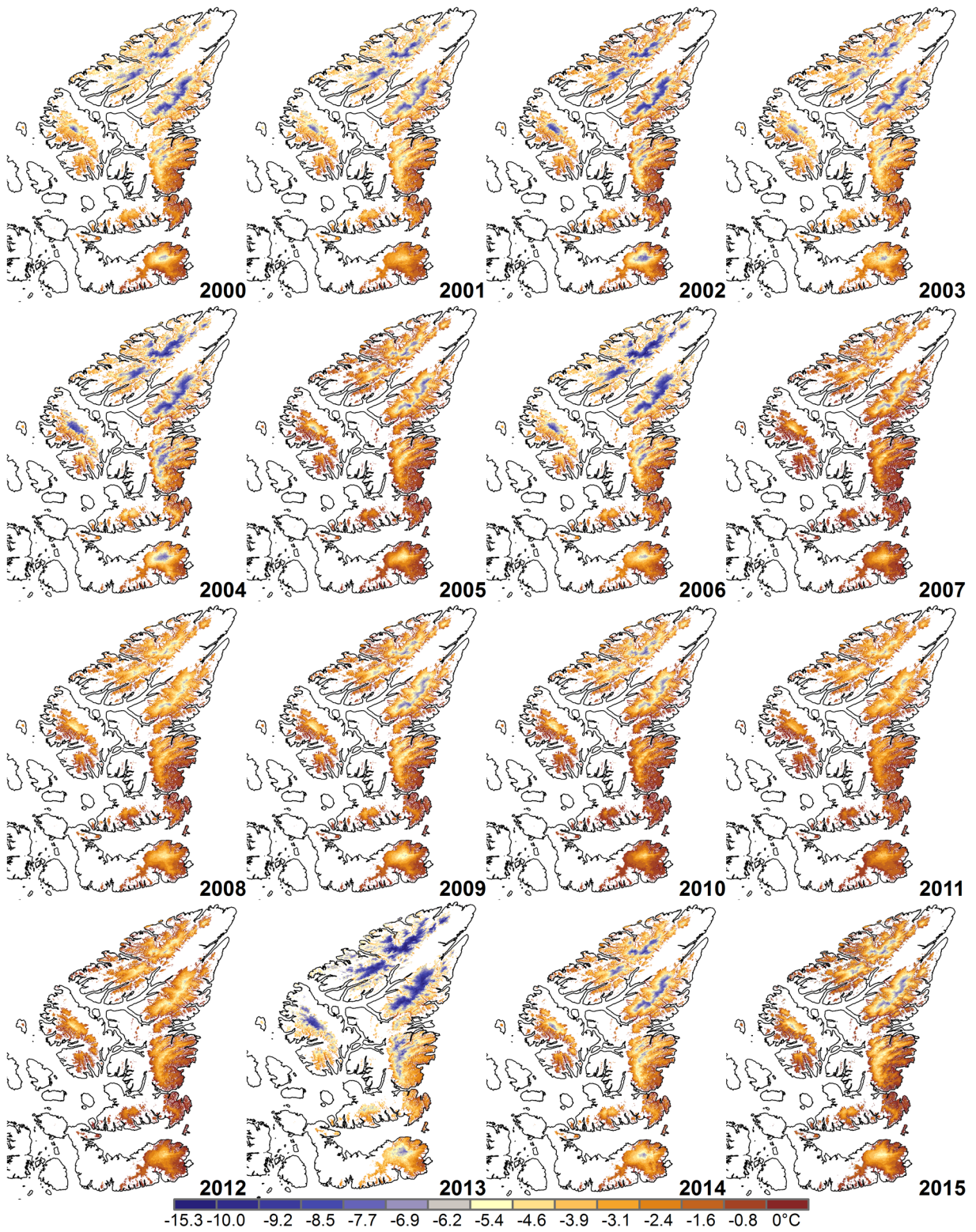


Figure 2-2 Mean summer clear-sky land surface temperature (°C) for the Queen Elizabeth Islands.

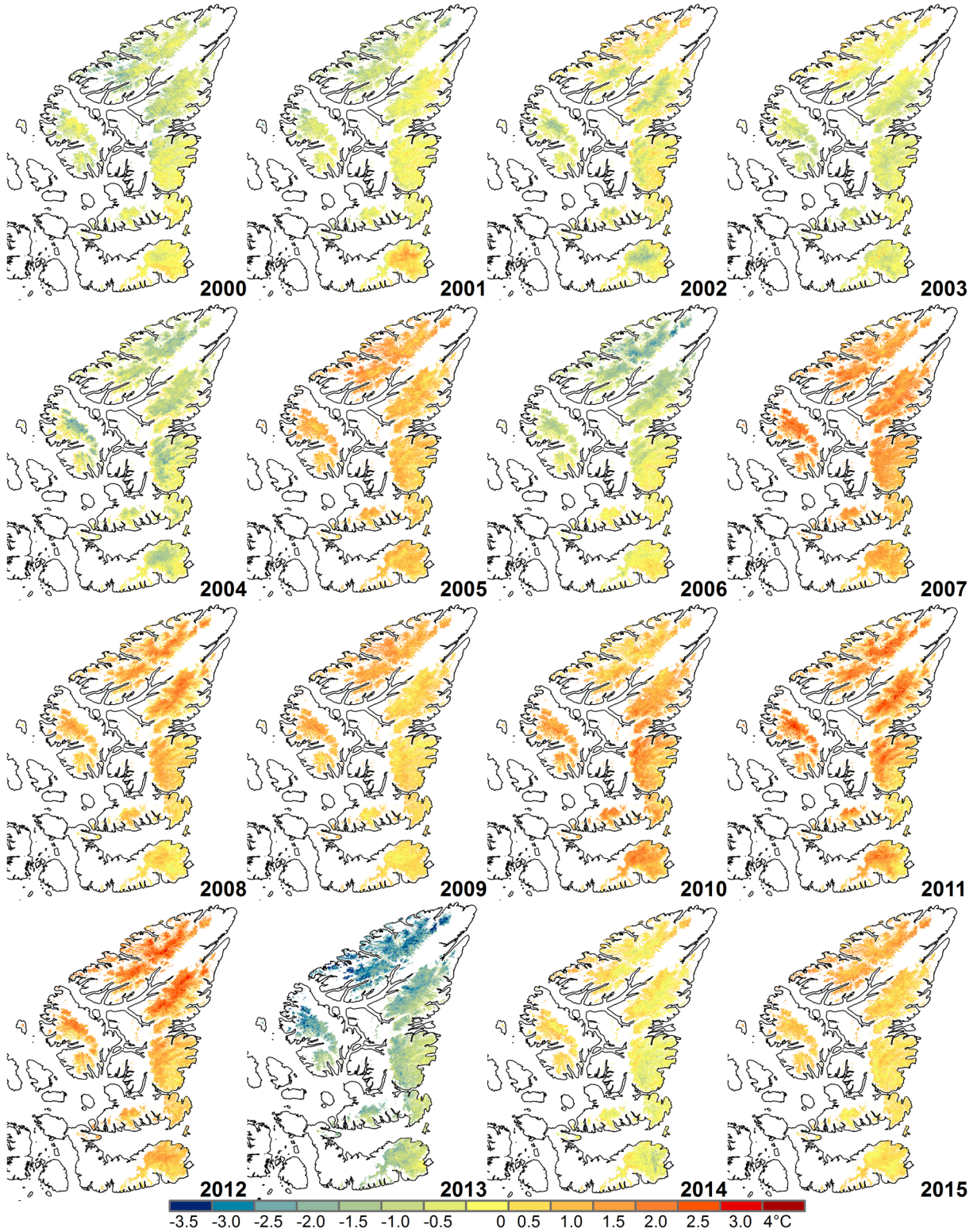


Figure 2-3 Mean summer clear-sky land surface temperature anomaly ($^{\circ}\text{C}$) relative to the 2000-2015 mean for the Queen Elizabeth Islands.

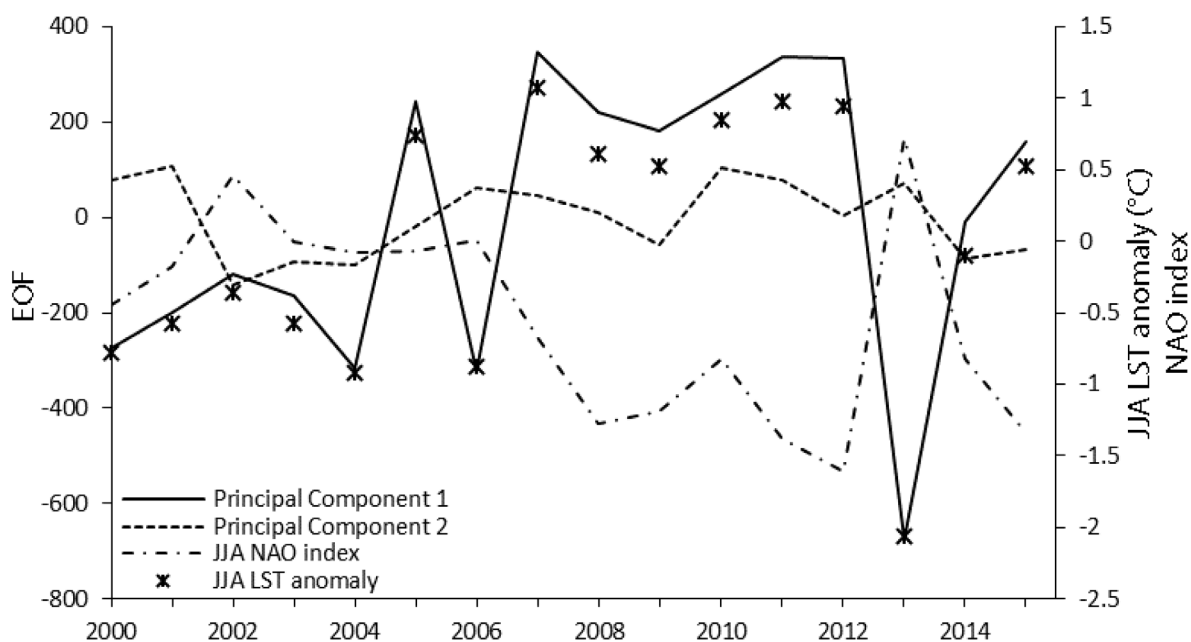


Figure 2-4 Empirical orthogonal function (EOF) for the first Principal Component of the LST time series for 2000-2015 (left-hand axis, solid black line segments). The mean summer (June – August) LST anomaly relative to the 200-2015 mean (°C) (black star) and the mean JJA NAO index for 2000-2015 (dashed curve) are plotted on the right-hand axis.

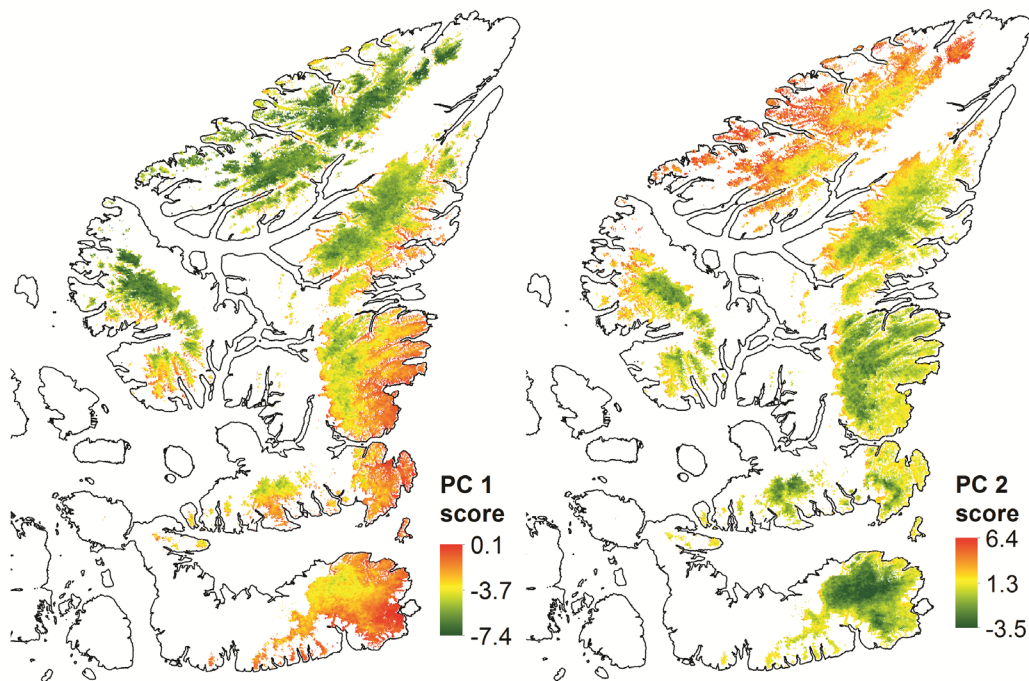


Figure 2-5 Component scores for the first two Principal Components of the mean summer clear-sky land surface temperature (Figure 2) for the Queen Elizabeth Islands.

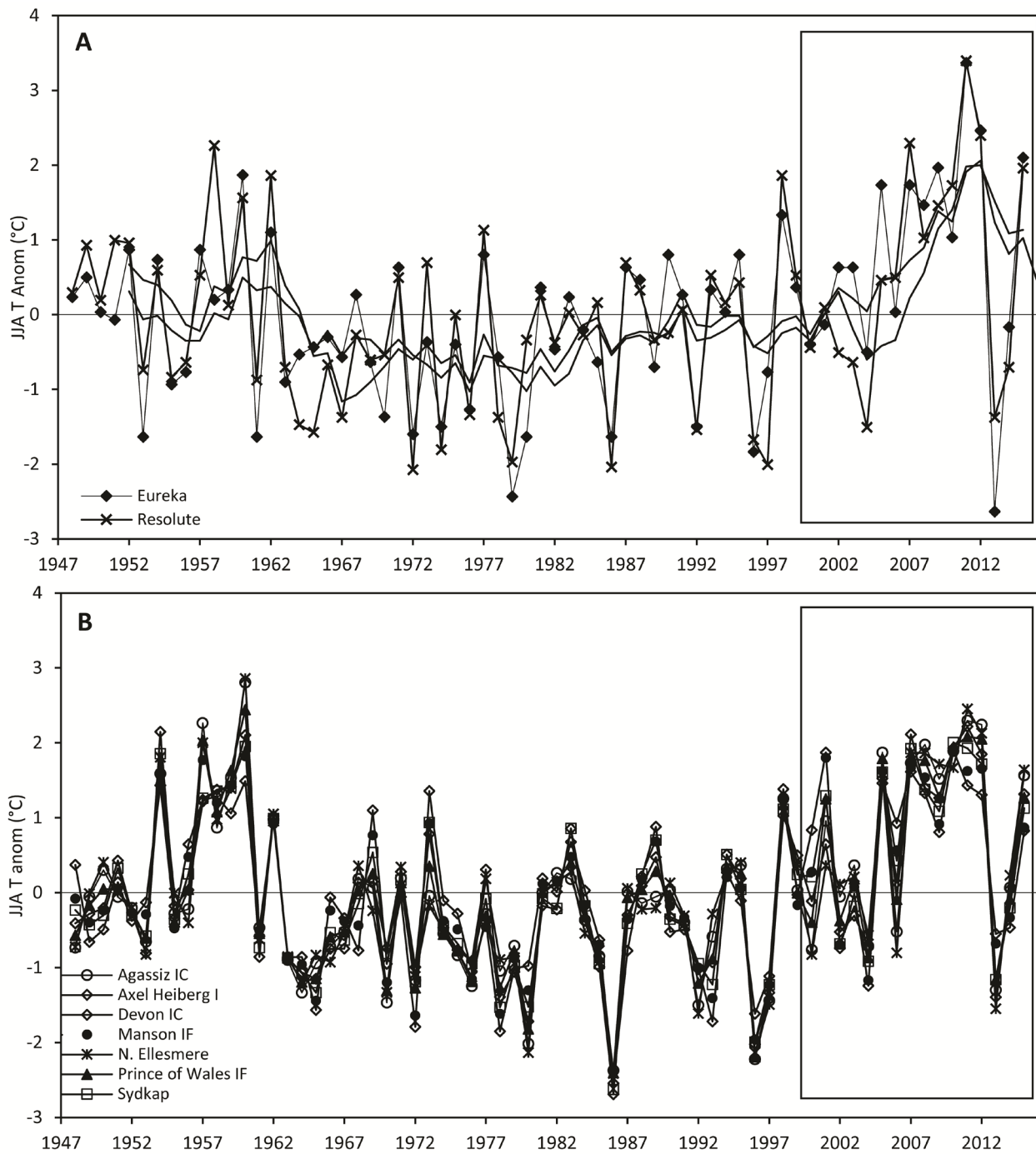


Figure 2-6 Annual anomalies (relative to the 1948-2015 mean) in (a) mean summer (June-August) near-surface air temperature at Eureka and Resolute; (b) mean summer 700 hPa air temperature for sites centered on the interior of each of the major glaciated regions in the QEI (all regions in Figure 1c except for the Meighen Ice Cap) from the NCEP/NCAR R1 Reanalysis. Black box indicates period of MODIS satellite record.

2.6 Chapter 2 Supplemental Materials

2.6.1: Analysis of clear-sky observations within each 8 day period

The number of clear-sky day observations within each 8 day period was computed from the MOD11A2 Qualify Flags. The total number of clear-sky observations for all 1 km x 1 km glacier-covered pixels in the QEI were computed for each 8 day period between day 153 and day 241 for 2000-2015. LST observations are given if at least 1 clear-sky observation is available during a given 8 day period. QEI-wide (area-averaged) clear-sky day observations were then computed by averaging all ice-covered pixels within the QEI (Figure 2-S2; Table 2-S1). The 16-year average number of clear-sky day observations for each 8 day period is presented in Figure 2-S3; the standard deviation is presented in Figure 2-S4.

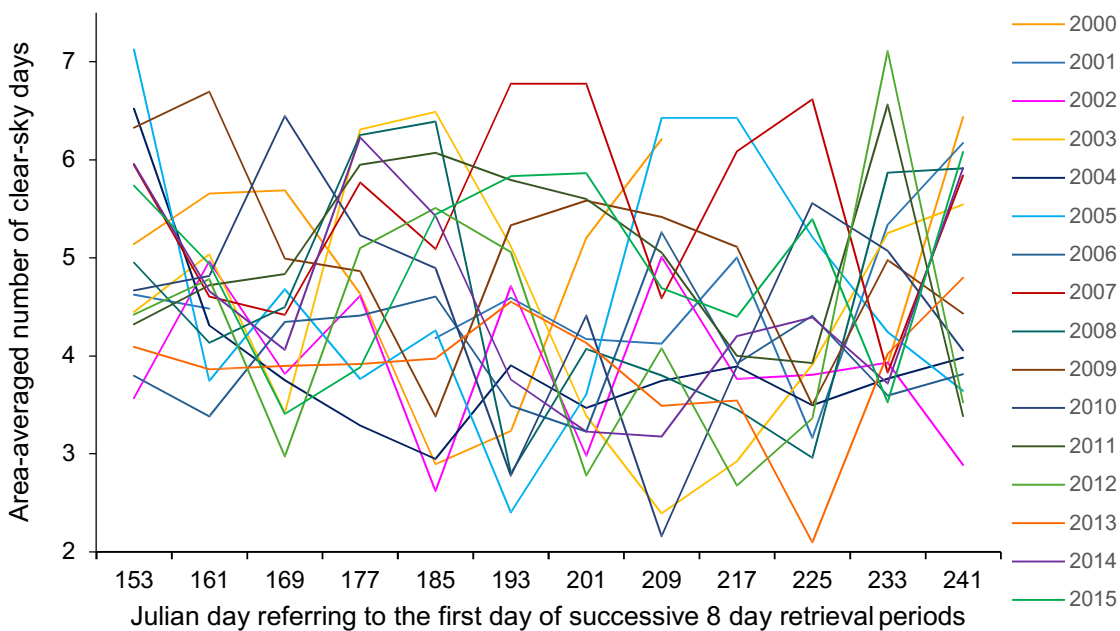


Figure 2-S1: Mean QEI-wide (area-averaged) number of clear-sky observations within individual 8 day periods for 2000-2015.

Table 2-S2: Mean QEI-wide clear-sky days (mean \pm 1SD) within each 8 day period between 1-2 June and 28-29 August for 2000-2015.

DOY	2000	2001	2002	2003	2004	2005	2006	2007	2008	2009	2010	2011	2012	2013	2014	2015	mean	median	stdev	variance
153	5.1 ± 1.9	4.6 ± 1.4	3.6 ± 1.7	4.4 ± 1.5	6.5 ± 1.1	7.1 ± 1.3	3.8 ± 1.5	5.9 ± 1.5	5.0 ± 1.4	6.3 ± 1.2	4.7 ± 2.0	4.3 ± 1.7	4.4 ± 1.7	4.1 ± 1.7	6.0 ± 1.3	5.7 ± 1.3	5.1 ± 1.5	4.8 ± 1.5	1.0 ± 0.3	1.1 ± 0.1
161	5.7 ± 1.6	4.5 ± 0.8	5.0 ± 1.3	5.0 ± 2.0	4.3 ± 1.3	3.7 ± 1.9	3.4 ± 1.5	4.6 ± 1.8	4.1 ± 1.7	6.7 ± 1.4	4.8 ± 1.5	4.7 ± 1.7	4.8 ± 1.2	3.9 ± 1.5	4.7 ± 1.4	4.9 ± 1.9	4.7 ± 1.5	4.7 ± 1.5	0.8 ± 0.3	0.6 ± 0.1
169	5.7 ± 1.8	no data	3.8 ± 1.9	3.4 ± 1.3	3.8 ± 1.4	4.7 ± 1.7	4.3 ± 1.5	4.4 ± 1.5	4.5 ± 1.7	5.0 ± 1.7	6.4 ± 1.6	4.8 ± 1.5	3.0 ± 1.3	3.9 ± 1.3	4.1 ± 1.6	3.4 ± 1.5	4.3 ± 1.6	4.3 ± 1.5	0.9 ± 0.2	0.8 ± 0.0
177	4.6 ± 1.5	NA	4.6 ± 1.6	6.3 ± 2.0	3.3 ± 1.6	3.8 ± 1.3	4.4 ± 1.2	5.8 ± 1.9	6.3 ± 2.0	4.9 ± 1.4	5.2 ± 1.6	6.0 ± 1.8	5.1 ± 1.9	3.9 ± 1.4	6.2 ± 1.9	3.9 ± 1.3	4.9 ± 1.6	4.9 ± 1.6	1.0 ± 0.3	1.0 ± 0.1
185	2.9 ± 1.4	4.2 ± 1.6	2.6 ± 1.4	6.5 ± 2.1	2.9 ± 1.4	4.3 ± 1.4	4.6 ± 1.4	5.1 ± 2.1	6.4 ± 1.8	3.4 ± 2.0	4.9 ± 1.7	6.1 ± 1.6	5.5 ± 1.7	4.0 ± 1.3	5.4 ± 1.5	5.4 ± 1.8	4.6 ± 1.6	4.7 ± 1.6	1.2 ± 0.3	1.5 ± 0.1
193	3.2 ± 1.3	4.6 ± 1.7	4.7 ± 1.4	5.1 ± 1.9	3.9 ± 1.4	2.4 ± 1.3	3.5 ± 1.4	6.8 ± 1.9	2.8 ± 1.1	5.3 ± 1.8	2.8 ± 1.2	5.8 ± 2.1	5.1 ± 1.7	4.6 ± 1.4	3.8 ± 1.7	5.8 ± 2.0	4.4 ± 1.6	4.6 ± 1.6	1.3 ± 0.3	1.6 ± 0.1
201	5.2 ± 1.9	4.2 ± 1.4	3.0 ± 1.4	3.4 ± 1.5	3.5 ± 1.3	3.6 ± 1.9	3.2 ± 1.7	6.8 ± 1.9	4.1 ± 1.7	5.6 ± 2.0	4.4 ± 1.3	5.6 ± 1.6	2.8 ± 1.3	4.1 ± 1.5	3.2 ± 1.5	5.9 ± 1.9	4.3 ± 1.6	4.1 ± 1.6	1.2 ± 0.2	1.4 ± 0.1
209	6.2 ± 1.7	4.1 ± 1.5	5.0 ± 1.9	2.4 ± 1.2	3.7 ± 1.6	6.4 ± 1.5	5.3 ± 2.1	4.6 ± 1.8	3.8 ± 1.5	5.4 ± 1.5	2.2 ± 1.1	5.1 ± 1.7	4.1 ± 1.6	3.5 ± 1.3	3.2 ± 1.7	4.7 ± 1.6	4.4 ± 1.6	4.4 ± 1.6	1.2 ± 0.2	1.5 ± 0.1
217	NA	5.0 ± 1.6	3.8 ± 1.3	2.9 ± 1.6	3.9 ± 1.4	6.4 ± 1.5	3.9 ± 1.2	6.1 ± 2.0	3.5 ± 1.4	5.1 ± 2.0	3.9 ± 1.2	4.0 ± 1.4	2.7 ± 1.1	3.5 ± 1.7	4.2 ± 2.0	4.4 ± 1.4	4.0 ± 1.5	3.9 ± 1.4	1.3 ± 0.3	1.6 ± 0.1
225	NA	3.2 ± 1.6	3.8 ± 1.9	3.9 ± 1.5	3.5 ± 1.6	5.2 ± 1.7	4.4 ± 1.4	6.6 ± 1.8	3.0 ± 1.2	3.5 ± 1.6	5.6 ± 2.6	3.9 ± 1.3	3.4 ± 1.5	2.1 ± 1.2	4.4 ± 2.3	5.4 ± 1.4	4.1 ± 1.6	3.9 ± 1.6	1.2 ± 0.4	1.4 ± 0.1
233	3.9 ± 1.4	5.3 ± 1.6	3.9 ± 1.6	5.3 ± 1.4	3.8 ± 1.5	4.2 ± 1.3	3.6 ± 1.6	3.8 ± 1.7	5.9 ± 1.2	5.0 ± 1.3	5.1 ± 1.5	6.6 ± 1.4	7.1 ± 1.1	4.0 ± 2.2	3.7 ± 1.5	3.5 ± 1.5	4.7 ± 1.5	4.1 ± 1.5	1.1 ± 0.2	1.2 ± 0.1
241	6.4 ± 1.2	6.2 ± 1.3	2.9 ± 1.3	5.5 ± 1.5	4.0 ± 1.8	3.6 ± 1.1	3.8 ± 1.7	5.8 ± 1.4	5.9 ± 1.4	4.4 ± 1.6	4.1 ± 1.6	3.4 ± 1.8	3.5 ± 1.5	4.8 ± 1.6	5.9 ± 1.5	6.1 ± 1.4	4.8 ± 1.5	4.6 ± 1.5	1.2 ± 0.2	1.4 ± 0.0
mean	4.9 ± 1.6	4.6 ± 1.5	3.9 ± 1.5	4.5 ± 1.6	3.9 ± 1.5	4.6 ± 1.5	4.0 ± 1.5	5.5 ± 1.8	4.6 ± 1.5	5.1 ± 1.6	4.5 ± 1.6	5.0 ± 1.6	4.3 ± 1.5	3.9 ± 1.5	4.6 ± 1.6	4.9 ± 1.6				
median	5.2 ± 1.6	4.5 ± 1.5	3.8 ± 1.5	4.7 ± 1.5	3.8 ± 1.4	4.3 ± 1.4	3.9 ± 1.5	5.8 ± 1.8	4.3 ± 1.5	5.1 ± 1.6	4.7 ± 1.5	4.9 ± 1.6	4.2 ± 1.5	3.9 ± 1.5	4.3 ± 1.5	5.2 ± 1.5				
stdev	1.2 ± 0.3	0.8 ± 0.3	0.8 ± 0.3	1.3 ± 0.3	0.9 ± 0.2	1.4 ± 0.3	0.6 ± 0.2	1.0 ± 0.2	1.3 ± 0.3	1.0 ± 0.3	1.2 ± 0.4	1.0 ± 0.2	1.3 ± 0.3	0.7 ± 0.3	1.1 ± 0.3	0.9 ± 0.2				
variance	1.5 ± 0.1	0.6 ± 0.1	0.7 ± 0.1	1.7 ± 0.1	0.8 ± 0.0	2.0 ± 0.1	0.4 ± 0.1	1.0 ± 0.1	1.6 ± 0.1	1.0 ± 0.1	1.4 ± 0.2	1.0 ± 0.0	1.7 ± 0.1	0.4 ± 0.1	1.2 ± 0.1	0.9 ± 0.1				

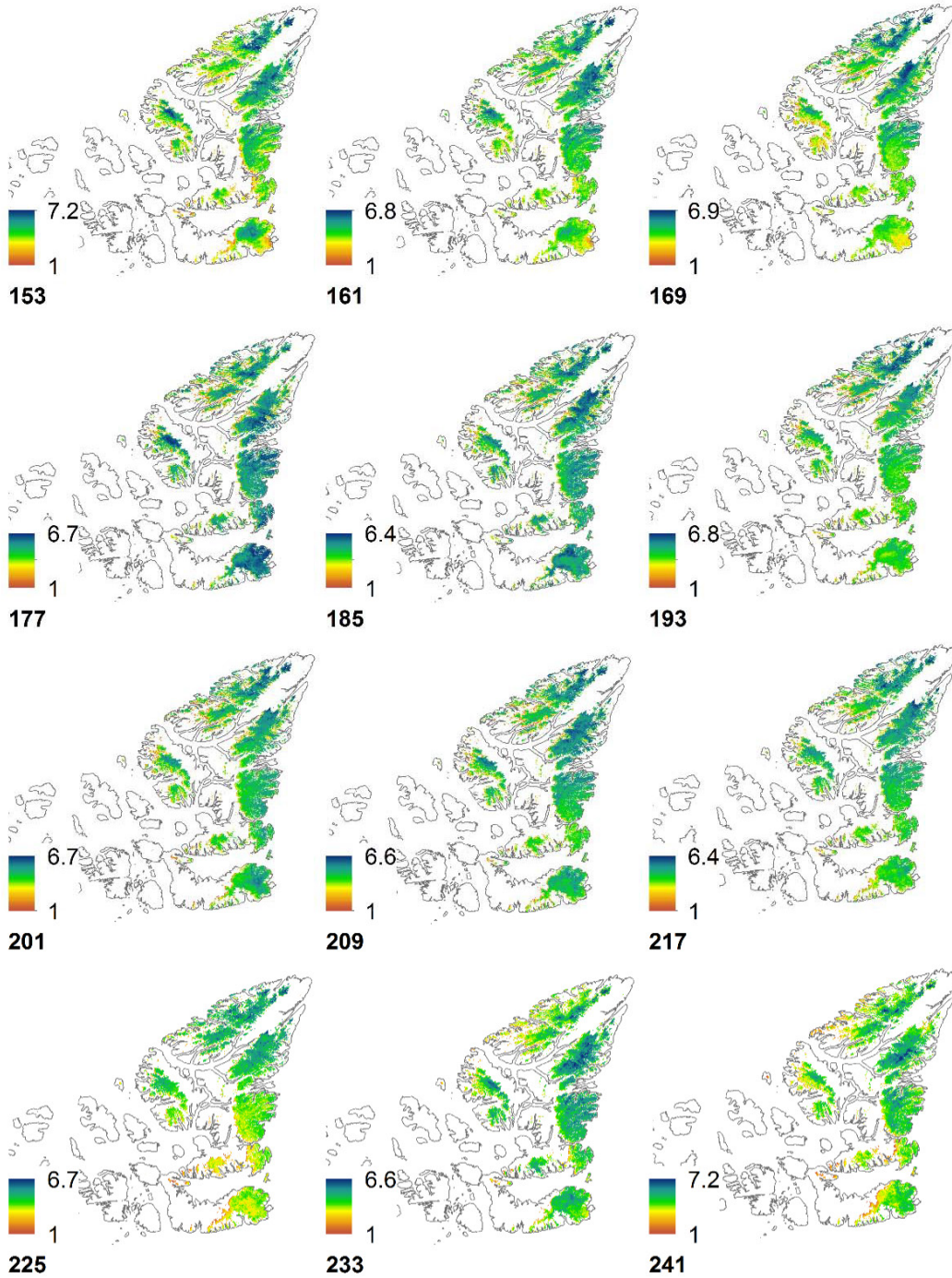


Figure 2-S3: Mean number of clear-sky observations during each 8 day period for 2000-2015.

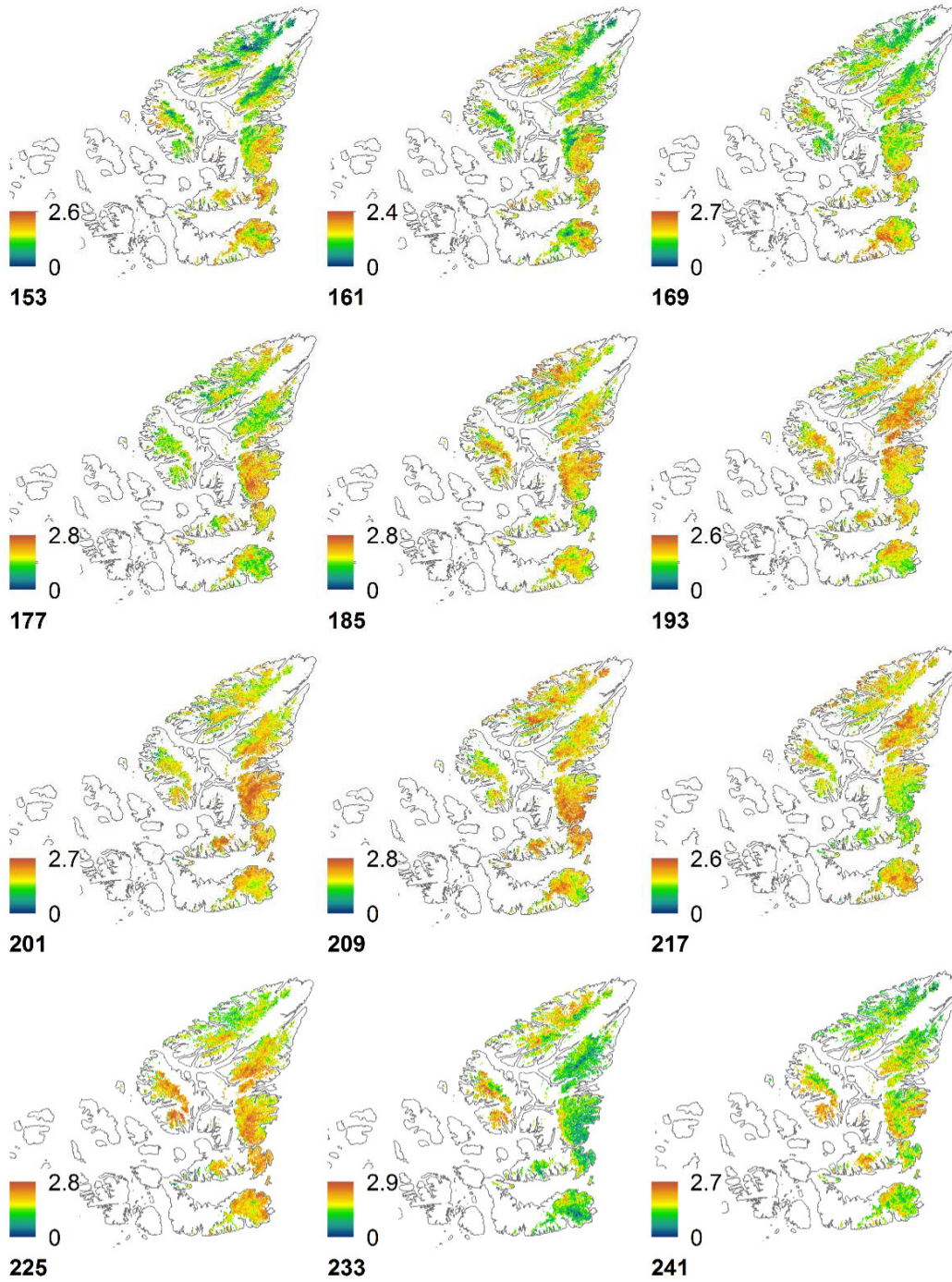


Figure 2-S4: Standard deviation of the number of clear-sky observations during each 8 day period for 2000-2015.

2.6.2: Occurrence of melt

Between 2000 and 2015, a temperature of 0°C was recorded for a small number ($<1\%$) of pixels prior to (days 121-145) and following (days 257-273) the June-August period (Figure 2-S5; Table 2-S6). The percentage of pixels experiencing a temperature $\geq 0^{\circ}\text{C}$ outside the JJA period was considerably less ($<1\%$) than during the June-August period ($> 50\%$). In most years, we observe a step change in the percentage of pixels experiencing melt (temperature $\geq 0^{\circ}\text{C}$) before and after the summer months. Given the small number of pixels experiencing melt outside of the June-August period, we restricted our analysis to the summer months (JJA). This approach facilitates comparison of data over time because it removes the need to adjust the length of the period of interest. However, the method does have limitations because changes in temperature are only monitored during the summer months. Thus, if a location already reaches the melting point regularly either prior to and/or following the JJA period, melt duration at that location would likely be underestimated. Similarly, if a location were to begin to reach the melting point outside the JJA period, this change would not be captured. The exclusion of these time periods is not believed to be significant for our study period. However, if surface temperatures continue to increase, we would also expect the length of the melt season to increase. This could warrant a revisit of the use of the JJA period to evaluate changes in glacier surface temperature.

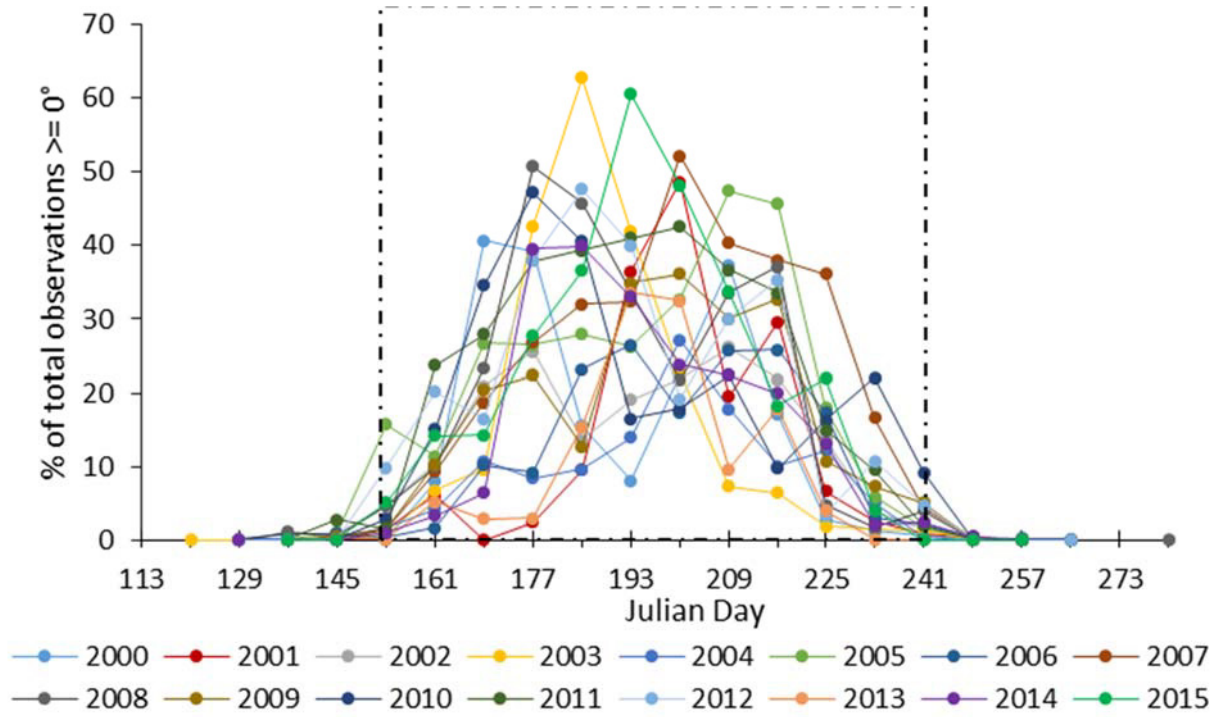


Figure 2-S5: Percentage of observations with $LST \geq 0^{\circ}\text{C}$ for each 8 day observation period from day 113 – 281 for 2000 to 2015. Percentage is calculated with respect to total number of pixels with LST observations for each date. The dotted lines delineate the study period (June-August) which spans day 153 – 241.

Table 2 - S6: Percentage of observations with a value $\geq 0^{\circ}\text{C}$. Data have not been filtered to remove pixels with LST error $>2^{\circ}\text{C}$. The number of available observations varies for each date.

	DOY	2000	2001	2002	2003	2004	2005	2006	2007	2008	2009	2010	2011	2012	2013	2014		
Melt onset	113																	
	121				<0.1													
	129			<0.1	<0.1	0.1		0.1		<0.1			<0.1		<0.1			
	137	<0.1	<0.1		<0.1	0.1	0.1	0.7		1.1	<0.1	<0.1	0.1	<0.1		<0.1		
	145		0.4	0.8	0.1	0.2	1.0	0.9	<0.1	0.5	0.6	0.1	2.7	0.2	0.1	<0.1	0.1	
June-August	153	0.1	1.5	4.8	0.7	1.6	15.8	0.3	1.6	4.6	1.5	2.8	1.5	9.9	0.2	1.0	5.0	
	161	8.0	6.1	10.4	6.8	4.3	11.4	1.7	9.4	9.9	10.3	15.1	23.7	20.2	5.2	3.3	14.2	
	169	40.7	DNE	21.0	9.6	10.7	26.7	10.1	18.7	23.4	20.4	34.6	27.9	16.5	2.9	6.4	14.3	
	177	39.1	2.4	25.6	42.7	8.4	26.5	9.1	26.8	50.8	22.4	47.2	38.0	38.0	3.0	39.5	27.7	
	185	15.5	9.5	13.6	62.8	9.7	27.9	23.1	32.1	45.7	12.7	40.6	39.4	47.6	15.4	39.9	36.6	
	193	8.1	36.5	19.1	41.9	13.9	26.2	26.5	32.4	33.6	34.9	16.6	41.1	40.0	33.6	33.0	60.5	
	201	22.6	48.7	21.8	22.9	27.2	32.7	17.4	52.2	21.8	36.1	17.8	42.6	19.2	32.5	23.9	48.3	
	209	37.2	19.5	26.2	7.3	17.8	47.4	25.7	40.3	33.6	30.0	22.3	36.7	30.0	9.7	22.4	33.7	
	217	17.1	29.6	21.9	6.4	10.1	45.7	25.8	38.0	37.1	32.7	9.8	33.6	35.4	17.8	19.9	18.3	
	225	2.7	6.7	13.8	1.9	12.2	17.9	17.3	36.2	4.7	10.8	16.3	15.0	3.4	4.0	13.2	22.0	
	233	1.2	2.6	3.9	1.5	5.1	5.9	3.0	16.6	1.6	7.4	22.0	9.5	10.7	0.1	2.1	4.1	
	241	0.5	0.8	1.4	1.2	0.3	1.7	2.1	4.3	4.0	5.1	9.2	2.0	4.8	<0.1	2.4	<0.1	
	249	0.1	0.4	0.1	0.2	<0.1	<0.1	0.4	0.3	0.1	0.2	0.2	0.1	0.2	<0.1	0.5	<0.1	
	Freeze-up	257	<0.1	<0.1	0.1	<0.1	<0.1	<0.1	0.2	<0.1	<0.1	<0.1	<0.1	<0.1	<0.1	<0.1	<0.1	<0.1
		265			0.0				0.1		<0.1		<0.1		<0.1			
273																		
281										<0.1								

2.6.3: Additional supporting material

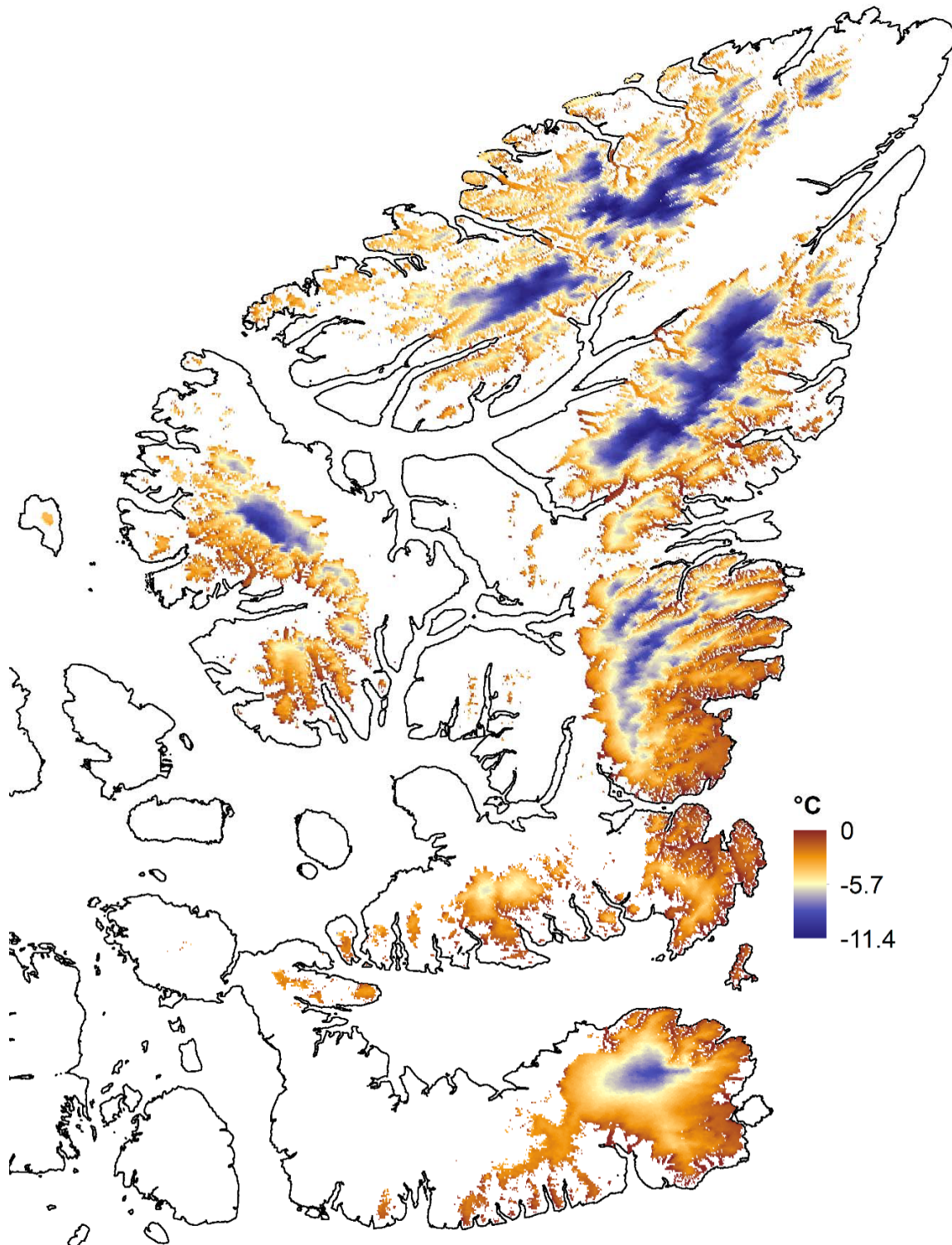


Figure 2-S7: 16-year average clear-sky mean summer land surface temperature (°C) for glaciated regions of the Queen Elizabeth Islands for the period 2000-2015.

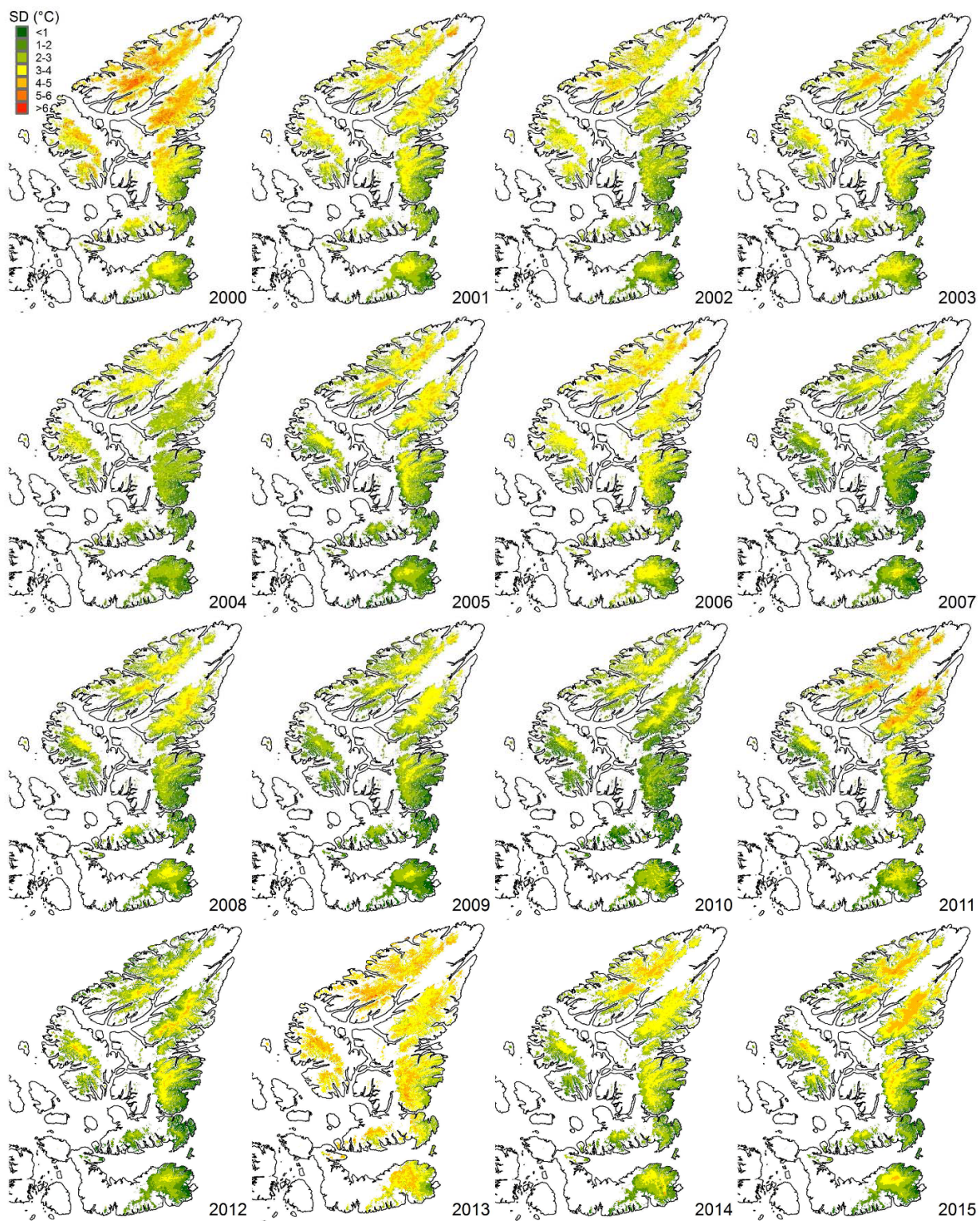


Figure 2-S8: Standard deviation of the mean summer clear-sky land surface temperature (°C) for the Queen Elizabeth Islands.

Table 2-S9: Location of sites used to calculate summer (June-August) 700 hPa air temperature for 2000-2015 from the NCEP/NCAR R1 Reanalysis. See *Sharp et al.* [2011] (Section 2.3.3).

Region	Latitude (N)	Longitude (E)
N. Ellesmere Island	80.6 - 83.1	267.7 - 294.1
Axel Heiberg Island	78.4 - 80.6	265.5 - 271.5
Agassiz Ice Cap	79.2 - 81.1	278.9 - 290.4
Prince of Wales Icefield	77.3 - 79.1	278.0 - 284.9
Sydkap	76.5 - 77.1	270.7 - 275.8
Manson Icefield	76.2 - 77.2	278.7 - 282.1
Devon Ice Cap	74.5 - 75.8	273.4 - 280.3

Table 2-S10: Difference between 2005-2009 and 2000-2004 average mean summer LST calculated in this study using all QEI glaciated pixels and by *Sharp et al.* [2011] using 23 km x 23 km cell blocks (Section 2.4).

	Agassiz IC	Axel Heiberg I	Devon & Coburg I	Manson IF	Northwest Ellesmere I	Prince of Wales IF	Sydkap IC
Difference in mean summer LST (°C): 2005-2009 minus 2000-2004 from <i>Sharp et al.</i> [2011]	1.29	1.82	0.88	1.19	0.98	1.32	1.37
Difference in mean summer LST (°C): 2005-2009 minus 2000-2004 from current study	1.08	1.47	0.70	0.70	1.25	0.99	1.17
Comparison of LST difference (°C) calculated from the current study and from <i>Sharp et al.</i> [2011]	-0.21	-0.35	-0.18	-0.49	0.27	-0.33	-0.20

2.7 References

- Ackerman, S. A., K. I. Strabala, P. W. Menzel, R. A. Frey, C. C. Moeller, and L. E. Gumley (1998), Discriminating clear sky from clouds with MODIS, *J. Geophys. Res.*, *103*(D24), 32141–32157, doi:10.1029/1998JD200032.
- Alt, B. T. (1978), Synoptic climate controls of mass-balance variations on Devon Island Ice Cap, *Arct. Alp. Res.*, *10*(1), 61–80, doi:10.2307/1550657.

- Alt, B. T. (1987), Developing synoptic analogs for extreme mass balance conditions on Queen Elizabeth Island ice caps, *Journal of Applied Climate*, 26(12), 1605-1623, doi: 10.1175/1520-0450(1987)026<1605:DSAFEM>2.0.CO;2.
- Arendt, A., et al. (2012), Randolph Glacier Inventory Vers. 3.0: a dataset of Global Glacier Outlines. Global Land Ice Measurements from Space, Boulder, CO. Digital media: http://www.glims.org/RGI/rgi32_dl.html.
- Bezeau, P., M. Sharp, D. Burgess, and G. Gascon (2013), Firn profile changes in response to extreme 21st-century melting at Devon Ice Cap, Nunavut, Canada, *J. Glaciol.*, 59(217), 981-991, doi:10.3189/2013JoG12J208.
- Bezeau, P., M. Sharp, and G. Gascon (2015), Variability in summer anticyclonic circulation over the Canadian Arctic Archipelago and west Greenland in the late 20th/early 21st centuries and its effects on glacier mass balance, *Int. J. Climatol.*, 35(4), 540-557, doi:10.1002/joc.4000.
- Box, J. E., X. Fetwweis, J. C. Stroeve, M. Tedesco, D.K. Hall, and K. Steffen (2012), Greenland ice sheet albedo feedback: thermodynamics and atmospheric drivers, *Cryosphere*, 6(4), 821-839, doi: 10.5194/tc-6-821-2012.
- Braithwaite, R. J. (2005), Mass balance characteristics of arctic glaciers, *Ann. Glaciol.*, 42, 225-229, doi: 10.3189/17275640578182899.
- Colbeck, S. C. (1982), An overview of seasonal snow metamorphism, *Rev. Geophys.*, 20(1), 45-61, doi: 10.1029/RG020i001p00045.
- Cuffey, K. M. and W. Paterson (2010), *The physics of glaciers*, 4th edn. Butterworth-Heinemann, Oxford.
- Flanner, M. G., C. S. Zender, J. T. Randerson, and P. J. Rasch PJ (2007), Present-day climate forcing and response from black carbon in snow, *J. Geophys. Res.*, 112, D11202, doi:10.1029/2006JD008003.
- Gardner, A. S., and M. Sharp (2007), Influence of the Arctic circumpolar vortex on the mass balance of Canadian high Arctic glaciers, *J. Climate*, 20(18), 4586-4598, doi: 10.1175/JCLI4268.1.

Gardner, A. S., G. Moholdt, B. Wouters, G. J. Wolken, D. O. Burgess, M. J. Sharp, J. G. Cogley, C. Braun, and C. Labine (2011), Sharply increased mass loss from glaciers and ice caps in the Canadian Arctic Archipelago, *Nature*, 473(7347), 357-360, doi:10.1038/nature10089.

Gardner, A. S., et al. (2013), A reconciled estimate of glacier contributions to sea level rise: 2003 to 2009, *Science*, 340(6134), 852-857, doi:10.1126/science.1234532.

Gascon, G., M. Sharp, and A. Bush (2013a), Changes in melt season characteristics on Devon Ice Cap, Canada, and their association with the Arctic atmospheric circulation, *Ann. Glaciol.*, 54, 101–110, doi:10.3189/2013AoG63A601.

Gascon, G., Sharp M., Burgess D., Bezeau P. and A. B. G. Bush (2013b), Changes in accumulation-area firn stratigraphy and meltwater flow during a period of climate warming: Devon Ice Cap, Nunavut, Canada, *J. Geophys. Res. Earth Surf.*, 118(4), 2380-2391, doi:10.1002/2013JF002838.

Hall D. K., R. S. Williams Jr, K. A. Casey, N. E. DiGirolamo, and Z. Wan (2006), Satellite-derived, melt-season surface temperature of the Greenland Ice Sheet (2000–2005) and its relationship to mass balance, *Geophys. Res. Lett.*, 33(11), L11501, doi:10.1029/2006GL026444.

Hall, D. K. J. E. Box, K. A. Casey, S. J. Hook, C. A. Shuman, and K. Steffen (2008a) Comparison of satellite-derived and in-situ observations of ice and snow surface temperatures over Greenland, *Remote Sens. Environ.*, 112(10), 3739-3749, doi: 10.1016/j.rse.2008.05.007.

Hall, D. K., R. S. Williams, S. B. Luthcke, and N. E. DiGirolamo (2008b), Greenland ice sheet surface temperature, melt and mass loss: 2000–2006, *J. Glaciol.*, 54(184), 81–93, doi:10.3189/002214308784409170.

Hall, D. K., J. C. Comiso, N. E. DiGirolamo, C. A. Shuman, J. R. Key, and L. S. Koenig (2012), A satellite-derived climate-quality data record of the clear-sky surface temperature of the Greenland ice sheet, *J. Clim.*, 25, 4785-4798, doi: 10.1175/JCLI-D-11-00365.1.

Hall, D. K., J. C. Comiso, N. E. DiGirolamo, C. A. Shuman, J. E. Box and L. S. Koenig (2013), Variability in the surface temperature and melt extent of the Greenland ice sheet from MODIS, *Geophys. Res. Lett.*, 40(10), 2114-2120, (doi:10.1002/grl.50240).

- Kalnay, E., et al. (1996), The NCEP/NCAR 40 year reanalysis project, *Bull. Am. Meteorol. Soc.*, 77(3), 437–471, doi:10.1175/1520-0477(1996)077<0437:TNYRP>2.0.CO;2.
- King, M. D., S. Platnick, P. Yang, G. T. Arnold, M. A. Gray, J. C. Ridei, S. A. Ackerman, and K. N. Liu (2004), Remote Sensing of Liquid Water and Ice Cloud Optical Thickness and Effective Radius in the Arctic: Application of Airborne Multispectral MAS Data, *J. Atmos. Ocean. Technol.*, 21(6), 857–875, doi:10.1175/1520-0426(2004)021<0857:RSOLWA>2.0.CO;2.
- Koenig, L. S., and D. K. Hall (2010), Comparison of satellite, thermochron and station temperatures at Summit, Greenland, during the winter of 2008/09, *J. Glaciol.*, 56(198), 735-741 (doi: 10.3189/002214310793146269).
- Koerner, R. M. (1977), Devon Island ice cap: core stratigraphy and paleoclimate, *Science*, 196(4285), 15-18, doi: 10.1126/science.196.4285.15.
- Koerner, R. M. (1979), Accumulation, ablation, and oxygen isotope variations on the Queen Elizabeth Islands ice caps, Canada, *J. Glaciol.*, 22(86), 25-41.
- Koerner, R. M. (2005), Mass balance of glaciers in the Queen Elizabeth Islands, Nunavut, Canada, *Ann. Glaciol.*, 42, 417–423, doi:10.3189/172756405781813122.
- Land Processes Distributed Active Archive Center (LP DAAC), MODIS Level 3 Global 1 km Grid SIN Version 5. NASA EOSDIS Land Processes DAAC, USGS Earth Resources Observation and Science (EROS) Center, Sioux Falls, South Dakota (<https://lpdaac.usgs.gov>), accessed Spetember 2014 - October 2015 at <http://e4ftl01.cr.usgs.gov>.
- Lenaerts, J. T. M., J. H. van Angelen, M. R. van den Broeke, A. S. Gardner, B. Wouters, and E. van Meijgaard (2013), Irreversible mass loss of Canadian Arctic Archipelago glaciers, *Geophys. Res. Lett.*, 40(5), 870–874, doi:10.1002/grl.50214.
- Machguth H., M. MacFerrin, D. van As, J. E. Box, C. Charalampidis, W. Colgan, R. S. Fausto, H. A. J. Meijer, E. Mosley-Thompson, and R. S. W. van de Wal (2016), Greenland meltwater storage in firm limited by near-surface ice formation, *Nat. Clim. Change*, 6, 390-393, doi: 10.1038/NCLIMATE2899.
- Pfeffer, W. T., and N. F. Humphrey (1998), Formation of ice layers by infiltration and refreezing of meltwater, *Ann. Glaciol.*, 26, 83-91.

Pfeffer, W. T. et al. (2014), The Randolph Glacier Inventory: a globally complete inventory of glaciers, *J. Glaciol.*, 60(221), 537-552, doi:10.3189/2014JoG13J176.

Radić V., A. Bliss, A. C. Beedlow, R. Hock, E. Miles, J. G. and Cogley (2014), Regional and global projections of twenty-first century glacier mass change in response to climate scenarios from global climate models, *Clim.. Dyn.*, 42(1-2), 37-58, doi:10.1007/s00382-013-1719-7.

Rajewicz, J., and S. J. Marshall SJ (2014), Variability and trends in anticyclonic circulation over the Greenland ice sheet, 1948-2013, *Geophys. Res. Lett.*, 41(8), 2842-2850, doi:10.1002/2014GL059255.

Sharp, M., D. O. Burgess, J. G. Cogley, M. Ecclestone, C. Labine, and G. J. Wolken (2011), Extreme melt on Canada's Arctic ice caps in the 21st century, *Geophys. Res. Lett.*, 38(11), L11501, doi:10.1029/2011GL047381.

Sharp, M., et al. (2015) [Arctic] Glaciers and ice caps (outside Greenland [in "State of the Climate 2014"]], *Bull. Am. Meteorol. Soc.*, 96(7), 135-137.

Shuman C. A., D. K. Hall, N. E. DiGirolamo, T. K. Mefford, and M. J. Schnaubelt (2014), Comparison of near-surface air temperatures and MODIS ice-surface temperatures at Summit, Greenland (2008-13), *J. Appl. Meteor. Climatol.*, 53(9), 2171 – 2180, doi:10.1175/JAMC-D-14-0023.1.

Strabala, K. I., S. A. Ackerman, and W. P. Menzel (1994), Cloud Properties inferred from 8–12- μm Data, *J. Appl. Meteor.*, 33(2), 212–229, doi:10.1175/15200450(1994)033<0212:CPIFD>2.0.CO;2.

Wan Z., and Z. L. Li (1997), A physical-based algorithm for retrieving land-surface emissivity and temperature from EOS/MOSI data, *IEE Transactions on Geoscience and Remote Sensing*, 35(4), 980-996.

Wan, Z., Y. Zhang, Q. Zhang, and Z. L. Li (2002), Validation of the land-surface temperature products retrieved from Terra Moderate Resolution Imaging Spectroradiometer data, *Remote Sens. Environ.*, 83(1-2), 163–180, doi:10.1016/S0034-4257(02)00093-7.

Wan, Z. M. (2008), New refinements and validation of the MODIS Land-Surface Temperature/Emissivity products, *Remote Sens. Environ.*, 112(1), 59–74, doi:10.1016/j.rse.2006.06.026.

Wang L., M. Sharp, B. Rivard, S. Marshall, and D. Burgess (2005), Melt season duration on Canadian Arctic ice caps, 2000-2004, *Geophys. Res. Lett.*, 32(19), L19502, doi: 10.1029/2005GL023962.

Wiscombe, W. J., and S. G. Warren (1980), A model for the spectral albedo of snow. I: Pure snow, *J. Atmos. Sci.*, 37(12), 2712-2732, doi: 10.1175.1520-0469(1980)037<2712:AMFTSA>2.0.CO;2.

Wolken G. J., M. Sharp, and L. Wang (2009), Snow and ice facies variability and ice layer formation on Canadian Arctic ice caps, 1999– 2005, *J. Geophys. Res.*, 114(F3), F03011, doi:10.1029/2008JF001173.

World Meteorological Organization (2015), Provisional Statement on the Status of Global Climate in 2011-2015, Press release No 13, 25 November 2015, <https://www.wmo.int>.

Zdanowicz, C., A. Smetny-Sowa, D. Fisher, N. Schaffer, L. Copland, J. Eley, and F. Dupont (2012), Summer melt rates on Penny Ice Cap, Baffin Island: Past and recent trends and implications for regional climate, *J. Geophys. Res.*, 117(F2), F02006, doi:10.1029/2011JF002248.

Chapter 3

Glacier albedo change in the Canadian High Arctic (2001-2015) and its relationship to recent climate warming

3.0 Abstract

Inter-annual variations and longer-term trends in annual glacier mass balance in Canada's Queen Elizabeth Islands (QEI) are largely attributable to changes in summer melt. The period 2005-2012 included some of the warmest summers in the region since at least the 1950s. The largest source of melt energy in the QEI in summer is net shortwave radiation, which is modulated by changes in glacier surface albedo. We used measurements from the Moderate Resolution Imaging Spectroradiometer (MODIS) sensors to investigate large scale spatial patterns and temporal variability in the summer surface albedo of QEI glaciers south of 80°N and their relationship to observed changes in glacier surface temperature from 2001 to 2015. Mean summer black-sky shortwave broadband albedo (BSA) decreased by $0.0038 \pm 0.0037 \text{ yr}^{-1}$ over that period. The bulk of this decrease occurred from 2008 to 2012 when mean summer BSA was anomalously low. Albedo declines were greatest in the west of the QEI and at lower elevations on the ice caps. On average, mean summer glacier surface temperatures increased by 0.51°C from 2001 to 2015. Overall, the BSA is negatively correlated with glacier surface temperature over this period.

3.1 Introduction

The area covered by glaciers and ice caps in the Queen Elizabeth Islands (QEI), Arctic Canada, was ~104,000 km² in 2000 [Arendt *et al.*, 2012]. From 2000 to 2015, summer mean glacier surface

temperatures in this region increased at a rate of $0.06 \pm 0.04^\circ\text{C yr}^{-1}$, and 2005-2012 air temperatures were $> 1.0^\circ\text{C}$ warmer than the 1948-2015 mean [Mortimer *et al.*, 2016]. QEI summer air and surface temperatures are strongly correlated with the annual and summer glacier mass balances, which have become increasingly negative since at least 2003 [Gardner *et al.*, 2013; Lenaerts *et al.*, 2013; Sharp *et al.*, 2015]. Inter-annual variations and longer-term trends in annual glacier mass balance in the QEI are dominated by changes in summer melt [Koerner, 2005], and net shortwave radiation is the largest source of melt energy on the QEI ice caps [Gascon *et al.*, 2013]. Variability in net shortwave radiation is strongly modulated by changes in the surface albedo [van den Broeke *et al.*, 2011; Tedesco *et al.*, 2016], the ratio of outgoing to incoming solar radiation.

The high albedo of fresh snow declines naturally due to settling and grain growth [Warren, 1982]. This initial decrease in albedo raises the shortwave energy absorption, leading to warming and/or melt, and a further lowering of the surface albedo. Warmer temperatures and increased snowpack water content further accelerate grain growth, leading to more rapid albedo declines that enhance surface warming and/or melt [Wiscombe and Warren, 1980; Colbeck, 1982]. A positive snow/ice albedo feedback has been linked to accelerated high-latitude warming, and is increasingly recognized as an important factor in explaining recent increases in rates of mass loss from the Greenland Ice Sheet [Tedesco *et al.*, 2016]. On ice caps and glaciers, enhanced summer warming and increased melt can lead to earlier and more widespread removal of the previous winter's snowpack, exposing underlying low-albedo glacier ice. Albedo decreases can also be caused by aerosol deposition [Warren and Wiscombe, 1980], enhanced biological activity on glacier surfaces [Fountain *et al.*, 2004], and accelerated release of impurities from snow and ice, which become concentrated at the snow/ice surface [Clarke and Noone, 1985; Conway *et al.*, 1996; Flanner *et al.*, 2007; Doherty *et al.*, 2010]. Given the observed increases in air and glacier surface

temperatures across the QEI [Mortimer *et al.*, 2016] we anticipate a reduction in the surface albedo in this region, unless warming is also accompanied by an increase in solid precipitation that is large enough to raise the surface albedo. The expected albedo reduction has, however, yet to be observed and quantified.

Decadal scale declines (~ 0.02 decade⁻¹) in the surface albedo of the Greenland Ice Sheet, which lies immediately to the east of the QEI, have been simulated using regional climate models, and documented using remote sensing data validated by in situ measurements [e.g. Stroeve *et al.*, 2005, 2013; Box *et al.*, 2012; Alexander *et al.*, 2014; Tedesco *et al.*, 2016]. Although global assessments of land surface albedo [e.g. He *et al.*, 2014] have included the QEI, these analyses were extremely broad in nature and the detailed spatial pattern of glacier albedo change and its variation over time are unknown. Between 2000 and 2015, measured increases in summer temperatures in the QEI were greatest in the north and west of the region [Sharp *et al.*, 2011; Mortimer *et al.*, 2016] but we do not know whether there is a similar spatial pattern in the albedo record. Field-based measurements provide information about the surface albedo at specific locations, but there are no long-term spatially distributed in-situ records of the surface radiation budget of glaciers and ice caps in the QEI.

Remote sensing methods permit evaluation of the surface albedo and its spatial and temporal variability at both the ice cap and regional scales. Here, we use measurements of surface albedo from the Moderate Resolution Imaging Spectroradiometer (MODIS) sensors to present the first near-complete picture of variations in the summer surface albedo of QEI glaciers and ice caps from 2001 to 2015. We assess the spatial and temporal variability in summer albedo and quantify the rate of albedo change across the QEI. We compare our 15-year summer albedo record with the summer mean land surface temperature (LST) record for 2001 to 2015 to investigate the

relationship between surface temperature and albedo changes, and to explore its spatial and temporal variability.

3.2 Data and Methods

3.2.1 MODIS albedo (MCD43A3)

Observations from the Moderate Resolution Imaging Spectroradiometers (MODIS), aboard the Terra (2000 to present) and Aqua (2002 to present) satellites, are used to assess the spatial and temporal evolution of the surface albedo over QEI glaciers and ice caps in summer (June-August). We use the MODIS combined Albedo 16-Day L3 Global 500 m gridded product (MCD43A3) Version 05 (<https://lpdaac.usgs.gov/>), which provides both white-sky (bihemispherical reflectance under isotropic conditions) and black-sky (directional hemispherical reflectance) shortwave broadband surface albedo [*Strahler et al.*, 1999; *Schaaf et al.*, 2011a and references therein]. MCD43A3 albedo is calculated every eight days for local solar noon from atmospherically corrected surface reflectances collected from both the Terra and Aqua satellites over a 16-day period [*Lutch et al.*, 2000; *Schaaf et al.*, 2002; *Gao et al.*, 2005]. A semi-empirical Bidirectional Reflectance Distribution Function (BRDF) model, which describes the surface scattering/reflectance of a target as a function of illumination, is used to estimate surface albedo from directional surface reflectance information recorded by the MODIS sensors [*Schaaf et al.*, 2002, 2011a, 2011b; *Jin et al.*, 2003; *Salomon et al.*, 2006]. MCD43A3 white- and black-sky albedos are estimated from the Level 2 surface reflectance products MOD09 and MYD09 for seven visible and near-infrared bands (spanning 0.4 to 2.4 μm) and three broad bands (shortwave (0.3-5.0 μm), visible (0.3-0.7 μm) and near infrared (0.7-5.0 μm)) in one of two ways. If sufficient (>7)

multi-date cloud-free observations with good angular sampling are acquired during a 16 day period to fully characterize the viewing/illumination geometry, a high quality full-inversion is run using a semi-empirical RossThick LiSparse Reciprocal (RTSLR) kernel-driven BRDF model [*Wanner et al.*, 1997; *Lutch et al.*, 2000; *Schaaf et al.*, 2002, 2011b]. If insufficient observations (<7) are available, then a lower quality magnitude inversion, which relies on a priori knowledge to scale an archetypal BRDF, is used to estimate the surface albedo [*Strugnell and Lutch*, 2001; *Schaaf et al.*, 2002; *Jin et al.*, 2003; *Liu et al.*, 2009]. Data quality flags, provided in the MCD43A2 data quality assessment product, indicate whether albedo values [for each pixel] were obtained from the full or magnitude inversions [*Schaaf et al.*, 2002, 2011a, 2011b].

MODIS surface reflectance products have a stated accuracy of 0.05 for solar zenith angles <75° [*Vermote et al.*, 2011; *Wang et al.*, 2012]. Extensive ground-truthing over high latitude snow and ice surfaces [e.g. *Greuell et al.*, 2007; *Box et al.*, 2012; *Alexander et al.*, 2014] has found the full-inversion data to be a good representation of the true surface albedo (RMSE within ± 0.04 of in-situ measurements, *Stroeve et al.* [2005]) for solar zenith angles <75°. Magnitude inversions produce lower quality albedo estimates than the full-inversion method but these data have proven to be sufficiently accurate to detect and monitor changes in surface albedo from one year to the next [*Schaaf et al.*, 2011b; *Stroeve et al.*, 2013]. The principal uncertainties in MODIS-derived surface albedos arise from cloud contamination and sensor degradation. Similarity in the spectral signatures of snow, ice and thin cloud makes it difficult to discriminate between these surface types [*Strabala et al.*, 1994; *King et al.*, 2004], and the conservative MODIS cloud mask tends to detect more clouds than actually occur over snow and ice [*Ackerman et al.*, 1998; *Hall et al.*, 2008]. Thus, the absence of observations for periods when clouds are present and the removal of data for periods when clouds are detected may introduce variability in the albedo record that is not representative

of true physical change. Despite this, the MCD43A3 albedo product has been found to provide a reasonable representation of the seasonal albedo cycle over glaciers and ice caps [e.g. *Stroeve et al.*, 2006]. Hence, in the absence of long-term ground measurements of glacier surface albedo in the QEI, we made the assumption that this is also the case in this region.

3.2.1.1 MODIS sensor degradation

The MODIS sensors are operating several years beyond their expected lifetimes and some of the instruments are degrading [*Wang et al.*, 2012]. Systematic (decreasing) temporal trends are present in the visible and NIR (bands 1-7) of the MODIS Version 05 data [*Lyapustin et al.*, 2014]. Calibration degradation effects, which are largely confined to the Terra sensor, are greatest in the blue band (B3) and decrease with increasing wavelength [*Lyapustin et al.*, 2014]. Over time, uncorrected sensor degradation gives rise to decreasing measured surface radiances, which may result in MODIS-derived albedo declines that are anomalous with respect to the true physical change. Decreasing global albedo trends attributed to un-corrected Terra sensor degradation have been quantified for several MODIS Version 05 derived products (Aerosol optical depth (AOD, ~27%), cloud optical thickness (COT, ~17%), and the Normalized Difference Vegetation Index (NDVI, ~0.01) [*Lyapustin et al.*, 2014 and references therein]), however, these assessments did not consider the MCD43A3 albedo product (or the MOD09A1/MYD09A1 daily reflectance products).

Previous work comparing MODIS-derived Version 05 albedo trends with in situ measurements over the Greenland Ice Sheet [e.g. *Box et al.*, 2012, *Stroeve et al.*, 2013; *Alexander et al.*, 2014; *Tedesco et al.*, 2016] largely discounted the notion that un-corrected Terra sensor degradation produced artificial declining albedo trends. However, investigation of surface albedo over the Greenland Ice Sheet's dry snow zone (2001-2013) concluded that much of the observed decline in broadband albedo from Terra-only data did result from sensor degradation [*Polashenski et al.*,

2015]. For the most part, the magnitude of the sensor-related albedo decline was smaller than the nominal uncertainty of the MODIS surface reflectance products [Vermotte *et al.*, 2011]. Terra sensor degradation is corrected for in the MODIS Version 06 data, which were not available at the time of writing. Recent analysis of surface albedo over the Greenland dry snow zone using these data for the 2001-2016 period did not find any significant trends in the visible-wavelength albedo [Casey *et al.*, 2016]. We note, however, there is no dry snow zone in the QEI. Albedo declines have also been measured over the Greenland Ice Sheet's wet snow zone using both the Version 05 and Version 06 MODIS data. The magnitude of the (2001-2016) albedo decrease is smaller for the Version 06 data and these smaller albedo declines (from the Version 06 data) are thought to be physically real [Casey *et al.*, 2016].

The combined MCD43A3 albedo dataset used here includes observations from both the Terra and Aqua sensors, so it is affected by degradation of the Terra sensor but the magnitude [of this effect] is smaller than it would be if Terra-only data were used. Polashenski *et al.* [2015] reported a <0.035 decade⁻¹ difference in the albedo trends measured by the Terra and Aqua sensors for a single MCD43A3 test pixel. Stroeve *et al.* [2013] presented the Terra-only (MOD), Aqua-only (MYD), and combined (MCD) albedo trends for a larger (50 km x 50 km) section of the Greenland Ice Sheet. The Terra-only declining albedo trend was 0.006 decade⁻¹ larger than the Aqua-only trend but it was only 0.002 decade⁻¹ larger than the combined MCD43A3 albedo trend (Table 1 in Stroeve *et al.* [2013]). Alexander *et al.* [2014] found good agreement between the summer (JJA) MCD43A3 black-sky shortwave broadband albedo and in situ albedo records from the Greenland Ice Sheet for 2000 to 2012. As reliable, long-term, spatially distributed, in situ albedo records do not exist for the QEI ice caps, a comparison of the MCD43A3 records with ground observations is not possible, and this is a limitation of this study.

Although it is generally accepted that Terra sensor degradation has resulted in anomalously large albedo declines over glaciated regions, the magnitude the artificial albedo declines measured over glaciers and ice sheets using the Version 05 data remains largely unknown. The aim of this study is to assess the spatial patterns of surface albedo and surface albedo change across the QEI. The MCD43A3 data have been shown to produce spatial and temporal patterns of albedo change that are consistent with both in situ measured and modelled data for the Greenland Ice Sheet [e.g. *Stroeve et al.*, 2013], which lies immediately east of the QEI. This gives us confidence in the spatial patterns of MODIS-derived surface albedo change presented here.

3.2.1.2 MCD43A3 data processing

Summer (1-2 June (day 153) to 28-29 August (day 241)) MODIS MCD43A3 and MCD43A2 Version 05 data for MODIS tiles h17v00, h16v00, h16v01, and h15v01 for the period 2001-2015 were obtained from the NASA/USGS Land Processes Distributed Active Archive Center (<http://lpdaac.usgs.gov/> accessed September 2014 to October 2015). Daytime clear-sky white- and black-sky shortwave broadband albedo data (MCD43A3) and accompanying quality assessment information (MCD43A2) were extracted from the hierarchical data format files and re-projected from the standard MODIS sinusoidal projection to a North America Albers Equal Area projection, WGS84 datum, 500 m resolution, using the MODIS re-projection tool version 4.1 (https://lpdaac.usgs.gov/tools/modis_reprojection_tool). The maximum summer (June-August) solar zenith angle over our study area (74°) was below the product's stated accuracy ($<75^\circ$), so no additional filtering was performed to remove data with high solar zenith angles. As the MCD43A3 albedo data for 2000 were extremely poor, we excluded them from our analysis. In that year, the difference between the white- and black-sky albedos was, on average 0.138, while in all other years the mean difference was between 0.010 and 0.007.

Additional processing was required for tiles h16v00 and h17v00, which cover the area north of 80°N, for the period 2000-2008. Parameter header files for these tiles, which are needed for data extraction and re-projection, were missing for this period, so new parameter header files were written for these tiles from existing data using the USGS's Land Data Products Evaluation (LDOPE) Facility's toolset cp_proj_param tool release 1.4 (LP DAAC 2004, <https://lpdaac.usgs.gov/tools>). Data for these tiles were not initially included in the regular MCD43A3 processing routine, and albedo values were processed at a later date using the lower quality Level 2 Gridded (L2G) data instead of the L2G-lite data as input [Stroeve *et al.*, 2013]. We found these data to be of considerably lower quality than both data for 2009 onward and data for areas south of 80°N (2001-2015). Specifically, the change in data processing method resulted in a distinct artefact, which is seen as a break in the data, where mean summer albedo is measurably higher for tiles that underwent L2G processing than it is for tiles subjected to L2G-lite processing. The general patterns and trends in the data from north and south of 80°N appear to be similar for the period 2001-2008. However, the notable difference in absolute albedo values prohibits a homogeneous analysis of the complete QEI albedo dataset for the period prior to 2009. For these reasons, we restricted our analysis to regions south of 80°N (tiles h15v01 and h16v01; total glacial area ~60 581 km²).

The white- and black sky albedos (representing completely diffuse and completely direct illumination, respectively) represent extreme estimates of the actual (blue-sky) bi-hemispheric surface albedo. If sufficient high-quality full-inversion MCD43A3 retrievals are available, it is possible to estimate the true blue-sky albedo as a function of the white- and black-sky albedos, the aerosol optical depth, and the cloud cover fraction [Román *et al.*, 2010]. In any given year, however, full inversion retrievals were available for <2% of all pixels in our study region, so both

full and magnitude inversions are used in our analysis. Given the limited number of high quality full-inversion retrievals over the QEI between 2001 and 2015 we chose not to interpolate the blue-sky albedo. Instead, we analyzed both the white- and black-sky albedos. The white-sky albedo was, on average, 0.008 lower than the black-sky albedo. To avoid redundancy, only results for the black-sky albedo (BSA), which are fully consistent with those obtained using the white-sky albedo (WSA), are presented here. The BSA was selected because our analysis focuses on albedo retrieved under clear-sky conditions. This approach is consistent with previous work using MCD43A3 data [e.g. *Alexander et al.*, 2014; *Tedesco et al.*, 2016].

3.2.2 MODIS LST (MOD11A2)

The Eight-Day L3 Global Land Surface Temperature and Emissivity product (MOD11A2) Version 05, which has been found to be a reasonable proxy for the duration and/or intensity of summer melting in the QEI [*Sharp et al.*, 2011; *Mortimer et al.*, 2016], was used to investigate the relationship between surface temperature and albedo. MOD11A2 daytime and night-time LSTs are computed from MODIS channels 31 (11 μm) and 32 (12 μm) using a split-window technique and all available daytime clear-sky scenes from the Terra satellite for sequential 8-day periods [*Wan et al.*, 2002]. These data have a spatial resolution of 1 km and nominal product accuracy of $\pm 1^\circ\text{C}$ but the accuracy can be as low as $\pm 2^\circ\text{C}$ over snow and ice surfaces [*Hall et al.*, 2008a; *Koenig and Hall*, 2010]. Pixels for which the average LST error (QC_Day LST error flag) exceeded 2°C were removed from the analysis and any remaining pixels having a temperature $>0^\circ\text{C}$ were assigned a temperature of 0°C [e.g. *Hall et al.*, 2008b; *Mortimer et al.*, 2016]. Uncertainties in the MOD11A2 LSTs arise mainly from cloud contamination [*Box et al.*, 2012; *Hall et al.*, 2012] and the removal of observations when clouds are detected [*Ackerman et al.*, 1998; *Hall et al.*, 2008a]. Variability in the number of clear-sky days within each observation

period and from one year to the next was not found to introduce significant variability in the MODIS-derived LST relative to the true surface temperature in the QEI [see *Mortimer et al.*, 2016]. MOD11A2 data were downloaded from (<https://lpdaac.usgs.gov/>, accessed September 2014 to October 2015) and re-projected to a North America Albers Equal Area projection, WGS84 datum, 1 km resolution.

3.2.3 Mean summer BSA and LST

QEI annual precipitation is low ($<400 \text{ mm yr}^{-1}$) and varies little from one year to the next. In contrast, the annual temperature range is large ($> 40^{\circ}\text{C}$) [*Braithwaite*, 2005]. Inter-annual variability in QEI annual mass balance is dominated by changes in the summer mass balance [*Koerner*, 2005], which, in turn is strongly correlated with summer air temperature [*Sharp et al.*, 2011]. Spatial and temporal patterns in BSA and LST were, therefore, evaluated for the summer months (June-August). For each year during the period 2001-2015, mean summer (JJA) BSA (Section 3.2.1) and LST (Section 3.2.2) were calculated for pixels having at least 7 of a possible 12 observations between 1-2 June (day 153) and 28-29 August (day 241). Mean summer BSA and LST anomalies were calculated on a pixel-by-pixel basis relative to the 2001-2015 mean for pixels having mean summer observations in 11 or more years. This constituted $\sim 83\%$ and $\sim 96\%$ of possible BSA and LST pixels, respectively. The rates of change in BSA and LST over the period 2001-2015 were determined from a linear regression of the 15 year records of mean summer LST and BSA. Consistent with the mean summer BSA and LST anomalies, regressions were computed on a pixel-by-pixel basis for all pixels having mean summer observations for 11 or more years.

To investigate the relationship between BSA and LST, linear correlations of the 15 year BSA (nearest neighbour resampling to 1 km x 1 km) and LST records were computed for pixels having LST and BSA observations in all years ($\sim 75\%$ of all possible pixels). To ensure that only data for

glaciated surfaces were retained, all BSA and LST outputs used in this analysis were clipped to the Randolph Glacier Inventory v3.2 region 32 Arctic Canada North reference polygons [Arendt *et al.*, 2012; Pfeffer *et al.*, 2014]. Surface elevations were obtained from the Canadian Digital Elevation Dataset (CDED) edition 3.0, scale 1:50 k, re-sampled to a 500 m resolution (Appendix I).

3.2.4 Minimum summer BSA

To investigate possible mechanisms causing albedo decline over different glacier surfaces, we used the minimum summer albedo to classify pixels according to surface type (i.e. bare ice or snow/firn). The albedo of bare ice ranges from ~ 0.2 to ~ 0.45 , but the albedo of debris-rich firn can be as low as ~ 0.30 [Cuffey and Paterson, 2010 Table 5.2]. Using a combination of visual comparison of the 2014 summer BSA data with Landsat 8 OLI imagery from 27-26 August 2014 and sensitivity analysis, we determined 0.3 to be an appropriate minimum summer BSA threshold to distinguish bare ice from firn and/or snow. For each year, if the minimum summer BSA was ≤ 0.3 , we assumed that bare ice was exposed at the surface at some point during that summer; however, the overlap between the albedos of ice and firn/snow may still result in misclassification of some pixels.

Pixels with a minimum summer BSA ≤ 0.3 in all 15 years, implying that bare ice was exposed at the surface at some point during each summer, were classified as bare ice (5% of pixels). Pixels having a minimum summer BSA > 0.3 in all 15 years, implying that bare glacier ice was never exposed at the surface during the summer and that the surface was always firn and/or snow-covered, were classified as firn (49% of pixels). Pixels having at least 1, but fewer than 15, minimum summer BSA observations ≤ 0.3 , which implied that bare ice was exposed in some, but not all, years; were placed in an intermediate category (46% of pixels). For each year, the average

QEI-wide minimum summer BSA was calculated for each category (bare ice, intermediate, firn). The mean rate of change in the minimum summer BSA over the 15 year record was computed from a linear regression of the annual minimum summer BSA record against time for all pixels having BSA observations in 11 or more years.

3.2.5 Climate model data

Outputs from regional climate models were used to identify forcings that could explain the spatial variability in the relationship between LST and BSA. Climate model outputs were used because field measurements of the surface radiation budget and precipitation are sparse (or non-existent) in the QEI. We used output from Canadian Fourth Generation Regional Climate Model (CanRCM4) from the Canadian Centre for Climate Modelling and Analysis (CCCma) [Flato *et al.*, 2000; Zadra *et al.*, 2008; von Salzen *et al.*, 2013]. This model is driven by the ERA-Interim Reanalysis for the period 1989-2009 and run at a 0.22° resolution (~25 km) for the Arctic Domain (<http://ec.gc.ca/ccmac-cccma>). Atmospheric parameters (surface upwelling and downwelling, shortwave and longwave radiation, near-surface air temperature, precipitation) were downloaded from CCCma (<http://www.cccma.ec.gc.ca/>, accessed February-April 2016), and summer (JJA) averages were calculated from the daily data for each year in the period 2001-2009. To permit comparison of BSA and LST with the climate model output, changes in mean summer BSA and LST were calculated for the 2001-2009 period (Figure 3-S2). We also considered using output from the CanRCM4 0.44° resolution (run up until 2015) and the Modèle Atmosphérique Régionale (MAR) version 3.2 but these model outputs were too coarse to discern spatial patterns in the surface radiation budget (including surface albedo) and precipitation at the ice cap scale. Further, in the case of MAR, available data covered only part of the QEI. The spatial resolution of the

CanRCM4 0.22° output provides broad spatial patterns of these variables across the QEI, but is too coarse to capture patterns related to the region's small-scale topography.

It is important to note, however, the CanRCM4 data are not directly comparable with the satellite-derived measurements of LST and albedo. The MODIS-derived LSTs [Wan *et al.*, 2002, 2008] relate to clear-sky conditions and are computed from 8 day averages (though data may not have existed for all 8 days [e.g. Box *et al.*, 2012; Hall *et al.*, 2012; Mortimer *et al.*, 2016, and references therein], but the mean summer near-surface air temperature data were calculated from daily averages of all-sky conditions. In addition, the near-surface air temperatures over pure ice and snow can exceed 0°C while the LST cannot. Further, the MCD43A3 BSA is calculated every 8 days from 16 days of multi-angular observations fitted to the BRDF model (Section 3.2.1, Schaaf *et al.* [2011a] and references therein), but the mean summer CanRCM4-derived albedo was computed from daily albedo estimates, and the CanRCM4 albedo parameterization underestimates albedo reductions resulting from snow grain metamorphism and light absorbing impurities [Namazi *et al.*, 2015]. The paucity of field measurements of surface energy balance and precipitation across the QEI prohibits validation of either the CanRCM4 model output or the MODIS-derived surface albedo data (which have a relatively high rate of data dropout, Section 3.6 Table 3-S1), and is a limitation of this study. For these reasons, the climate model outputs are only used to infer overall trends and to identify parameters that may explain some of the observed variability in the relationship between BSA and LST that could warrant further investigation when improved model and satellite data become available.

3.3 Results

3.3.1 Mean summer glacier albedo: 2001 to 2015

Annual maps of mean summer shortwave broadband BSA for 2001 to 2015 are presented for all QEI glaciers and ice caps south of 80°N (hereafter referred to simply as QEI) (Figure 3-2 and Tables 3-1 and 3-2). The QEI-wide mean summer BSA, averaged across all 15 years, was 0.545 ± 0.102 (mean \pm 1 standard deviation). The lowest QEI-wide mean summer BSA (0.482 ± 0.118) was recorded in 2011 while the highest (0.580 ± 0.097) was recorded in 2003 (Table 3-2). The 2010-2015 mean summer BSA was 0.047 lower than that during the first pentad (2001-2005). Low summer BSAs during the second half of the study period are consistent with high summer air and glacier surface temperature anomalies in the QEI from 2007 to 2015 [Mortimer *et al.*, 2016]. The mean summer BSA for the seven regions shown in Figure 3-1 was computed by averaging the mean summer BSA for all glaciated pixels within each region. Consistent with the QEI-wide mean summer BSA, the lowest mean summer BSA for each region occurred in 2011 (Table 3-2). The highest mean summer BSA was recorded in 2003 for all regions except Manson Icefield, where it was recorded in 2005 (Table 3-2).

In general, mean summer BSA is lower around the margins of the ice masses than in the higher elevation interior regions (Figure 3-2). Aggregating the 2001-2015 average mean summer BSA into 50 m elevation bins, we observe a linear rate of BSA increase with elevation (0.0082 per 50 m elevation bin, $r^2 = 0.98$). During years when the QEI-wide mean summer BSA was low (e.g. 2011), we observed a broad zone of low albedo values (< 0.4) around the margins of the major ice masses (Figure 3-2). Conversely, in years when the mean summer BSA was high (e.g. 2003), this zone was much less obvious. High data dropout (the QEI-wide mean dropout rate ranged from 11.4% (2001) to 19.4% (2009), Section 3.6 Table 3-S1), particularly on the summits of the Devon

Ice Cap, Sydkap Ice Cap, and the Axel Heiberg Island ice caps may produce a negative albedo bias for these regions since the albedo is typically greater at higher elevations.

3.3.2 BSA anomalies: 2001 to 2015

Mean summer BSA anomalies were computed on a pixel-by-pixel basis relative to the 2001-2015 mean (Section 3.2.3). Negative (positive) albedo anomalies indicate a larger (smaller) absorbed fraction of incoming shortwave radiation relative to the 15 year mean. QEI-wide and regional BSA anomalies were positive from 2001 to 2006 and negative from 2007 to 2012 (Figure 3-3 and Table 3-3). Positive BSA anomalies were observed in 2013 and 2014 while 2015 saw a return to negative anomalies. Consistent with the mean summer BSA, the most negative QEI-wide and regional BSA anomalies were recorded in 2011 while the most positive anomalies occurred in 2004, except on the Devon and Sydkap Ice Caps where the most positive BSA anomaly was recorded in 2003 (Table 3-3). In 2011 and 2012, when the QEI-wide mean summer BSA anomaly was strongly negative, > 90% of pixels had negative BSA anomalies. Conversely, in 2003 and 2004, when the QEI-wide mean summer BSA anomaly was strongly positive > 85% of pixels in the region had positive mean summer BSA anomalies.

The sign of the mean summer BSA anomaly varies both within and between regions (Figure 3-3). In 2007, when mean summer glacier surface temperatures (LST) were anomalously high [Mortimer *et al.*, 2016] (Section 3.4.1), mean summer BSA anomalies were negative along the margins of most ice masses but were positive at higher elevations, and the QEI-wide mean summer BSA anomaly was near zero (-0.0107 ± 0.0346). In 2013, when the regional mean BSA was anomalously high and mean summer LSTs were anomalously low [Mortimer *et al.*, 2016] (Section 3.4.1), BSA anomalies across most of the study area had a spatial pattern similar to that of 2007 but of opposite sign. This implies that during extreme warm (cold) years, the spatial pattern of

BSA anomalies is likely driven by a similar regional-scale pattern of atmospheric forcing, but of opposite sign. We also observed a distinct east-west divide in the sign of the BSA anomaly in both 2005 and 2010. In 2005, BSA anomalies were predominantly negative on Axel Heiberg Island, but mainly positive elsewhere. The opposite situation occurred in 2010. Finally, high spatio-temporal variability in the sign of the BSA anomaly over Prince of Wales Icefield, Manson Icefield, and Devon Ice Cap (particularly in 2007 and 2008) may reflect inter-annual variations in summer precipitation in this region, which is located close to open water sources in Baffin Bay and Nares Strait (Figure 3-1).

3.3.3 BSA change: 2001 to 2015

To determine whether there was a measurable change in the MODIS-derived mean summer BSA over the period 2001-2015, we performed a linear regression analysis (Section 3.2.3). Between 2001 and 2015 the QEI-wide (south of 80°N) summer mean BSA decreased at a rate of $0.0038 \pm 0.0037 \text{ yr}^{-1}$ ($r = 0.59$ $p < 0.02$, Figure 3-4a and Table 3-4). Assuming a constant rate of change, this equates to a total reduction in mean summer BSA of 0.057 over the 15 year period. Strong negative anomalies in mean summer BSA from 2008 to 2012 (Figure 3-3 and Table 3-3) suggest that the bulk of the albedo decrease occurred during that 5 year period. The measured rate of BSA decline ($-0.038 \pm 0.037 \text{ decade}^{-1}$) exceeds that attributed to uncorrected Terra sensor degradation ($\sim -0.002 \text{ decade}^{-1}$, Section 3.2.1.1) and the total change (-0.057) is greater than the stated product uncertainty (0.050). Therefore, we are confident that a reduction in mean summer BSA did occur over the 2001-2015 period. In light of the reported albedo declines resulting from uncorrected Terra sensor degradation [Lyapustin et al., 2014; Polashenski et al., 2015; Tedesco et al., 2016], it is likely that the true albedo change is less than that reported here. Given the uncertainties as to the magnitude of this degradation effect [Lyapustin et al., 2014] (Section 3.2.1.1) we elected not

to attempt to correct for sensor degradation, but instead present the values obtained directly from the MCD43A3 Version 05 data (Section 3.2.1.2). The BSA reduction calculated here is comparable to reductions reported for other Arctic glaciers and the Greenland Ice Sheet using similar methods but slightly different time periods [e.g. *Greuell et al.*, 2007; *Box et al.*, 2012; *Stroeve et al.*, 2013; *Alexander et al.*, 2014; *Tedesco et al.*, 2016].

Between 2001 and 2015, the area-averaged mean summer (JJA) incoming solar radiation over ice covered surfaces in the QEI, computed from daily means of NCEP/NCAR R1 Reanalysis data [*Kalnay et al.*, 1996] (<http://www.esrl.noaa.gov/psd/data/gridded/>), ranged from 350 W m⁻² (clear-sky downward solar flux) to 306 W m⁻² (all-sky downward solar flux). Assuming the solar radiation received at the surface was constant over the 15 year period, our measured BSA reduction (-0.0038 yr⁻¹) translates to a total increase in area-averaged absorbed solar radiation of between 1.3 and 1.7 MJ over the 15 year period. For a surface already at the melting point, this equates to an increase in (area-averaged) summer melt of between 0.45 and 0.52 m w.e. [*Cuffey and Paterson*, 2010 Table 5.1].

Between 2001 and 2015, > 87% of pixels analyzed experienced a decrease in mean summer BSA, with the remaining pixels experiencing a slight increase (Figure 3-4a). BSA increases were confined to high elevation regions (Figure 3-4a) and may indicate an increase in summer snowfall or riming events, particularly in the east of the QEI where glaciers are in close proximity to open water in Baffin Bay and Nares Strait (Figure 3-1). Summer air and surface temperatures, which were anomalously warm during the period 2005-2012, have previously been positively correlated with the maximum open water extent in the QEI's inter-island channels [*Koerner*, 1977].

Spatially, there is a general tendency towards increasing rates of albedo decline at lower elevations around ice cap margins, and there is an east-west gradient in the magnitude of the measured albedo

decline (Figure 3-4a). Regionally-averaged rates of mean summer BSA change on Axel Heiberg Island and Meighen Ice Cap in the western QEI ranged from $-0.0057 \pm 0.0045 \text{ yr}^{-1}$ to $-0.0059 \pm 0.0024 \text{ yr}^{-1}$. In the east, the rate was between $-0.0033 \pm 0.0037 \text{ yr}^{-1}$ (Prince of Wales Icefield) and $-0.0042 \pm 0.0039 \text{ yr}^{-1}$ (Sydkap Ice Cap) (Table 3-4). This east-west spatial pattern in the magnitude of the albedo decrease is consistent with the spatial pattern of LST increase described by *Mortimer et al.* [2016] for the entire QEI [including areas north of 80°N] for the period 2000-2015, where the MODIS-derived mean summer LST change was two to four times higher in the north and west of the QEI than in the southeast. It is also similar to the spatial pattern of snow accumulation on ice caps in the QEI described by *Koerner* [1979], where the accumulation rate decreases from east to west across the QEI. Strong warming in the west, where snow accumulation is also low, likely results in earlier snowpack removal and greater lowering of the surface albedo in these (western) regions.

To explore whether there are any other spatial patterns in the mean summer BSA record that differ from the long-term (linear) trend, we performed a Principal Components Analysis of the 15 year mean summer BSA record. Only the first Principal Component (PC1, Figure 3-4d), which explains 46% of the variance in the mean summer BSA record, had eigenvalues greater than one. This component's scores are generally positive along the high-elevation central spine of the eastern QEI and strongly negative over Axel Heiberg Island in the western QEI and at low elevations along the margins of ice masses (Figure 3-4c), consistent with the pattern of BSA change described previously (Figure 3-4a). For PC1, the highest Empirical Orthogonal Functions (EOFs) (29.6 and 20.1) correspond to the years with the lowest mean summer BSA (2011 and 2012), while the lowest EOFs (-16.4 and -18.2) correspond to the years (2003 and 2004) with the highest mean summer BSA (Figure 3-5). The departure from zero is much larger for the minimum scores than for the

maximum scores, suggesting that positive and negative BSA anomalies are likely to have been caused by an atmospheric forcing with the same spatial pattern (but reversed signs of forcing anomalies). In general, years with low (high) EOFs also had anomalously high (low) LSTs (Section 3.4.1, Table 3-S2).

Investigating the potential influence of atmospheric forcings on the BSA, we found the EOFs for PC1 to be well (negatively) correlated with the mean summer NAO index ($r = -0.87$, $p < 0.001$, Figure 5), derived by averaging the June-August monthly mean NAO indices for 2001 to 2015 (<http://www.cpc.ncep.noaa.gov>). The correlation between PC1 and the JJA NAO index is consistent with the finding of *Mortimer et al.* [2016], which found good agreement between the 2000-2015 LST record and the summer NAO index, suggesting that inter-annual variability in both the BSA and LST records is related to similar forcing. *Box et al.* [2012] also reported good correspondence between the JJA NAO index and the strength of the ice-albedo feedback over Greenland in the period 2007-2011. During 2009-2011 in particular, strong negative NAO indices, associated with persistent anticyclonic circulation, strengthened the ice-albedo feedback over the Greenland Ice Sheet [*Box et al.*, 2012].

3.3.4 Minimum summer BSA

The 15-year average QEI-wide minimum summer BSA was 0.41 ± 0.12 . Between 2001 and 2015 the QEI-wide minimum summer BSA decreased at a rate of $0.0049 \pm 0.0050 \text{ yr}^{-1}$ ($r = 0.71$, $p < 0.01$, Table 3-4) and ~85% of pixels analyzed experienced a decrease in the minimum summer BSA over the study period. Minimum summer BSA declines were smallest ($+0.001$ to -0.002 yr^{-1} for BSA minima < 0.2) for pixels having the lowest 15-year average minimum summer BSA (Figure 3-6b). Higher rates of minimum summer BSA declines ($\sim -0.006 \text{ yr}^{-1}$ to $\sim -0.007 \text{ yr}^{-1}$) were observed for pixels having a 15-year minimum summer BSA > 0.325 . The smaller albedo declines measured

for lower minimum albedo values suggests limited albedo reductions over glacier ice relative to those occurring over firn and snow-covered areas [e.g. *Alexander et al.*, 2014].

Pixels were placed into three broad categories –bare ice, intermediate, firn– according to the minimum summer BSA (Section 3.2.4). Linear regression of the annual minimum summer BSA against time for the 15 year record shows a reduction in minimum summer BSA for all three surface type categories over the period 2001-2015. In general, the minimum summer BSA of all three categories decreased from 2001-2012 but increased from 2013 onward (Figure 3-6c). The magnitude of the BSA decline was roughly three times smaller for the bare ice category ($-0.0013 \pm 0.0040 \text{ yr}^{-1}$) than for the intermediate ($-0.0043 \pm 0.0043 \text{ yr}^{-1}$) and firn ($-0.0035 \pm 0.0029 \text{ yr}^{-1}$) categories. Where bare ice is regularly exposed at the surface during the summer, minimum BSA declines likely result from an increase in light absorbing impurities, surface ponding, and/or biological activity [*Conway et al.*, 1996; *Fountain et al.*, 2004; *Flanner et al.*, 2007; *Doherty et al.*, 2010]. Light absorbing impurities (mineral dust, soot, and other aerosols), micro-organisms (cyanobacteria and algae) and ponded water are highly absorptive in the visible spectrum and have been found to alter the visible albedo of snow and ice [e.g. *Clarke and Noone*, 1985; *Flanner et al.*, 2007; *Doherty et al.*, 2010, 2013; *Dumont et al.*, 2014]. To investigate whether there has been an increase in these parameters (light absorbing impurities, biological activity, and/or ponded water) we analyzed trends in the MCD43A3 visible albedo (0.3-0.7 μm). Because Terra sensor calibration degradation effects are greatest in the visible and near-infrared wavelengths (Section 3.2.1.1, *Lyapustin et al.* [2014]), we use changes in the minimum summer visible broadband BSA only as an indicator of whether or not decreases in albedo within the visible spectrum are likely to have occurred. Between 2001 and 2015 the QEI-wide minimum summer visible broadband BSA changed at a rate of $-0.0059 \pm 0.0053 \text{ yr}^{-1}$. Visible broadband BSA reductions were observed for

the intermediate ($-0.0070 \pm 0.0056 \text{ yr}^{-1}$) and firm ($-0.0050 \pm 0.0049 \text{ yr}^{-1}$) categories; change for the bare ice category ($-0.0038 \pm 0.0042 \text{ yr}^{-1}$) was at the lower end of the detection limit. These decreases in minimum visible BSA suggest that the coverage of light-absorbing impurities, microorganisms, and/or ponded water increased over snow/firm and intermediate areas in the QEI over the 2001-2015 period. This could account for some of the measured declines in the minimum summer BSA.

For the firm and intermediate categories, decreases in the minimum summer albedo can also result from an increase in the mean snow grain size and water content of snow [*Warren and Wiscombe, 1980; Colbeck, 1982; Warren, 1982; Tedesco et al., 2016*]. Previous work has used model simulations to estimate changes in mean grain size and their contribution to the total albedo change [e.g. *Tedesco et al., 2016*]. Such simulations are not available for our study area. The rate and/or degree of snow metamorphism increases with temperature, and frequent melt events further accelerate albedo declines by enhancing the consolidation of individual snow grains [*Colbeck, 1982; Warren, 1982*]. Between 2000 and 2015, QEI-wide mean summer LST increased by $0.06 \pm 0.04^\circ\text{C yr}^{-1}$ and melt was observed at all locations at some point during this time [*Mortimer et al., 2016*; for which data from regions north of 80°N are also considered]. Given the observed surface warming, it is reasonable to expect that the rate of grain metamorphism would have also increased during this time period. If this is the case, minimum summer BSA declines for the firm category could be attributable to increases in some combination of grain size, water content, surface accumulation of light absorbing impurities, biological activity, and/or the extent of ponded water. For the intermediate category, albedo declines can also result from an increase in the extent of bare ice exposure at the glacier surface (in addition to the processes outlined for the firm category). We use the minimum summer BSA to infer changes in the extent of bare ice exposure at the glacier

surface and to investigate its inter-annual variability. Since the MCD43A3 data are only produced every 8 days (Section 3.2.1), changes in the duration of bare ice exposure were not investigated, and only changes in areal extent were analyzed. For each year, the total area having a minimum summer albedo ≤ 0.3 was calculated. Between 2001 and 2015, the total area classified as bare ice ranged from 7179 km² (2004) to 18949 km² (2012) and the linear rate of increase in bare ice area was 532 km² yr⁻¹ ($r = 0.65$, $p < 0.01$). This increase in the area of bare ice exposed at the glacier surface is consistent with the observed increase in summer glacier surface temperatures between 2000 and 2015 [*Mortimer et al.*, 2016], which has been used as a proxy for the duration and/or intensity of summer melting. A longer and/or more intense melt season can increase bare ice exposure by either earlier removal of the winter snowpack (increasing the duration of ice exposure) or exposure of new areas of bare ice (increase in exposed ice extent). Years with anomalously high LSTs also had larger areas of bare ice exposed and there is reasonable correspondence between these records ($r = 0.57$, $p < 0.05$). There is good agreement ($r = -0.93$, $p < 0.001$) between the 15 year records of mean summer BSA and extent of bare ice exposure, suggesting that changes in the area of bare ice exposed at the glacier surface in the summer are important in modulating the mean summer albedo in the QEI. It is reasonable to conclude that increases in bare ice exposure contributed to some of the measured declines in minimum summer BSA for the intermediate category.

Our analysis of minimum summer shortwave and visible broadband BSA suggests that there were increases in the exposure of light absorbing impurities, micro-organisms, and/or ponded water, bare ice extent, mean grain size, and the water content of snow over glaciated regions in the QEI over the period 2001-2015. Model simulations of the Greenland Ice Sheet found that, when considered separately, changes in surface grain size and bare ice exposure time explained 54% and

65%, of the variability in the satellite-derived albedo record between 1996 and 2012 [Tedesco *et al.*, 2016]. In the QEI, minimum summer BSA declines were ~3 times smaller for the bare ice category than for the intermediate and firn categories. Since the albedo of bare ice can only be lowered by increasing the coverage of light absorbing impurities, micro-organisms, and/or ponded water, we suggest that changes in mean snow grain size and water content, and/or bare ice exposure played a larger role in the decreases in QEI minimum summer BSA.

3.4 Comparison of glacier surface albedo and temperature changes

3.4.1 Mean summer land surface temperatures: 2001 to 2015

Between 2001 and 2015, QEI-wide (QEI south of 80°N) mean summer LST (15 year mean: $-2.62 \pm 1.41^{\circ}\text{C}$) increased at a rate of $0.034 \pm 0.037^{\circ}\text{C yr}^{-1}$ (Figure 3- 4b and Table 3-4). The 15 year period (2001-2015) is characterized by four consecutive years with anomalously low LSTs (2001-2004) and six consecutive years with positive LST anomalies (2007-2012) (Section 3.6, Figure 3-S1, Tables 3-1, 3-S3, and 3-S4). Mean summer LST change was greatest at high elevations where the mean summer LST is lower and there is more potential for surface warming. Since the temperature of pure ice and snow cannot exceed 0°C, the magnitude of any possible LST change is limited at low elevations where the LST regularly reaches 0°C in the summer [see Mortimer *et al.*, 2016]. The 15 year record of mean summer LST was, as expected, negatively correlated ($r = -0.75$, $p < 0.01$) with the 15 year record of mean summer BSA, which points to a positive ice-albedo feedback which would promote enhanced rates of glacier mass loss in the QEI.

3.4.2 Spatial patterns of relationship between BSA and LST

Linear correlation of the 15 year LST and BSA records was used to investigate the spatial pattern in the relationship between temperature and albedo (Section 3.2.3). Negative correlations were observed for ~91% of pixels (Figure 3-4d) and the average correlation coefficient (r) of all pixels analyzed was -0.41 ($p < 0.2$), much smaller than obtained using the annual means ($r = -0.75$, $p < 0.01$, Section 3.4.1). This weak negative correlation may be due, in part, to the fact that the albedo continues to decline once the surface temperature has reached the pressure melting point. The spatial pattern of correlation coefficients (Figure 3-4d) more closely resembles the pattern of mean summer BSA change (Figure 3-4a) than it does that of mean summer LST change (Figure 3-4b). At lower elevations, around the margins of the ice masses, where mean summer LST approaches the pressure melting point (PMP) during summer, albedo declines were large but LST increases were small, and the correlation between LST and BSA was strongly negative. This likely indicates that, for surfaces at temperatures near the PMP, melt (which can result in an increase ponded water and the release of light absorbing impurities which become concentrated on the surface) is an important influence on albedo declines.

Spatially, there is considerable variability in the relationship between the LST and BSA records (Figure 3-4d). Correlations are strongly negative ($r < -0.6$) along outlet glaciers and around ice cap margins and weakly negative ($r > -0.2$) and/or positive in the interior of most ice masses. In the eastern QEI (eastern Ellesmere Island and Devon Island), correlations are generally weaker on the maritime facing (eastern) slopes ($r \sim -0.2$ to ~ -0.6) than on the continental (western) margins ($r < -0.6$) of the same ice masses, with the exception of the peninsula to the south of Cadogan Inlet on Prince of Wales Icefield (Figure 3-4d, black box) where the correlation was strongly negative ($r < -0.75$). Despite a high data dropout rate in the interior regions of most ice masses, Figure 3-4d appears to show positive correlations along the central high-elevation spine of the eastern QEI

where the mean summer BSA and LST both increased. Finally, areas with strong negative (positive) correlations tend to have negative (positive) loadings for PC1 of the 15 year mean summer BSA record (Figure 3-4c).

3.4.3 Discussion of spatial patterns in the relationship between BSA and LST

The spatial pattern of correlation coefficients (between BSA and LST, Figure 3-4d) points to a complex and varying relationship between surface temperature and surface albedo in the QEI over the period 2001-2015. Since field measurements of the surface radiation budget and precipitation are sparse (or non-existent) in the QEI, outputs from the CCMA's CanRCM4 (Section 3.2.5) were used to identify forcings that could explain the spatial variability in the relationship between LST and BSA. Between 2001 and 2009, the modelled QEI-wide means of summer incoming shortwave radiation, near-surface air temperature and MODIS-derived LST all increased, and the mean summer outgoing shortwave radiation and MODIS-derived BSA both decreased (Section 3.6 Table 3-S5). These increases in incoming shortwave radiation are consistent with the occurrence of persistent positive mean summer 500 hPa geopotential height anomalies over the Canadian Arctic and western Greenland between 2007 and 2012 [*Gascon et al.*, 2013; *Rajewicz and Marshall*, 2014; *Bezeau et al.*, 2015]. Mean annual precipitation decreased over all ice masses (Section 3.6 Table 3-S5); summer precipitation increased over the summit of Devon Ice Cap between 2001 and 2009.

The CanRCM4 output reveals east-west differences in the summer net radiation budget which may explain some of the east-west differences in the relationship between LST and BSA (Section 3.4.2). The 2001 to 2009 mean summer net shortwave radiation over Axel Heiberg Island (84 W m^{-2}) and Sydkap Ice Cap (85 W m^{-2}) was considerably larger than that over ice caps in the bordering Baffin Bay (54 to 66 W m^{-2}) (Table 3-S6). No such east-west difference was observed for the 2001 to

2009 mean summer net longwave radiation. Investigation of the 500 hPa geopotential height anomalies from NCEP/NCAR Reanalysis data [Kalnay *et al.*, 1996] during the 2001-2015 period indicates that, in general, there was a persistent ridge over the north and west of the QEI during warm summers and a trough in that region during colder years [Mortimer *et al.*, 2016]. Strong and persistent anticyclonic circulation maximizes the amount of incoming shortwave radiation incident at the air-ice interface which promotes enhanced surface warming and has previously been associated with extreme negative mass balance years in the QEI [Alt, 1987; Gardner and Sharp, 2007; Gascon *et al.*, 2013].

Differences in the net radiation budget alone do not appear to explain the high spatial variability in the relationship between the LST and BSA records observed in the eastern QEI. In the eastern QEI, surface warming and albedo declines were smaller on the maritime (eastern) sides of ice masses than on their continental (western) sides, and positive correlations between the 15 year LST and BSA records were observed at higher elevations in the interior of ice masses (Figure 3-4d). The occurrence of regions with positive correlations may indicate a negative ice-albedo feedback in which warming is associated with an increase in albedo which dampens further warming [e.g. Box *et al.*, 2012]. These positive correlations, together with the east-west differences in the relationship between BSA and LST in the eastern QEI, may point to a potential role for summer precipitation variability in modulating the inter-annual variability in BSA (and its relationship to LST) in the eastern QEI where ice masses are in close proximity to open water sources in Baffin Bay and Nares Strait (Figure 3-1).

Snow accumulation rates in the QEI are largely a function of distance from the moisture source, and Baffin Bay contributes >20% of the total moisture delivered to maritime-facing slopes in the southeast QEI [Koerner, 1979]. Increased open water extent during warm years promotes

atmospheric convection, which strengthens the advection of warm moist air masses into Baffin Bay [Koerner, 1977]. The high elevation regions of eastern Ellesmere and Devon Islands act as a barrier to this increased moisture transport [Koerner, 1979]. As a result, precipitation is deposited on the eastern maritime slopes, raising the albedo and limiting surface warming and hence melt (negative ice-albedo feedback, e.g. Box *et al.* [2012]). In the eastern QEI, positive correlations were mainly confined to higher elevations where >50% of annual precipitation occurs during the summer, and where loadings for PC1 of the mean summer BSA were strongly positive (Figure 3-4c), suggesting that variability in summer precipitation may have the ability to alter the albedo in this region.

In contrast, on the western (lee side) side of ice masses on eastern Ellesmere and Devon Islands, the correlation between LST and BSA was strongly negative. In these regions, warmer air and glacier surface temperatures result in albedo decreases, leading to further surface warming (positive ice-albedo feedback). Koerner [1979] attributed the existence of a dry area with low amounts of snow accumulation centered on western Ellesmere Island to the precipitation-shadowing effect of the surrounding mountains. The presence of a barrier to moisture transport from the east limits precipitation on the western (lee) side of the eastern ice masses and adiabatic heating of descending air masses results in warm dry air which promotes warming and enhances albedo decline.

3.5 Summary and conclusions

We have presented the first account of summer mean shortwave broadband albedo variations over glaciated surfaces of the QEI (South of 80°N) from 2001 to 2015. QEI mean summer black-sky albedo decreased by $0.0038 \pm 0.0037 \text{ yr}^{-1}$ over that time period. Strong negative BSA anomalies from 2008 to 2012 suggest that the bulk of the BSA decline occurred during this 5 year period.

Albedo declines were greatest in the west and at lower elevations. Mean summer glacier surface temperatures increased by 0.51°C during the 2001-2015 period and the 15 year BSA record is negatively correlated with the 15 year record of glacier surface temperatures. The complex topography of the QEI results in considerable spatial variation in the relationship between surface temperature and albedo. Positive correlations observed at high elevations on eastern Ellesmere Island may point to a positive ice-albedo feedback where warmer temperatures are associated with enhanced summer precipitation (as snow and/or rime) which raises the albedo and limits warming and melt. In other areas warming appears to drive albedo decline and promote further surface warming, leading to increased melt, runoff, and glacier mass loss.

Table 3-1. Clear-sky BSA and LST for glaciated regions of the QEI south of 80°N; ± 1 standard deviation. Anomalies are with respect to the 2001-2015 mean.

Year	BSA mean	BSA min	BSA mean anomaly	BSA min anomaly	% area with missing BSA data	LST mean	LST mean anomaly	% area with missing LST data
2001	0.567 \pm 0.108	0.417 \pm 0.135	0.0199 \pm 0.0550	0.0030 \pm 0.0690	11.4	-3.1 \pm 1.5	-0.38 \pm 0.53	5.4
2002	0.569 \pm 0.116	0.447 \pm 0.138	0.0297 \pm 0.0453	0.0448 \pm 0.0686	19.8	-3.2 \pm 1.8	-0.49 \pm 0.61	5.2
2003	0.580 \pm 0.097	0.446 \pm 0.127	0.0366 \pm 0.0346	0.0374 \pm 0.0653	15.1	-3.4 \pm 1.6	-0.75 \pm 0.45	5.2
2004	0.575 \pm 0.105	0.447 \pm 0.127	0.0383 \pm 0.0392	0.0484 \pm 0.0692	21.5	-3.6 \pm 2.0	-0.86 \pm 0.71	5.2
2005	0.556 \pm 0.114	0.434 \pm 0.137	0.0126 \pm 0.0365	0.0254 \pm 0.0661	15.4	-2.1 \pm 1.3	0.60 \pm 0.33	5.2
2006	0.557 \pm 0.109	0.426 \pm 0.131	0.0169 \pm 0.0316	0.0219 \pm 0.0512	19.5	-3.2 \pm 1.7	-0.46 \pm 0.52	5.2
2007	0.536 \pm 0.126	0.429 \pm 0.148	-0.0096 \pm 0.0375	0.0175 \pm 0.0511	13.5	-1.7 \pm 1.2	0.97 \pm 0.43	5.3
2008	0.525 \pm 0.110	0.376 \pm 0.122	-0.0185 \pm 0.0330	-0.0336 \pm 0.0471	17.0	-2.3 \pm 1.2	0.41 \pm 0.42	5.2
2009	0.522 \pm 0.112	0.381 \pm 0.130	-0.0200 \pm 0.0314	-0.0250 \pm 0.0470	19.4	-2.4 \pm 1.5	0.32 \pm 0.35	5.2
2010	0.533 \pm 0.103	0.399 \pm 0.122	-0.0133 \pm 0.0367	-0.0134 \pm 0.0457	13.0	-1.7 \pm 1.2	0.94 \pm 0.49	5.3
2011	0.482 \pm 0.118	0.364 \pm 0.132	-0.0639 \pm 0.0371	-0.0481 \pm 0.0455	13.3	-1.9 \pm 1.0	0.83 \pm 0.59	5.5
2012	0.504 \pm 0.112	0.362 \pm 0.128	-0.0421 \pm 0.0332	-0.0507 \pm 0.0473	13.3	-2.1 \pm 1.2	0.63 \pm 0.44	5.3
2013	0.568 \pm 0.093	0.413 \pm 0.121	0.0265 \pm 0.0463	0.0076 \pm 0.0731	12.8	-4.4 \pm 1.7	-1.66 \pm 0.64	5.2
2014	0.550 \pm 0.013	0.388 \pm 0.124	0.0086 \pm 0.0395	-0.0186 \pm 0.0664	13.3	-3.0 \pm 1.5	-0.30 \pm 0.47	5.2
2015	0.522 \pm 0.102	0.394 \pm 0.131	-0.0169 \pm 0.0674	-0.0094 \pm 0.0700	15.8	-2.4 \pm 1.4	0.19 \pm 0.31	1.2

Table 3-2. Clear-sky mean summer BSA for glaciated regions of the QEI south of 80°N; ± 1 standard deviation.

Year	QEI	Agassiz IC	Axel Heiberg I	Devon & Coburg I	Manson IF	Meighen IC	Prince of Wales IF	Sydkap IC
2001	0.567 \pm 0.108	0.538 \pm 0.124	0.531 \pm 0.121	0.593 \pm 0.085	0.541 \pm 0.101	0.615 \pm 0.079	0.576 \pm 0.112	0.570 \pm 0.084
2002	0.569 \pm 0.116	0.562 \pm 0.131	0.541 \pm 0.129	0.577 \pm 0.092	0.532 \pm 0.112	0.563 \pm 0.049	0.589 \pm 0.121	0.544 \pm 0.085
2003	0.580 \pm 0.097	0.561 \pm 0.112	0.524 \pm 0.112	0.605 \pm 0.069	0.551 \pm 0.085	0.522 \pm 0.056	0.595 \pm 0.099	0.591 \pm 0.064
2004	0.575 \pm 0.105	0.553 \pm 0.119	0.532 \pm 0.118	0.588 \pm 0.079	0.557 \pm 0.102	0.585 \pm 0.040	0.594 \pm 0.109	0.579 \pm 0.078
2005	0.556 \pm 0.114	0.534 \pm 0.124	0.465 \pm 0.139	0.585 \pm 0.085	0.554 \pm 0.092	0.502 \pm 0.084	0.578 \pm 0.111	0.534 \pm 0.086
2006	0.557 \pm 0.109	0.546 \pm 0.126	0.495 \pm 0.110	0.572 \pm 0.088	0.542 \pm 0.105	0.526 \pm 0.050	0.578 \pm 0.110	0.546 \pm 0.090
2007	0.536 \pm 0.126	0.522 \pm 0.138	0.443 \pm 0.133	0.570 \pm 0.094	0.504 \pm 0.113	0.478 \pm 0.076	0.559 \pm 0.130	0.503 \pm 0.095
2008	0.525 \pm 0.110	0.522 \pm 0.120	0.415 \pm 0.116	0.548 \pm 0.078	0.515 \pm 0.100	0.481 \pm 0.076	0.547 \pm 0.107	0.497 \pm 0.102
2009	0.522 \pm 0.112	0.524 \pm 0.118	0.428 \pm 0.108	0.536 \pm 0.089	0.479 \pm 0.104	0.489 \pm 0.056	0.553 \pm 0.111	0.511 \pm 0.090
2010	0.533 \pm 0.103	0.542 \pm 0.116	0.515 \pm 0.112	0.530 \pm 0.087	0.479 \pm 0.095	0.537 \pm 0.074	0.557 \pm 0.104	0.509 \pm 0.086
2011	0.482 \pm 0.118	0.477 \pm 0.128	0.390 \pm 0.119	0.512 \pm 0.100	0.445 \pm 0.096	0.409 \pm 0.064	0.507 \pm 0.115	0.442 \pm 0.100
2012	0.504 \pm 0.112	0.475 \pm 0.117	0.414 \pm 0.114	0.547 \pm 0.090	0.471 \pm 0.102	0.425 \pm 0.065	0.523 \pm 0.109	0.485 \pm 0.093
2013	0.568 \pm 0.093	0.550 \pm 0.105	0.540 \pm 0.089	0.582 \pm 0.079	0.548 \pm 0.095	0.611 \pm 0.041	0.576 \pm 0.099	0.591 \pm 0.068
2014	0.550 \pm 0.103	0.528 \pm 0.116	0.475 \pm 0.118	0.580 \pm 0.074	0.539 \pm 0.096	0.571 \pm 0.053	0.564 \pm 0.101	0.560 \pm 0.073
2015	0.522 \pm 0.117	0.508 \pm 0.132	0.429 \pm 0.125	0.539 \pm 0.095	0.498 \pm 0.105	0.437 \pm 0.082	0.558 \pm 0.108	0.497 \pm 0.115
average	0.545 \pm 0.102	0.526 \pm 0.116	0.488 \pm 0.112	0.568 \pm 0.079	0.516 \pm 0.094	0.517 \pm 0.055	0.562 \pm 0.104	0.538 \pm 0.079

Table 3-3. Clear-sky mean summer BSA anomaly (with respect to 2001-2015 mean) for glaciated regions of the QEI south of 80°N; ± 1 standard deviation.

Year	QEI	Agassiz IC	Axel Heiberg I	Devon & Coburg I	Manson IF	Meighen IC	Prince of Wales IF	Sydkap IC
2001	0.0202 \pm	0.0075 \pm	0.0408 \pm	0.0225 \pm	0.0234 \pm	0.0979 \pm	0.0116 \pm	0.0300 \pm
	0.0555	0.0571	0.0709	0.0421	0.0567	0.0434	0.0534	0.0542
2002	0.0299 \pm	0.0316 \pm	0.0658 \pm	0.0240 \pm	0.0148 \pm	0.0460 \pm	0.0269 \pm	0.0204 \pm
	0.0451	0.0385	0.0526	0.0384	0.0446	0.0201	0.0436	0.0438
2003	0.0370 \pm	0.0305 \pm	0.0436 \pm	0.0411 \pm	0.0352 \pm	0.0048 \pm	0.0309 \pm	0.0531 \pm
	0.0346	0.0313	0.0367	0.0324	0.0337	0.0234	0.0347	0.0353
2004	0.0386 \pm	0.0234 \pm	0.0516 \pm	0.0337 \pm	0.0506 \pm	0.0684 \pm	0.0373 \pm	0.0464 \pm
	0.0391	0.0344	0.0407	0.0365	0.0414	0.0258	0.0388	0.0392
2005	0.0127 \pm	0.0039 \pm	-0.0191 \pm	0.0224 \pm	0.0357 \pm	-0.0149 \pm	0.0141 \pm	0.0057 \pm
	0.0365	0.0261	0.0466	0.0322	0.0362	0.0360	0.0308	0.0305
2006	0.0172 \pm	0.0156 \pm	0.0215 \pm	0.0173 \pm	0.0239 \pm	0.0086 \pm	0.0145 \pm	0.0120 \pm
	0.0313	0.0303	0.0423	0.0342	0.0277	0.0297	0.0272	0.0293
2007	-0.0107 \pm	-0.0077 \pm	-0.0316 \pm	0.0001 \pm	-0.0142 \pm	-0.0400 \pm	-0.0058 \pm	-0.0316 \pm
	0.0374	0.0330	0.0434	0.0293	0.0338	0.0265	0.0399	0.0328
2008	-0.0179 \pm	-0.0081 \pm	-0.0446 \pm	-0.0211 \pm	-0.0030 \pm	-0.0371 \pm	-0.0175 \pm	-0.0136 \pm
	0.0330	0.0265	0.0449	0.0316	0.0278	0.0267	0.0261	0.0479
2009	-0.0200 \pm	-0.0061 \pm	-0.0374 \pm	-0.0249 \pm	-0.0388 \pm	-0.0304 \pm	-0.0120 \pm	-0.0107 \pm
	0.0313	0.0217	0.0393	0.0301	0.0274	0.0296	0.0264	0.0394
2010	-0.0140 \pm	0.0120 \pm	0.0340 \pm	-0.0394 \pm	-0.0395 \pm	0.0201 \pm	-0.0080 \pm	-0.0303 \pm
	0.0366	0.0237	0.0337	0.0294	0.0259	0.0312	0.0235	0.0283
2011	-0.0657 \pm	-0.0534 \pm	-0.0861 \pm	-0.0587 \pm	-0.0730 \pm	-0.1106 \pm	-0.0574 \pm	-0.0916 \pm
	0.0363	0.0323	0.0407	0.0366	0.0267	0.0212	0.0333	0.0454
2012	-0.0434 \pm	-0.0559 \pm	-0.0647 \pm	-0.0228 \pm	-0.0473 \pm	-0.0995 \pm	-0.0423 \pm	-0.0506 \pm
	0.0328	0.0288	0.0378	0.0293	0.0305	0.0282	0.0266	0.0385
2013	0.0272 \pm	0.0230 \pm	0.0579 \pm	0.0223 \pm	0.0323 \pm	0.0942 \pm	0.0134 \pm	0.0532 \pm
	0.0459	0.0444	0.0624	0.0372	0.0405	0.0361	0.0410	0.0418
2014	0.0087 \pm	0.0019 \pm	-0.0032 \pm	0.0178 \pm	0.0233 \pm	0.0539 \pm	0.0020 \pm	0.0215 \pm
	0.0393	0.0362	0.0428	0.0400	0.0384	0.0229	0.0349	0.0445
2015	-0.0164 \pm	-0.0190 \pm	-0.0443 \pm	-0.0188 \pm	-0.0183 \pm	-0.0822 \pm	-0.0032 \pm	-0.0313 \pm
	0.0672	0.0823	0.0904	0.0354	0.0590	0.0478	0.0674	0.0721

Table 3-4. 2001-2015 BSA and LST change for glaciated regions of the QEI south of 80°N; ± 1 standard deviation.

	QEI	Agassiz IC	Axel Heiberg I	Devon & Coburg I	Manson IF	Meighen IC	Prince of Wales IF	Sydkap IC
Mean	-0.0038 \pm	-0.0032 \pm	-0.0057 \pm	-0.0038 \pm	-0.0039 \pm	-0.0059 \pm	-0.0033 \pm	-0.0042 \pm
BSA (yr ⁻¹)	0.0037	0.0039	0.0045	0.0027	0.0037	0.0024	0.0037	0.0039
Minimum	-0.0049	-0.0042	-0.0076	-0.0034	-0.0046	-0.0065	-0.0054 \pm	-0.0053 \pm
BSA (yr ⁻¹)	± 0.0051	± 0.0048	± 0.0057	± 0.0042	± 0.0055	± 0.0044	0.0049	0.0048
LST	0.03 \pm	0.05 \pm	0.08 \pm	0.02 \pm	0.01 \pm	0.11 \pm	0.03 \pm	0.03 \pm
(°C yr ⁻¹)	0.04	0.03	0.04	0.03	0.02	0.03	0.03	0.03

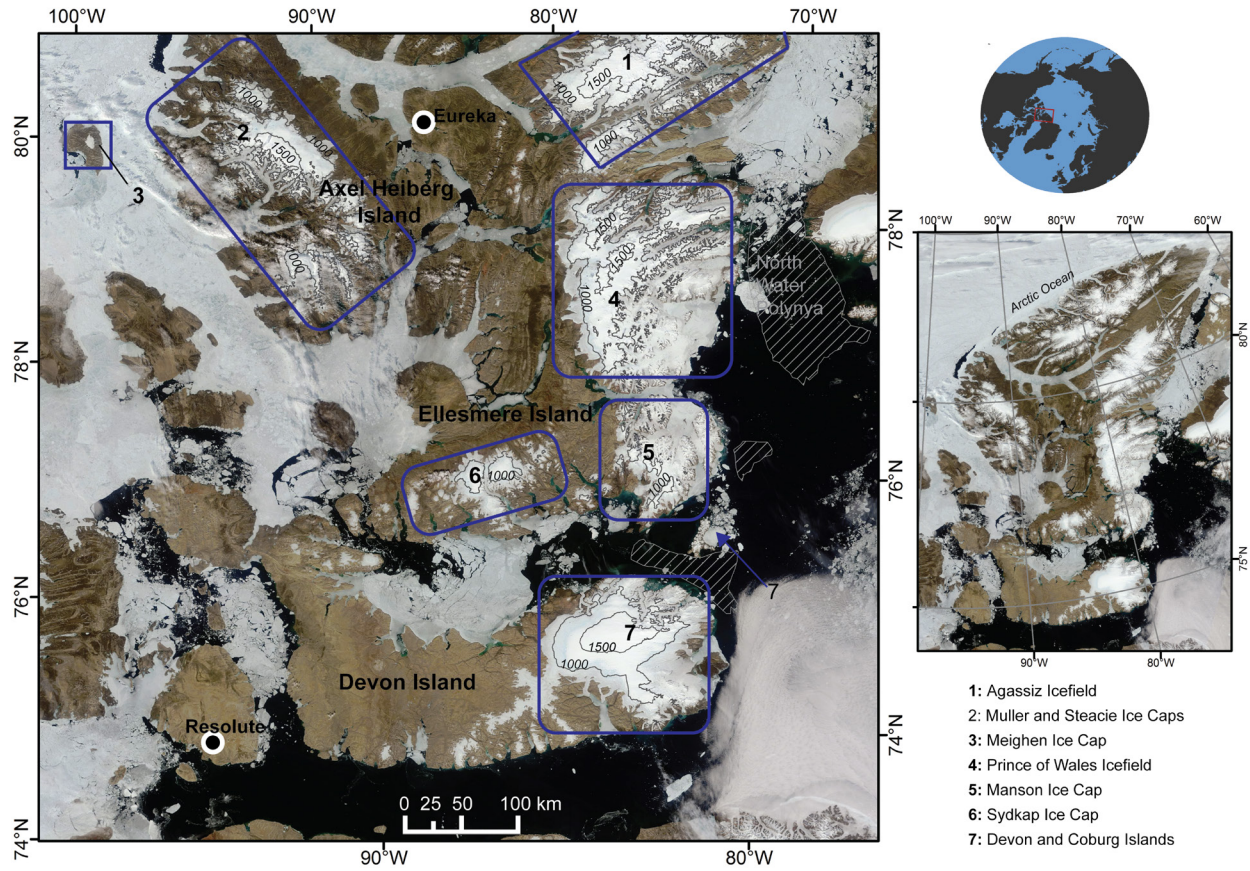


Figure 3-1 Glaciated regions of the Queen Elizabeth Islands, Arctic Canada. Only ice south of 80°N (see inset, right) are used in our analysis. Blue boxes indicate approximate area of the seven different regions used in our analysis.

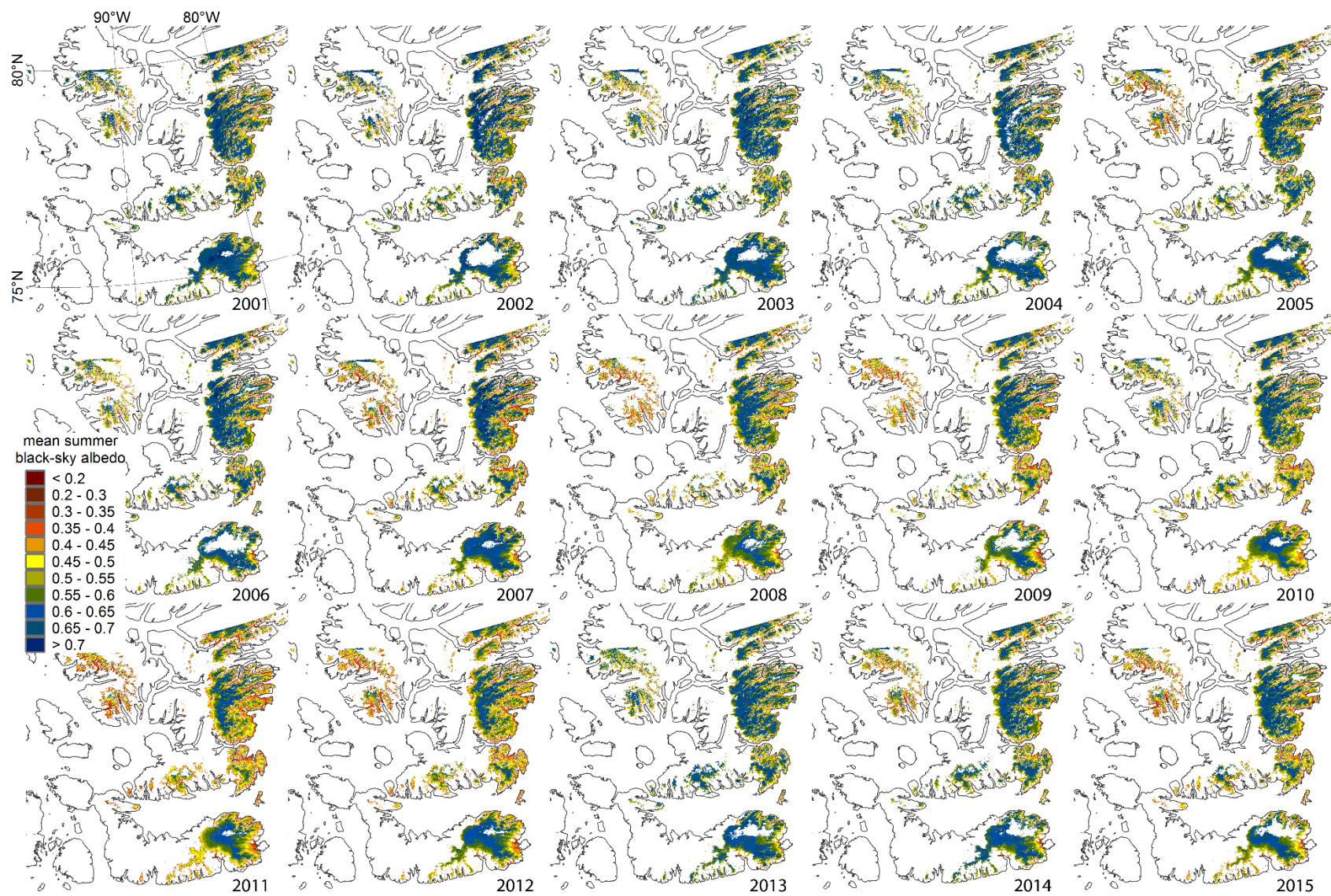


Figure 3-2 Annual summer mean clear-sky shortwave broadband black-sky albedo over the Queen Elizabeth Islands glaciers and ice caps south of 80°N for the period 2001-2015. White areas within glaciated terrain indicate no data.

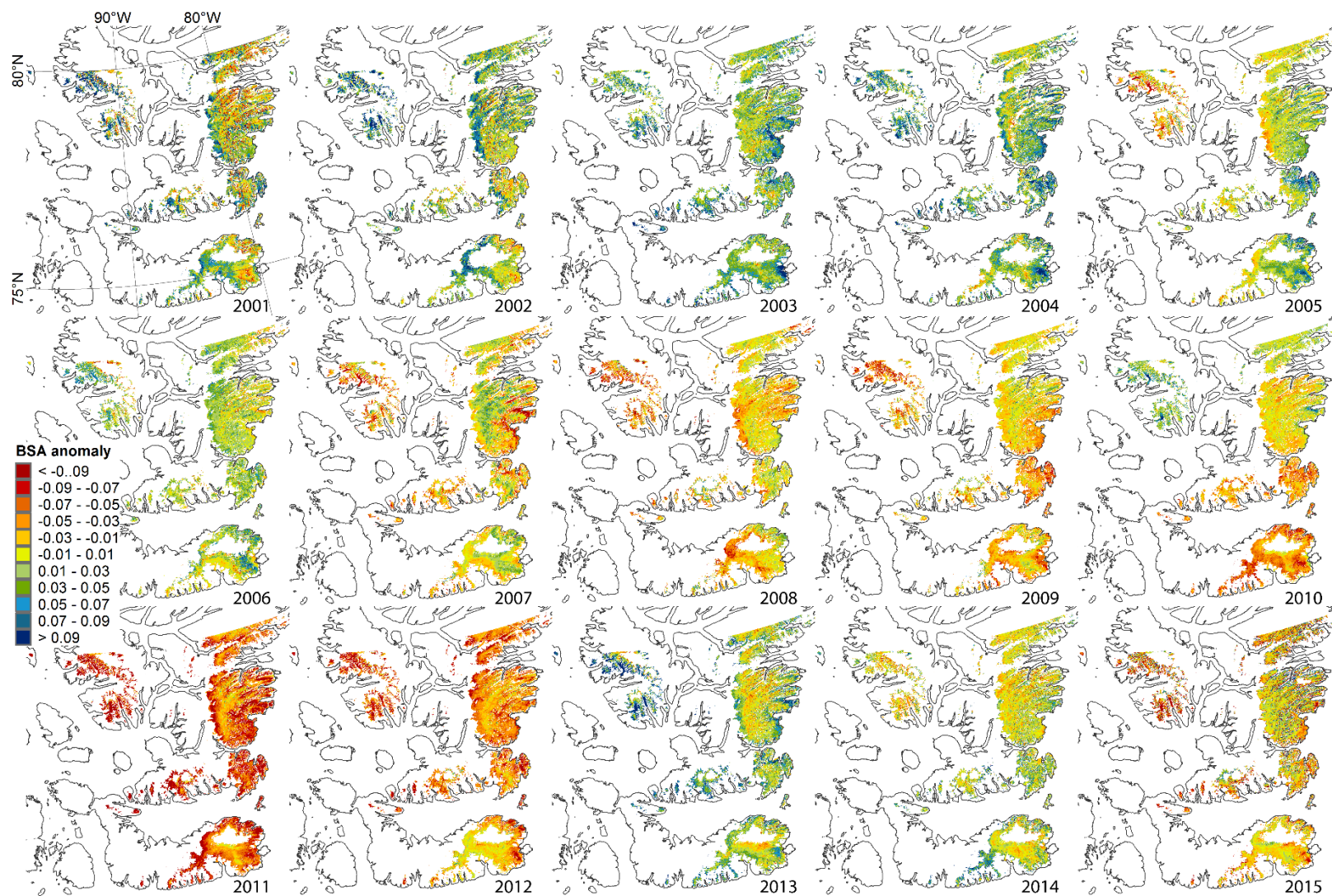


Figure 3-3 Annual summer mean clear-sky shortwave broadband black-sky albedo anomaly relative to the 2001-2015 mean over the Queen Elizabeth Islands glaciers and ice caps south of 80°N for the period 2001-2015. White areas within glaciated terrain indicate no data.

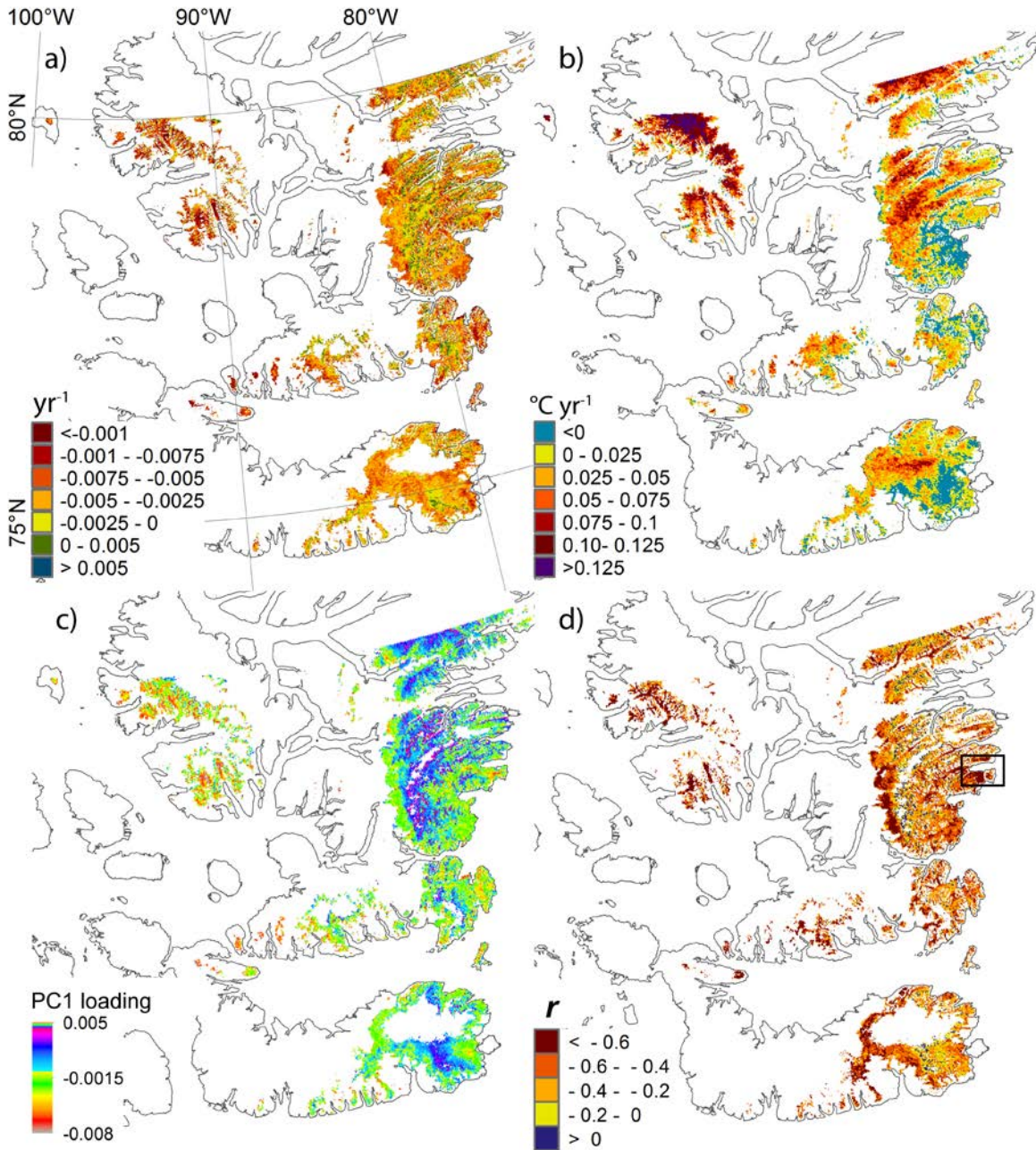


Figure 3-4 (a) Linear rate of change in mean summer clear-sky shortwave broadband black-sky albedo (yr^{-1}) and (b) mean summer clear-sky land surface temperature ($^{\circ}\text{C yr}^{-1}$) for 2000 to 2015 for the Queen Elizabeth Islands south of 80°N for pixels having 11 or more mean summer observations. (c) Component loadings for the first Principal Component of the 15-year mean summer clear-sky shortwave broadband black-sky albedo record, (d) Pearson Correlation Coefficient of the 15 year mean summer clear-sky shortwave broadband black-sky albedo (Figure 2) and mean summer clear-sky land surface temperature (Figure 3-S1) records for 2001 to 2015 for pixels with annual mean summer LST and BSA for all 15 years of observation. Black box shows location of Cadogan Inlet (Section 3.4.3). White areas within glaciated terrain indicate no data.

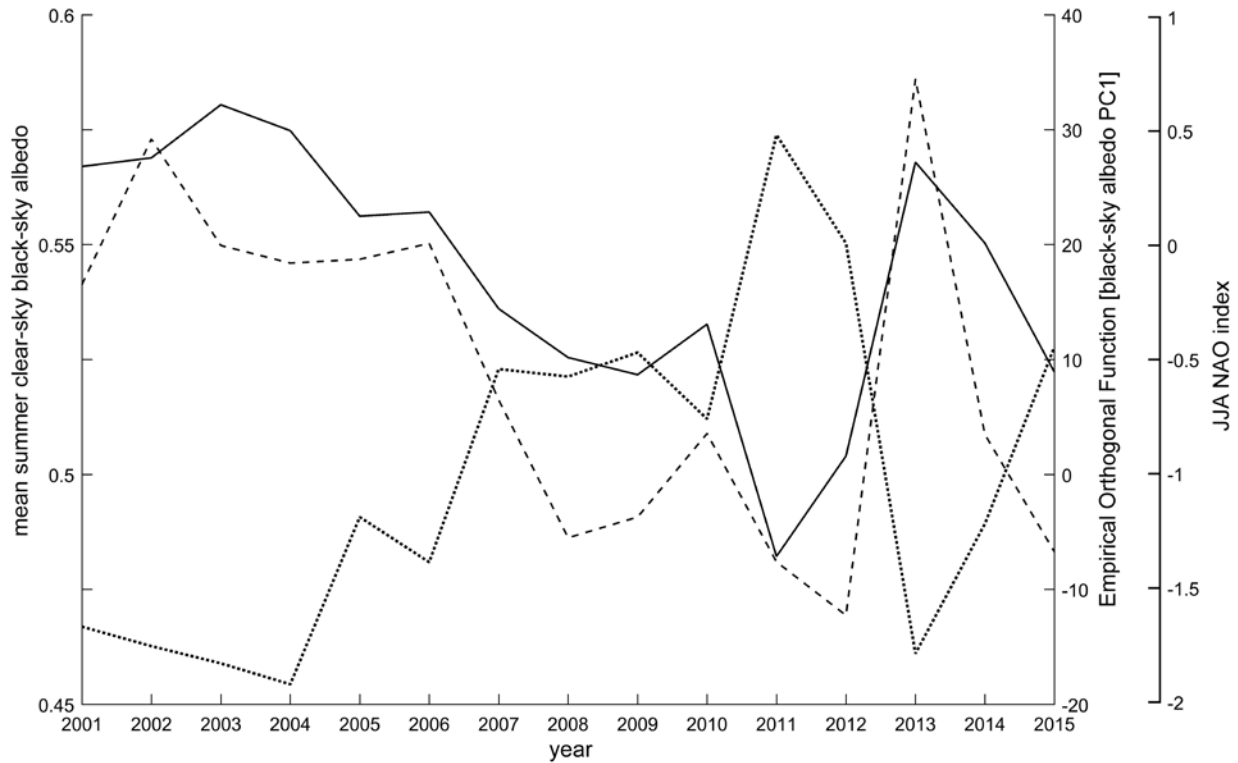


Figure 3-5 Mean summer BSA (solid line) and JJA NAO index (dashed line), Empirical Orthogonal Functions (EOFs) for the First Principal Component of the 15 year mean summer BSA record (dotted line) for 2001 to 2015.

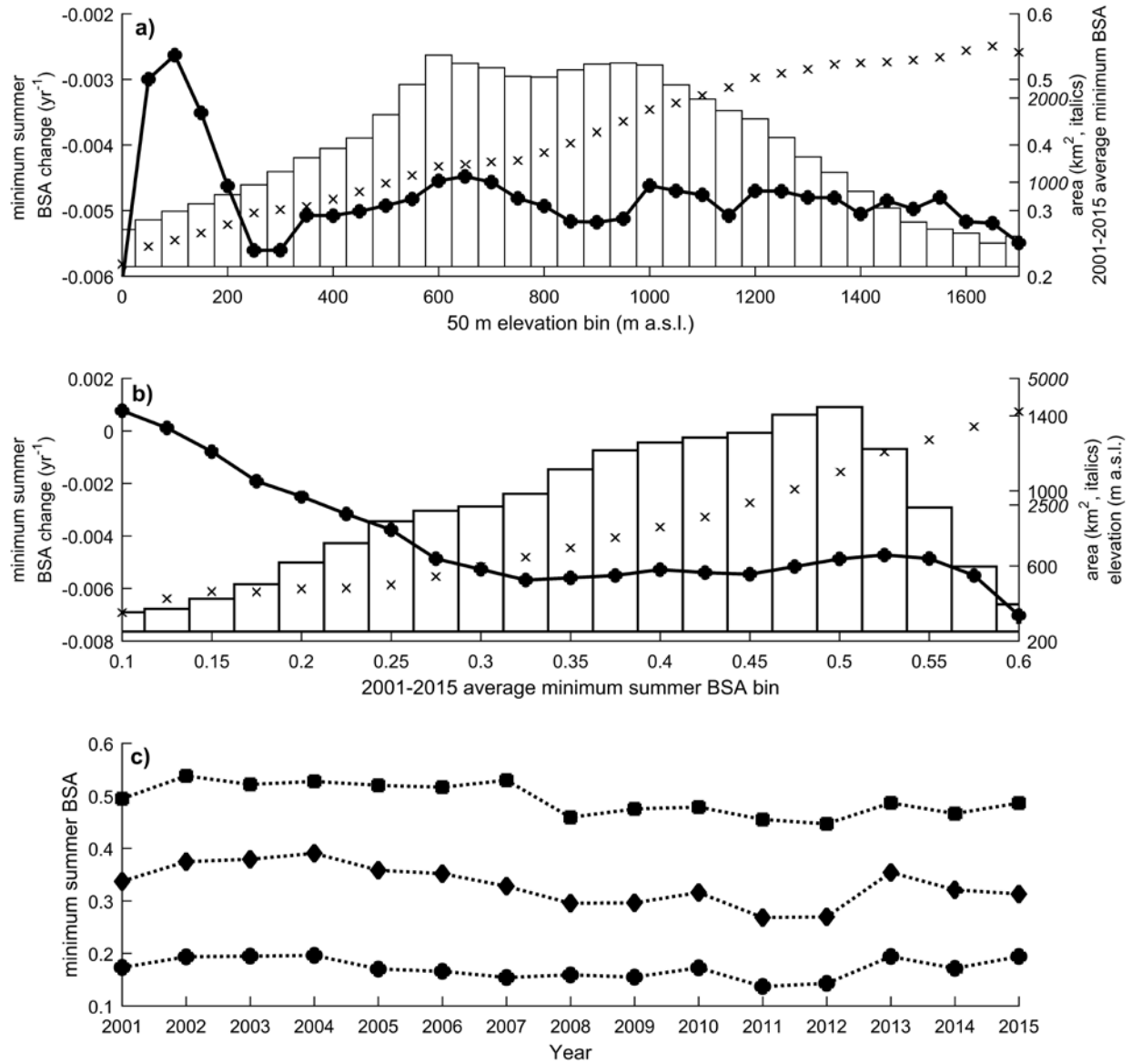


Figure 3-6 (a) Minimum summer clear-sky shortwave broadband black-sky albedo change for 2001 to 2015, averaged by 50 meter elevation bins. Right-hand axis: average 15-year minimum summer clear-sky shortwave broadband black-sky albedo (stars) and surface area (bar graph) for each elevation bin. (b) Minimum summer clear-sky shortwave broadband black-sky albedo change for 2001 to 2015, averaged by 0.025 BSA bins from 0.1 to 0.6 according to the 15-year average minimum summer BSA. Right-hand axis: 'X' indicates average elevation (m a.s.l.) and area (bar graph) for each minimum BSA bin. (c) Minimum summer BSA for bare-ice (circles), intermediate (diamonds), and firn (squares) categories described in Section 3.2.4 for 2001-2015.

3.6 Chapter 3 Supplemental materials

3.6.1 Introduction

The following figures and tables present data that support the conclusions, but are not essential. Figure 3-S1 presents the LST anomalies for 2001-2015. These data are similar to those presented in Chapter 2 [and *Mortimer et al.* 2016]. The data differs in the time period (anomalies are calculated with respect to the 2001-2015 mean instead of 2000-2015) and the area of interest (this chapter presents only data for regions south of 80°N whereas Chapter 2 [and *Mortimer et al.* 2016] included regions north of 80°N). These data are summarised in Tables 3-S3 and 3-S4. Figure 3-S2 presents the BSA and LST change for the 2001-2009 period, calculated to enable comparison with the Can RCM4 climate model output. These parameters are summarized in Tables 3-S5 and 3-S6. The spatial and temporal variability of missing albedo observations is described in Table 3-S1. Table 3-S2 provides similar information to that presented in Figure 3-5 but also includes the mean summer LST.

Table 3-S1: Percentage of all possible pixels having at least 7 or a possible 12 clear-sky shortwave broadband black-sky albedo observations during each summer (days 153-241).

Year	QEI	Agassiz IC	Axel Heiberg I	Devon & Coburg I	Manson IF	Meighen IC	Prince of Wales IF	Sydkap IC
2001	88.6	90.4	71.4	92.3	90.8	87.5	94.3	80.9
2002	80.2	90.4	60.7	73.0	90.5	87.5	91.6	65.7
2003	84.9	90.4	65.0	83.8	89.2	87.5	93.1	79.4
2004	78.5	90.4	64.7	73.0	80.4	87.5	85.7	74.2
2005	84.6	90.4	67.0	82.8	90.8	87.5	93.6	69.7
2006	80.5	90.4	60.1	70.8	90.7	87.5	92.8	75.2
2007	86.5	90.4	63.0	90.3	90.8	86.3	94.1	76.0
2008	83.0	90.4	55.2	86.8	90.8	85.6	94.1	54.3
2009	80.6	90.1	58.3	75.0	90.7	84.4	94.0	57.3
2010	87.0	90.3	66.6	89.5	90.7	87.1	94.1	78.6
2011	86.7	89.9	63.5	91.5	90.7	83.7	94.1	73.7
2012	86.7	90.0	64.4	91.1	90.7	79.8	94.1	73.8
2013	87.2	93.2	68.9	83.2	93.6	89.0	96.0	82.9
2014	86.7	93.1	67.7	82.9	93.4	89.0	95.9	80.7
2015	84.2	92.9	64.7	78.7	93.6	84.8	94.4	72.3

Table 3-S2: Comparison of Empirical Orthogonal Functions (EOFs) for the First Principal Component, QEI-wide mean summer BSA, and LST.

Year	PC1 EOF	BSA	LST (°C)	PC1 EOF Rank	BSA Rank	LST Rank
2001	-13.2	0.567	-3.08	11	5	10
2002	-14.9	0.569	-3.18	12	3	12
2003	-16.4	0.580	-3.45	14	1	13
2004	-18.2	0.575	-3.56	15	2	14
2005	-3.7	0.556	-2.09	8	7	5
2006	-7.6	0.557	-3.16	10	6	11
2007	9.2	0.536	-1.72	5	9	1
2008	8.5	0.525	-2.28	6	11	6
2009	10.6	0.522	-2.37	4	13	7
2010	4.8	0.533	-1.75	7	10	2
2011	29.6	0.482	-1.86	1	15	3
2012	20.1	0.504	-2.06	2	14	4
2013	-15.6	0.568	-4.36	13	4	15
2014	-4.3	0.550	-3.00	9	8	9
2015	11.1	0.522	-2.43	3	12	8

Table 3-S3: Clear-sky mean summer land surface temperature (°C) for glaciated regions of the Queen Elizabeth Islands south of 80°N; ± 1 standard deviation.

Year	QEI	Agassiz IC	Axel Heiberg I	Devon & Coburg I	Manson IF	Meighen IC	Prince of Wales IF	Sydkap IC
2001	-3.1 \pm 1.5	-3.6 \pm 1.6	-3.7 \pm 1.6	-2.5 \pm 1.0	-2.1 \pm 1.0	-5.4 \pm 0.7	-3.4 \pm 1.5	-3.0 \pm 1.1
2002	-3.2 \pm 1.8	-3.3 \pm 1.8	-3.8 \pm 1.9	-3.2 \pm 1.8	-1.9 \pm 1.2	-3.3 \pm 0.6	-3.3 \pm 1.9	-2.9 \pm 1.4
2003	-3.4 \pm 1.6	-3.9 \pm 1.6	-4.0 \pm 1.7	-3.2 \pm 1.4	-2.1 \pm 1.0	-3.4 \pm 0.5	-3.7 \pm 1.6	-3.2 \pm 1.0
2004	-3.6 \pm 2.0	-3.8 \pm 2.0	-4.0 \pm 2.3	-3.3 \pm 1.7	-2.3 \pm 1.2	-3.4 \pm 0.2	-3.9 \pm 2.1	-3.1 \pm 1.3
2005	-2.1 \pm 1.3	-2.4 \pm 1.3	-2.2 \pm 1.5	-2.0 \pm 1.2	-1.2 \pm 0.7	-2.0 \pm 0.3	-2.4 \pm 1.4	-1.6 \pm 0.8
2006	-3.2 \pm 1.7	-3.7 \pm 1.7	-3.8 \pm 1.9	-2.8 \pm 1.4	-1.9 \pm 1.0	-3.7 \pm 0.4	-3.5 \pm 1.9	-2.5 \pm 1.1
2007	-1.7 \pm 1.2	-1.7 \pm 1.2	-1.7 \pm 1.2	-1.8 \pm 1.0	-1.0 \pm 0.7	-1.6 \pm 0.2	-1.9 \pm 1.3	-1.3 \pm 0.7
2008	-2.3 \pm 1.2	-2.5 \pm 1.1	-2.4 \pm 1.4	-2.4 \pm 1.2	-1.4 \pm 0.8	-3.1 \pm 0.6	-2.4 \pm 1.3	-1.9 \pm 1.0
2009	-2.4 \pm 1.5	-2.6 \pm 1.5	-2.2 \pm 1.4	-2.3 \pm 1.4	-1.3 \pm 0.8	-2.3 \pm 0.2	-2.7 \pm 1.6	-2.1 \pm 1.1
2010	-1.7 \pm 1.2	-1.9 \pm 1.2	-2.0 \pm 1.4	-1.6 \pm 0.9	-0.9 \pm 0.6	-2.2 \pm 0.3	-2.0 \pm 1.2	-1.2 \pm 0.7
2011	-1.9 \pm 1.0	-2.1 \pm 1.1	-1.7 \pm 1.1	-1.8 \pm 0.9	-1.4 \pm 0.7	-1.4 \pm 0.4	-2.1 \pm 1.0	-1.4 \pm 0.7
2012	-2.1 \pm 1.2	-2.3 \pm 1.2	-2.2 \pm 1.2	-2.0 \pm 1.1	-1.1 \pm 0.8	-1.7 \pm 0.8	-2.4 \pm 1.3	-1.6 \pm 0.9
2013	-4.4 \pm 1.7	-4.8 \pm 1.8	-5.2 \pm 1.8	-3.9 \pm 1.4	-3.1 \pm 1.1	-5.0 \pm 0.5	-4.5 \pm 1.8	-4.2 \pm 1.3
2014	-3.0 \pm 1.5	-3.1 \pm 1.5	-2.7 \pm 1.7	-3.0 \pm 1.4	-2.1 \pm 1.0	-2.7 \pm 0.2	-3.4 \pm 1.6	-2.7 \pm 1.1
2015	-2.4 \pm 1.4	-2.6 \pm 1.5	-2.4 \pm 1.5	-2.4 \pm 1.3	-1.4 \pm 0.9	-1.9 \pm 0.3	-2.8 \pm 1.5	-2.2 \pm 1.1
average	-2.6 \pm 1.4	-2.8 \pm 1.5	-2.8 \pm 1.5	-2.5 \pm 1.2	-1.6 \pm 0.8	-2.9 \pm 0.4	-2.9 \pm 1.5	-2.3 \pm 1.0

Table 3-S4: Clear-sky mean summer land surface temperature anomaly (°C) relative to the 2001-2015 mean for glaciated regions of the Queen Elizabeth Islands south of 80°N; ± 1 standard deviation.

Year	QEI	Agassiz IC	Axel Heiberg I	Devon & Coburg I	Manson IF	Meighen IC	Prince of Wales IF	Sydkap IC
2001	-0.38 \pm	-0.62 \pm	-0.79 \pm	0.07 \pm	-0.40 \pm	-2.38 \pm	-0.41 \pm	-0.68 \pm
	0.53	0.35	0.47	0.54	0.38	0.74	0.32	0.51
2002	-0.49 \pm	-0.34 \pm	-0.85 \pm	-0.61 \pm	-0.19 \pm	-0.50 \pm	-0.33 \pm	-0.55 \pm
	0.61	0.50	0.63	0.66	0.46	0.58	0.52	0.59
2003	-0.75 \pm	-0.98 \pm	-1.03 \pm	-0.62 \pm	-0.43 \pm	-0.57 \pm	-0.73 \pm	-0.88 \pm
	0.45	0.38	0.47	0.43	0.36	0.41	0.38	0.46
2004	-0.86 \pm	-0.79 \pm	-1.10 \pm	-0.75 \pm	-0.61 \pm	-0.49 \pm	-0.97 \pm	-0.74 \pm
	0.71	0.71	0.93	0.61	0.48	0.38	0.70	0.53
2005	0.60 \pm	0.61 \pm	0.77 \pm	0.57 \pm	0.50 \pm	0.90 \pm	0.57 \pm	0.72 \pm
	0.33	0.31	0.35	0.32	0.35	0.28	0.30	0.38
2006	-0.46 \pm	-0.79 \pm	-0.89 \pm	-0.21 \pm	-0.18 \pm	-0.76 \pm	-0.51 \pm	-0.11 \pm
	0.52	0.44	0.56	0.38	0.36	0.40	0.49	0.31
2007	0.97 \pm	1.22 \pm	1.28 \pm	0.70 \pm	0.68 \pm	1.26 \pm	1.04 \pm	1.05 \pm
	0.43	0.39	0.46	0.37	0.30	0.24	0.32	0.36
2008	0.41 \pm	0.44 \pm	0.59 \pm	0.12 \pm	0.33 \pm	-0.18 \pm	0.58 \pm	0.45 \pm
	0.42	0.44	0.39	0.33	0.28	0.45	0.38	0.39
2009	0.32 \pm	0.35 \pm	0.71 \pm	0.21 \pm	0.37 \pm	0.57 \pm	0.23 \pm	0.26 \pm
	0.35	0.24	0.39	0.28	0.22	0.30	0.30	0.36
2010	0.94 \pm	1.06 \pm	0.94 \pm	0.93 \pm	0.75 \pm	0.68 \pm	0.94 \pm	1.12 \pm
	0.49	0.40	0.45	0.48	0.47	0.22	0.54	0.46
2011	0.83 \pm	0.82 \pm	1.25 \pm	0.74 \pm	0.24 \pm	1.45 \pm	0.86 \pm	0.91 \pm
	0.59	0.46	0.55	0.56	0.45	0.28	0.55	0.52
2012	0.63 \pm	0.70 \pm	0.72 \pm	0.59 \pm	0.58 \pm	1.16 \pm	0.60 \pm	0.71 \pm
	0.44	0.48	0.61	0.39	0.30	0.68	0.38	0.46
2013	-1.66 \pm	-1.82 \pm	-2.27 \pm	-1.41 \pm	-1.42 \pm	-2.02 \pm	-1.56 \pm	-1.91 \pm
	0.64	0.54	0.62	0.58	0.55	0.72	0.55	0.64
2014	-0.30 \pm	-0.11 \pm	0.22 \pm	-0.44 \pm	-0.42 \pm	0.31 \pm	-0.45 \pm	-0.32 \pm
	0.47	0.31	0.36	0.49	0.39	0.44	0.37	0.40
2015	0.19 \pm	0.24 \pm	0.45 \pm	0.13 \pm	0.20 \pm	0.91 \pm	0.14 \pm	0.04 \pm
	0.31	0.31	0.33	0.29	0.21	0.26	0.27	0.33

Table 3-S5: 2001-2009 change in mean summer temperature, short- and longwave radiation, precipitation, and albedo for selected glaciated regions south of 80°N.

	Near-surface air temperature (°C yr ⁻¹) ^a	Incoming SW radiation (Wm ⁻² yr ⁻¹) ^a	Outgoing SW radiation (Wm ⁻² yr ⁻¹) ^a	Incoming LW radiation (Wm ⁻² yr ⁻¹) ^a	Outgoing SW radiation (Wm ⁻² yr ⁻¹) ^a	Summer precipitation (kg m ⁻² yr ⁻¹) ^a	Annual precipitation (kg m ⁻² yr ⁻¹) ^a	BSA (yr ⁻¹) ^b	LST (°C yr ⁻¹) ^c
QEI	0.10	0.48	-0.61	-0.15	0.38	-596.2	-3532.0	-0.007	0.16
Axel Heiberg I	0.32	-0.10	-3.85	0.02	1.47	-763.1	-4572.7	-0.014	0.25
Devon & Coburg I	0.14	-0.26	-0.35	0.51	0.56	-278.2	-2459.8	-0.007	0.10
Manson IF	0.01	-0.27	-0.14	0.20	0.06	-429.2	-3059.0	-0.007	0.12
Prince of Wales IF	0.01	1.37	0.54	-0.71	-0.12	-771.0	-3878.9	-0.005	0.16
Sydkap IC	0.28	-0.58	-3.49	0.47	1.35	-755.1	-4068.1	-0.009	0.19

^a variables from the CanRCM4, summer (JJA) averages computed from daily averages

^b mean summer clear-sky shortwave broadband black-sky albedo from MCD34A3 data

^c mean summer clear-sky land surface temperature from MOD11A1 data

Table 3-S6: Eight year average (2001-2009) mean summer temperature, short- and longwave radiation, precipitation, and albedo for selected glaciated regions south of 80°N.

	Near-surface air temperature (°C) ^a	Incoming SW radiation (W m ⁻²) ^a	Outgoing SW radiation (W m ⁻²) ^a	Incoming LW radiation (W m ⁻²) ^a	Outgoing SW radiation (W m ⁻²) ^a	Total summer precipitation (kg m ⁻²) ^a	Total annual precipitation (kg m ⁻²) ^a	BSA ^b	LST (°C) ^c
QEI	-3.18	254.2	190.8	260.0	297.3	10333.4	88300.8	0.56	-2.76
Axel Heiberg I	-1.40	238.3	154.2	266.2	308.2	8743.7	69379.2	0.50	-3.08
Devon I & Coburg I	-2.61	251.5	185.2	261.7	299.1	11923.2	104068.8	0.58	-2.60
Manson IF	-1.90	237.1	177.1	275.6	304.4	11923.2	116683.2	0.53	-1.67
Prince of Wales IF	-4.45	268.0	213.9	252.0	290.3	10333.4	88300.8	0.58	-3.01
Sydkap IC	-0.26	214.7	129.5	280.6	313.9	11128.3	94608.0	0.55	-2.40

^a variables from the CanRCM4, summer (JJA) averages computed from daily averages

^b mean summer clear-sky shortwave broadband black-sky albedo from MCD34A3 data

^c mean summer clear-sky land surface temperature from MOD11A1 data

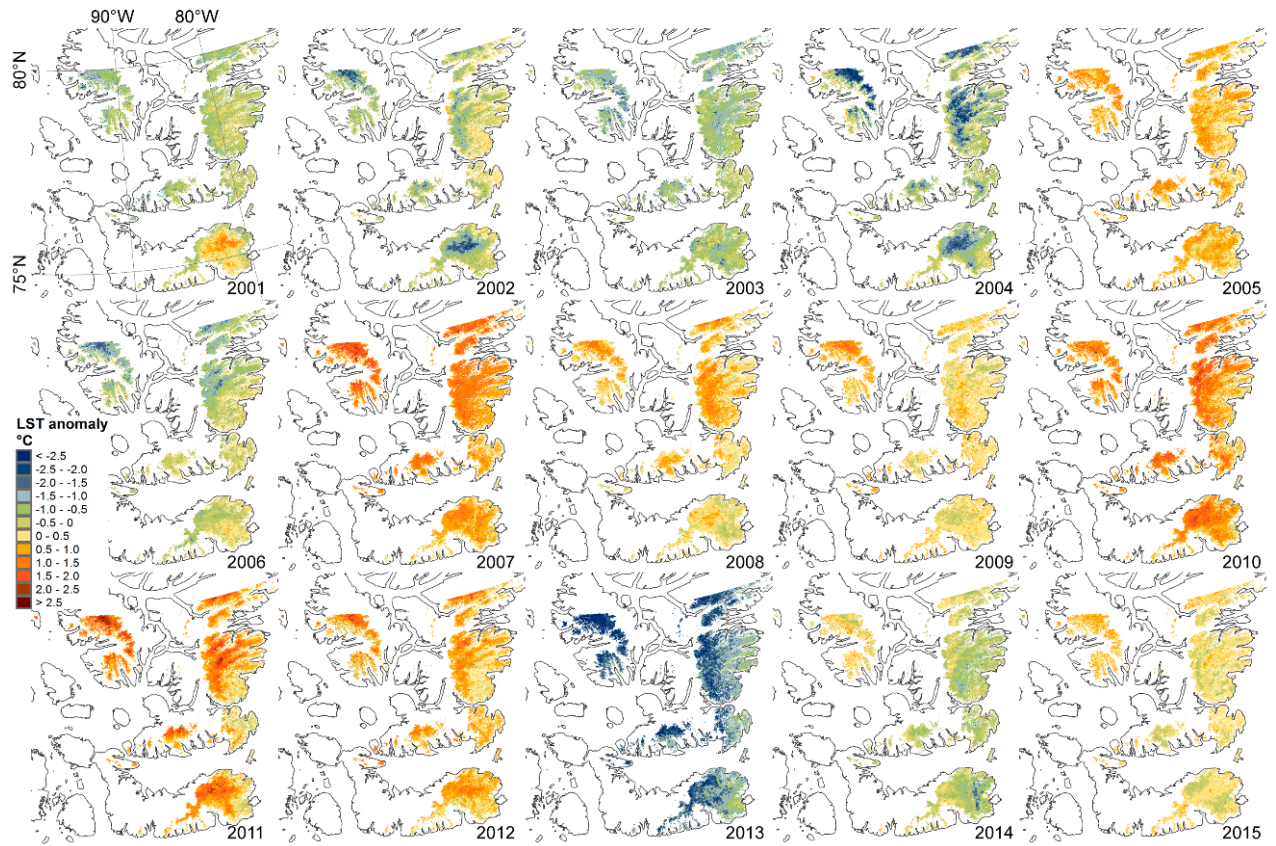


Figure 3-S1: Clear-sky mean summer land surface temperature anomaly (°C) relative to the 2001-2015 mean for glaciated regions of the Queen Elizabeth Islands south of 80°N.

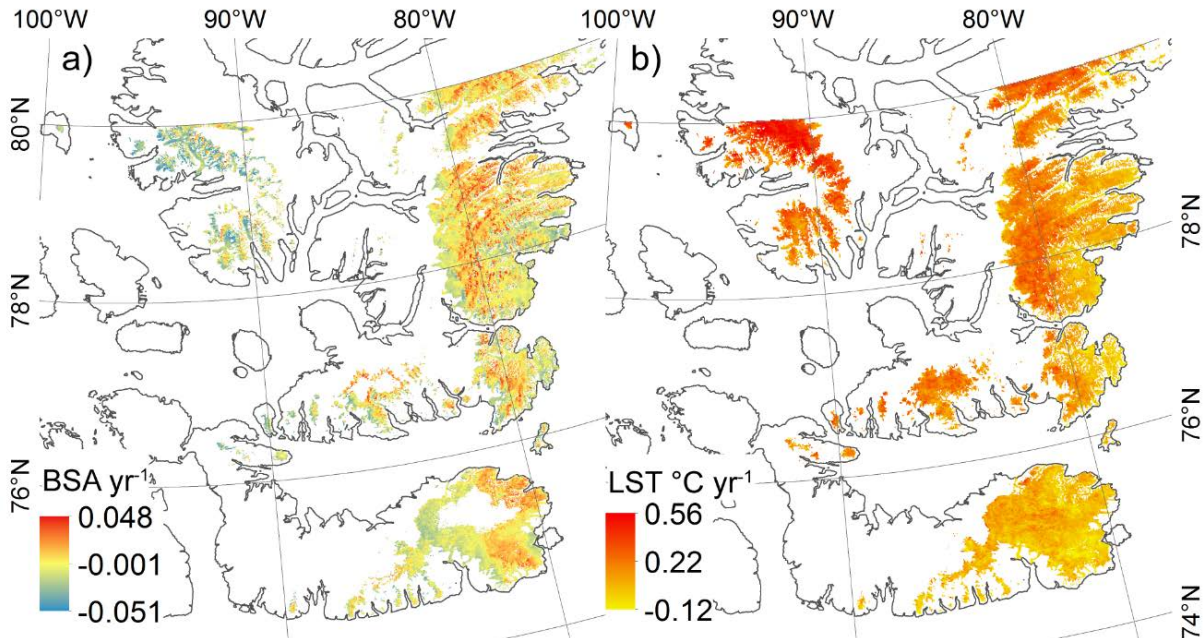


Figure 3-S2: Linear rate of change in (a) mean summer clear-sky shortwave broadband black-sky albedo (yr^{-1}) and (b) mean summer clear-sky land surface temperature ($^{\circ}\text{C yr}^{-1}$) for 2001-2009 for the Queen Elizabeth Islands south of 80°N for pixels having seven or more mean summer (JJA) observations.

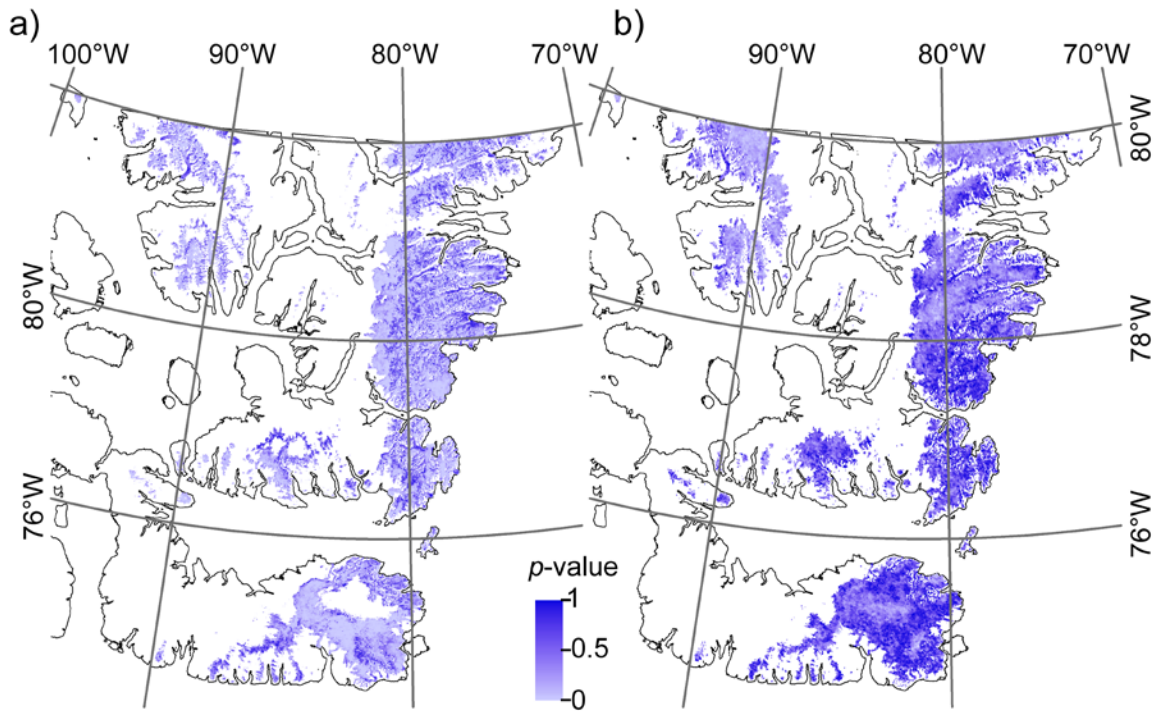


Figure 3-S3: p-value for linear regression of the 15 year BSA (a) and LST (b) records shown in figures 4-4a and 4-4b.

3.7 References

- Ackerman, S. A., K. I. Strabala, P. W. Menzel, R. A. Frey, C. C. Moeller, and L. E. Gumley (1998), Discriminating clear sky from clouds with MODIS, *J. Geophys. Res.*, *103*(D24), 32141–32157, doi:10.1029/1998JD200032.
- Alexander, P. M., M. Tedesco, X. Fettweis, R. S. W. van de Wal, C. J. P. P. Smeets, and M. R. van den Broeke (2014), Assessing spatiotemporal variability and trends in modeled and measured Greenland Ice Sheet albedo (2000-2013), *The Cryosphere*, *8*(6), 2293-2312, doi: 10.5194/tc-8-2293-2014.
- Alt, B. T. (1987), Developing synoptic analogs for extreme mass balance conditions on Queen Elizabeth Island ice caps, *Journal of Applied Climate*, *26*(12), 1605-1623, doi: 10.1175/1520-0450(1987)026<1605:DSAFEM>2.0.CO;2.
- Arendt, A., et al. (2012), Randolph Glacier Inventory Vers. 3.0: a dataset of Global Glacier Outlines. Global Land Ice Measurements from Space, Boulder, CO. Digital media: http://www.glims.org/RGI/rgi32_dl.html.
- Bezeau, P., M. Sharp, and G. Gascon (2015), Variability in summer anticyclonic circulation over the Canadian Arctic Archipelago and west Greenland in the late 20th/early 21st centuries and its effects on glacier mass balance, *Int. J. Climatol*, *35*(4), 540-557, doi:10.1002/joc.4000.
- Box, J. E., X. Fetwweis, J. C. Stroeve, M. Tedesco, D.K. Hall, and K. Steffen (2012), Greenland ice sheet albedo feedback: thermodynamics and atmospheric drivers, *Cryosphere*, *6*(4), 821-839, doi: 10.5194/tc-6-821-2012.
- Braithwaite, R. J. (2005), Mass balance characteristics of arctic glaciers, *Ann. Glaciol.*, *42*, 225-229, doi: 10.3189/17275640578182899.
- Casey, K. A., C. M. Polashenski, J. Chen, and M. Tedesco (2016), Impact of MODIS sensor calibration updates on Greenland Ice Sheet albedo trends, AGU annual fall meeting, 12 December, C13B-0813.
- Clarke, A. D., and K. J. Noone (1985), Soot in the Arctic snowpack: a cause for perturbations in radiative transfer, *Atmospheric Environment*, *19*(12), 2045-2053, doi: 10.1016/0004-6981(85)90113-1.

- Colbeck, S. C. (1982), An overview of seasonal snow metamorphism, *Rev. Geophys.*, 20(1), 45-61, doi: 10.1029/RG020i001p00045.
- Conway, H., A. Gades, and C.F. Raymond (1996), Albedo of dirty snow during conditions of melt, *Water Resour. Res.*, 32(6), 1716-1718, doi: 10.1029/96WR00712.
- Cuffey, K. M. and W. Paterson (2010), *The physics of glaciers*, 4th edn. Butterworth-Heinemann, Oxford.
- Doherty, S. J., S. G. Warren, T. C. Grenfell, A. D. Clarke, and R. E. Brandt (2010), Light absorbing impurities in Arctic snow, *Atmos. Chem Phys*, 10(23), 11647-11680, doi: 10.5194/acp-10-11647-2010.
- Doherty, S. J., T. C. Grenfell, S. Forsstrom, D. L. Hegg, R. E. Brandt, and S. G. Warren (2013), Observed vertical redistribution of black carbon and other insoluble light-absorbing particles in melting snow, *J. Geophys. Res.-Atmos.*, 118(11), 5553-5569, doi: 10.1002/jgrd.50235.
- Dumont, M., E. Brun, G. Picard, M. Michou, Q. Libois, J. R. Petit, M. Geyer, S. Morin, and B. Josse (2014), Contribution of light absorbing impurities in snow to Greenland's darkening since 2009, *Nat. Geosci.*, 7(7), 509-512, doi: 10.1038/ngeo2180.
- Flanner, M. G., C. S. Zender, J. T. Randerson, and P. J. Rasch PJ (2007), Present-day climate forcing and response from black carbon in snow, *J. Geophys. Res.*, 112, D11202, doi:10.1029/2006JD008003.
- Flato, G. M., G. J. Boer, W. G. Lee, N. A. McFarlane, D. Ramsden, M. C. Reader, and A. J. Weaver (2000), The Canadian Centre for Climate Modelling and Analysis global coupled model and its climate, *Climate Dynamics*, 16(6), 451-467, doi: 10.1007/s003820050339.
- Fountain, A.G., M. Tranter, T. H. Nylén, and D. R. Müller (2004), Evolution of cryoconite holes and their contribution to meltwater runoff from glaciers in the McMurdo Dry Valleys, Antarctica, *J. Glaciol.*, 50(168), 35-45, doi: 10.3189/172756504781830312.
- Gardner, A. S., and M. Sharp (2007), Influence of the Arctic circumpolar vortex on the mass balance of Canadian high Arctic glaciers, *J. Climate*, 20(18), 4586-4598, doi: 10.1175/JCLI4268.1.

- Gardner, A. S., et al. (2013), A reconciled estimate of glacier contributions to sea level rise: 2003 to 2009, *Science*, 340(6134), 852-857, doi:10.1126/science.1234532.
- Gao, F., C. B. Schaaf, A. H. Strahler, A. Roesch, W. Lucht, and R. Dickenson (2005), MODIS bidirectional reflectance distribution function and albedo Climate Modelling Grid products and the variability of albedo for major vegetation types, *J. Geophys. Res.-Atmos.*, 110, D01104, doi: 10.1029/2004JD005190.
- Gascon, G., M. Sharp, and A. Bush (2013), Changes in melt season characteristics on Devon Ice Cap, Canada, and their association with the Arctic atmospheric circulation, *Ann. Glaciol.*, 54, 101–110, doi:10.3189/2013AoG63A601.
- Greuell, W., J. Kohler, F. Obleitner, P. Glowacki, K. Melvold, E. Bernsen, and J. Oerlemans (2007), Assessment of interannual variations in the surface mass balance of 18 Svalbard glaciers from the Moderate Resolution Imaging Spectroradiometer/Terra albedo product, *J. Geophys. Res.*, 112, D07105, doi: 10.1029/2006JD007245.
- Hall, D. K. J. E. Box, K. A. Casey, S. J. Hook, C. A. Shuman, and K. Steffen (2008a), Comparison of satellite-derived and in-situ observations of ice and snow surface temperatures over Greenland, *Remote Sens. Environ.*, 112(10), 3739-3749, doi: 10.1016/j.rse.2008.05.007.
- Hall, D. K., R. S. Williams, S. B. Luthcke, and N. E. DiGirolamo (2008b), Greenland ice sheet surface temperature, melt and mass loss: 2000–2006, *J. Glaciol.*, 54(184), 81–93, doi:10.3189/002214308784409170.
- Hall, D. K., J. C. Comiso, N. E. DiGirolamo, C. A. Shuman, J. R. Key, and L. S. Koenig (2012), A satellite-derived climate-quality data record of the clear-sky surface temperature of the Greenland ice sheet, *J. Clim.*, 25, 4785-4798, doi: 10.1175/JCLI-D-11-00365.1.
- He, T., S. L. Lian, and D. X. Song (2014), Analysis of global land surface albedo climatology and spatial-temporal variation during 1981-2010 from multiple satellite products, *J. Geophys. Res.-Atmos.*, 119(17), 10281-10298, doi: 10.1002/2014/JD021667.
- Jin, Y., C. B. Schaaf, C. E. Woodcock, F. Gao, X. Li, and A. H. Strahler (2003), Consistency of MODIS surface BRDF/Albedo retrievals: 1. Algorithm performance, *J. Geophys. Res.* 108(D5), 4158, doi: 10.1029/2002JD002803.

Kalnay, E., et al. (1996), The NCEP/NCAR 40 year reanalysis project, *Bull. Am. Meteorol. Soc.*, 77(3), 437–471, doi:10.1175/1520-0477(1996)077<0437:TNYRP>2.0.CO;2.

King, M. D., S. Platnick, P. Yang, G. T. Arnold, M. A. Gray, J. C. Ridei, S. A. Ackerman, and K. N. Liu (2004), Remote Sensing of Liquid Water and Ice Cloud Optical Thickness and Effective Radius in the Arctic: Application of Airborne Multispectral MAS Data, *J. Atmos. Ocean. Technol.*, 21(6), 857–875, doi:10.1175/1520-0426(2004)021<0857:RSOLWA>2.0.CO;2.

Koenig, L. S., and D. K. Hall (2010), Comparison of satellite, thermochron and station temperatures at Summit, Greenland, during the winter of 2008/09, *J. Glaciol.*, 56(198), 735-741 (doi: 10.3189/002214310793146269).

Koerner, R. M. (1977), Devon Island ice cap: core stratigraphy and paleoclimate, *Science*, 196(4285), 15-18, doi: 10.1126/science.196.4285.15.

Koerner, R. M. (1979), Accumulation, ablation, and oxygen isotope variations on the Queen Elizabeth Islands ice caps, Canada, *J. Glaciol.*, 22(86), 25-41.

Koerner, R. M. (2005), Mass balance of glaciers in the Queen Elizabeth Islands, Nunavut, Canada, *Ann. Glaciol.*, 42, 417–423, doi:10.3189/172756405781813122.

Land Processes Distributed Active Archive Center (LP DAAC) USGS EROS Data Center (2004) MODIS Land data operational product evaluation (LDOPE) tools, Release 1.4, 30 April 2001, LDOPE Tools User's Manual, 103 pages.

Land Processes Distributed Active Archive Center (LP DAAC), MODIS Albedo 16-day Level 3 Global 500 m Grid SIN Version 5 (MCD43A3v05). NASA EOSDIS Land Processes DAAC, USGS Earth Resources Observation and Science (EROS) Center, Sioux Falls, South Dakota (<https://lpdaac.usgs.gov>), accessed September 2014 - October 2016 at <http://e4ftl01.cr.usgs.gov>.

Land Processes Distributed Active Archive Center (LP DAAC), MODIS Level 3 Global 1 km Grid SIN Version 5. NASA EOSDIS Land Processes DAAC, USGS Earth Resources Observation and Science (EROS) Center, Sioux Falls, South Dakota (<https://lpdaac.usgs.gov>), accessed September 2014 - October 2015 at <http://e4ftl01.cr.usgs.gov>.

- Lenaerts, J. T. M., J. H. van Angelen, M. R. van den Broeke, A. S. Gardner, B. Wouters, and E. van Meijgaard (2013), Irreversible mass loss of Canadian Arctic Archipelago glaciers, *Geophys. Res. Lett.*, *40*(5), 870–874, doi:10.1002/grl.50214.
- Liu, J., C. B. Schaaf, A. H. Strahler, Z. Jiao, Y. Shuai, Q. Zhang, M. Román, J. A. Augustine, and E. G. Dutton (2009), Validation of Moderate Resolution Imaging Spectroradiometer (MODIS) albedo retrieval algorithm: Dependence of albedo on solar zenith angle, *J. Geophys. Res.-Atmos.*, *114*, D01106, doi:10.1029/2008JD009969.
- Lucht, W., C. B. Schaaf, and A. H. Strahler (2000), An algorithm for the retrieval of albedo from space using semiempirical BRDF models, *IEEE Transactions on Geoscience and Remote Sensing*, *38*, 977-998.
- Lyapustin, A., Y. Wang, X. Xiong, G. Meister, S. Platnick, R. Levy, B. Franz, S. Korin, T. Hilker, J. Tucker, F. Hall, P. Sellers, A. Wu, and A. Angal (2014), Scientific impact of MODIS C5 calibration degradation and C6+ improvements, *Atmos. Meas. Tech.*, *7*(12), 4353-4365, doi:10.5194/amt-7-4353-2014.
- Mortimer, C. A., M. Sharp, and B. Wouters (2016), Glacier surface temperatures in the Canadian high arctic, 2000-2015, *J. Glaciol.*, *62*(23), 963-975, doi: 10.1017/jog.2016.80.
- Namazi, M., K. Von Salzes, and J. N. S. Cole (2015), Simulation of black carbon in snow and its climate impact in the Canadian Global Climate Model, *Atmos. Chem. Phys.*, *15*(18), 10887-10904, doi: 10.5194/acp-15-10887-2015.
- Pfeffer, W. T. et al. (2014), The Randolph Glacier Inventory: a globally complete inventory of glaciers, *J. Glaciol.*, *60*(221), 537-552, doi:10.3189/2014JoG13J176.
- Polashenski, C. M., J. E. Dibb, M. G. Flanner, J. Y. Chen, Z. R. Courville, A. M. Lai, J. J. Schauer, M. M. Shafer and M. Bergin (2015), Neither dust nor black carbon causing apparent albedo decline in Greenland's dry snow zone: Implications for MODIS C5 surface reflectance, *Geophys. Res. Lett.*, *42*(12), 9319-9327, doi: 10.1002/2015GL065912.
- Rajewicz, J., and S. J. Marshall SJ (2014), Variability and trends in anticyclonic circulation over the Greenland ice sheet, 1948-2013, *Geophys. Res. Lett.*, *41*(8), 2842-2850, doi:10.1002/2014GL059255.

- Román, M. O., C. B. Schaaf, P. Lewis, F. Gao, G. P. Anderson, J. L. Privette, A. H. Strahler, C. E. Woodcock, and M. Barnsley (2010), Assessing the coupling between surface albedo derived from MODIS and the fraction of diffuse skylight over spatially-characterized landscapes, *Remote Sens. Environ.*, 114(4), 738-760, doi: 10.1016/j.rse.2009.11.014.
- Salomon, J. G., C. B. Schaaf, A. H. Strahler, F. Gao, and Y. Jin (2006), Validation of the MODIS Bidirectional Reflectance Distribution Function and Albedo retrievals using combined observations from the Aqua and Terra platforms, *IEEE Transactions on Geoscience and Remote Sensing*, 44(6), 1555-1565.
- Schaaf, C. B., et al. (2002), First operational BRDF, albedo nadir reflectance products from MODIS, *Remote Sens. Environ.*, 83(1), 135-148, doi: 10.1016/S0034-4257(02)00091-3.
- Schaaf, C. L. B., J. Liu, F. Gao, and A. H. Strahler (2011a), MODIS albedo and reflectance anisotropy products from Aqua and Terra. In B. Ramachandran Justice C and M Abrams (Eds), Land remote sensing and global environmental change: NASA's earth observing system and the science of ASTER and MODIS. Remote Sensing and Digital Image Processing Series, vol 11, Springer-Verlag (873 pp).
- Schaaf, C. B., Z. Wang, and A. H. Strahler (2011b), Commentary on Wang and Zender – MODIS snow albedo bias at high solar zenith angles relative to theory and in situ observations in Greenland, *Remote Sens. Environ.*, 115(5), 1296-1300, doi: 10.1016/j.rse.2011.01.002.
- Sharp, M., D. O. Burgess, J. G. Cogley, M. Ecclestone, C. Labine, and G. J. Wolken (2011), Extreme melt on Canada's Arctic ice caps in the 21st century, *Geophys. Res. Lett.*, 38(11), L11501, doi:10.1029/2011GL047381.
- Sharp, M., et al. (2015) [Arctic] Glaciers and ice caps (outside Greenland [in "State of the Climate 2014"], *Bull. Am. Meteorol. Soc.*, 96(7), 135-137.
- Strabala, K. I., S. A. Ackerman, and W. P. Menzel (1994), Cloud Properties inferred from 8–12- μm Data, *J. Appl. Meteor.*, 33(2), 212–229, doi:10.1175/15200450(1994)033<0212:CPIFD>2.0.CO;2.
- Strahler, A. H., et al. (1999), MODIS BRDF/Albedo product: algorithm theoretical basis document version 5.0.

Stroeve, J. C., J. Box, F. Gao, S. Liang, A. Nolin, and C. Schaaf (2005), Accuracy assessment of the MODIS 16-day albedo product for snow: Comparison with Greenland in situ measurements, *Remote Sens. Environ.*, *94*(1), 46-60, doi: 10.1016/j.rse.2004.09.001.

Stroeve, J. C., J. Box, and T. Haran (2006), Evaluation of the MODIS (MOD10A1) daily snow albedo product over the Greenland Ice Sheet, *Remote Sens. Environ.*, *105*(2), 155-171, doi: 10.1016/j.rse.2006.06.009.

Stroeve, J., J. E. Box, Z. Wang, C. Schaaf, and A. Barret (2013), Re-evaluation of MODIS MCD43 Greenland albedo accuracy and trends, *Remote Sens. Environ.*, *138*, 199-214, doi: 10.1016/j.rse.2013.07.023.

Strugnell, N., and W. Lucht (2001), Continental-scale albedo inferred from AVHRR data, land cover class and field observations of typical BRDFs, *J. Clim.*, *14*(7), 1360-1376, doi: 10.1175/1520-0442(2001)014<1360:AATICS>2.0.CO;2.

Tedesco M., S. Doherty, X. Fettweis, P. Alexander, J. Jeyaratnam, and J. Stroeve (2016), The darkening of the Greenland ice sheet: trends, drivers, and projections (1981-2100), *The Cryosphere*, *10*, 477-496, doi: 10.5194/tc-10-477-2016.

van den Broeke, M. R., C. J. P. P. Smeets, and R. S. W. van de Wal (2011), The seasonal cycle and interannual variability of surface energy balance and melt in the ablation zone of the west Greenland ice sheet, *The Cryosphere*, *5*(2), 377-390, doi: 10.5194/tc-5-377-2011.

Vermote, E. F., S. Y. Kotchenova, and J. P. Ray (2011), MODIS surface reflectance user's guide. MODIS Land Surface Reflectance Science Computing Facility, version 1.

von Salzen, K., J. F. Scinocca, N. A. McFarlane, J. Li, J. N. S. Cole, D. Plummer, D. Verseghy, M. C. Reader, X. Ma, M. Lazare, and L. Solheim (2013), The Canadian Fourth Generation Atmospheric Global Climate Model (CanAM4). Part I: representation of physical processes, *Atmosphere-Ocean*, *51*(1), 104-125, doi: 10.1080/07055900.2012.755610.

Wan, Z., Y. Zhang, Q. Zhang, and Z. L. Li (2002), Validation of the land-surface temperature products retrieved from Terra Moderate Resolution Imaging Spectroradiometer data, *Remote Sens. Environ.*, *83*(1-2), 163–180, doi:10.1016/S0034-4257(02)00093-7.

- Wan, Z. M. (2008), New refinements and validation of the MODIS Land-Surface Temperature/Emissivity products, *Remote Sens. Environ.*, *112*(1), 59–74, doi:10.1016/j.rse.2006.06.026.
- Wang, Z., C. B. Schaaf, M. J. Chopping, A. H. Strahler, J. Wang, M. O. Román, A. V. Rocha, C. E. Woodcock, and Y. Shuai (2012), Evaluation of Moderate-resolution Imaging Spectroradiometer (MODIS) snow albedo product (MCD43A) over tundra, *Remote Sens. Environ.*, *117*, 264-280, doi: 10.1016/j.rse.2011.10.002.
- Wanner, W., A. H. Strahler, B. Hu, P. Lewis, J. P. Muller, X. Li, C. L. B. Schaaf, and M. J. Barnsley (1997), Global retrieval of bidirectional reflectance and albedo over than from EOS MODIS and MISR data: theory and algorithm, *J. Geophys. Res.* *102*(D14), 17143-17162, doi: 10.1029/96JD03295.
- Warren, S. G. (1982), Optical properties of snow, *Reviews of Geophysics*, *20*(1), 67-89, doi: 10.1029/RG020i001p00067.
- Warren, S. G., and W. J. Wiscombe (1980), A model for the spectral albedo of snow. II Snow containing atmospheric aerosols, *J. Atmos. Sci.*, *37*(12), 2734-2745, doi: 10.1175/1520-0469(1980)037<2734:AMFTSA>2.0.CO;2.
- Wiscombe, W. J., and S. G. Warren (1980), A model for the spectral albedo of snow. I: Pure snow, *J. Atmos. Sci.*, *37*(12), 2712-2732, doi: 10.1175.1520-0469(1980)037<2712:AMFTSA>2.0.CO;2.
- Zadra, A., D. A. Caya, J. E. Cote, B. E. Dugas, C. Jones, R. E. Laprise, K. A. Winger, and L. P. Caron (2008), The next Canadian regional climate model, *Phys. Can.*, *64*(2), 75-83.

Chapter 4

Influence of recent warming and ice dynamics on glacier surface elevations in the Canadian High Arctic, 1995-2014

4.0 Abstract

Repeat airborne laser altimetry measurements show widespread thinning (surface lowering) across glaciated surfaces in Canada's Queen Elizabeth Islands (QEI) since 1995. Rates of thinning, averaged for 50 m elevation bins, were more than three times larger from 2005/06 to 2012/14 than during the previous two pentads. Strong negative dh/dt anomalies from 2005/06 to 2012/14, relative to the 1995-2012/14 mean, suggest that most of the measured thinning occurred during the most recent 5-6 year period when mean summer land surface temperatures (LSTs) were anomalously high and the mean summer black-sky shortwave broadband albedo (BSA) was anomalously low, relative to the 2000/01-2015 period, and upper-air (700 hPa) and near surface (2 m) air temperatures were between 0.8°C and 1.5°C warmer than the 1995-2012 mean. Comparisons of dh/dt with mean summer LST and BSA measurements from the Moderate Resolution Spectroradiometers (MODIS) and surface longitudinal strain rates, computed from surface velocity fields derived from RADARSAT 1/2, and LandSat-7 EMT+ data, suggest that surface elevation changes were driven mainly by changes in climate, except along most fast-flowing outlet glaciers where changes in ice dynamics seem to have played an important role. Where longitudinal strain rates were high ($|du/dx|$ in excess of 0.01 yr⁻¹; e.g. on sections of the Otto, Antoinette, Wykeham, Ekblaw, Southeast 1 and 2 glaciers) there was generally good correspondence between regions of compressive (extensional) flow and thickening (thinning).

4.1 Introduction

Cumulative mass loss from glaciers and ice caps in the Canadian Arctic (which includes the Queen Elizabeth Islands (QEI)) from 2002/03 to 2014/15, estimated using data from the Gravity Recovery and Climate Experiment (GRACE), was -762.6 Gt [*Sharp et al.*, 2015]). Glacier mass balances in the QEI which contains 14% of the global glacier area outside of the major ice sheets of Greenland and Antarctica, have been consistently negative since measurements began in the late 1950s [*Koerner*, 2005; *Sharp et al.*, 2011], and the rate of mass loss from the region nearly tripled between 2004-2006 and 2007-2009 [*Gardner et al.*, 2011; *Lenaerts et al.*, 2013; *Millan et al.*, 2017]. Changes in the elevation of a glacier surface are controlled by the basal-climatic mass balance of the glacier (the sum of the climatic and basal mass balances) and by ice dynamics. For a glacier in steady state, the climatic mass balance of a region of a glacier (the sum of the surface and internal mass balances) is balanced by the flux divergence (the difference between the vertically integrated mass fluxes into and out of the region) [*Cogley et al.*, 2011]. In the QEI, glacier mass change for the period 1991-2015 was attributed primarily to the surface mass balance, with ice dynamics accounting for only ~10% of observed mass loss [*Millan et al.*, 2017].

In a glacier's accumulation zone, warmer air and surface temperatures increase both the amount of melt and the depth of meltwater percolation into the firn layer, simultaneously raising the near-surface ice/firn temperature through latent heat release during freezing and increasing the rate of firn densification [*Pfeffer and Humphrey*, 1998; *Zdanowicz et al.*, 2012; *Bezeau et al.*, 2013]. These processes both result in lowering of the glacier's surface elevation. In the ablation area, where bare glacier ice is exposed at the surface during the summer, warmer summer mean air and surface temperatures result in increased melting and mass loss, and thus in glacier thinning. Changes in surface accumulation rates (via solid precipitation, wind redistribution of snow, and/or

avalanching) can also alter the elevation of the glacier surface. However, annual precipitation in the QEI is low (<400 mm w.e. yr^{-1} , *Braithwaite, 2005*) and inter-annual variability in precipitation is small compared to variability in melt rates. Inter-annual variability and longer term trends in the annual mass balance of QEI glaciers are thus controlled primarily by variability in summer air temperatures and melt [*Koerner, 2005*].

Recent increases in summer melt rates, inferred from QEI summer land surface temperatures (LST) (which increased by nearly 1°C from 2000-2015; *Mortimer et al., 2016*), are therefore expected to have resulted in thinning of these ice masses unless there was a compensating reduction in rates of ice flow. Higher air and surface temperatures drive decreases in albedo (the ratio of outgoing to incoming solar radiation) which enhance surface warming and/or melt, leading to further decreases in the surface albedo [*Warren and Wiscombe, 1980; Colbeck, 1982*]. This positive ice-albedo feedback was observed over the majority of the QEI ice cover (south of 80°N) from 2001-2015, when the regional glacier mean summer black-sky shortwave broadband albedo (BSA) decreased by 0.057 [*Mortimer and Sharp, in review*], and is expected to have enhanced surface melt rates and glacier thinning.

Changes in ice flow, inferred from variations in ice surface velocity, alter the mass transferred into and/or out of a region of a glacier, resulting in localized thinning or thickening. Flow velocities of outlet glaciers in the QEI can be highly variable [e.g. *Short and Gray, 2005; Burgess and Sharp, 2008; Williamson et al., 2008*] and may result in changes in ice thickness that are largely independent of changes in climate. Surface velocities on QEI glaciers and ice-caps were relatively stable over the period 1991-2015, except along outlet glaciers where large variations in velocity ($> \sim 20$ m yr^{-1}) were common [*van Wychen et al., 2016, 2017; Millan et al., 2017*]. Rapid changes in surface velocity in the eastern QEI during this period were linked to changes in glacier thickness

[*van Wychen et al.*, 2016]. However, such comparisons were limited to only three glaciers (Dobbin, Parrish, and Trinity), and the extent to which recent changes in glacier surface elevation elsewhere in the QEI are linked to changes in ice dynamics is not well known.

Repeat airborne altimetry measurements made over ice caps in the QEI in 1995 and 2000 revealed overall thinning (generally $<0.5 \text{ m yr}^{-1}$) during this 5-year period, although strong thinning at lower elevations was replaced by thickening at higher elevations in the interior of most ice masses [*Abdalati et al.*, 2004]. Using the flux imbalance method, *Colgan et al.* [2008] inferred thickening (or no change in surface elevation) in the northwest sector of the Devon Ice Cap during this same time-period, and thinning in the southeast. However, it is not known whether these spatial patterns of glacier and ice cap surface elevation change have persisted to the present day. Repeat satellite laser altimetry revealed QEI-wide surface lowering (average dh/dt : $-0.38 \pm 0.04 \text{ m yr}^{-1}$) between 2003 and 2009 [*Gardner et al.*, 2011, 2013], but the relative contributions of changes in climatic mass balance and ice dynamics to the rate of elevation change (dh/dt) were not examined. Here, spatial and temporal patterns in rates of glacier surface elevation change (dh/dt) for the period 1995-2014 are investigated from repeat-track airborne altimetry data collected over the QEI from NASA's Airborne Topographic Mapper (ATM). Changes in remotely-sensed ice surface temperature, albedo, and surface longitudinal strain rates are compared with measured changes in dh/dt to qualitatively assess the relative influences of changes in the climatic mass balance and ice dynamics on glacier and ice cap surface elevations between 2000 and 2014.

4.2 Data and methods

4.2.1 Repeat airborne altimetry measurements

Repeat-track measurements of glacier and ice cap surface elevations in the QEI were acquired by airborne laser altimetry in the springs of 1995, 2000, 2005, 2006, 2011, 2012, 2014, and 2015 using NASA's Airborne Topographic Mapper (ATM) conical laser scanning system(s) [Krabill, 2010, 2012]. The conical laser scanner emits sequential pulses of energy towards the Earth's surface. The time taken for an emitted pulse to return to the receiver, known as the two-way travel time (TWTT), is recorded by the sensor [Martin *et al.*, 2012]. Precise measurements of the aircraft positioning and attitude, obtained from inertial sensors (accelerometer and gyroscope) and GPS systems, are then used to compute surface elevations from the TWTT. The ATM T1 10° off-nadir scanner system, which has a 140 m wide swath, 1-3 m footprint, ground spacing of 2-5 m (depending on aircraft speed), and nominal vertical accuracy of <0.2 m, was used in 1995 [Krabill *et al.*, 2002; Abdalati *et al.*, 2004]. From 2000 to 2006 (pre-Operation IceBridge) data were collected using the ATM T2 15° system (250 m swath width, 1 m footprint, ~2 m ground spacing (depending on aircraft speed), nominal vertical accuracy of <0.2m; Krabill *et al.*, 2002; Abdalati *et al.*, 2004; Krabill, 2014ab). Between 2011 and 2015, the ATM T4 30° system (230 m swath width, 0.5 m footprint, measurement density of 1 laser shot per <1 m², nominal vertical accuracy <0.1 m) was used [Martin *et al.*, 2012; Krabill, 2014ab].

Comparison of the surface elevations of coincident points measured in different airborne altimetry surveys enables calculation of the rate of elevation change between the two surveys at a specific location. NASA's Level 4 Surface Elevation Rate of Change, Version 1 product (IDHDT4; Krabill, 2014a) uses the ATM wide-scan Level 1B Qfit Elevation and Return Strength dataset to obtain estimates of surface elevation change. The IDHDT4 routine identifies locations where the track spacing of overlapping data from two different campaign years (referred to as the reference and test data) is < 200 m. For each reference data point, all test data points within a 2.5 m search

radius are identified. If the number of data pairs for a given reference data point is > 500 , the absolute surface elevation difference for each data pair is computed. Data pairs having an absolute elevation difference > 300 m are removed and dh/dt for a given overlap location is computed by dividing the average elevation change of all remaining data pairs by the time-period between measurements [Krabill, 2014b]. Outputs are provided as discrete points with a nominal spatial resolution 250 m x 250 m, referenced to the WGS84 ellipsoid. IDHDT4 surface elevation change estimates do not account for crustal uplift, which for the QEI was estimated to be < 7 mm yr⁻¹ from continuous dGPS measurements made between 2008 and 2014 at a station on bedrock adjacent to the Devon Ice Cap (B. Danielson pers. comm. 2015). Elevation measurement accuracy from NASA's ATM instruments is < 10 cm [Krabill et al., 2002] and < 5.4 cm for the more recent scanner systems [Kwok et al., 2012; Martin et al., 2012]. Uncertainty assessments specific to the IDHDT4 product are not provided since the ILATM1B data, which are used as input, undergo extensive quality assessment. Instead, the RMS error (largely dependent on surface roughness) and the number of points used in each calculation are provided and can be combined with visual interpretation of graphical outputs to qualitatively interpret the accuracy of the data [Krabill, 2014b]. Investigation of these parameters revealed no clear relationships between rates of elevation change, RMS error, number of data points, and location, so no additional filtering beyond that described below was performed.

IDHDT4 data from the QEI for the 1995-2014 period were obtained from the National Snow and Ice Data Centre (<http://nsidc.org/data/idhdt4>, downloaded 6 July – 22 August 2016). Data from 2015 were not included due to their limited spatial coverage and the failure of the wide-swath scanner [Krabill, 2014a, updated 2016]. To ensure that only measurements over glaciated surfaces were retained, the IDHDT4 data were clipped to the Randolph Glacier Inventory (RGI) version

5.0 Arctic Canada North region 32 polygons [Arendt *et al.*, 2012; Pfeffer *et al.*, 2014]. The RGI polygons are referenced to the 1999/2000 glacier extent and do not include all small rock outcrops within ice caps. Summer 2013 LandSat 7 ETM+ and 2014 LandSat 8 OLI images were used to manually identify and remove IDHDT4 data that were not located over ice (usually data collected over small rock outcrops and areas exposed by glacier retreat since 1999/2000). Such data, which typically showed very small elevation changes ($\sim \pm 0.001 \text{ m yr}^{-1}$), accounted for $\sim 1\%$ of all IDHDT4 data falling within the RGI polygons.

Airborne altimetry surveys were conducted every ~ 5 years between 1995 and 2012, but coverage varies between surveys. Surveys were conducted over the Devon Ice Cap and the Prince of Wales Icefield in 2005, the remaining ice masses were surveyed in 2006. The northern portion of Prince of Wales Icefield (Ekblaw, Leffert, and Stygge glaciers) was surveyed in both 2005 and 2006. Since these glaciers are known to exhibit large variations in surface velocity (Section 4.1), dh/dt in these regions may not be representative of changes across the entire Prince of Wales Icefield. Therefore, we did not attempt to adjust the 2005 surface elevations using the 2005-2006 elevation difference and only the more comprehensive 2005 ATM data were used for the Prince of Wales Icefield. Coverage over the Manson Icefield and Sydkap Ice Cap is limited after 2006. Airborne altimetry surveys were conducted over most ice masses in both 2011 and 2012. The exception to this was northern Ellesmere Island, where ice masses were surveyed in 2014, but not in 2011 or 2012. Mean 2011-2012 dh/dt for areas surveyed in both 2011 and 2012 was $-0.83 \pm 0.60 \text{ m yr}^{-1}$ with little variation between ice masses. To avoid redundancy, only data for 2012 are presented here. To evaluate spatial and temporal patterns in dh/dt during the 1995-2012/2014 period, data were aggregated into three epochs: 1995-2000, 2000-2005/2006, 2005/2006-2012/2014. This approach is consistent with earlier work [e.g. Abdalati *et al.*, 2004; Arendt *et al.*, 2006] which

regards ~5 years as the optimal time interval between repeat ATM surveys to minimise the effects of inter-annual variability in melt and accumulation on the measured elevation change.

4.2.2 MODIS data

4.2.2.1 MOD11A2 LST

Satellite-derived measurements of land surface temperature (LST) and surface albedo from the Moderate Resolution Imaging Spectroradiometers (MODIS), onboard the Terra (2000 to present) and Aqua (2002 to present) satellites (<https://lpdaac.usgs.gov/>), were used to examine the likely influence of changes in the climatic mass balance on observed changes in glacier surface elevation. Estimates of LST were obtained from the Eight-Day L3 Global Land Surface Temperature and Emissivity product (MOD11A2) Version 05, which computes daytime and night-time LST from MODIS channels 31 (11 μm) and 32 (12 μm) using a split-window technique and all available daytime clear-sky scenes from the Terra satellite for sequential 8 day periods [*Wan et al.*, 2002]. A conservative cloud mask is used to remove observations when clouds are present [*Ackerman et al.*, 1998]. Variability in the number of clear-sky days within each observation period and from one year to the next did not introduce significant variability in the MODIS-derived LST relative to the true surface temperature in the QEI [see *Mortimer et al.*, 2016 and references therein]. Mean summer daytime LST from MOD11A2 has been found to be a reasonable proxy for the duration and/or intensity of summer melting in the QEI [*Sharp et al.*, 2011; *Mortimer et al.*, 2016]. MOD11A2 has a spatial resolution of 1 km x 1 km and a nominal product accuracy of $\pm 1^\circ\text{C}$ [*Wan et al.*, 2008], but the accuracy can be as low as $\pm 2^\circ\text{C}$ over snow and ice surfaces [*Hall et al.*, 2008a; *Koenig and Hall*, 2010]. Pixels for which the average LST error (QC_Day LST error flag) exceeded 2°C were removed from the analysis and any remaining pixels having a temperature $> 0^\circ\text{C}$ were assigned a temperature of 0°C [e.g. *Hall et al.*, 2008b; *Mortimer et al.*, 2016].

4.2.2.2 MCD43A3 albedo

Estimates of surface albedo were obtained from the MODIS combined Albedo 16-Day L3 Global 500 m gridded product (MCD43A3) Version 05 (<https://lpdaac.usgs.gov/>). MCD43A3 albedos are estimated from the Level 2 surface reflectance products (MOD09 and MYD09) for seven visible and near-infrared bands (spanning 0.4 to 2.4 μm) and three broad bands (shortwave (0.3-5.0 μm), visible (0.3-0.7 μm) and near infrared (0.7-5.0 μm) [*Lutch et al.*, 2000]. A semi-empirical Bidirectional Reflectance Distribution Function (BRDF) model, which describes the surface scattering/reflectance of a target as a function of illumination, is used to estimate surface albedo from directional surface reflectance information recorded by the MODIS sensors [*Gao et al.*, 2005]. MCD43A3 white-sky (bihemispherical reflectance under isotropic conditions) and black-sky (directional hemispherical reflectance) albedos are calculated every eight days using atmospherically-corrected surface reflectance values collected by both the Terra and Aqua satellites over a 16 day period [*Strahler et al.*, 1999; *Schaaf et al.*, 2002, 2011, and references therein]. MODIS surface reflectance data have a stated accuracy of 0.005 for solar zenith angles $<75^\circ$ [*Vermote et al.*, 2011]. Comprehensive quality assessment information is provided in the MCD43A2 companion data product [*Schaaf et al.*, 2002]. High quality full-inversion retrievals (where reflectance data collected during each 16 day period are used as input for a semi-empirical RossThick LiSparse Reciprocal kernel-driven BRDF model to compute the surface albedo [*Wanner et al.*, 1997; *Lutch et al.*, 2000; *Schaaf et al.*, 2002]) account for $<2\%$ of pixels in our study region so we also include the lower quality, magnitude inversion data (when there are <7 observations during a 16 day period the albedo is computed using a priori knowledge to scale an archetypal BRDF) [*Strahler et al.*, 1999].

Consistent with previous work using MCD43A3 data [e.g. *Alexander et al.*, 2014; *Tedesco et al.*, 2016; *Mortimer and Sharp*, in review], only trends in the black-sky broadband shortwave albedo (BSA), which are fully consistent with the white-sky albedo (WSA), are evaluated here. MCD43A3 data for 2000 were extremely poor and were excluded from our analysis. In that year, the difference between the white- and black- sky albedos was, on average, 0.138 while in other years the mean difference was between 0.010 and 0.007 [*Mortimer and Sharp*, in review].

Data for regions north of 80°N (tiles h16v00 and h17v00) prior to 2009 were not initially included in the MCD43A3 processing routine, and were processed at a later date using the lower quality Level 2 Gridded (L2G) data as input [*Stroeve et al.*, 2013]. QEI mean summer albedo derived from MCD43A3 data is measurably higher for the L2G data than for tiles subjected to the L2G-lite processing. This resulted in an artefact in the data, seen as a clear break in the data, where the absolute albedo values for regions north of 80°N were higher prior to 2009, prohibiting a homogeneous analysis of albedo change across the QEI and restricting our analysis to regions south of 80°N from 2001 onward [see *Mortimer and Sharp*, in review].

Cloud contamination results in the absence of data when clouds are present. In addition, similarity in the spectral signatures of snow, ice, and thin cloud makes it difficult to discriminate between these surface types [*Strabala et al.*, 1994; *King et al.*, 2004], and the conservative MODIS cloud mask tends to detect more clouds than are actually present over snow and ice [*Ackerman et al.*, 1998; *Hall et al.*, 2008]. The absence of data when clouds are present may introduce variability in the albedo record that is not representative of true physical change. However, the MCD43A3 albedo product has been found to provide a reasonable representation of the seasonal albedo cycle of the Greenland Ice Sheet [e.g. *Stroeve et al.*, 2006], immediately adjacent to the QEI. In the

absence of long-term ground measurements of surface albedo in the QEI, we made the assumption that this is also the case in this region.

4.2.2.2.1 MODIS sensor degradation

Degradation of the MODIS sensor onboard the Terra satellite [Wang *et al.*, 2012] is associated with systematically decreasing temporal trends in the visible and NIR bands of the MODIS Version 05 data [Lyapustin *et al.*, 2014 and references therein]. Early comparisons of MODIS Version 05 albedo with in situ measurements largely discounted the notion that un-corrected sensor degradation produced artificial declining albedo trends [e.g. Box *et al.*, 2012; Alexander *et al.*, 2014; Tedesco *et al.*, 2016]. More recently, however, Polashenski *et al.* [2015] found that albedo declines over the Greenland Ice Sheet's dry snow zone were largely attributable to Terra sensor degradation, but the magnitude of the measured albedo decline was smaller than the nominal uncertainty of the MODIS surface reflectance products [Vermote *et al.*, 2011]. Terra sensor degradation is corrected for in the newer Version 06 albedo products and analysis of these data for the period 2001-2016 found no trend in visible wavelength albedo over the dry snow zone of the Greenland Ice Sheet [Casey *et al.*, 2016]. There are no dry snow zones in the QEI. Over the Greenland Ice Sheet's wet snow zone, albedo declines (2001-2016) were observed from both the Version 05 and Version 06 data. Trends calculated from the Version 06 data were smaller than those computed from the Version 05 data and are thought to be physically real [Casey *et al.*, 2016].

The combined MCD43A3 dataset used here is affected by degradation of the Terra sensor as it includes data from both the Terra and Aqua sensors; however, the effect of sensor degradation is smaller than it would be if only Terra data were used. Stroeve *et al.* [2013] found the Terra-only declining albedo trend to be $0.006 \text{ decade}^{-1}$ larger than the Aqua only trend, but the MCD43A3 trend was only $0.002 \text{ decade}^{-1}$ larger (than the Aqua-only trend). In addition, Alexander *et al.*

[2014] found good agreement between the summer MCD43A3 black-sky albedo and in situ albedo records from the Greenland Ice Sheet for 2000-2012. Although degradation of the Terra sensor is corrected for in the Version 06 data. These data were not available at the time of writing so the older Version 05 data were used here. The Version 05 have been shown to produce spatial and temporal patterns of albedo change that are consistent with both in situ and modelled data for the Greenland Ice Sheet (immediately adjacent to the QEI), which gives us confidence in the broad spatial patterns of albedo change used here to interpret dh/dt .

4.2.2.3 Mean summer LST and BSA

Inter-annual variability in the annual mass balance of QEI glaciers and ice cap is dominated by variability in the summer mass balance which, in turn, is largely controlled by changes in summer air temperature [Koerner, 2005]. Changes in LST and BSA were therefore computed for the summer months (1-2 June to 28-29 August). All available MOD11A2 and MCD43A3 data and accompanying quality assessment information (MCD43A2) for MODIS tiles h16v00, h17v00, h16v01, and h15v01 were downloaded from the NASA/USGS Land Processes Distributed Active Archive Center (<https://lpdaac.usgs.gov/> accessed September 2014 to October 2015). Together, these data provide complete coverage of the QEI. Data were re-projected to a North American Albers Equal Area projection, WGS84 datum, 1 km (LST) and 500 m (BSA) resolution using the MODIS re-projection tool version 4.1 (https://lpdaac.usgs.gov/tools/modis_reprojection-tool). Full descriptions of the LST and BSA data processing methods used here are provided in *Mortimer et al.* [2016] and *Mortimer and Sharp* [in review], respectively.

4.2.3 Comparison of dh/dt with LST, BSA, and du/dx

To investigate the influences of changes in the glacier climatic mass balance and ice dynamics on the surface elevations of glaciers and ice caps, the airborne-derived measurements of dh/dt were compared with measured changes in MODIS-derived LST [Mortimer *et al.*, 2016], BSA [Mortimer and Sharp, in review], and surface longitudinal strain rates.

4.2.3.1 Mass balance: MODIS-derived LSTs were strongly correlated with annual mass change estimates derived from GRACE data during the period 2003/04 - 2014/2015 ($r = -0.82$; $p < 0.01$) and have been used previously as a proxy for the intensity and/or duration of summer melt [Hall *et al.*, 2006; Sharp *et al.*, 2011; Mortimer *et al.*, 2016]. Variability in net absorption of shortwave radiation, which is usually the largest source of melt energy in the QEI in the summer [Gascon *et al.*, 2013], is modulated by changes in the surface albedo [Van den Broeke *et al.*, 2011; Tedesco *et al.*, 2016]. Albedo decreases enhance surface melt rates, resulting in increased runoff, rates of firn compaction and densification, and rates of glacier thinning. Here, we use changes in these two variables to infer changes in the glacier climatic mass balance. The basal mass balance, which is typically small relative to the climatic mass balance [Cuffey and Paterson, 2010], is not included in our assessment. For each IDHDT4 data point, the corresponding LST and BSA changes were extracted. The signs (increase/decrease) of the changes in these two variables were then used to investigate the likely influences of changes in climatic mass balance on dh/dt [Section 4.6 Table 4-S1].

Good quality MODIS-derived BSA (Version 05) data are available only for regions of the QEI south of 80°N beginning in 2001, so availability of the full combination of LST, BSA, and dh/dt data was limited to areas south of 80°N . This excluded the whole of northern Ellesmere Island, $\sim 73\%$ of the Agassiz Ice Cap, $\sim 23\%$ of the combined area of the Mueller and Steacie Ice Caps, and $\sim 36.5\%$ of the Meighen Ice Cap. Given this limitation, we compared dh/dt with both BSA and

LST change for areas south of 80°N while, for areas north of 80°N, we compared dh/dt with LST change alone. Since ATM measurements were always collected in the spring, they were compared with measurements of mean summer LST and BSA from the previous summer. LST change was computed for the period 2000-2011 (2000-2013 for northern Ellesmere Island) and BSA change was calculated for the period 2001-2011. Linear regressions were performed on a pixel by pixel basis for all pixels having mean summer LST and BSA observations for at least half the years in each time interval following the methods of *Mortimer et al.* [2016] and *Mortimer and Sharp* [in review]. Since the presence of clouds results in missing LST and BSA data, LST and BSA change measurements are not available for all IDHDT4 data points. BSA data are particularly sparse, especially over the interiors of the Mueller and Devon Ice Caps [see *Mortimer and Sharp*, in review]. Comparisons of LST, BSA, and dh/dt were only conducted for IDHDT4 data points having corresponding BSA and LST observations. This constituted ~83% and 96% of possible IDHDT4 points, respectively.

4.2.3.2 Ice dynamics: Along-flow changes in the flux divergence can alter the elevation of a glacier surface, as longitudinally compressive (extensional) flow results in thickening (thinning) of the glacier [*Cuffey and Paterson*, 2010]. To assess the influences of changes in ice dynamics on rates of surface elevation change on QEI glaciers and ice caps, dh/dt was compared with surface longitudinal strain rates (du/dx) computed from surface velocity fields published by *van Wychen et al.* [2016, 2017]. Annual mean surface velocities (summer to summer) were derived from LandSat 7 ETM+ data for 1999-2010, winter (February) velocities were derived from RADARSAT-1 (2000, 2006-2010) and RADARSAT-2 (2009-2015) data. The spatial resolution of these datasets is 100 m and measurement uncertainties are 19 m yr⁻¹ and 8.7 m yr⁻¹ respectively for the LandSat-derived annual surface velocities and the RADARSAT-derived winter velocities

[van Wychen *et al.*, 2016, 2017]. van Wychen *et al.* [2016] found winter velocities to be ~14% lower on average than the annual velocities and this difference increased to 15-25% towards the termini of most glaciers. The RADARSAT-derived surface velocities have broader spatial coverage than the Landsat-derived measurements, which are confined mainly to larger and faster flowing outlet glaciers. In most regions, calculations of du/dx were limited to 2000 and 2006-2015 (RADARSAT data), and, in many locations were limited to the period after 2011. As such, du/dx measurements from 2013-2015 (the period following the most recent dh/dt measurements) were also included to ensure sufficient data coverage along all ATM survey lines [Section 4.6 Table S-2].

Surface velocities along the ATM-flight lines were extracted every 100 m and the average surface velocity of 1 km long segments was computed. Longitudinal strain rates (du/dx) were calculated from these discrete 1 km long segments, with a 100 m overlap between successive du/dx measurements to reduce the effect of the choice of start and end points, and then smoothed with a 1 km moving average filter to remove noise from the data. For consistency between regions, a 1 km averaging length was used throughout, even though this may have introduced additional noise to the data. The ATM flight lines do not always follow glacier flowlines and they cut across them in large regions of the ice masses, so longitudinal strain rates were not always computed for flow-parallel segments. In our analysis, du/dx was computed along the entire length of each ATM flight line and was not adjusted for differences between the alignment of the flightline and the direction of ice flow.

Attempts were made to quantify the expected magnitude of surface elevation change along glacier flowlines using the flux imbalance method. However, our calculations of the flux divergence overestimated the observed dh/dt by nearly one order of magnitude -an amount much larger than

can be explained by the omission of surface mass balance. This discrepancy is most likely due to the fact that our calculation of dh/dt from du/dx [along a flowline] assumed one-dimensional flow and did not account for lateral spreading (compression) as ice exits (enters) a constriction. In addition, the ATM-flight lines do not always follow the central flowline of the glacier, so the extracted velocities may not always be the actual peak velocities in a given cross profile. Therefore, we did not correct for dh/dt using the measured du/dx . Instead, we compared the relative magnitude of du/dx to identify locations where ice dynamics were likely an important contributor to changes in surface elevation. Specifically, locations where du/dx was large, and of opposite sign of dh/dt , were taken to indicate that ice dynamics made an important contribution to dh/dt , and we were careful not to interpret dh/dt as a straightforward indicator of mass change.

4.3 Results

Comparisons of the rates of surface elevation change between epochs 1: 1995-2000, 2: 2000-2005/06, and 3: 2005/06-2012/14 show considerable temporal variability in the rate of surface elevation change over the period 1995-2012/14. For all regions except northern Ellesmere Island, rates of thinning, aggregated into 50 m elevation bins according to the average ellipsoid heights in the two end-years of each campaign period (Figure 4-1), were ~3 to 6.5 times larger during the final epoch than in the previous two. On northern Ellesmere Island, however, dh/dt was only ~1 to 2 times larger in the most recent campaign period, likely owing to lower summer air and surface temperatures in that region in 2013 and 2014 [Mortimer *et al.*, 2016] and positive glacier mass balances in 2013 [Sharp *et al.*, 2015].

Higher rates of thinning after 2005/06 are consistent with a period of strong positive anomalies in air and surface temperatures, and negative anomalies in surface albedo (relative to the 2000/01-2015 period), across the QEI ice caps from 2005-2012 [*Mortimer et al.*, 2016; *Mortimer and Sharp*, in review], as well as with increasingly negative glacier mass balances since the mid 2000s [*Sharp et al.*, 2011; *Gardner et al.*, 2013; *Lenaerts et al.*, 2013; *Millan et al.*, 2017]. Specifically, the annual mean in-situ climatic mass balance, derived by averaging the annual balances measured at four sites in the Canadian Arctic, was ~3.5 times more negative between 2005/06 and 2012 than it was between 1995 and 2005/06 (computed from data presented in *Sharp et al.* [2015]) and the annual mass loss estimates for this region from GRACE data increased at a mean rate of 11.6 Gt yr⁻¹ between 2003/04 and 2011/12 [*Mortimer et al.*, 2016, update from *Gardner et al.*, 2011]. Mean summer (JJA) air temperatures at 700 hPa geopotential height, obtained from the NCEP/NCAR R1 Reanalysis [*Kalnay et al.*, 1996] and centered over each of the major ice masses [see *Sharp et al.*, 2011; *Mortimer et al.*, 2016], were between 0.8°C and 1.4°C higher during 2007-2012 compared with the 1995-2012 mean, while summer near-surface (2 m) air temperatures at Eureka and Resolute Bay were 1.2°C and 1.5°C warmer than the 1995-2012 mean (<http://climate.weather.gc.ca>). Further, mean summer LSTs for this period (2007-2012; available since 2000) were 0.63°C to 1.08°C warmer than the 2000-2015 mean [*Mortimer et al.*, 2016].

Between 1995 and 2012/14, widespread thinning (surface lowering) was observed over QEI glaciers and ice caps (Figure 4-2), consistent with increasingly negative glacier mass balances and higher air and land surface temperatures observed across the region since at least 2000 [*Gardner et al.*, 2011, 2013; *Sharp et al.*, 2011, 2015; *Lenaerts et al.*, 2013; *Mortimer et al.*, 2016; *Millan et al.*, 2017]. In this study, thinning (thickening) is defined as $|dh/dt| \geq 0.02 \text{ m yr}^{-1}$; intermediate values ($|dh/dt| < 0.02 \text{ m yr}^{-1}$) are taken to imply no significant change in surface elevation [see

Abdalati et al., 2004]. For the period 1995 to 2012/14, thinning was greatest ($< -0.5 \text{ m yr}^{-1}$) at lower elevations along the margins of the major ice masses, and there is a general trend towards lower rates of thinning at higher elevations. Thickening was observed on the east-facing slopes of the southern Prince of Wales Icefield (between ~ 400 and 850 m a.s.l.) and on the Agassiz Ice Cap (above $\sim 1500 \text{ m a.s.l.}$). High rates of dh/dt (thinning $< -0.5 \text{ m yr}^{-1}$ or thickening $> 0.2 \text{ m yr}^{-1}$) were observed along portions of six previously identified [*Copland et al.*, 2003; *van Wychen et al.*, 2016] surge-type glaciers on the Northern Ellesmere Island (Otto Glacier), Mueller (Thompson Glacier) and Agassiz (Antoinette Glacier) Ice Caps and the Prince of Wales Icefield (Taggart Lake, Ekblaw, and Wykeham glaciers). Regions of many of these glaciers underwent significant fluctuations ($> \sim 20 \text{ m yr}^{-1}$) in surface velocity between 1999 and 2015 [*van Wychen et al.*, 2016; 2017; *Millan et al.*, 2017].

4.3.1 dh/dt by epoch

(a) 1995-2000

Surface elevation changes of glaciers in the QEI during the period 1995-2000 were reported by *Abdalati et al.* [2004]. This time interval is included here to allow evaluation of spatial and temporal patterns of dh/dt over the entire 1995-2012/14 period. Briefly, from 1995-2000, thinning occurred at lower elevations around the margins of the ice masses as well as along the Thompson (Mueller Ice Cap), and Strand (Steacie Ice Cap) glaciers on Axel Heiberg Island, the Otto Glacier (northern Ellesmere Island), and the Leffert Glacier (Prince of Wales Icefield) (Figure 4-S3). Either thickening or no change in surface elevation ($dh/dt \geq -0.02 \text{ m yr}^{-1}$) was observed at higher elevations in the interior of most ice masses. Thickening was especially pronounced ($> +0.2 \text{ m yr}^{-1}$)

¹) on the northern Grant Ice Cap, northern Ellesmere Island, at low elevations ($< \sim 750$ m a.s.l.), along the east-facing slopes of the Prince of Wales Icefield (mean dh/dt : $\sim +0.34$ m yr⁻¹), and along the lower 5-18 km of the Antoinette Glacier, Agassiz Ice Cap (mean dh/dt : $\sim +0.37$ m yr⁻¹).

(b) 2000-2005/06

The period 2000-2005/06 was also characterized by thickening at higher elevations and thinning at lower elevations (Figure 4-S4). A spatial pattern of dh/dt similar to that of the previous epoch was observed over much of the Prince of Wales Icefield, with the exception of the Ekblaw Glacier which thickened at an average rate of $+0.33$ m yr⁻¹ along its lower ~ 40 km. This thickening is consistent with a marked decrease in the glacier's near-terminus surface velocities between 2000 (~ 500 m yr⁻¹) and 2015 (~ 150 - 200 m yr⁻¹) [*van Wychen et al.*, 2016], which would have resulted in longitudinally compressive flow and thickening. During the previous epoch, dh/dt along the lower ~ 40 km of Ekblaw Glacier ranged from ~ -0.2 to $+0.2$ m yr⁻¹.

Thinning or no change in surface elevation ($dh/dt \leq +0.02$ m yr⁻¹) occurred across the northwest sector of the Devon Ice Cap above ~ 1250 m a.s.l. where thickening (mean dh/dt : $+0.04$ m yr⁻¹) occurred during the previous epoch. On the Agassiz Ice Cap, thickening (mean dh/dt : $\sim +0.05$ m yr⁻¹; local $dh/dt > 0.1$ m yr⁻¹) occurred at higher elevations, while thinning (mean dh/dt : ~ -0.08 m yr⁻¹) was observed in the north-northeast -a region that experienced thickening (mean dh/dt : $\sim +0.04$ m yr⁻¹) during the previous epoch. In the western QEI, thickening was observed across much of the interior of the Mueller Ice Cap, where thinning (up to ~ -0.2 m yr⁻¹) occurred during the previous epoch. Thinning (< -0.2 m yr⁻¹) was observed across the southern portion of northern Ellesmere Island's ice masses which, in general, thickened (by up to $+0.1$ m yr⁻¹) during the previous epoch. The only exception was the Otto Glacier which thinned throughout its lowermost

~ 45 km during the first two epochs (mean 1995-2000 dh/dt : -0.47 m yr^{-1} ; mean 2000-2006 dh/dt : -0.41 m yr^{-1}).

(c) 2005/06-2012/14

With a few exceptions, namely the Southeast 1 and 2 glaciers (Devon Ice Cap) which thickened by ~ 0.35 and 0.17 m yr^{-1} , respectively, thinning occurred nearly everywhere during the period 2005/06-2012/14 (Figure 4-S5). Thickening along the middle sections of the Southeast 1 and 2 Glaciers is consistent with previously identified dynamically-induced thickness changes attributed to slow downglacier propagation of a surge front [*Burgess and Sharp, 2008*]. Overall, rates of thinning decreased from $< -0.6 \text{ m yr}^{-1}$ around the margins of most ice masses to between ~ -0.4 and -0.2 m yr^{-1} in their interiors. Lower rates of thinning (0.2 m yr^{-1} or less) and/or no detectable changes ($|dh/dt| < 0.02 \text{ m yr}^{-1}$) in surface elevation were observed over the interior regions of the Devon and Agassiz Ice Caps, and along the southernmost transect across the Prince of Wales Icefield between ~ 400 and 750 m a.s.l.

4.3.2 dh/dt anomalies

To further investigate the temporal variability in the rate of glacier surface elevation change, dh/dt anomalies for each epoch were computed relative to the 1995-2012/14 mean (Figure 4-3). For each epoch, the closest data point to the corresponding point from the 1995-2012 data set (1995-2014 for northern Ellesmere Island) within a search radius of 150 m was identified and the dh/dt anomaly for each data pair was computed. Nearly all data pairs (99.98%; 89% for northern Ellesmere Island) had negative anomalies during the final epoch (2005/06-2012/14), while the first two epochs were characterized by largely positive dh/dt anomalies (Figure 4-3). During the first (1995-2000) and second (2000-2005/06) epochs, negative dh/dt anomalies were observed for only 7.2% (12% for

northern Ellesmere Island) and 8.6% (28% for northern Ellesmere Island) of data pairs, respectively.

For the 1995-2000 epoch, negative anomalies occurred primarily on the Agassiz Ice Cap, the Prince of Wales Icefield, and the Otto Glacier, northern Ellesmere Island (Figure 4-3). Thickening and positive dh/dt anomalies were observed over the northwest sector of the Devon Ice Cap during 1995-2000. *Abdalati et al.* [2004] speculated that thickening in this region may have been the result of increased precipitation. However, in situ mass balance measurements from this region were negative during the 1995-2000 period, with increasingly negative annual mass balances from ~1997 onward [World Glacier Monitoring Service, 2016]. Investigation of surface elevation changes using the flux imbalance method [see *Colgan et al.*, 2008] and surface mass budget modelling discounted the notion that thickening was the result of increased precipitation. Instead, *Colgan et al.* [2008] suggested that any apparent thickening was most likely the result of downward penetration of the Neoglacial cold wave, which would have stiffened the ice near the bed, reducing outflow from the interior of the ice cap and causing thickening there.

From 2000 to 2005/06, negative dh/dt anomalies were clustered on the northern halves of both the Agassiz Ice Cap and the northern Ellesmere Island Icefields, with the exception of the extreme north-eastern part of the Grant Ice Cap, which had positive dh/dt anomalies. During the final epoch (2005/06-2012/14), in which dh/dt anomalies were negative in all regions, the Agassiz Ice Cap experienced the least negative dh/dt anomalies (mean dh/dt anomaly ~ -0.1 m yr⁻¹). The largest negative dh/dt anomalies (< -1 m yr⁻¹) were located along the lower 20-25 km of the Wykeham Glacier, Prince of Wales Icefield, and likely reflect dynamically-induced thinning given that this glacier's near-terminus surface velocities increased consistently between 2007/08 (~ 200 m yr⁻¹) and 2015 (~ 450 m yr⁻¹) [*van Wychen et al.*, 2016]. Over northern Ellesmere Island, positive dh/dt

anomalies from 2006 to 2014 were mainly confined to the lower ~34 km of the Otto Glacier and may be linked to a marked reduction ($> 600 \text{ m yr}^{-1}$) in near-terminus (lower ~2 km) surface velocities from 2008 to 2013 [van Wychen *et al.*, 2016]. We note that, except where thickness changes were dynamically induced (e.g. Otto Glacier, Section 4.4.2), differences in dh/dt anomalies between northern Ellesmere Island and the rest of the QEI (for which dh/dt anomalies were computed with respect to 1995-2012) are likely attributable to lower air and ice surface temperatures in 2013 when mean summer LSTs were 2-4°C lower than in 2011 and 2012. This would be associated with lower rates of surface melting and thinning.

Overall, there was a reduction in ice surface elevations across the QEI between 1995 and 2012/2014. Strong negative dh/dt anomalies during the 2005/06-2012/14 period suggest that the bulk of this thinning occurred during the most recent 5-6 year period. During all epochs, there is a general trend of decreasing rates of thinning with increasing elevation. Thickening (or no measurable change in surface elevation $dh/dt \geq -0.02 \text{ m yr}^{-1}$) was observed at higher elevations during the first two epochs, whereas all regions exhibited thinning during the final epoch. Large surface elevation changes ($dh/dt < -1 \text{ m yr}^{-1}$ and/or $> 0.2 \text{ m yr}^{-1}$) occurred along regions of several outlet glaciers, and are likely tied to ice deformation associated with rapid changes in longitudinal gradients in glacier surface velocity (Section 4.4.2).

4.4 Comparison of dh/dt with LST, BSA, and ice dynamics for 2000-2012/14

To investigate the relative influences of changes in the glacier climatic mass balance and ice dynamics on observed changes in glacier and ice cap surface elevation, the ATM-derived dh/dt values were compared with measured changes in MODIS-derived LST [Mortimer *et al.*, 2016],

BSA [*Mortimer and Sharp*, in review], and surface longitudinal strain rates (du/dx) for the 2000-2012/14 period (Section 4.2.3). Briefly, between 2000 and 2012/14, either thickening or no change in surface elevation ($dh/dt \geq -0.02 \text{ m yr}^{-1}$) was observed at higher elevations in the interior of most ice masses (Figure 4-4a). Local thickening $> +0.2 \text{ m yr}^{-1}$ was observed at low elevations in the interior of the southern Prince of Wales Icefield (between ~ 380 and 700 m a.s.l.), and along sections of the Wykeham, Ekblaw, and Antoinette glaciers, as well as on the eastern Devon Ice Cap where the north-south running ATM survey line crosses the Southeast 1 and 2 glacier drainage basins.

Changes in the elevation of a glacier surface are controlled by the basal-climatic mass balance of the glacier and by ice dynamics. Annual precipitation in the QEI is low ($< 400 \text{ mm w.e. yr}^{-1}$, *Braithwaite* [2005]) and variability in the annual glacier mass balance is dominated by changes in summer melt [*Koerner*, 2005]. Changes in the mean summer LST and BSA are therefore used to infer changes in the glacier climatic mass balance (Section 4.2.3.1). Specifically, an increase (decrease) in LST, together with a decrease (increase) in BSA, is taken to imply a high probability of a negative (positive) change in climatic mass balance. Under this scenario, if the LST change is positive and BSA change is negative, thinning is expected unless there was a compensating reduction in surface longitudinal velocity gradients.

During the 2000-2012/14 period, where surface velocities were low ($< \sim 20 \text{ m yr}^{-1}$, see van Wychen and others, 2016), as seen in the interior regions of the ice masses, there was generally good agreement between the trends in LST and BSA (Figure 4-4 c, 4-4 d) and the sign of dh/dt (Figure 4-4a). There were, however, some exceptions, namely in the interior of southern Prince of Wales Icefield (between ~ 380 and 700 m a.s.l.), and at high elevations on the Agassiz Ice Cap ($> \sim 1750 \text{ m a.s.l.}$) and northern Prince of Wales Icefield ($> \sim 1000 \text{ m a.s.l.}$). Conversely, where surface

velocities were high ($> \sim 75 \text{ m yr}^{-1}$), for example along many outlet glaciers [see *van Wychen et al.*, 2016, 2017; *Millan et al.*, 2017], the sign of dh/dt was often opposite of what would have been expected from observed changes in LST and BSA, which suggests that, in addition to changes in the glacier climatic mass balance, evolving ice dynamics made an important contribution to dh/dt along fast-flowing outlet glaciers.

To assess the relative influence of changing ice flow on observed changes in glacier and ice cap surface elevation, du/dx (computed for 1 km long segments, Section 4.2.3.2) was compared with dh/dt for the period 2000-2012/14. $|du/dx|$, averaged from all available data for the 1999-2015 period, is shown in Figure 4b. In general, $|du/dx|$ was at least one order of magnitude larger along outlet glaciers (where $|dh/dt|$ can exceed 1 m yr^{-1}) than elsewhere (where $|dh/dt|$ is typically less than 0.5 m yr^{-1}). The large and distinct difference in the relative magnitude of du/dx between regions with large and spatially variable dh/dt and regions where dh/dt was smaller and more spatially uniform, provides a means of differentiating between areas where ice dynamics (in addition to changes in glacier mass balance) are likely to have significantly influenced dh/dt and areas where changes in the glacier mass balance are likely to have been the primary driver of changes in the rate of glacier surface elevation change.

4.4.1 Low longitudinal strain rates

Where $|du/dx|$ is consistently low, changes in ice dynamics are expected to have played only a minor role in the observed short-term (< 20 years) changes in surface elevation [*Cuffey and Paterson*, 2010]. Instead, thinning and/or thickening are likely to have resulted from changes in the climatic mass balance of the glacier. Between 2000 and 2011/13, QEI-wide mean summer LST increased by $0.17 \pm 0.07 \text{ }^\circ\text{C yr}^{-1}$ and 98.7% of pixels experienced an increase in LST. During this time (2000-2012/14), 87% of the dh/dt observations with corresponding LST change

measurements were negative, implying thinning (Figure 4-4c). In the ablation area, where surface lowering coincided with an increase in LST [and du/dx was small], thinning probably implies a loss of glacier mass. In the accumulation area, however, a reduction in the elevation of the glacier surface that coincided with an increase in LST does not necessarily imply glacier mass loss. Higher air and surface temperatures increase both the amount of melt and the depth of meltwater penetration into the firn layer. Enhanced meltwater percolation and subsequent refreezing releases latent heat, simultaneously raises the temperature of the firn and increases the rate of firn densification [Pfeffer and Humphrey, 1998], resulting in a lowering of the glacier surface. Field observations from the Devon and Penny Ice Caps have found an increase in both firn density and temperature of the firn (which increases the rate of firn densification) [Zdanowicz *et al.*, 2012; Bezeau *et al.*, 2013] as well as the growth of large ice bodies within the firn layer [Gascon *et al.*, 2013].

Reductions in the surface albedo enhance warming and melt rates via the positive ice-albedo feedback, resulting in thinning. Comparison of the sign of dh/dt and LST with BSA change for regions south of 80°N shows that, in most instances where $|du/dx|$ was low ($|du/dx|$ smaller than 0.003 yr⁻¹, Figure 4-4b), thinning and an increase in LST coincided (as expected) with a decrease in BSA (Figure 4-4d). There were, however, some exceptions, particularly on the Prince of Wales Icefield. At higher elevations on northern Prince of Wales Icefield (> ~1000 m a.s.l.) thinning often coincided with an increase in both LST and BSA, while thickening along the interior of the southernmost transect across Prince of Wales Icefield (between ~380 and 700 m a.s.l.) coincided with an increase in LST and a decrease in BSA.

Previous work identified local clusters of positive correlations between mean summer LST and BSA at high elevations in eastern Ellesmere Island from 2001-2015 that may indicate a locally

positive feedback between surface temperature and albedo, whereby, increased solid precipitation during warm summers [see *Koerner, 1979*] both raises the albedo and results in thickening [*Mortimer and Sharp, in review*]. During the 2001-2011 period, increases in both LST and BSA were observed at higher elevations on northern Prince of Wales Icefield ($> \sim 1000$ m a.s.l.), eastern Ellesmere Island, yet this region experienced thinning (instead of thickening). If, indeed, the measured increases in mean summer BSA during 2001-2015 are indicative of an increase in summer snowfall and/or riming events, we suggest that, at higher elevations on the northern Prince of Wales Icefield, any increases in precipitation during the 2001-2011 period were sufficient to increase the BSA but insufficient to prevent an increase in melt rates (expected on the basis of the LST change). In this case, increased surface temperatures and melt rates likely enhanced rates of firn densification and the growth of ice bodies within the firn layer, resulting in thinning. However, since high quality precipitation observations over the QEI ice caps are limited, we were unable to determine whether changes in precipitation were responsible for the measured increase in BSA.

Along the central portion of the southernmost transect on Prince of Wales Icefield, thickening coincided with an increase in LST and a decrease in BSA between 2001 and 2011. We note that *Millan et al. [2017]* identified a surge on Glacier 9 (southern Prince of Wales Icefield) with peak velocities occurring in 2006 followed by a slowdown from 2010 onward. The termination of this surge event may have resulted in local thickening during the latter part of the study period. This glacier runs perpendicular to the southernmost flight line on Prince of Wales Icefield so variations in du/dx associated with such a surge event were not fully captured.

Elsewhere, across most of the southernmost portion of Prince of Wales Icefield du/dx was low, and we would have expected an increase in LST and a decrease in BSA to correspond with thinning (rather than the thickening that was observed). During the slightly longer 2001-2015 period,

however, this region experienced an increase in both LST and BSA, thought to be indicative of a localized negative ice-albedo feedback linked to locally higher amounts of solid precipitation in the summer which may account for the observed thickening [see *Mortimer and Sharp*, in review]. Differences in the sign of BSA change between these two periods (2001-2011 versus 2001-2015) result from differences in end dates; BSA anomalies (relative to the 2001-2015 period) were negative in 2011 but positive in 2013 and 2014 (2012 and 2015 also had negative BSA anomalies) [*Mortimer and Sharp*, in review]. Positive correlations between BSA and LST were not observed in this region of southeast Prince of Wales Icefield during the 2001-2011 period but were observed during the 2001-2015 period. Warmer temperatures and frequent melt events increase the mean snow grain size and water content of snow which lowers the albedo [*Warren and Wiscombe*, 1980; *Colbeck*, 1982; *Warren*, 1982; *Tedesco et al.*, 2016]. It is, therefore, possible for a location to experience an increase in summer solid precipitation, which may result in thickening, while at the same time experiencing a decrease in BSA and an increase LST. The combined effects of increased precipitation, increased snow grain size, and higher water content of the snow, therefore, provide a plausible explanation for the coincidence of thickening with an increase in LST and a decrease in BSA observed in the interior of southern Prince of Wales Icefield.

4.4.2 Large longitudinal strain rates

Areas of high $|du/dx|$ ($|du/dx|$ in excess of 0.01 yr^{-1}) were confined mainly to outlet glaciers (Figure 4-4b; Section 4.6 Table 4-S2). In these regions, dh/dt was also large ($< -1 \text{ m yr}^{-1}$; $> +0.2 \text{ m yr}^{-1}$) and highly variable (Figure 4-4b, Figure 4-5). During the 2000-2015 period, longitudinal strain rates in excess of $\sim 0.05 \text{ yr}^{-1}$ were observed along the Otto, Ekblaw, Wykeham, and Antoinette glaciers (Figure 4-4b, 4-5). Localized thinning and/or thickening rates in excess of 1 m yr^{-1} were observed on the Otto, Antoinette, Leffert, and Thompson glaciers between 2000 and 2012/14

(Figure 4-4a). Locations identified from Figure 4b as having large $|du/dx|$ ($|du/dx|$ in excess of 0.01 yr^{-1}) were investigated further. Specifically, the sign of dh/dt was compared with the sign of du/dx to determine whether areas of thinning (thickening) corresponded with locations of extensional (compressive) flow (Figure 4-5). Comparison of these data finds that, regions where dh/dt was appreciably different from zero ($dh/dt: < -1 \text{ m yr}^{-1}; > +0.2 \text{ m yr}^{-1}$) coincided with regions where du/dx was also significantly different than zero ($|du/dx|$ in excess of 0.01 yr^{-1}). In these locations, a positive (negative) dh/dt generally coincided with a negative (positive) du/dx (Figure 4-5). Negative (positive) du/dx indicates longitudinally extensional (compressive) flow.

In detail, longitudinal extension ($\sim 0.05 \text{ yr}^{-1}$) over the lowermost $\sim 5 \text{ km}$ of the Antoinette Glacier, Agassiz Ice Cap, coincided with thinning ($< -1 \text{ m yr}^{-1}$) (Figure 4-5b). Alternating zones of longitudinal extension ($> +0.01 \text{ yr}^{-1}$) and longitudinal compression ($< -0.01 \text{ yr}^{-1}$) over the lowermost $\sim 30\text{-}35 \text{ km}$ of the glacier appear to coincide with areas of thinning and thickening respectively (Figure 5b), but dh/dt measurements are sparse over the lower $\sim 17 \text{ km}$. Above $\sim 40 \text{ km}$ from the terminus, $|du/dx|$ was low ($|du/dx| < 0.003 \text{ yr}^{-1}$) and dh/dt was small (mean $dh/dt: -0.07 \pm 0.1 \text{ m yr}^{-1}$). Thickening (mean $dh/dt: +0.25 \text{ m yr}^{-1}$) and longitudinal compression ($\sim -0.02 \text{ yr}^{-1}$) occurred along the middle portion (between ~ 22 and 40 km from the terminus) of the Wykeham Glacier, eastern Prince of Wales Icefield (Figure 4-5d) while longitudinal extension ($> +0.05 \text{ yr}^{-1}$) and thinning ($< -1 \text{ m yr}^{-1}$) occurred in the lowermost $\sim 5 \text{ km}$. In the uppermost $\sim 15 \text{ km}$, thinning (mean $dh/dt: -0.45 \text{ m yr}^{-1}$) generally coincided with longitudinally extending flow.

Along the Ekblaw Glacier (Figure 4-5c), 60 km to the north, longitudinal extension ($> +0.1 \text{ yr}^{-1}$) in the lowermost $\sim 5 \text{ km}$ coincided with thinning (up to $\sim -1 \text{ m yr}^{-1}$ between 2005 and 2012; only limited data are available for 2000-2012). Between ~ 15 and 38 km from the terminus, alternating zones of longitudinal compression (at $\sim 21, 26, 33 \text{ km}$ from the terminus, up to -0.03 yr^{-1}) and

longitudinal extension (at ~18, 22, and 30 km from terminus, up to $+0.02 \text{ yr}^{-1}$) generally coincided with either thickening (up to $+0.28 \text{ m yr}^{-1}$) or no change in surface elevation ($dh/dt \geq -0.02 \text{ m yr}^{-1}$; mean dh/dt along this section: 0.003 m yr^{-1}), although local thinning (up to -0.067 m yr^{-1}) was observed ~32 km from the terminus. Finally, longitudinal extension ($> 0.05 \text{ yr}^{-1}$) and thinning ($\sim -0.25 \text{ m yr}^{-1}$) were observed in the uppermost part of Ekblaw Glacier (above ~40 km from the terminus).

On northern Ellesmere Island, longitudinal extension ($\sim +0.08 \text{ yr}^{-1}$) along the lowermost ~5-10 km of Otto Glacier (Figure 4-5a) coincided with thinning (mean dh/dt : -1.34 m yr^{-1} , localized $dh/dt < -2 \text{ m yr}^{-1}$). Longitudinal compression ($\sim -0.05 \text{ yr}^{-1}$) ~10 km from the terminus appears to correspond with local thickening, although dh/dt measurements for this location are extremely sparse. Above ~10-12 km from the terminus, longitudinal extension (mean du/dx : $+0.006 \text{ yr}^{-1}$; local maximum: $+0.05 \text{ yr}^{-1}$) coincided with thinning (mean dh/dt : -0.31 m yr^{-1}), except at ~32 km from the terminus where longitudinal compression (-0.008 yr^{-1}) is associated with a depression in the surface topography.

Measurements of dh/dt on the Southeast 1 and 2 glaciers (Figure 4-5e), eastern Devon Ice Cap, are restricted to the 2005-2012 period. Distinct zones of thinning and thickening are observed on these glaciers (Figure 4-S5). Although these glaciers are known to have surged in the past [*Burgess and Sharp, 2008*], values of du/dx were only moderate (Figure 4-4b). Thinning and longitudinal extension were observed along the lowermost ~10 km (mean dh/dt : -1.2 m yr^{-1} ; mean du/dx : $\sim 0.004 \text{ yr}^{-1}$, local maximum $\sim +0.029 \text{ yr}^{-1}$) and uppermost ~25 km of the Southeast 1 Glacier (mean dh/dt : -0.28 m yr^{-1} , mean du/dx : $+0.003 \text{ yr}^{-1}$, local maximum $\sim +0.028 \text{ yr}^{-1}$), while longitudinal compression (mean du/dx : -0.003 yr^{-1} , local minimum -0.017 yr^{-1}) and thickening (mean dh/dt : $+0.34 \text{ m yr}^{-1}$, localized thickening up to $\sim +0.74 \text{ m yr}^{-1}$) dominated the section of the glacier

between ~10 and ~30 km from its terminus. Maximum surface velocities ($> 100 \text{ m yr}^{-1}$) occurred ~30 km up-glacier from the terminus and coincide with a change from longitudinal compression (and thickening) downglacier to longitudinal extension (and thinning) upglacier. This feature likely corresponds with a previously identified surge front, thought to be propagating into more slowly moving ice at lower elevations [*Burgess and Sharp, 2008*]. Similar relationships between dh/dt and du/dx are observed on Southeast 2 Glacier, located immediately to the south.

4.5 Discussion and conclusions

4.5.1 Discussion

During the 2000-2012/14 period, in areas where $|du/dx|$ was large ($|du/dx|$ in excess of 0.01 yr^{-1} ; Figure 4-b), there was generally good correspondence between regions of extension (compression) and negative (positive) dh/dt (Figure 4-5), suggesting that, where du/dx is large, ice dynamics are an important influence on patterns of dh/dt in the QEI. This inference is further supported by the apparent inconsistency between the sign of dh/dt and the signs of LST and BSA change (Figure 4-4c, 4-4d) that is found in regions where $|du/dx|$ is large (Figure 4-4b). The highest rates of thinning ($< -1 \text{ m yr}^{-1}$; Figure 4-4a) were observed along outlet glaciers where flow was strongly extensional (Figures 4-4b, 4-5). In contrast, where $|du/dx|$ was small ($|du/dx|$ less than 0.003 yr^{-1} ; Figure 4-4b) changes in glacier surface elevation were likely the result of changes in the glacier mass balance, as thinning almost always coincided with an increase in LST and a decrease in BSA. Exceptions (for small $|du/dx|$) may be tied to local variations in precipitation. Quality precipitation data are needed to investigate the spatial and temporal variability in precipitation over eastern Ellesmere Island and its influence on the surface energy and mass balance but, unfortunately, do not exist for

QEI ice caps. Enhanced rates of firn densification and the formation of ice bodies within the firn layer likely contributed to surface lowering in the accumulation zone of most ice masses. Where this is the case, thinning does not imply a loss of glacier mass.

The relationship between dh/dt and elevation (Figure 4-6) shows a general reduction in the rate of thinning with increasing elevation, except along outlet glaciers. From Figure 4-6, a large amount of scatter in both the sign and magnitude of dh/dt , is observed below ~ 800 m a.s.l. The large spread in dh/dt at lower elevations corresponds, for the most part, with outlet glaciers (lighter colours in Figure 4-6 a-c, blue and red crosses in Figure 4-6d), where variations in dh/dt were inferred to be attributable largely to changes in ice dynamics (Section 4.4). These data are characterised by a reduction in the rate of thinning (or more rapid thickening) with increasing elevation up to a local maximum, beyond which point dh/dt decreases with increasing elevation. In contrast, data from low-elevation regions not located along outlet glaciers display much less variability in dh/dt at a given elevation, and the magnitude of thinning decreases steadily with increasing elevation. For all data, there is a near linear decrease in the rate of thinning with increasing elevation above ~ 1000 m a.s.l., except on northern Ellesmere Island where higher rates of thinning are observed between ~ 750 and 1500 m a.s.l..

The initial airborne altimetry surveys of 1995 and 2000 were designed to cover the widest parts of the QEI ice masses and, where possible, traverse significant outlet glaciers [Abdalati *et al.*, 2004]. As such, the resulting dh/dt measurements are unevenly distributed across the QEI and tend to be biased toward outlet glaciers. In developing estimates of glacier and ice cap mass loss on the basis of laser altimetry, the relation between dh/dt and elevation is often parameterized and used to extrapolate from point measurements to estimate rates of dh/dt for a larger region [e.g. Arendt *et al.*, 2002; Abdalati *et al.*, 2004; Bamber *et al.*, 2005; Howat *et al.*, 2008; Gardner *et al.*, 2011].

These relationships are then used to produce estimates of volume and mass change for un-surveyed areas. Previous studies [e.g. *Abdalati et al.*, 2004; *Arendt et al.*, 2006; *Gardner et al.*, 2012] noted large uncertainties in extrapolating dh/dt measurements derived from repeat airborne altimetry surveys to obtain regional volume change estimates, but did not address the potential influence of changing ice dynamics on the relationship between dh/dt and elevation. Given the large variability in dh/dt in our dataset, particularly along outlet glaciers where variability appears to be governed primarily by differences in ice dynamics, we did not attempt to establish a quantitative relationship between dh/dt and elevation.

Existing altimetry-based estimates of QEI glacier mass change were published prior to the production of annual QEI-wide surface velocity fields. As such, the influence of changing ice dynamics on surface elevations was not considered when rates of mass change were estimated from altimetry data. *Gardner et al.* [2011, 2013] used a mass-budget model, repeat satellite laser altimetry measurements from the Ice Cloud and land Elevation Satellite (ICESat), and repeat gravimetry using data from the GRACE satellites to produce 'consensus' estimates of QEI glacier mass change for the period 2003-2009. To obtain a QEI-wide estimate of glacier mass change, *Gardner et al.* [2011, 2013] used a third order polynomial of the ICESat-derived dh/dt versus elevation to upscale the measured dh/dt data to the entire QEI ice cover. Examination of these data shows considerable scatter in the annual dh/dt (high standard deviation) for elevation bins below ~700 or 800 m a.s.l. [*Gardner et al.*, 2011, Supplemental Figure S5]. This scatter is consistent with that observed in the ATM-derived dh/dt data presented here (Figure 4-6), which we attribute to patterns of surface elevation change along outlet glaciers that are strongly influenced by variations in ice dynamics. Although there was good agreement between the mass change estimates obtained by all three methods (GRACE, mass budget, ICESat), consideration of ice dynamics as a possible

influence on dh/dt may help to reduce some of the differences between results obtained using different methods. However, we recognise that *Gardner et al.* [2011, 2013] could not have assessed the influence of ice dynamics on the relationship between dh/dt and surface elevation change because QEI-wide surface velocity fields for the period 2003-2009 were not available prior to ~2012/2014 (although some sub-regional estimates were available for shorter time periods).

4.5.2 Conclusion

Repeat airborne laser altimetry measurements show widespread thinning of QEI glaciers and ice caps between 1995 and 2012/14. The bulk of this thinning occurred during the 2005/06-2012/14 period when rates of thinning were > 3 times larger than during the previous two pentads. Our analysis shows that changes in the surface elevation of the QEI ice caps between 2000 and 2012/14 are attributable to the combined effects of ice dynamics and changes in climatic mass balance. Over a majority of the QEI's glaciated surfaces, longitudinal gradients in glacier surface velocity were negligible, suggesting that ice dynamics were probably not a major influence on observed patterns of surface elevation change. In these regions, thinning generally coincided with an increase in LST and a decrease in BSA, implying that, in areas where $|du/dx|$ was small, dh/dt was controlled primarily by changes in glacier mass balance. Along fast-flowing outlet glaciers (e.g. Otto, Ekblaw, Wykeham, and Antoinette glaciers), however, $|du/dx|$ was at least an order of magnitude larger than in the interior regions of the ice masses. In these regions, thinning (thickening) generally coincided with locations of persistent extensional (compressive) flow, suggesting that, in addition to changes in the glacier mass balance, ice dynamics also influenced spatial patterns of dh/dt and their changes over time.

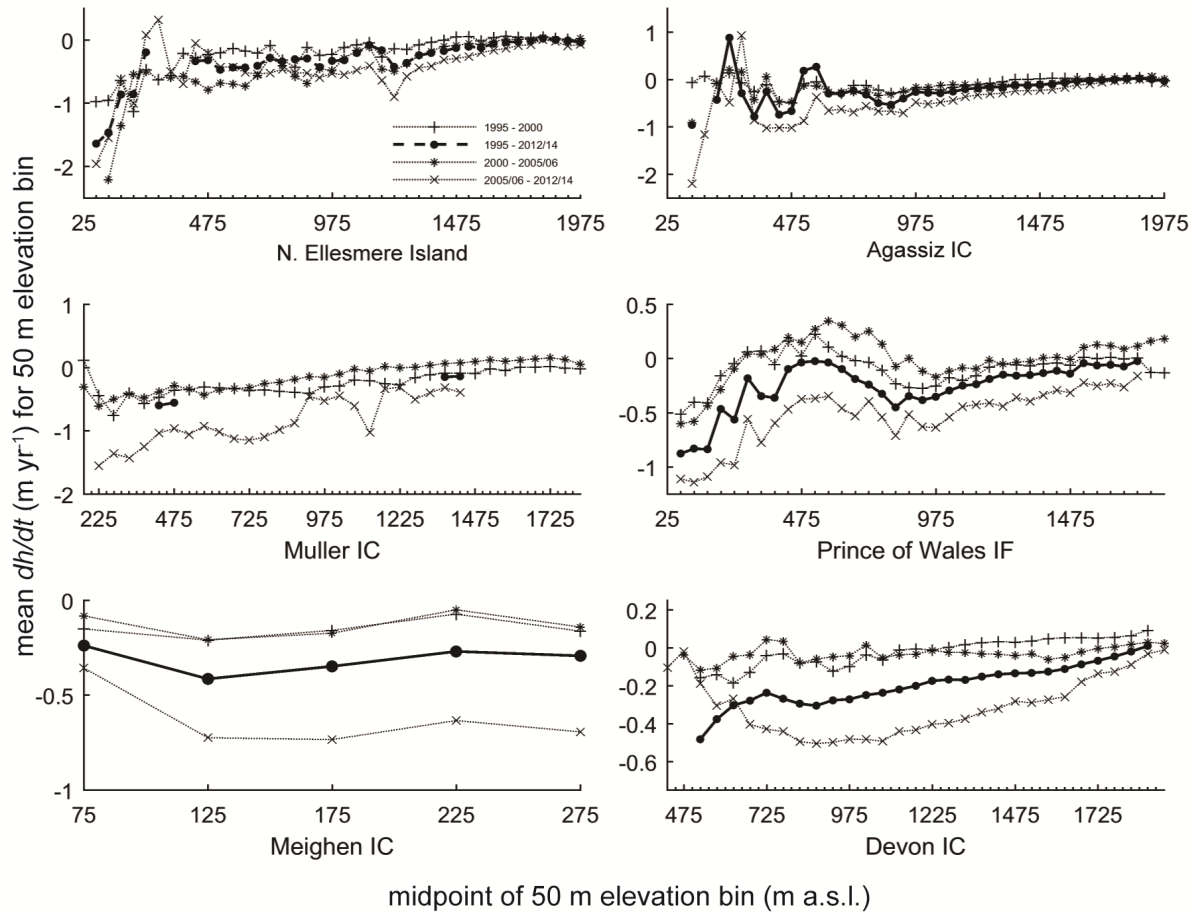


Figure 4-1: Mean dh/dt for 50 m elevation bins for glaciated regions in the QEI between 1995 and 2012/14.

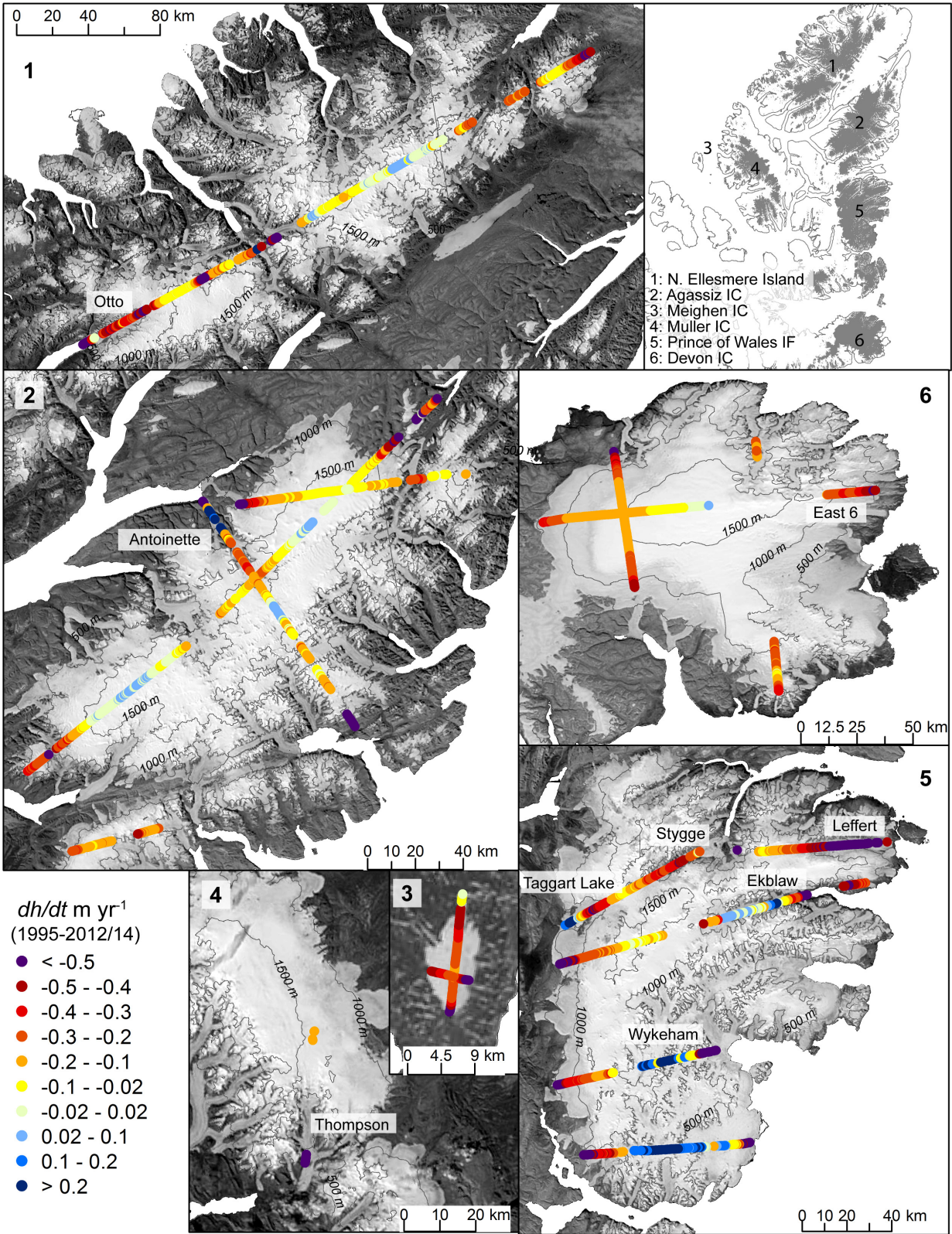


Figure 4-2: Rate of surface elevation change (m yr^{-1}) over glaciated regions in the QEI between 1995 and 2012/14 from repeat airborne altimetry data (IDHDT4), elevation contours from CDED DEM 1:50k.

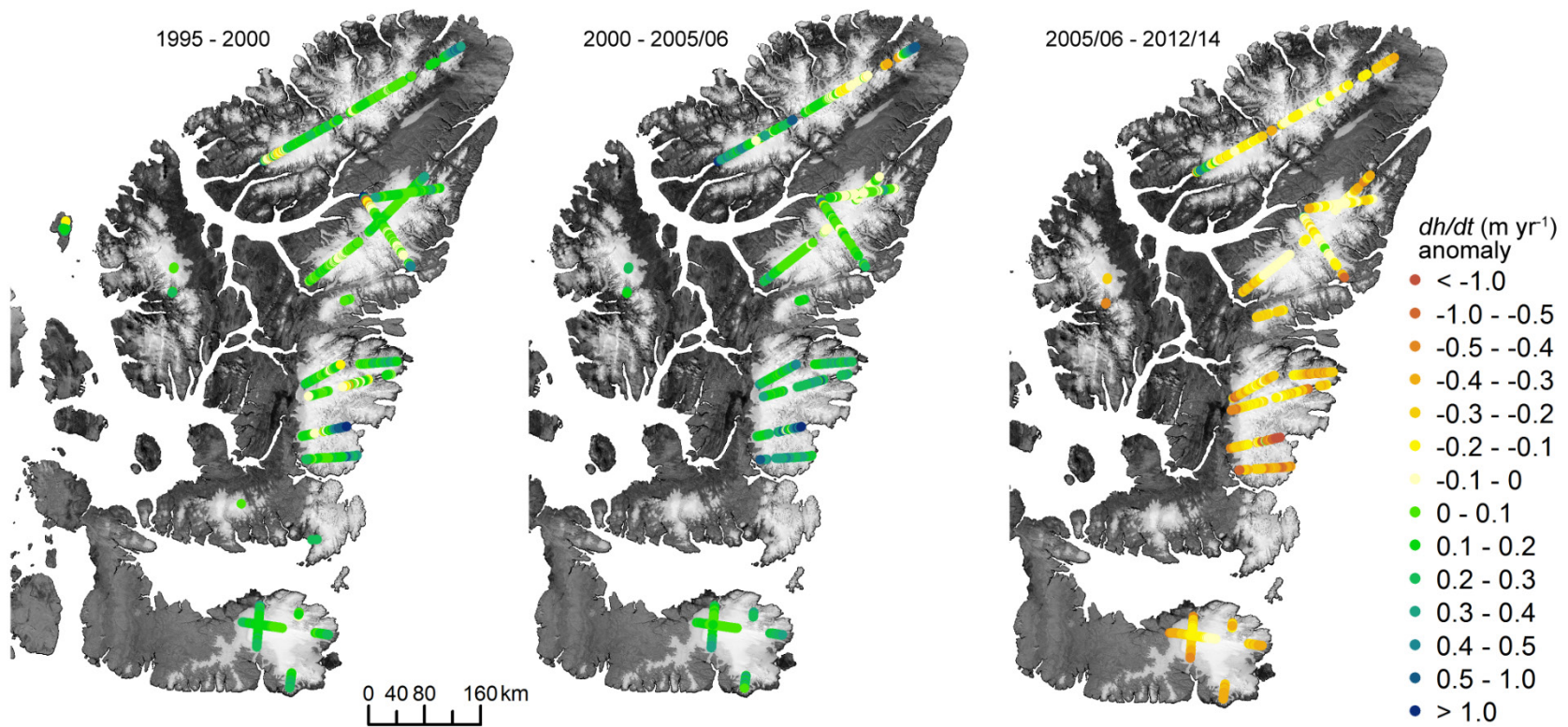


Figure 4-3: dh/dt anomalies (m yr⁻¹) relative to the 1995-2012/14 mean for the 1995-2000, 2000-2005/06, and 2005/06-2012/14 periods.

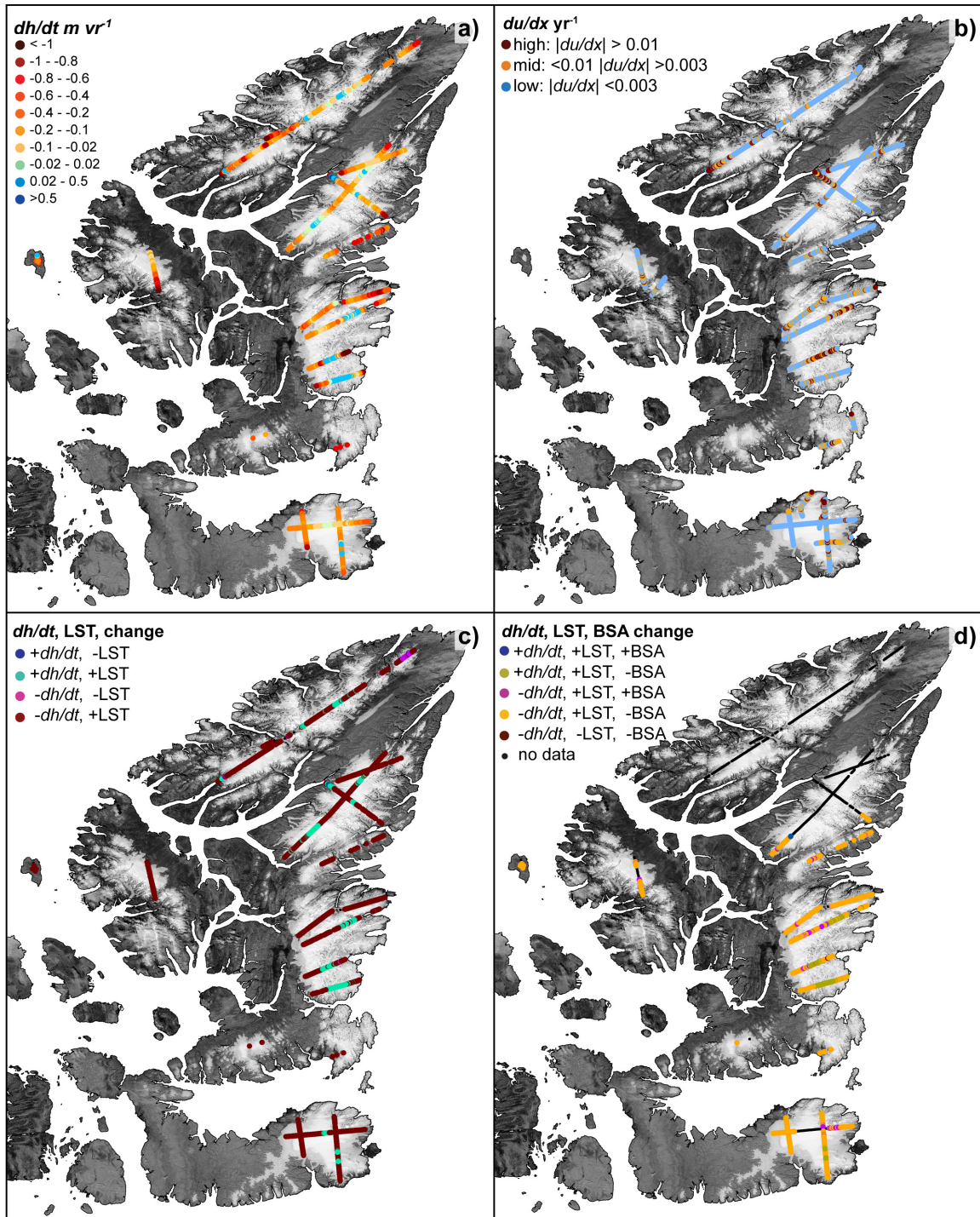


Figure 4-4: comparison of surface elevation change, longitudinal strain rates, temperature and albedo change for the 2000-2012/14 period. a) dh/dt ($m\ yr^{-1}$) for 2000-2012/14, b) mean du/dx (yr^{-1}) from available velocity data between 2000 and 2015, c) comparison of dh/dt with mean summer LST change, d) comparison of dh/dt with mean summer LST and BSA change for areas south of $80^{\circ}N$.

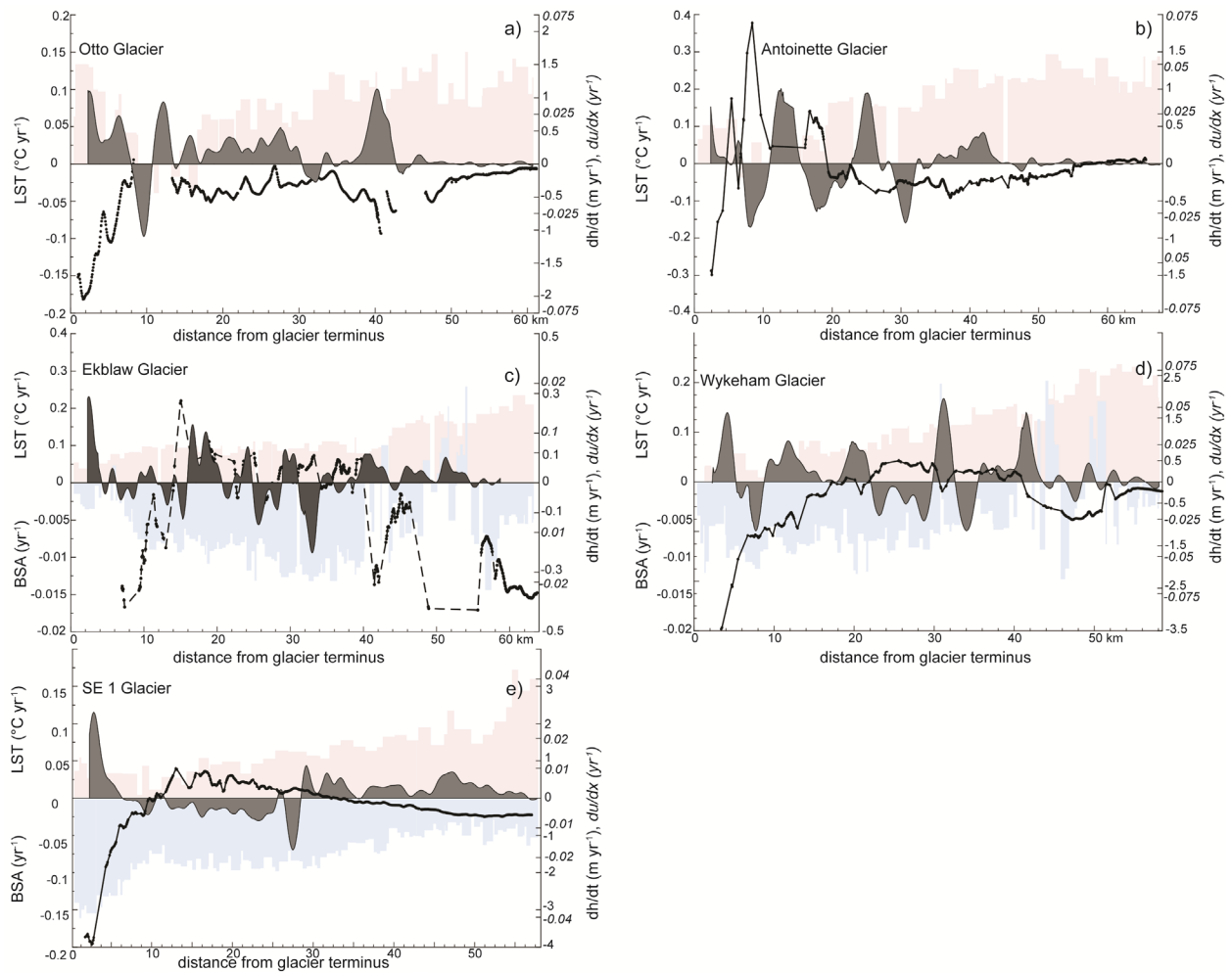


Figure 4-5: Comparison of dh/dt and du/dx for specific glaciers identified as having large longitudinal strain rates and large and highly variable dh/dt in Figure 4. Right-hand axis: mean du/dx (yr^{-1} , solid grey) computed from available annual and velocity data between 1999/2000 and 2015 (italic text). Black line indicates rate of surface elevation change (dh/dt m yr^{-1} , solid text) for 2000-2012/14 (2005-2012 for Southeast 1). Left-hand axis: pink and blue bar graphs indicate rate of LST ($^{\circ}\text{C yr}^{-1}$) and BSA (yr^{-1}) change. For glaciers where both LST and BSA data are available, rate of LST change is indicated on the upper left-hand axis and BSA change on the lower left-hand axis.

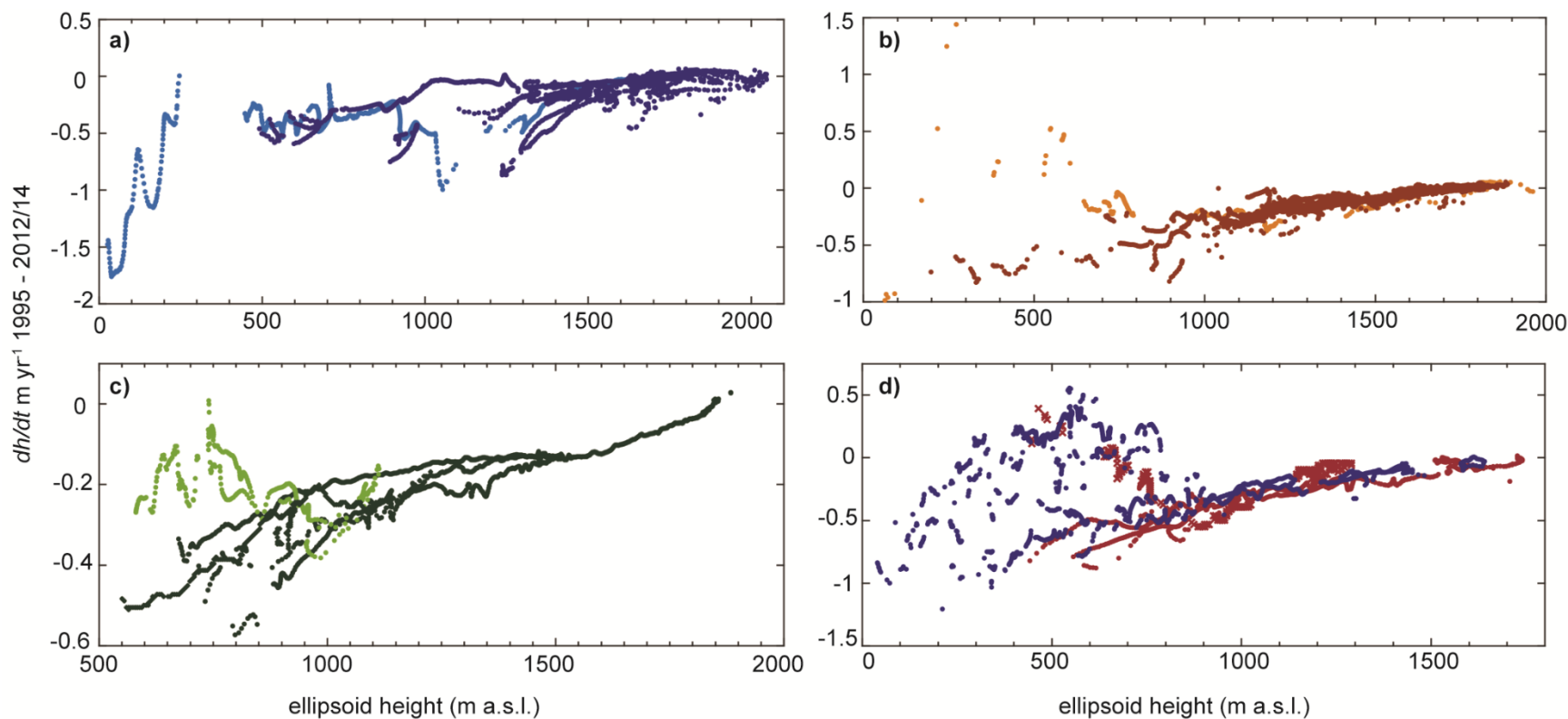


Figure 4-6: dh/dt (m yr^{-1}) versus surface elevation (ellipsoid height, m a.s.l.) over glaciated regions in the QEI between 1995 and 2012/14 shown in Figure 1. a) northern Ellesmere Island, Otto Glacier shown in light blue, b) Agassiz Ice Cap, Antoinette Glacier centerline shown in light orange. c) Devon Ice Cap, data from Belcher and East 6 Glaciers shown in light green. d) Prince of Wales Icefield divided into eastern (blue) and western (red) portions, data for Taggart Lake Glacier indicated by red crosses.

4.6 Chapter 4 Supplemental material

Table 4-S1: sign of change in LST, BSA, and dh/dt for the period 2000-2012, QEI south of 80°N.

	Variables	Causes/explanations	Examples/observations
thickening	+ dh/dt , + LST, + BSA	Longer and/or more intense melt season and reduction in proportion of SW radiation absorbed, thickening	Almost none (not significant) 0.2% of data on both the Devon Ice Cap and Prince of Wales Icefield. 0.8% of data on Agassiz Ice Cap.
	+ dh/dt , +LST, -BSA	Longer and/or more intense melt season and increase in proportion of SW radiation absorption, thickening -increased precipitation, enhanced melt	Eastern Devon Ice Cap where N-S running transect crosses SE 1 and 2 drainage basins (3.1% of Devon Ice Cap data). Prince of Wales Icefield (20.1% of data): <i>Outlet glaciers:</i> Ekblaw Glacier (between ~16 and 43 km from terminus, below ~750 m a.s.l.), Wykeham Glacier (20 km long section in middle between ~24 and 44 km from terminus, between ~550 and 800 m a.s.l.), <i>Other:</i> southernmost transect of Prince of Wales Icefield: 30-25 km long section between ~380 and 700 m a.s.l. (low du/dx)
	+ dh/dt , - LST, + BSA	Shorter and/or less intense melt season (colder), or saturation of LST signal, reduction in proportion of SW radiation absorbed, thickening	Not observed
	+ dh/dt , - LST, -BSA	Shorter and/or less intense melt season (colder) or saturation of the LST signal, increase in proportion of SW radiation absorption, thickening	Not observed
thinning	- dh/dt , + LST, + BSA	Longer and/or more intense melt season, reduction in proportion of SW radiation absorbed, thinning	Prince of Wales Icefield (~5.3% of data): mid-high elevations in central part of icefield, west 1000-1250 m a.s.l.) Scattered observations also found on: Devon Ice Cap (higher elevations (> 1150 m a.s.l.) the in east ~4.9% of Devon Ice Cap data points), higher elevations of Agassiz Ice Cap (> ~1750 m a.s.l.), and Muller Ice Cap (~17% of data points but few total data point). High elevations (>1000 m a.s.l.) of N-S running transect that begins at terminus of Thompson Glacier, ~25 km from terminus). Lack of continuous data in these regions makes it difficult to determine if these observations are artifacts or definite trends in the data.
	- dh/dt , + LST, - BSA	Longer and/or more intense melt season, increase in proportion of SW radiation absorption, thinning	Observed almost everywhere. 83.8% of QEI data points south of 80°N with corresponding LST and BSA change observations. Regionally: Agassiz (91.5%), Axel (82.5%), Devon Ice Cap (91.8%), Meighen Ice Cap (100%), Prince of Wales Icefield (73.8%)
	- dh/dt , - LST, + BSA	Shorter and/or less intense melt season, reduction in proportion of SW radiation absorbed, thinning	Not observed
	- dh/dt , - LST, - BSA	Shorter and/or less intense melt season, increase in proportion of SW radiation absorbed, thinning	Almost none (not significant) 0.6% of data on Prince of Wales Icefield

Table 4-S2: comparison of dh/dt , du/dx , and surface velocities along QEI outlet glaciers.

		dh/dt (2000-2012/14, m yr ⁻¹)	Longitudinal strain rate (du/dx , yr ⁻¹)	Velocity (m yr ⁻¹) (adapted from <i>van Wychen et al.</i> [2016, 2017])
Agassiz IC	Antoinette	<p>Overall thinning with along-glacier variability Mean 2000-12 dh/dt: -0.12 ± 0.24 m yr⁻¹</p> <p>Spatial variability: Distinct zones of thickening/thinning. Sparse data over lowermost ~17 km Thinning (~ -1 m yr⁻¹) on lowermost 5 km. Thickening (mean dh/dt from sparse data: $+0.52$ m yr⁻¹) between ~5 and 17 km from terminus, with localized thickening >1 m yr⁻¹. Above ~40 km from terminus, mean dh/dt: -0.07 ± 0.1 m yr⁻¹</p> <p>Temporal variability* 2000-06: -0.06 ± 0.20 m yr⁻¹ 2006-12: -0.21 ± 0.41 m yr⁻¹ *Limited data over lowermost ~15 km during 2000-06 so temporal differences not fully representative.</p>	<p>Along-glacier variability: zones of compression and extension Alternating zones of extension ($>+0.01$ yr⁻¹) and compression (<-0.01 yr⁻¹) over lower ~30-35 km appear to coincide with areas of thinning and thickening (see Figure 5a) but dh/dt measurements over the lower ~17 km are sparse. <u>Extension</u> over lowermost ~5 km (mean du/dx: ~ 0.006, maximum ~ 0.035 yr⁻¹), coincides with thinning. Extension ($\sim +0.1$ yr⁻¹) at ~12 and 25 km from terminus. <u>Compression</u> at ~8km (-0.03 yr⁻¹) and ~18 km (-0.024 yr⁻¹) from terminus coincide with thickening ($+1.9$ m yr⁻¹ and $+0.7$ m yr⁻¹, respectively). Compression at ~30 km; may coincide with lower rates of thinning Above ~40 km from terminus du/dx was low (> -0.003 yr⁻¹) dh/dt was small (mean dh/dt: -0.07 ± 0.1 m yr⁻¹)</p>	<p>Slowdown Surface velocities along ATM flight line (data from <i>van Wychen et al.</i> [2016]): Above ~40 km from terminus surface velocities are low ($<15-20$ m yr⁻¹). Below ~40 km from terminus velocities are higher ($> \sim 150$ m yr⁻¹) and more variable. Antoinette Glacier centerline proper [<i>van Wychen et al.</i>, 2016]: Near-terminus surface velocity decrease from ~100 m yr⁻¹ in 2000 to stagnant in 2015. Deceleration occurred over ~5-7 year period and at end of period is stagnant. Reduction in dynamic discharge from 0.04 Gt yr⁻¹ in 2000 to 0 Gt yr⁻¹ in 2012 (stagnant). Classified as pulse-type glacier by <i>van Wychen et al.</i> [2016]</p>
Muller IC	Thompson	<p>Thinning along entire length of glacier Mean 2000-12 dh/dt: -0.56 ± 0.19 m yr⁻¹</p> <p>Spatial variability: Higher rates of thinning below where glacier enters constriction ~28 km from terminus. Mean dh/dt for lowermost ~28 km: -0.65 ± 0.15 m yr⁻¹; above 28 km dh/dt: -0.38 ± 0.13 m yr⁻¹</p> <p>Temporal: Stronger thinning during 2006-12 (-0.99 m yr⁻¹) compared with 2000-06 (-0.25 m yr⁻¹). Mild thickening in uppermost ~2.5 km during 2000-06.</p>	<p>Moderate du/dx with locally higher rates. Heterogeneous du/dx, no discernable pattern of compression or extension but du/dx data are limited to 2000 and 2011-2015.</p> <p>Low-moderate du/dx (less than 0.01 yr⁻¹) with locally higher rates (greater than 0.01 yr⁻¹). Mild extension (mean du/dx: $\sim +0.0004$ yr⁻¹) over lowermost ~25 km (up to $\sim +0.015$ yr⁻¹); corresponds with increase in rates of thinning toward terminus.</p> <p>du/dx feature: compression-extension-compression, in excess of ~ 0.020 yr⁻¹] between ~20 and 28 km from terminus coincides with where ice enters a constriction and is forced around a cliff. This feature coincides with a region of lower rates of thinning (thickening during 2000-06) surrounded by higher rates of thinning.</p>	<p>Slowdown Surface velocities along ATM flight line obtained from <i>van Wychen et al.</i> [2016] and are limited to 2000 and 2011-2015. Lowermost ~8-10 km, surface velocities up to ~ 25 m yr⁻¹ in 2011-2015 compared with 2000. 2011-2015 velocities at 10 km from terminus and between ~15 and 32 km from terminus ~ 10 to 40 m yr⁻¹ higher compared with 2000. Localized slower velocities at ~34 km from terminus where 2011-2015 velocities were 25-30 m yr⁻¹ lower than in 2000. <i>Copland et al.</i> [2003]: Possible surge-type glacier determined from presence of large looped and folded moraines across terminus in 1959 and 1999, ~ 0.75 km advance between 1959 and 1999.</p>

Prince of Wales IF	Leffert	<p>Thinning along entire length of glacier Mean 2000-12 dh/dt: -0.50 ± 0.27 m yr⁻¹</p> <p><u>Spatial</u>: stronger thinning along lower ~40 km, mean dh/dt along this section -0.7 m yr⁻¹, localized thinning up to -1.05 m yr⁻¹.</p> <p>Stronger thinning between ~10 and 25 km from terminus (mean dh/dt: -0.84 ± 0.12 m yr⁻¹). Lower rates of thinning (-0.22 ± 0.07 m yr⁻¹) in uppermost 20 km</p> <p>Increase in rate of thinning until ~10km from terminus; decrease in rate of thinning over lower ~10 km</p> <p><u>Temporal</u>: stronger thinning in 2005-12 2000-05: -0.22 ± 0.22 m yr⁻¹ 2005-12: -0.73 ± 0.30 m yr⁻¹</p>	<p>Moderate but variable du/dx Extension ($\sim +0.01$ yr⁻¹) near terminus (lower ~3 km) but lower rates of thinning (~ -0.3 m yr⁻¹ compared with < -1 m yr⁻¹ ~11 km from terminus). Low du/dx between ~3 km and ~15 km from terminus. Higher rates of du/dx between ~16 and 32 km from terminus and have <u>alternating zones of compression and extension</u> in the region. Extension at ~24 km from terminus coincides with locally higher rate of thinning (~ -0.8 m yr⁻¹). Consistent extension above ~34 km from the terminus (mean du/dx: $+0.001$ yr⁻¹; local maximum: 0.005 yr⁻¹)</p> <p><u>du/dx vs. dh/dt</u>: Overall pattern of du/dx (increase in rate of thinning until ~10km from terminus and decrease in rate of thinning over lower ~10 km) does not fully correspond with du/dx. Local variations in dh/dt, superimposed upon large-scale thinning trend may be linked to local variations in du/dx but not clear. Lack of correspondence may be due, in part, lack of temporal coverage in du/dx (limited to 2000 and 2012-2015)</p>	<p>Slowdown Surface velocities along ATM flight line (which is close to centerline) obtained from <i>van Wychen et al.</i> [2016].</p> <p><u>Temporal</u> Reduction in near-terminus velocities from ~80 m yr⁻¹ in 2000 to ~30 m yr⁻¹ in 2012. Decrease in dynamic discharge from 0.02 Gt yr⁻¹ in 2000 to 0.00 Gt yr⁻¹ in 2012. Velocity data limited to 2000 and 2011-2015.</p> <p><u>Spatial</u>: Velocities increase from drainage divide to ~40 km from terminus (35-45 m yr⁻¹). Lower velocities (10-30 m yr⁻¹) between ~15 and 30 km from terminus. Sharp increase (~ 20 m yr⁻¹) in velocity at ~15 km from terminus.</p>
	Ekblaw	<p>Overall thinning with along-glacier variability 2000-12 mean dh/dt -0.12 ± 0.17 m yr⁻¹</p> <p><u>Spatial variability</u>: Slight thickening (mean dh/dt $+0.03$ m yr⁻¹) between ~15 and ~45 km from terminus with slight thinning (-0.067 m yr⁻¹) at ~32 km from terminus; thinning above ~45 km and below ~15 km from terminus. Mean dh/dt for uppermost ~22 km: -0.27 ± 0.11 m yr⁻¹. Few data points in lowermost ~10 km but suggests thinning during 2000-12.</p> <p><u>Temporal variability</u> 2000-05: thickening (0.11 ± 0.22 m yr⁻¹) especially over lowermost ~45 km ($+0.26 \pm 0.18$ m yr⁻¹); no data for lower ~5 km. 2005-12: thinning (-0.34 ± 0.21 m yr⁻¹).</p>	<p>High du/dx with alternating zones of compression/extension <u>Extension</u>: lowermost ~5 km ($>+0.1$ yr⁻¹) coincides with thinning, up to ~1 m yr⁻¹ during 2005-2012, sparse data for 2000-2012.</p> <p><u>Alternating zones of extension</u> between ~15 and 38 km from terminus (mean du/dx: $+0.0002$ yr⁻¹). Extension (up to $+0.02$ yr⁻¹) at ~18, 22, and 30 km from terminus. Compression (up to -0.03 yr⁻¹) at ~26, and 33 km from terminus tend to coincide with thickening. Extension ~38-42 km from terminus coincides with localized thinning (~ -0.3 m yr⁻¹).</p> <p>Ice enters constriction ~50 km from terminus, above this location du/dx is low (± 0.005 yr⁻¹ and standard deviation of dh/dt is small (0.11 m yr⁻¹))</p>	<p>Slowdown Along ATM flight line (obtained from <i>van Wychen et al.</i> [2016]): Decrease in surface velocity over entire lower ~25-30 km (during 2000-2015) and magnitude of slowdown increases toward terminus.</p> <p><u>Ekblaw centerline proper</u> [<i>van Wychen et al.</i>, 2016]: Decrease in near-terminus surface velocity from ~500 m yr⁻¹ in 2000 to ~150-200 m yr⁻¹ in 2015 (not currently stagnant). Increase in dynamic discharge between 2000 (0.14 Gt yr⁻¹) and winters 20006 and 2007 (0.20 Gt yr⁻¹), decrease to 0.11 Gt yr⁻¹ in 2012 and 0.07 Gt yr⁻¹ in 2014. Terminus retreat (~ 0.5 km) between 2000 and 2014.</p> <p>Classified as pulse-type glacier by <i>van Wychen et al.</i> (2016)</p>
	Wykeham*	<p>Overall thinning with along-glacier variability Mean 2000-12 dh/dt: -0.27 ± 0.55 m yr⁻¹</p> <p><u>Spatial variability</u>: thickening in middle Thickening ($+0.25$ m yr⁻¹) between ~22 and ~40 km from terminus Thinning: mean dh/dt -1.2 m yr⁻¹ between ~3 km and ~13 km from terminus; no data for lowermost ~3 km. Thinning (-0.45 m yr⁻¹) over uppermost ~15 km.</p> <p><u>Temporal variability</u>: 2000-05: thickening ($+0.27 \pm 0.37$ yr⁻¹) 2005-12: thinning (-0.39 ± 0.64 m yr⁻¹)</p> <p>* Note: location of Wykeham ATM line differs significantly from central flowline</p>	<p>Along-glacier variability Middle compression, upper and lower extension</p> <p><u>Extension</u> specially pronounced in lowermost ~5 km ($>+0.05$ yr⁻¹), increases towards terminus and was particularly strong ($>+0.1$ yr⁻¹) from ~2011 onward. Spatiotemporal variability in du/dx corresponds with increase in rates of thinning.</p> <p>Moderate extension over lower ~20 km; except for compression ~4 km from terminus; corresponds generally with thinning. Extension between ~40 and 50 km from terminus also corresponds with thinning.</p> <p><u>Compression</u>: local compression ~4 km from terminus. Compression (~ -0.02 yr⁻¹) between ~20 and 30 km from terminus generally corresponds with thickening.</p>	<p>Speedup Surface velocities <u>along ATM flight line</u> obtained from <i>van Wychen et al.</i> [2016]: <u>Temporal</u>: increase in surface velocity between 1999-2000 and 2004-2005, decrease from 2004-2005 to 2007-2008. Consistent increase in near-terminus surface velocity (lowermost ~5 km) from 2009-2015. Temporal differences in surface velocity increase towards terminus.</p> <p><u>Spatial</u>: generally high surface velocities (>150 m yr⁻¹) along much of the length of this glacier, especially the lowermost 40 km.</p> <p><u>Wykeham Glacier centerline proper</u> [<i>van Wychen et al.</i>, 2016]: Increase in surface velocity across lowermost ~5 km from ~200-300 m yr⁻¹ in 2000 to 500 m yr⁻¹ in 2015. Dynamic discharge 0.17 Gt yr⁻¹ in 2000 and >0.30 Gt yr⁻¹ 2011 onward. Terminus retreat of ~1 km between 2000 and 2014. Classified as surge-type glacier by <i>van Wychen et al.</i> [2016].</p>

	Taggart Lake North*	<p>Thinning along entire length of glacier Mean 2000-12 dh/dt: -0.30 ± 0.17 m yr⁻¹</p> <p><u>Spatial variability</u>: 2000-2012 Maximum thinning (0.67 m yr⁻¹) ~15 km from margin. Higher rates of thinning (2000-12 dh/dt: -0.49 m yr⁻¹) between ~12 and 20 km from margin in all time periods. Lesser rate of thinning above ~25 km from margin (mean dh/dt -0.14 0.05 m yr⁻¹) No data for lowermost ~10 km.</p> <p><u>Temporal variability</u>: 2000-05: no change ($+0.005 \pm 0.016$ m yr⁻¹) 2005-12: thinning (-0.45 ± 0.22)</p> <p>*Note: analysis restricted to northernmost ATM line in Taggart Lake drainage basin.</p>	<p>Moderate du/dx, along-glacier variability du/dx limited to 2000 and 2011-2015.</p> <p><u>Compression</u> (< -0.025 or 0.03 yr⁻¹) below ~8 km, coincident dh/dt data only available for 2005-12 but shows trend towards lower rates of thinning towards margin and thickening ~2 km from margin. Compression between ~8 and ~12km from terminus except in 2000. <u>Extension</u> ($\sim +0.02$ yr⁻¹) between ~12 and 20 km, magnitude decreases up-glacier, coincides with higher rates of thinning. Local extension (~ 0.035 yr⁻¹) feature ~8 km in 2011 and 2012 from terminus but lack of corresponding dh/dt data.</p> <p>Moderate and spatially homogeneous du/dx (between $+0.004$ yr⁻¹ and -0.004 yr⁻¹) in uppermost ~10 km; mild thinning.</p>	<p>Slowdown Surface velocities along ATM flight line (data from <i>van Wychen et al.</i> [2016]): <u>Temporal</u>: higher surface velocities in 2000 compared with 2011-2015 period (~ 10-20 m yr⁻¹ higher). Maximum surface velocities occur ~5 km from margin in all years. <u>Spatial</u>: In 2000, consistent increase in surface velocities from drainage divide (0-20 m yr⁻¹) to ~5 km from margin (~ 110 m yr⁻¹), consistent decrease in surface velocity along lower 5 km to ~30 m yr⁻¹ at margin. <u>Spatiotemporal</u>: Maximum 2011-2015 velocity 2011-2015 ~80 m yr⁻¹. During 2011-2015, reduction in velocity towards margin begins farther up-glacier (at ~12 km from margin) than in 2000. 2011-2015 velocity profile relatively flat between ~12 and 5 km from terminus with local velocity minimum ~8 km from terminus. This local minimum was not observed in 2000. Observed surge in 1999 into a proglacial lake. Terminus advanced ~3 km between 1959 and 1999. Distinctive shear margin, extensive surface folding [<i>Copland et al.</i>, 2003].</p>
	East 6*	<p>Thinning along entire length of glacier Mean 2000-2012 dh/dt along lowermost ~20 km* -0.36 ± 0.12 m yr⁻¹ <u>Spatial variability</u>: Higher rates of thinning (< -0.5 m yr⁻¹) towards margin <u>Temporal variability</u>: Increase in rate of thinning between 2000-2005 (-0.09 ± 0.07 m yr⁻¹) and 2005-2012 (-0.58 ± 0.16 m yr⁻¹). *Note: only the lower 20 km of this transect is on East 6 Glacier and it but does not follow the outlet glacier proper; it is north of the main glacier trunk.</p>	<p>Low du/dx, with locally higher rates, and very little variability</p> <p><u>Local extension</u> (0.015 yr⁻¹, ~16 km from terminus) followed by compression (~ -0.015 yr⁻¹, ~12 km from terminus) may correspond with locally higher(lower) rates of thinning but not definitive.</p> <p>du/dx is generally low (± 0.003 yr⁻¹) with little along-glacier variability, except between ~12 and 16 km from margin</p>	<p>No measurable change Surface velocities along ATM flight line (data from <i>van Wychen et al.</i> [2017]): Consistent low velocities (< 20 m yr⁻¹) along ATM flight line. No measurable change (no change in excess of 20 m yr⁻¹) in surface velocity between 2009 and 2015.</p> <p>East 6 glacier proper from <i>van Wychen et al.</i> [2015]: ~20 m yr⁻¹ velocity reduction between 2010 and 2011. 2015 velocities were lowest during observation period (2009-2015). Dynamic discharge for East 6 proper was 0 Gt yr⁻¹ during 2009-2015.</p>
Devon IC	SE1 [SE 2 similar, only SE1 presented]	<p>Distinct zones of thinning and thickening Thickening in middle, thinning above and below. Mean 2006-12 dh/dt*: SE1 -0.19 ± 0.67 m yr⁻¹; <u>Spatial</u>: Thinning (mean dh/dt: -1.2 ± 1.2 m yr⁻¹) over lowermost ~10km, thinning increases toward terminus (up to -3.9 m yr⁻¹). No data for lowermost ~4-5 km. Thickening (mean dh/dt: $\sim +0.34$ m yr⁻¹; local maximum: $+0.79$ m yr⁻¹) between ~10 and 30 from terminus. Thinning in upper ~25 km (mean dh/dt: ~ -0.28 m yr⁻¹). <u>Temporal</u>: Data along glacier only available for 2005-2012. N-S running transect on eastern Devon Ice Cap, crosses SE1 drainage basin. Data at this location are available for 2000-2005 and 2000-2012 and show thickening (> 0.1 m yr⁻¹); corroborates thickening observed during 2005-2012.</p>	<p>Distinct zones of compression and extension</p> <p><u>Extension</u> over lowermost ~10 km mean (du/dx: $\sim +0.004$ yr⁻¹, local maximum: $\sim +0.029$ yr⁻¹) coincides with thinning. Extension over uppermost ~25 km (mean du/dx: $\sim +0.003$ yr⁻¹; local maximum: $\sim +0.028$ yr⁻¹), corresponds with thinning.</p> <p><u>Compression</u> (mean du/dx: -0.003 yr⁻¹, local minimum -0.017 yr⁻¹) between ~10 and 30 km from terminus, coincides with thickening.</p> <p>Distinct shift from compression to extension ~30 km from terminus. Corresponds with maximum surface velocity (> 100 m yr⁻¹).</p>	<p>Spatial variability Surface velocities along ATM flight line obtained from <i>van Wychen et al.</i> [2017]. Velocity data only available for 2009-2015, with no data for 2011, so temporal variability not assessed.</p> <p><u>Spatial</u>: maximum velocities (> 100 m yr⁻¹) occur ~30 km up-glacier from terminus. Near drainage divide, surface velocities are below ~15 m yr⁻¹; velocities along lowermost ~10 km are between ~3 and 15 m yr⁻¹.</p> <p>Dynamic discharge for Southeast 1 and 2 glaciers 0.03 Gt yr⁻¹ in 2009 and 2010, 0.04 Gt yr⁻¹ in 2011 and 2012 [<i>van Wychen et al.</i>, 2017]. <i>Burgess and Sharp</i> [2008] identified possible surge-type behaviour from calculations of flux divergence.</p>

N. Ellesmere I.	Otto	<p>Overall thinning with spatiotemporal variability. Mean 2000-2014 dh/dt: -0.41 ± 0.38 m yr⁻¹</p> <p><u>Spatial variability</u> Strong thinning, along lowermost ~5 km (mean dh/dt: -1.34 ± 0.46 m yr⁻¹; localized thinning <-2 m yr⁻¹) and between ~35 and 45 km (mean dh/dt: -0.55 ± 0.13 m yr⁻¹) from terminus. Missing data between ~5 and ~15 km from terminus where thickening ($+0.34$ m yr⁻¹) was observed during 2006-2014. Lesser rate of thinning (mean dh/dt: -0.17 ± 0.12 m yr⁻¹) in uppermost ~15 km.</p> <p><u>Temporal variability</u> Little difference in glacier-wide average dh/dt between 2000-2006 (mean dh/dt: -0.40 ± 0.26 m yr⁻¹) and 2006-2014 (mean dh/dt: -0.41 ± 0.49 m yr⁻¹), but spatial differences in dh/dt between time periods are observed.</p> <p><u>Spatiotemporal</u> More along-glacier variability in 2006-2014 compared with 2000-2006. Pronounced area of thickening between ~6 and 15 km from terminus (mean dh/dt: $\sim +0.34$ m yr⁻¹) only observed in 2006-14 but there was a considerable amount of missing data for the 2000-2006 period. More expansive up-glacier zone of thinning ($dh/dt < -0.4$ m yr⁻¹) in 2006-2014 (~15 km long, between 35 and 50 km from terminus) compared to 2000-2006 (~6 km long, ~40-46 km from terminus).</p>	<p>du/dx high near terminus, elsewhere du/dx is moderate</p> <p>du/dx highest in lower ~5-10 km (up to $\sim +0.8$ yr⁻¹). Above ~12 km from terminus du/dx is moderate (> -0.01 yr⁻¹ or $< +0.01$ yr⁻¹).</p> <p><u>Extension</u> on lower ~5-10 km ($\sim +0.08$ yr⁻¹), coincides with strong thinning. Extension above ~10-12 km from terminus (mean du/dx: $+0.006$ yr⁻¹, local maximum: $+0.05$ yr⁻¹), except for at ~32 km from terminus (compression).</p> <p><u>Compression</u> ~10 km from the terminus (~ -0.05 yr⁻¹) appears to correspond with thickening, however, dh/dt measurements for this location are extremely sparse.</p> <p>Above ~45 km from terminus du/dx is low (> -0.003 yr⁻¹ or $< +0.003$ yr⁻¹) and dh/dt is spatially homogeneous.</p>	<p>Variable velocity</p> <p>Surface velocities along ATM flight line obtained from <i>van Wychen et al.</i> [2016].</p> <p><u>Temporal</u>: 2013-2015 winter velocities along entire length of ATM flight line lower during 2013-2015 compared with 2000. >65 m yr⁻¹ increase in velocity over lowermost ~20 km between 2000 and 2007.</p> <p><u>Spatiotemporal</u>: Marked reduction in velocity (~ 250 m yr⁻¹) over lowermost ~5 km) between 2012 and 2013, Temporal divergence in surface velocities began ~20 km from terminus.</p> <p><u>Otto Glacier centerline proper</u> [<i>van Wychen et al.</i>, 2016]: Increase in surface velocity over lower 10 km from ~200-400 m yr⁻¹ in 2000 to ~600-700 m yr⁻¹ in 2007 and 2008 (lower 5 km) followed by a reduction in surface velocity along lowermost ~5 km from 2009 onward ($\sim 250-300$ m yr⁻¹ in 2009-2010) and terminus region stagnant in 2013-2015. Decrease in dynamic discharge from 0.11 Gt yr⁻¹ in 2000 to 0.09 Gt yr⁻¹ in 2012.</p> <p>Confirmed surge-type glacier: <i>Copland et al.</i> [2003] observed surging in 1959 and 1999. ~2km terminus advance 1959-1999. Heavy crevassing, not surging in 1950.</p>
-----------------	------	---	---	--

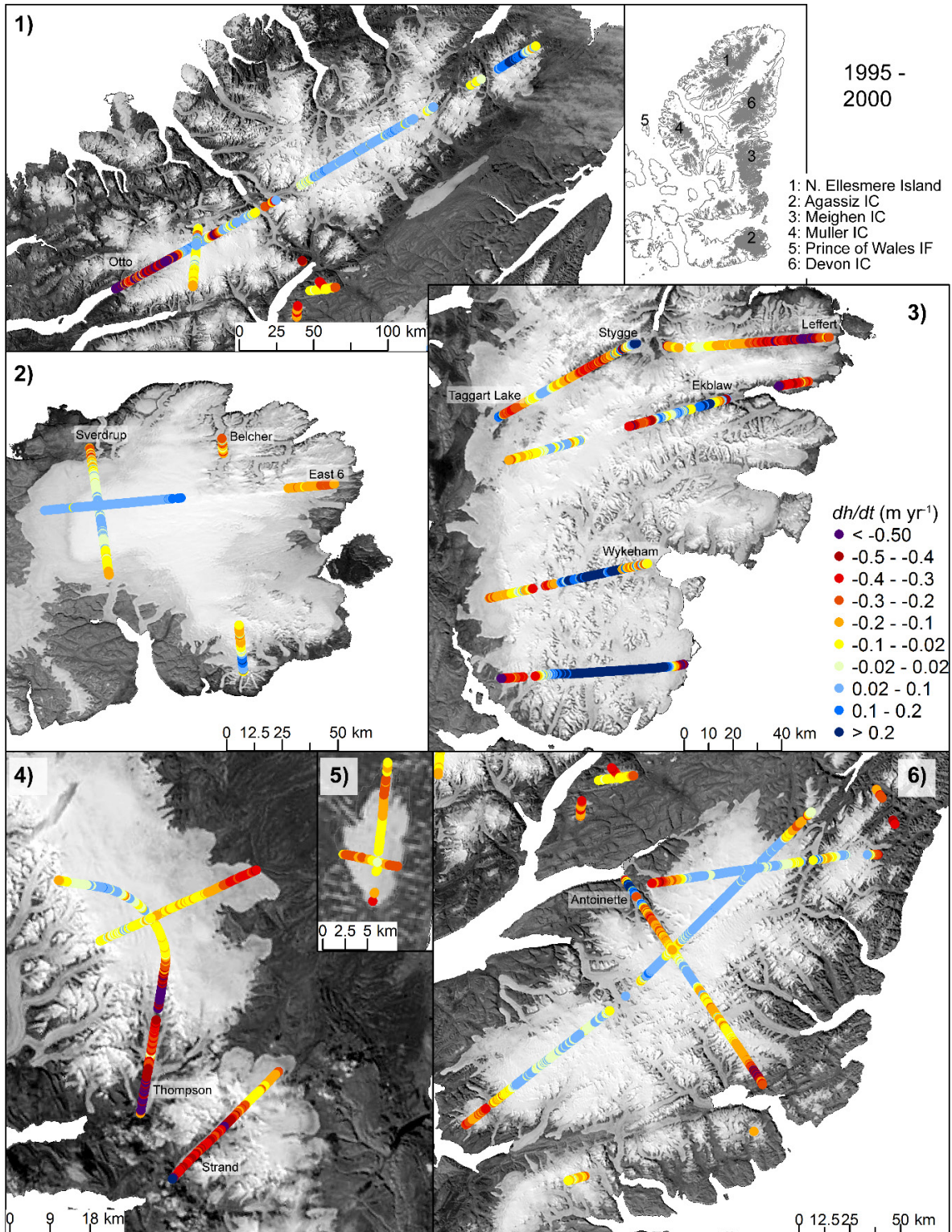


Figure 4-S3: Rate of surface elevation change (m yr^{-1}) over glaciated regions in the QEI between 1995 and 2000 from repeat airborne altimetry data (IDHDT4), surface elevations from CDED DEM 1:50k. Similar data are presented in *Abdalati et al.* [2004].

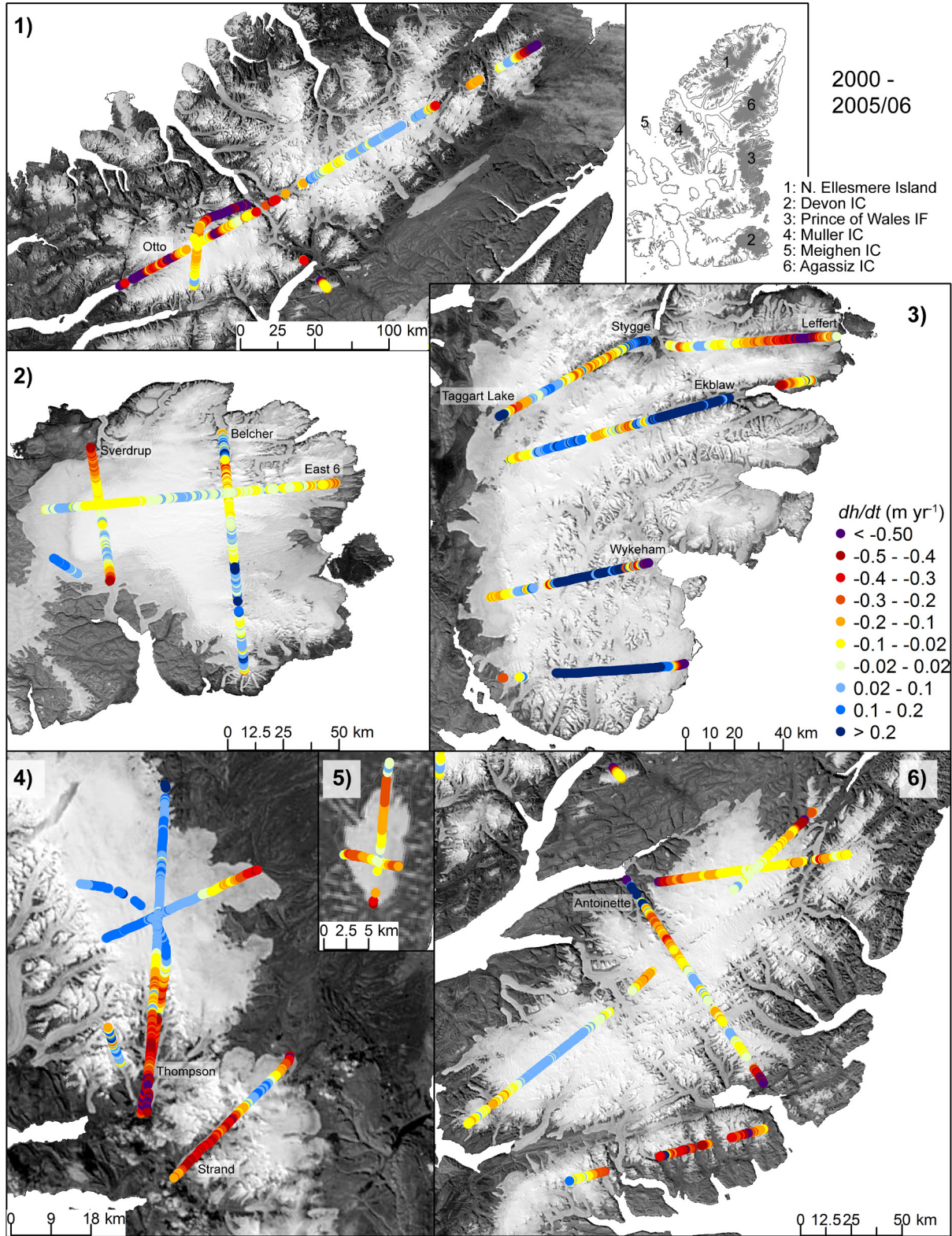


Figure 4-S4: Rate of surface elevation change (m yr^{-1}) over glaciated regions in the QEI between 2000 and 2005/06 from repeat airborne altimetry data (IDHDT4), surface elevations from CEDD DEM 1:50k.

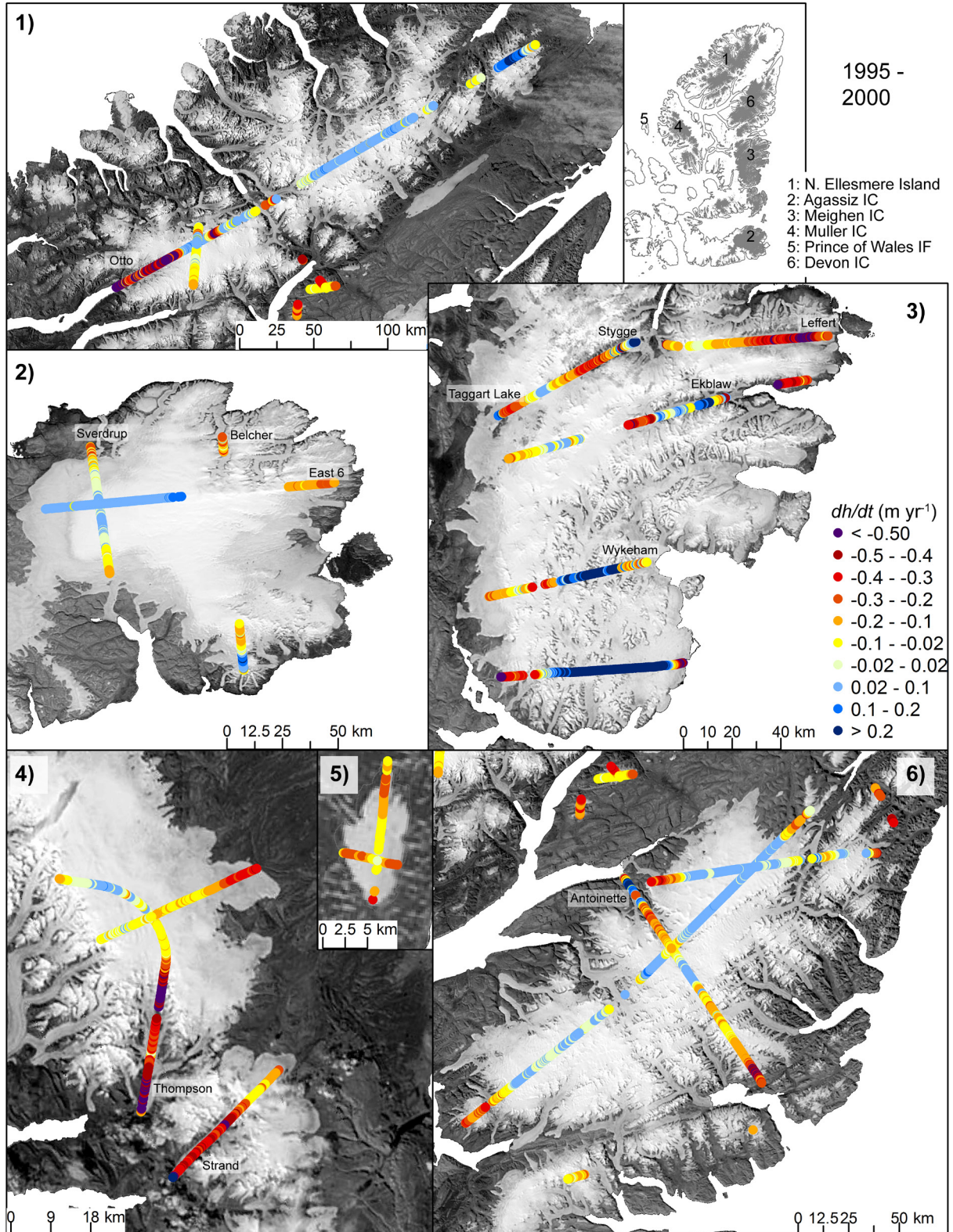


Figure 4-S5: Rate of surface elevation change (m yr⁻¹) over glaciated regions in the QEI between 2005/06 and 2012/14 from repeat airborne altimetry data (IDHDT4), surface elevations from CDED DEM 1:50k.

4.7 References

- Abdalati, W., W. Krabill, E. Frederick, S. Manizade, C. Martin, J. Sonntag, R. Swift, R. Thomas, J. Yungel, and R. Koerner (2004), Elevation changes of ice caps in the Canadian Arctic Archipelago, *J. Geophys. Res.*, *109*(F04007), doi: 10.1029/2003JF000045.
- Ackerman, S. A., K. I. Strabala, P. W. Menzel, R. A. Frey, C. C. Moeller, and L. E. Gumley (1998), Discriminating clear sky from clouds with MODIS, *J. Geophys. Res.*, *103*(D24), 32141–32157, doi:10.1029/1998JD200032.
- Alexander, P. M., M. Tedesco, X. Fettweis, R. S. W. van de Wal, C. J. P. P. Smeets, and M. R. van den Broeke (2014), Assessing spatiotemporal variability and trends in modeled and measured Greenland Ice Sheet albedo (2000-2013), *The Cryosphere*, *8*(6), 2293-2312, doi: 10.5194/tc-8-2293-2014.
- Arendt, A. A., K. A. Echelmeyer, W. D. Harrison, C. S. Lingle, and V. B. Valentine (2002), Rapid wastage of Alaska Glaciers and their contribution to rising sea level, *Science*, *297*(5580), 382-386, doi: 10.1126/science.1072497.
- Arendt, A., K. Echelmeyer, W. Harrison, C. Lingle, S. Zirnheld, V. Valentine, B. Ritchie, and M. Druckenmiller (2006), Updated estimates of glacier volume changes in the western Chugach Mountains, Alaska, and a comparison of regional extrapolation methods, *J. Geophys. Res.: Earth Surf.*, *111*(F3), doi: 10.1029/2005JF000436
- Arendt, A., et al. (2012), Randolph Glacier Inventory Vers. 3.0: a dataset of Global Glacier Outlines. Global Land Ice Measurements from Space, Boulder, CO. Digital media: http://www.glims.org/RGI/rgi32_dl.html.
- Bamber, J. L., W. Krabill, W. Raper, J. A. Dowdeswell, and J. Oerlemans (2005), Elevation changes measured on Svalbard glaciers and ice caps from airborne laser data, *Ann. Glaciol.*, *42*(1), 202-208, doi: 10.3189/172756405781813131.
- Bezeau, P., M. Sharp, D. Burgess, and G. Gascon (2013), Firn profile changes in response to extreme 21st-century melting at Devon Ice Cap, Nunavut, Canada, *J. Glaciol.*, *59*(217), 981-991, doi:10.3189/2013JoG12J208.

- Box, J. E., X. Fetwweis, J. C. Stroeve, M. Tedesco, D.K. Hall, and K. Steffen (2012), Greenland ice sheet albedo feedback: thermodynamics and atmospheric drivers, *Cryosphere*, 6(4), 821-839, doi: 10.5194/tc-6-821-2012.
- Braithwaite, R. J. (2005), Mass balance characteristics of arctic glaciers, *Ann. Glaciol.*, 42, 225-229, doi: 10.3189/17275640578182899.
- Burgess, D., and M. J. Sharp (2008), Recent changes in thickness of the Devon Island ice cap, Canada, *J. Geophys. Res.*, 113(B07204), 1-18, doi: 10.1029/2007/JB005238.
- Cogley, J. G., R. Hock, L. A. Rasmussen, A. A. Arendt, A. Bauder, R. J. Braithwaite, P. Jansson, G. Kaser, M. Möller, L. Nicholson, and M. Zemp (2011), Glossary of Glacier Mass Balance and Related Terms, IHP-VII Technical Documents in Hydrology No. 86, IACS Contribution No. 2, UNESCO-IHP, Paris.
- Colbeck, S. C. (1982), An overview of seasonal snow metamorphism, *Rev. Geophys.*, 20(1), 45-61, doi: 10.1029/RG020i001p00045.
- Colgan W., J. Davis, and M. Sharp (2008), Is the high-elevation region of Devon Ice Cap thickening?, *J. Glaciol.*, 54(186), 428-436, doi: 10.3189/002214308785837084.
- Copland, L., M. J. Sharp, and J. A. Dowdeswell (2003), The distribution and flow characteristics of surge-type glaciers in the Canadian High Arctic, *Ann. Glaciol.*, 36(1), 73-81, doi:10.3189/172756403781816301.
- Cuffey, K. M. and W. Paterson (2010), *The physics of glaciers*, 4th edn. Butterworth-Heinemann, Oxford.
- Gao, F., C. B. Schaaf, A. H. Strahler, A. Roesch, W. Lutch, and R. Dickenson (2005), MODIS bidirectional reflectance distribution function and albedo Climate Modelling Grid products and the variability of albedo for major vegetation types, *J. Geophys. Res.-Atmos.*, 110, D01104, doi: 10.1029/2004JD005190.
- Gardner, A. S., G. Moholdt, B. Wouters, G. J. Wolken, D. O. Burgess, M. J. Sharp, J. G. Cogley, C. Braun, and C. Labine (2011), Sharply increased mass loss from glaciers and ice caps in the Canadian Arctic Archipelago, *Nature*, 473(7347), 357-360, doi:10.1038/nature10089.

Gardner, A. S., G. Moholdt, A. Arendt, and B. Wouters (2012), Accelerated contributions of Canada's Baffin and Bylot Island glaciers to sea level rise over the past half century, *The Cryosphere*, 6, 1103-1125, doi: 10.5194/tc-6-1103-2012.

Gardner, A. S., et al. (2013), A reconciled estimate of glacier contributions to sea level rise: 2003 to 2009, *Science*, 340(6134), 852-857, doi:10.1126/science.1234532.

Gascon, G., M. Sharp, and A. Bush (2013), Changes in melt season characteristics on Devon Ice Cap, Canada, and their association with the Arctic atmospheric circulation, *Ann. Glaciol.*, 54, 101–110, doi:10.3189/2013AoG63A601.

Hall D. K., R. S. Williams Jr, K. A. Casey, N. E. DiGirolamo, and Z. Wan (2006), Satellite-derived, melt-season surface temperature of the Greenland Ice Sheet (2000–2005) and its relationship to mass balance, *Geophys. Res. Lett.*, 33(11), L11501, doi:10.1029/2006GL026444.

Hall, D. K. J. E. Box, K. A. Casey, S. J. Hook, C. A. Shuman, and K. Steffen (2008a), Comparison of satellite-derived and in-situ observations of ice and snow surface temperatures over Greenland, *Remote Sens. Environ.*, 112(10), 3739-3749, doi: 10.1016/j.rse.2008.05.007.

Hall, D. K., R. S. Williams, S. B. Luthcke, and N. E. DiGirolamo (2008b), Greenland ice sheet surface temperature, melt and mass loss: 2000–2006, *J. Glaciol.*, 54(184), 81–93, doi:10.3189/002214308784409170.

Howat, I. M., B. E. Smith, I. Joughin, and T. A. Scambos (2008), Rates of southeast Greenland ice volume loss from combined ICESat and ASTER observations, *Geophys. Res. Lett.*, 35(17), doi: 10.1029/2008GL034496.

Koenig, L. S., and D. K. Hall (2010) Comparison of satellite, thermochron and station temperatures at Summit, Greenland, during the winter of 2008/09, *J. Glaciol.*, 56(198), 735-741 (doi: 10.3189/002214310793146269).

Koerner, R. M. (1979), Accumulation, ablation, and oxygen isotope variations on the Queen Elizabeth Islands ice caps, Canada, *J. Glaciol.*, 22(86), 25-41.

Koerner, R. M. (2005), Mass balance of glaciers in the Queen Elizabeth Islands, Nunavut, Canada, *Ann. Glaciol.*, 42, 417–423, doi:10.3189/172756405781813122.

Krabill, W. B., W. Abdalati, E. B. Frederick, S. S. Manizade, C. F. Martin, J. G. Sonntag, R. N. Swift, R. H. Thomas, and J. G. Yungel (2002), Aircraft laser altimetry measurement of elevation changes of the Greenland Ice Sheet: Techniques and accuracy assessment, *J. Geodyn.*, 34, 357-376, doi: 10.1016/s0264-3707(02)00040-6.

Krabill, W. B. (2010), updated 2016. *IceBridge ATM L2 Icessn Elevation, Slope, and Roughness. Version 2*. [Greenland 2011,2012,2014,2015]. Boulder, Colorado USA: NASA DAAC at the National Snow and Ice Data Center. <http://dx.doi.org/10.5067/CPRXXK3F39RV>, accessed July 2016.

Krabill, W. B. (2012), *Pre-IceBridge ATM LIB Qfit Elevation and Return Strength, Version 1*. [Greenland and Arctic Canada 1995, 2000, 2005, 2006]. Boulder, Colorado USA. NASA National Snow and Ice Data Center Distributed Active Archive Center. doi: <http://dx.doi.org/10.5067/8Q93SAT2LG3Q>, accessed February – July 2014

Krabill, W. B. (2014a), updated 2016, *IceBridge ATM L4 Surface elevation rate of change, Version 1* [Greenland and arctic Canada 1995-2015] Boulder, Colorado USA: NASA DAAC at the National Snow and Ice Data Center. <http://dx.doi.org/10.5067/BCW6CI3TXOCY>, accessed 6 July – 22 August 2016

Krabill, W. B. (2014b), updated 30 June 2016, IceBridge ATM L4 Surface elevation rate of change Version 1 user guide, <http://nsidc.org/data/docs/daac/icebridge/idhdt4/index.html>.

Kwok, R., G. F. Cunningham, S. S. Manizade, and W. B. Krabill (2012), Arctic sea ice freeboard from IceBridge acquisitions in 2009: Estimates and comparisons with ICESat, *J. Geophys. Res.*, 117(C2), doi: 10.1029/2011JC007654.

Land Processes Distributed Active Archive Center (LP DAAC) USGS EROS Data Center (2004) MODIS Land data operational product evaluation (LDOPE) tools, Release 1.4, 30 April 2001, LDOPE Tools User's Manual, 103 pages.

Land Processes Distributed Active Archive Center (LP DAAC), MODIS Albedo 16-day Level 3 Global 500 m Grid SIN Version 5 (MCD43A3v05). NASA EOSDIS Land Processes DAAC, USGS Earth Resources Observation and Science (EROS) Center, Sioux Falls, South Dakota (<https://lpdaac.usgs.gov>), accessed September 2014 - October 2016 at <http://e4ftl01.cr.usgs.gov>.

Land Processes Distributed Active Archive Center (LP DAAC), MODIS Level 3 Global 1 km Grid SIN Version 5. NASA EOSDIS Land Processes DAAC, USGS Earth Resources Observation and Science (EROS) Center, Sioux Falls, South Dakota (<https://lpdaac.usgs.gov>), accessed Spetember 2014 - October 2015 at <http://e4ftl01.cr.usgs.gov>.

Lenaerts, J. T. M., J. H. van Angelen, M. R. van den Broeke, A. S. Gardner, B. Wouters, and E. van Meijgaard (2013), Irreversible mass loss of Canadian Arctic Archipelago glaciers, *Geophys. Res. Lett.*, *40*(5), 870–874, doi:10.1002/grl.50214.

Lucht, W., C. B. Schaaf, and A. H. Strahler (2000), An algorithm for the retrieval of albedo from space using semiempirical BRDF models, *IEEE Transactions on Geoscience and Remote Sensing*, *38*, 977-998.

Lyapustin, A., Y. Wang, X. Xiong, G. Meister, S. Platnick, R. Levy, B. Franz, S. Korkin, T. Hilker, J. Tucker, F. Hall, P. Sellers, A. Wu, and A. Angal (2014), Scientific impact of MODIS C5 calibration degradation and C6+ improvements, *Atmos. Meas. Tech.*, *7*(12), 4353-4365, doi:10.5194/amt-7-4353-2014.

Martin, C. F., W. B. Krabill, S. S. Manizade, R. L. Russell, J. G. Sonntag, R. N. Swift, and J. K. Yungel (2012), Airborne topographic mapper calibration procedures and accuracy assessment. NASATM-2012-215891.

Millan, R., J. Mougnot, and E. Rignot (2017), Mass budget of the glaciers and ice caps of the Queen Elizabeth Islands, Canada, from 1991 to 2015, *Environ. Res. Lett.*, *12*(02), 1-8, doi: 10.1088/1748-9326/aa5b04.

Mortimer, C. A., M. Sharp, and B. Wouters (2016), Glacier surface temperatures in the Canadian high arctic, 2000-2015, *J. Glaciol.*, *62*(23), 963-975, doi: 10.1017/jog.2016.80.

Mortimer, C. A. and M. Sharp, Glacier albedo change in the Canadian High Arctic (2001-2015) and its relationship to recent climate warming, in review for *J. Geophys. Res.: Earth Surface*.

Pfeffer, W. T., and N. F. Humphrey (1998) Formation of ice layers by infiltration and refreezing of meltwater, *Ann. Glaciol.*, *26*, 83-91.

Pfeffer, W. T. et al. (2014), The Randolph Glacier Inventory: a globally complete inventory of glaciers, *J. Glaciol.*, *60*(221), 537-552, doi:10.3189/2014JoG13J176.

Polashenski, C. M., J. E. Dibb, M. G. Flanner, J. Y. Chen, Z. R. Courville, A. M. Lai, J. J. Schauer, M. M. Shafer and M. Bergin (2015), Neither dust nor black carbon causing apparent albedo decline in Greenland's dry snow zone: Implications for MODIS C5 surface reflectance, *Geophys. Res. Lett.*, 42(12), 9319-9327, doi: 10.1002/2015GL065912.

Schaaf, C. B., et al. (2002), First operational BRDF, albedo nadir reflectance products from MODIS, *Remote Sens. Environ.*, 83(1), 135-148, doi: 10.1016/S0034-4257(02)00091-3.

Schaaf, C. L. B., J. Liu, F. Gao, and A. H. Strahler (2011), MODIS albedo and reflectance anisotropy products from Aqua and Terra. In B. Ramachandran Justice C and M Abrams (Eds), Land remote sensing and global environmental change: NASA's earth observing system and the science of ASTER and MODIS. Remote Sensing and Digital Image Processing Series, vol 11, Springer-Verlag (873 pp).

Sharp, M., D. O. Burgess, J. G. Cogley, M. Ecclestone, C. Labine, and G. J. Wolken (2011), Extreme melt on Canada's Arctic ice caps in the 21st century, *Geophys. Res. Lett.*, 38(11), L11501, doi:10.1029/2011GL047381.

Sharp, M., et al. (2015) [Arctic] Glaciers and ice caps (outside Greenland [in "State of the Climate 2014"], *Bull. Am. Meteorol. Soc.*, 96(7), 135-137.

Short, N. H., and A. L. Gray (2005), Glacier dynamics in the Canadian High Arctic from RADARSAT-1 speckle tracking, *Can. J. Remote Sens.*, 30(3), 504-509.

Strahler, A. H. et al. (1999), MODIS BRDF/Albedo product: algorithm theoretical basis document version 5.0.

Stroeve, J., J. E. Box, Z. Wang, C. Schaaf, and A. Barret (2013), Re-evaluation of MODIS MCD43 Greenland albedo accuracy and trends, *Remote Sens. Environ.*, 138, 199-214, doi: 10.1016/j.rse.2013.07.023.

Tedesco M., S. Doherty, X. Fettweis, P. Alexander, J. Jeyaratnam, and J. Stroeve (2016), The darkening of the Greenland ice sheet: trends, drivers, and projections (1981-2100), *The Cryosphere*, 10, 477-496, doi: 10.5194/tc-10-477-2016.

van den Broeke, M. R., C. J. P. P. Smeets, and R. S. W. van de Wal (2011), The seasonal cycle and interannual variability of surface energy balance and melt in the ablation zone of the west Greenland ice sheet, *The Cryosphere*, 5(2), 377-390, doi: 10.5194/tc-5-377-2011.

van Wychen, W., J. Davis, D. O. Burgess, L. Copland, L. Gray, M. Sharp, and C. Mortimer (2016), Characterizing interannual variability of glacier dynamics and dynamic discharge (1999-2015) for the ice masses of Ellesmere and Axel Heiberg Islands, Nunavut, Canada, *J. Geophys. Res.- Earth Surf.*, 121, 39-63, doi:10.1002/2015JF003708.

van Wychen, W., J. Davis, L. Copland, D. O. Burgess, L. Gray, M. Sharp, J. A. Dowdeswell, and T. J. Benham (2017), Variability in ice motion and dynamic discharge from the Devon Ice Cap, Nunavut, Canada, *J. Glaciol.*, 1-14, doi: 10.1017/jog.2017.

Vermote, E. F., S. Y. Kotchenova, and J. P. Ray (2011), MODIS surface reflectance user's guide. MODIS Land Surface Reflectance Science Computing Facility, version 1.

Wan, Z., Y. Zhang, Q. Zhang, and Z. L. Li (2002), Validation of the land-surface temperature products retrieved from Terra Moderate Resolution Imaging Spectroradiometer data, *Remote Sens. Environ.*, 83(1-2), 163–180, doi:10.1016/S0034-4257(02)00093-7.

Wan, Z. M. (2008), New refinements and validation of the MODIS Land-Surface Temperature/Emissivity products, *Remote Sens. Environ.*, 112(1), 59–74, doi:10.1016/j.rse.2006.06.026.

Wang, Z., C. B. Schaaf, M. J. Chopping, A. H. Strahler, J. Wang, M. O. Román, A. V. Rocha, C. E. Woodcock, and Y. Shuai (2012), Evaluation of Moderate-resolution Imaging Spectroradiometer (MODIS) snow albedo product (MCD43A) over tundra, *Remote Sens. Environ.*, 117, 264-280, doi: 10.1016/j.rse.2011.10.002.

Wanner, W., A. H. Strahler, B. Hu, P. Lewis, J. P. Muller, X. Li, C. L. B. Schaaf, and M. J. Barnsley (1997), Global retrieval of bidirectional reflectance and albedo over than from EOS MODIS and MISR data: theory and algorithm, *J. Geophys. Res.* 102(D14), 17143-17162, doi: 10.1029/96JD03295.

Warren, S. G. (1982), Optical properties of snow, *Reviews of Geophysics*, 20(1), 67-89, doi: 10.1029/RG020i001p00067.

Warren, S. G., and W. J. Wiscombe (1980), A model for the spectral albedo of snow. II Snow containing atmospheric aerosols, *J. Atmos. Sci.*, 37(12), 2734-2745, doi: 10.1175/1520-0469(1980)037<2734:AMFTSA>2.0.CO;2.

Williamson, S., M. Sharp, J. Dowdeswell, and T. Benham (2008), Iceberg calving rates from northern Ellesmere Island ice caps, Canadian Arctic, 1999-2003, *J. Glaciol.*, 54(186), 391-400, doi: 10.3189/00221430878537048.

World Glacier Monitoring Service Fluctuations of Glaciers (2016), Devon Ice Cap NW, Canada (WGMS_ID: 39), *Fluctuations of Glaciers Database*, version 2016-08-16, doi: 10.5904/wgms-fog-2016-08.

Zdanowicz, C., A. Smetny-Sowa, D. Fisher, N. Schaffer, L. Copland, J. Eley, and F. Dupont (2012), Summer melt rates on Penny Ice Cap, Baffin Island: Past and recent trends and implications for regional climate, *J. Geophys. Res.*, 117(F2), F02006, doi:10.1029/2011JF002248.

Chapter 5

Conclusions

5.1 Summary

This thesis investigated changes in glacier and ice cap surface elevation over the Queen Elizabeth Islands (QEI), Arctic Canada, for the period 1995-2014, as well as changes in QEI land surface temperature and albedo for the period 2000(01)-2015. Measurements of mean summer (June-August) glacier surface temperatures (LSTs) and shortwave broadband black-sky surface albedo (BSA, regions south of 80°N) from NASA's Moderate Resolution Spectroradiometer (MODIS), were used to provide the first near-complete picture of LST and BSA changes for all glacier covered surfaces in the QEI. Repeat airborne surface elevation measurements from NASA's Airborne Topographic Mapper (ATM) conical laser scanning system were used to investigate the spatial and temporal variability in rates of surface elevation change (dh/dt) over QEI glaciers and ice caps (1995-2014) and their relationship with observed changes in LST, BSA, and surface longitudinal strain rates (du/dx), for the period 2000-2012/14.

This thesis identified strong positive LST anomalies (relative to the 2000-2015 mean; Chapter 2), negative BSA anomalies (relative to the 2001-2015 mean; Chapter 3), and strong thinning (relative to the 1995-2012/14 mean; Chapter 4) since ~2005/06. This is consistent with previously reported increases in rates of glacier mass loss from the QEI since the mid to late 2000s [e.g. *Gardner et al.*, 2011; 2013; *Sharp et al.*, 2011, *Lenearths et al.*, 2013; *Millan et al.*, 2017]. Between 2000(01) and 2015, mean summer QEI-wide LSTs increased at a rate of $0.06 \pm 0.04 \text{ }^\circ\text{C yr}^{-1}$ (total increase of 0.96°C over 16 years), and the mean summer BSA (measured for areas south of 80°N for 2001-2015) decreased at a rate of $-0.0038 \pm 0.0037 \text{ yr}^{-1}$ (total decrease of 0.057 over 15 years). A period

of strong positive(negative) LST(BSA) anomalies during the period ~2007-2012 suggests that the bulk of the observed warming and decreases in albedo occurred during this 5 year period. LST(BSA) increases(decreases) were strongest in the west and north of the QEI. LST increases were greatest at higher elevations in the interior of the ice masses, while BSA declines were greatest at lower elevations around the margins of the ice masses. Between 1995 and 2014, surface lowering was observed across most of the QEI where repeat ATM data were available and the rate of thinning was ~3 times greater during the 2005/06-2012/14 period than during the previous two pentads.

5.2.1 LST change

5.2.1.1 Summary: Mean summer clear-sky daytime LST, averaged across all glaciated surfaces in the QEI, for the period 2000-2015 was $-3.3 \pm 1.8^{\circ}\text{C}$. During this 16 year period, mean summer LSTs increased over 93% of the QEI's ice cover and nearly all (99.9%) glaciated pixels recorded at least one LST observation of 0°C , suggesting that melt occurred at all elevations and all locations in the region at some point during the study period. Comparison of mean summer LST with annual mass change estimates from GRACE for 2003/2004-2014/2015 identified a strong correlation ($r = -0.82$; $p < 0.01$) between these two records, confirming that variations in annual mass balance in the QEI are strongly influenced by variations in summer air temperature. Chapter 2 identified strong surface warming in the north and west of the QEI, consistent with the spatial pattern of warming described by *Sharp et al.* [2011] for a shorter time period and with less complete spatial coverage. There is good agreement ($r > 0.91$, $p > 0.001$) between the LST record of *Sharp et al.* [2011], obtained from 23 km x 23 km boxes centered on the higher elevations of the QEI's seven major ice masses, and the LST record presented in this thesis for all glaciated surfaces in the QEI. This suggests that, under current climatic conditions, a spatially distributed sample of LST

measurements from high-elevation locations in the QEI may be sufficient to determine the sign and approximate magnitude of LST changes in the region and to identify broad spatial patterns. The point-based method of *Sharp et al.* [2011], however, does not allow for evaluation of the complete spatial structure of LST change, which would enable comparison with changes in the surface albedo (Chapter 3), and glacier surface elevation change (Chapter 4).

MODIS data are only available since 2000. Near-surface (2 m; <http://climate.weather.gc.ca>) and upper air (700 hPa; NCEP/NCAR R1 Reanalysis, *Kalnay et al.* [1994]) temperatures, available since 1948, were used to place the 16 year record of mean summer LSTs into a longer-term context. Close coupling between the mean summer LSTs and 700 hPa air temperatures for the period 2000-2015 (Manson Icefield $r > 0.78$, all other regions $r \geq 0.86$; $p < 0.001$), and good agreement between the 68 year records of near-surface and upper-air temperatures ($r > 0.79$), suggests that the 2007-2012 period, when mean summer LSTs were anomalously high, was also anomalously warm relative to the last 68 years.

5.2.1.2 Limitations: This thesis used the mean summer (JJA) LST, computed from 8-day MODIS LST data (MOD11A2), to infer changes in the duration and/or intensity of summer melt [e.g. *Hall et al.*, 2006; *Sharp et al.*, 2011]. With continued warming, the utility of the methods and approach used in this thesis will become more limited, because, once a surface reaches the pressure melting point (PMP), no further increase in the intensity of the melt season can be detected. In addition, once a surface regularly reaches the PMP during the JJA period, no further increases in melt duration can be detected for that surface. However, higher atmospheric temperatures over a surface that is at the PMP will result in melting, runoff, and mass loss. Between 2000 and 2015, at lower elevations around the margins of the ice masses the 8-day LST regularly reached 0°C during the JJA period. On average, 5.5% of pixels had 9 or more of a possible 11 eight-day LST observations

$\geq 0^{\circ}\text{C}$; values ranged from $< 1\%$ in anomalously cold years (e.g. 2000 and 2001) to $\sim 12\%$ in anomalously warm years (e.g. 2007 and 2012) (Chapter 2, Table 2-S6).

Secondly, by restricting analysis of LST to the JJA period, any potential changes in LST occurring outside of this period were not captured. The JJA period was selected as it corresponds to the melt season used previously by *Sharp et al.* [2011], which was obtained by extending the melt season duration of *Wang et al.* [2005], estimated from QuikSCAT data for 2000-2004, outward by two standard deviations to ensure that all possible melt days were captured. Between 2000 and 2015, an LST $\geq 0^{\circ}\text{C}$ was recorded for $< 1\%$ of pixels prior to and following the JJA period (compared with for $> 50\%$ of pixels during the summer months), indicating that the bulk of the surface melt occurred during JJA. Restricting our analysis of LST to the summer months, therefore, does not appear to have resulted in the exclusion of significant melt periods (outside of the JJA period). The use of a static melt season (JJA) facilitates comparison of summer LST over multiple years. However, with continued warming, the length of the melt season will likely increase, so, in the future, a revisit of the use of the JJA period to monitor changes in glacier surface temperature may be warranted.

5.2.2 BSA change

5.2.1.1 Summary: The QEI-wide mean(minimum) summer BSA, averaged across all 15 years, was 0.545 ± 0.102 (0.41 ± 0.12). Between 2001 and 2015 $>87\%$ (85%) of pixels experienced a decrease in mean (minimum) summer BSA. Analysis of the minimum summer black-sky visible ($0.3\text{-}0.7\ \mu\text{m}$) and shortwave ($0.3\text{-}5.0\ \mu\text{m}$) broadband albedos, suggests that measured decreases in mean summer broadband shortwave BSA were the result of increases in bare ice extent, mean grain size and water content of snow, as well as of increased exposure of light absorbing impurities and/or micro-organisms, and/or in the extent of ponded water on the glacier surfaces [*Clarke and*

Noone, 1985; Conway *et al.*, 1996; Fountain *et al.*, 2004; Doherty *et al.*, 2010]. The 15 year BSA record was negatively correlated with the 15 year LST record for 91% of pixels having BSA and LST observations in all 15 years (75% of possible pixels). Output from the Canadian Regional Climate Model (CanRCM4), available at a 0.22° resolution for the period 2001-2009 [Flato *et al.*, 2000; Zadra *et al.*, 2008; van Salzen *et al.*, 2013], shows an increase in incoming shortwave radiation and near-surface air temperatures, as well as a decrease in outgoing shortwave radiation and mean annual precipitation over the QEI south of 80°N (Chapter 3, Table 3-S5). Larger amounts of incoming shortwave radiation, combined with a lower surface albedo mean that more energy would be available for melt and warming. Importantly, the negative correlation between LST and BSA, indicative of a positive ice-albedo feedback, will enhance rates of glacier mass loss in the QEI.

5.2.1.2 Limitations: Principal uncertainties in the assessment of spatial and temporal variability of surface albedo presented in Chapter 3 arise from: (i) high data dropout resulting from the absence of data when clouds are present [Hall *et al.*, 2008], and (ii) degradation of the sensors aboard the Terra satellite [Wang *et al.*, 2012] which may have resulted in artificially high albedo declines in the dataset used in this study (Chapter 3 Section 3.2.1.1, and references therein).

(i) Missing data: Difficulties in discriminating between ice, snow, and thin cloud [Strabala *et al.*, 1994; King *et al.*, 2004], as well as the conservative MODIS cloud mask [Ackerman *et al.*, 1998] that tends to detect more clouds than are in fact present over snow and ice [Hall *et al.*, 2008], resulted in the absence of a considerable amount of data; especially over high-elevation regions of the Devon Ice Cap, Sydkap Ice Cap, and Axel Heiberg Island. There is considerably more missing data in the albedo record compared to the LST record. LST is calculated from thermal infrared channels 31 and 32 which have bandwidths of 10.78 – 11.28 μm and 11.77 - 12.27 μm , respectively

[Wan *et al.*, 2002]. MCD43A3 albedos are calculated for seven visible and near-infrared bands (spanning 0.4 to 2.4 μm) and the broadband shortwave albedo is calculated from spectral-to-broadband conversion [Strugnell *et al.*, 2001]. Higher incidence of data loss due to cloud cover, as well as difficulties in discriminating between clouds and snow/ice surfaces (mentioned previously), at lower visible and shortwave compared to the thermal-infrared wavelengths may, in part, explain the higher amount of missing albedo data compared to the LST data.

In this thesis, the mean summer BSA for each year, was only computed if there were a minimum of 7 of the possible 12 MCD43A3 observations (Chapter 3, Section 3.2.3). During the 2001-2015 period, between 11.4% (2001) and 19.4% (2009) of ice covered pixels south of 80°N had no data. These high annual data dropout rates were further compounded when calculating the 15-year rate of BSA change, as BSA change was only computed for pixels having at least 11 of 15 years of observation. Therefore, the QEI-wide rate of BSA change reported in Chapter 3, as well as the mean summer BSA for each year, are biased towards areas with data coverage. Measured BSA declines were greater at lower elevations, so the absence of data at higher elevations may have resulted in reported BSA decreases that are larger than the actual value.

BSA increases were observed at high elevations on eastern Ellesmere and Devon Islands. The large amount of missing data in these regions made it difficult to determine whether instances of BSA increase were simply noise in the data, or, whether they were representative of a larger area where BSA increased. Similar issues, relating to the absence of data, arose when interpreting spatial pattern(s) in the relationship between LST and BSA. Correlations between the 15 year LST and BSA records were only computed for pixels having LST and BSA observations in all years (75% of possible pixels; Chapter 3 Section 3.2.3). Comparison of the LST and BSA data found instances of positive correlation between LST and BSA (Chapter 3, Figure 3-4d). These data were

mainly located at high elevations on eastern-facing slopes of the eastern QEI, and appear as a strip of data separating areas of negative correlations (lower elevations) from large areas having no data (higher elevations). Owing to the absence of data at higher elevations in the interior of most ice masses, it is not known whether these high elevation pixels with positive correlations between LST and BSA are representative of a larger area that encompasses the full high elevation region (of these ice caps, where there are no data), or whether they are simply scattered data points that are not indicative of any broad spatial trend. The use of surface albedo products from multiple sensors [e.g. *Shuai et al.*, 2011; *He et al.*, 2014, and references therein] may improve the spatial coverage of the surface albedo presented here. The MODIS MCD43A3 product was selected for this thesis due to the high repeat cycle (1-2 days) of the combined Aqua and Terra satellites, as well as the availability of a broadband albedo product free of charge.

(ii) Sensor degradation: As outlined in Chapter 3 (Section 3.2.1.1) the MODIS sensors are operating beyond their expected lifespan and some of the sensors are degrading, particularly those onboard the Terra satellite [*Wang et al.*, 2012]. Degradation of the Terra sensor may have resulted in BSA decreases reported in this thesis, from MCD43A3 Version 05 data, which are lower than the true albedo change [*Lyapustin et al.*, 2014; *Polashenski et al.*, 2015]. Sensor degradation is not believed to have substantially altered the broad spatial pattern(s) of mean summer BSA presented in this thesis (discussed in detail in Chapter 3 Section 3.2.1.1). Effects of Terra sensor degradation are supposed to be corrected for in the Version 06 MODIS data, release 8 July 2016 [*Schaaf and Wang*, 2015]. Over the dry snow zone of the Greenland Ice Sheet, no significant trends in visible-wavelength albedo were detected from the Version 06 data [*Casey et al.*, 2016]; however, albedo declines in this region were detected from the Version 05 data [*Polashenski et al.*, 2015]. Importantly for this thesis, there are no dry snow zones in the QEI. Both the Version 05 and

Version 06 data identified albedo declines in the wet snow zone of the Greenland Ice Sheet, but the magnitude of the albedo decrease is smaller for the Version 06 data [Casey *et al.*, 2016]. At present, there are no substantive comparative studies detailing the differences between Version 05 and Version 06 albedo data, and resultant albedo trends, over large glaciated regions. This, however, does not mean that important differences in albedo values between these two versions do not exist. Comparison of Version 05 and Version 06 data is still in its early stages, so any such discrepancies, if they exist, have yet to be reported in detail for glaciated regions.

Attempts were made to include the Version 06 MCD43A3 data in this thesis. Following data processing, however, large artifacts were identified in the data, which prohibited calculation of the mean summer BSA. In addition, calibrations were less stable for the most recent data, particularly from ~2014 onward [Casey *et al.*, 2016]. Once the artifacts in the MCD43A3 Version 06 data are corrected, and sensor calibrations are stabilized for the period 2014 onward, results presented in this thesis should be updated using the newer Version 06 MODIS data.

5.2.3 Surface elevation change

5.2.1.1 Summary: Repeat ATM measurements showed widespread thinning of QEI glaciers and ice caps between 1995 and 2012/2014 (Chapter 4 Section 4.3). Thinning in excess of 0.5 m yr^{-1} was observed at lower elevations along the margins of the ice masses. Thickening was observed on the east-facing slopes of southern Prince of Wales Icefield (between ~400 and 850 m a.s.l.) and Agassiz Ice Cap (above ~1500 m a.s.l.). Large variations in both the sign and magnitude of dh/dt were observed along many outlet glaciers (e.g. Otto, Antoinette, Ekblaw, Leffert, Wykeham, Thompson, SE1 and 2 glaciers).

Comparison of dh/dt with measured changes in LST and BSA, as well as with surface longitudinal strain rates (du/dx), suggests that, in most regions, dh/dt is controlled mainly by the climatic mass balance, except along fast-flowing outlet glaciers where ice dynamics appear to also be important. For outlet glaciers where dh/dt data were available, there was good agreement between zones of thickening (thinning) and longitudinal compression (extension), supporting the notion that ice dynamics make an important contribution to dh/dt along many outlet glaciers. Importantly, Chapter 4 demonstrated that, in the absence of the necessary data to compute the full three-dimensional flux divergence, evaluation of the relative magnitude of du/dx within a region can be a useful tool for identifying areas where ice dynamics may be an important (i.e. areas with relatively high du/dx) cause of changes in glacier surface elevation.

5.2.1.2 Limitations: The investigation of the relative influences of ice dynamics and climatic mass balance on observed changes in glacier and ice cap surface elevation, presented in Chapter 4, makes the simplifying assumption that longitudinal strain is balanced solely by vertical strain. Attempts to quantify the expected magnitude of dh/dt from the surface longitudinal strain rate (du/dx) were unsuccessful, so this assumption is likely not valid. Lateral spreading (compression) as ice exits (enters) a constriction were not accounted for in this one-dimensional assessment. To better constrain the relative influence of du/dx and mass balance on dh/dt , future work should, at a minimum, use the full two-dimensional surface velocity field so that both the longitudinal and horizontal strain components can be taken into consideration. Three dimensional bedrock topography is available for specific QEI outlet glaciers [*Paden et al.*, 2016] and, combined with assumptions about the vertical velocity profile (e.g. depth-averaged velocity is 80% of surface velocity [*Cuffey and Paterson*, 2010]) may permit calculation of the full three dimensional flux divergence.

Repeat ATM measurements of the QEI ice cover are sparse, so the available dh/dt data do not fully characterize the spatial [and temporal] variability of surface elevation change across the region. The temporal patterns of dh/dt presented in this thesis are, however, consistent with reports of increasingly negative mass balances [*Sharp et al.*, 2011] and enhanced rates of mass loss [*Gardner et al.*, 2013] in the QEI since the mid to late 2000s, as well as with anomalously high surface temperatures (Chapter 2) and low surface albedo (Chapter 3) during 2007-2012.

Estimates of dh/dt from Ice, Cloud, and land Elevation Satellite (ICESat) retrievals, are available for the QEI from fall 2003 to fall 2009 [e.g. *Gardner et al.*, 2011]. These data have a broader spatial coverage, but a much coarser spatial resolution (~ 70 m diameter footprint, *Zwally et al.* [2011]) than the airborne ATM data. Given the paucity of airborne-derived dh/dt measurements, I considered including ICESAT-derived dh/dt data in this thesis. However, the ICESat data have very limited spatial coverage over the QEI after 2008, so the dh/dt record was only 5 years long (fall 2003 - fall 2008). This time period was deemed too short for calculation of LST and/or BSA trends. For short ($< \sim 5$ -10 years) time periods, the presence of extreme warm/cold years, as well as the choice of start and end dates, was found to influence both the sign and magnitude of LST and/or BSA change. This prohibited comparison of ICESAT-derived dh/dt with LST and BSA changes. Inclusion of the ICESat data with no additional comparisons, did not provide any new insights beyond what has already been published [*Gardner et al.*, 2011; 2013].

5.2 Discussion of LST, BSA, and dh/dt

5.2.1 Large-scale spatial patterns and climate

The temporal pattern of mean summer LST and BSA anomalies was found to be strongly linked to the North Atlantic Oscillation (NAO) index, which is based on the surface sea-level pressure

difference between the Azores High (subtropical) and Icelandic (subpolar) Low. The first Principal Component (PC1) of the 16 year LST ($r = -0.79$, $p < 0.001$) and 15 year BSA ($r = -0.87$, $p < 0.001$) records, which closely resemble the pattern of LST and BSA change, were well correlated with the annual NAO index (Chapters 2 and 3). In years with strong positive (negative) LST and negative (positive) BSA anomalies (e.g. 2007-2012; 2013) the NAO index was positive (negative). *Box et al.* [2012] have suggested that strong anticyclonic circulation over southern Greenland during 2009-2011, when the JJA NAO index was negative, enhanced the strength of the ice-albedo feedback resulting in higher rates of melt and mass loss from the Greenland Ice Sheet. A similar phenomenon may have occurred in the QEI.

Extreme mass balance years in the QEI have previously been associated with the strength and geometry of the July circumpolar vortex that alters the distribution and intensity of regions of high and low pressure across the QEI [*Alt*, 1987; *Gardner and Sharp*, 2007]. During warm (cold) summers, a persistent ridge (trough) in the 500 hPa geopotential height anomalies (NCEP/NCAR Reanalysis R1 data, *Kalnay et al.* [1996]) was centered over the north and west of the QEI (Chapter 2 Section 2.3.1). This configuration appears to be tied to the increased warming and albedo declines observed in the north and east of the QEI during 2007-2012. For example, strong warming and albedo declines over Axel Heiberg and northwest Ellesmere Islands, coincided with the presence of a ridge of high pressure centered over the north and west of the QEI that was often observed in years when the NAO index was negative.

Strong, persistent anticyclonic circulation maximizes the incoming shortwave radiation received at the air-ice interface, and a lower albedo increases the proportion of incoming solar radiation that is absorbed, providing more energy for warming and melt. During the period for which CanRCM4 climate model data were available (2000-2009), modelled incoming shortwave radiation and near-

surface air temperatures increased, while the incoming longwave radiation and annual precipitation decreased (Chapter 3 Section 3.4.3). Spatially, the net shortwave radiation was consistently higher in the west than in the east. No such (east-west) differences were observed in the net longwave radiation. This spatial pattern in net shortwave radiation is consistent with the east-west differences in BSA change, as well as the northwest-southeast pattern of air and surface temperature change.

5.2.2 Small scale features and precipitation

Although the broad spatial and temporal patterns in mean summer LST and BSA closely resemble the configuration of the 500 hPa geopotential surface, the complex physiography of the QEI results in considerable local variation in how these regional-scale atmospheric forcings are manifested. This is illustrated by the considerable variability in LST and BSA change within individual ice masses. For example, LST declines were observed in southeast Devon Ice Cap, as well as Manson Icefield, and in the southern coastal region of eastern Prince of Wales Icefield below ~500 m a.s.l.. Conversely, large LST increases were observed on the western side of these same ice masses. The eastern part of these ice masses borders Baffin Bay (which is the primary moisture source for southeast QEI) and is downwind of the North Water (NOW) polynya. These open water sources probably assist in moderating LSTs over low-lying areas of Devon Ice Cap, Manson Icefield and southeast Prince of Wales Icefield, and may explain the smaller rates of LST change in these regions.

BSA increases were observed along a high-elevation central spine located on the eastern facing slopes of the eastern QEI, above the low-lying areas where LST decreased. Comparison of the 15-year LST and BSA records found instances of positive correlations between LST and BSA along this high elevation central spine [in the eastern QEI]. These positive correlations suggest the

presence of a negative ice-albedo feedback (Chapter 3 Section 3.4.2). Given that both the mean summer LST and BSA increased in this region, enhanced solid precipitation during warm summers, which temporarily raises the surface albedo, provides a possible explanation for the observed positive correlations. More than 60% of the annual precipitation along this high-elevation central spine occurs in the summer, compared with < 40% at lower elevations (Chapter 3, Figure 3-S3). Variations in summer precipitation may, therefore, affect rates of surface warming and albedo decline, and hence rates of mass loss, along maritime-facing slopes of the eastern QEI.

Variability in annual precipitation in the QEI is low compared to the variability in summer temperatures [Braithwaite, 2005], and, it is generally accepted that variations in precipitation play only a minor role in variability of QEI annual mass balance [Koerner, 2005; Sharp *et al.*, 2011]. However, investigation of spatial and temporal variability in mean summer LST and BSA, presented in this thesis, as well as differences in rates of glacier surface elevation change (Chapter 4, discussed below), identified regional differences in rates of warming and albedo change that may be linked to local variations in precipitation. QEI accumulation rates decrease from east to west [Koerner, 1979] (a spatial pattern that is consistent with the spatial pattern of LST and BSA change described in Chapters 2 and 3), and variability in open water extent in QEI's inter-island channels has previously been correlated with summer temperatures in the QEI [Koerner, 1977]. I propose that variability in open water extent in Baffin Bay and Nares Strait, results in variability in summer precipitation which, leads to variability in summer and annual mass balance in maritime regions of the eastern QEI. Future work investigating a possible relationship between precipitation, open water extent, and mass change in this region would be valuable.

5.2.3 Feedbacks: LST, BSA, elevation change and climate in the eastern QEI

Observed albedo increases may limit surface warming and reduce rates of melt and mass loss. If, as suggested (Chapter 3 Section 3.4.3), the positive ice-albedo feedback observed on eastern Ellesmere and Devon Islands is a result of increased solid precipitation during warm summers, thickening of glaciers in this region would be expected (unless there was a corresponding increase in flow). Attempts were made to use measurements of dh/dt from repeat airborne ATM surveys to determine whether regions of positive correlations between LST and BSA corresponded with areas of glacier thickening (or lower rates of thinning). The available dh/dt data are sparse, and, especially on the Prince of Wales Icefield, a considerable fraction of these data comes from large outlet glaciers where dh/dt is strongly influenced by ice dynamics (large du/dx) (Chapter 4 Section 4.4.2). Since a majority of the dh/dt data for the region having positive correlations between LST and BSA (eastern Prince of Wales Icefield) were located in areas where du/dx was large, it was not possible to determine whether the observed thickening was attributable to changes in ice dynamics or surface mass balance.

5.3 Concluding remarks

This thesis used MODIS-derived LST and BSA, and airborne-derived dh/dt to evaluate the spatial and temporal variability of changes in temperature, albedo and rates of surface elevation change across the QEI. When interpreted together, these data point to a possible influence of summer precipitation on the mass balance of the eastern maritime-facing areas of ice caps on Ellesmere and Devon Islands, which may be related to the extent of open water in Baffin Bay and Nares Strait. However, no single dataset clearly demonstrated that warm summers are, in fact, tied to an increase in summer solid precipitation and riming events, which temporarily raise the surface albedo and suppress further warming. In each dataset, however, there are suggestions that something other than summer temperature enhances variability in glacier mass balance in the eastern QEI.

Throughout much of this thesis changes in LST and BSA were used to infer changes in the climatic mass balance, while changes in precipitation, which alter accumulation rates, were neglected. Future work should focus on evaluation of spatial and temporal trends in precipitation within and between ice masses in the QEI. Such an assessment requires (reliable) climate model output at a sufficient spatial resolution to permit evaluation of spatial trends at the ice cap scale. These data are not available at present.

5.4 References

Alt, B. T. (1987), Developing synoptic analogs for extreme mass balance conditions on Queen Elizabeth Island ice caps, *Journal of Applied Climate*, 26(12), 1605-1623, doi: 10.1175/1520-0450(1987)026<1605:DSAFEM>2.0.CO;2.

Box, J. E., X. Fetwweis, J. C. Stroeve, M. Tedesco, D.K. Hall, and K. Steffen (2012), Greenland ice sheet albedo feedback: thermodynamics and atmospheric drivers, *Cryosphere*, 6(4), 821-839, doi: 10.5194/tc-6-821-2012.

Braithwaite, R. J. (2005), Mass balance characteristics of arctic glaciers, *Ann. Glaciol.*, 42, 225-229, doi: 10.3189/17275640578182899.

Casey, K. A., C. M. Polashenski, J. Chen, and M. Tedesco (2016), Impact of MODIS sensor calibration updates on Greenland Ice Sheet albedo trends, AGU annual fall meeting, 12 December, C13B-0813.

Clarke, A. D., and K. J. Noone (1985), Soot in the Arctic snowpack: a cause for perturbations in radiative transfer, *Atmospheric Environment*, 19(12), 2045-2053, doi: 10.1016/0004-6981(85)90113-1.

Conway, H., A. Gades, and C.F. Raymond (1996), Albedo of dirty snow during conditions of melt, *Water Resour. Res.*, 32(6), 1716-1718, doi: 10.1029/96WR00712.

Cuffey, K. M. and W. Paterson (2010), *The physics of glaciers*, 4th edn. Butterworth-Heinemann, Oxford.

Doherty, S. J., S. G. Warren, T. C. Grenfell, A. D. Clarke, and R. E. Brandt (2010), Light absorbing impurities in Arctic snow, *Atmos. Chem Phys*, *10*(23), 11647-11680, doi: 10.5194/acp-10-11647-2010.

Flato, G. M., G. J. Boer, W. G. Lee, N. A. McFarlane, D. Ramsden, M. C. Reader, and A. J. Weaver (2000), The Canadian Centre for Climate Modelling and Analysis global coupled model and its climate, *Climate Dynamics*, *16*(6), 451-467, doi: 10.1007/s003820050339.

Fountain, A.G., M. Tranter, T. H. Nylén, and D. R. Müller (2004), Evolution of cryoconite holes and their contribution to meltwater runoff from glaciers in the McMurdo Dry Valleys, Antarctica, *J. Glaciol.*, *50*(168), 35-45, doi: 10.3189/172756504781830312.

Gardner, A. S., and M. Sharp (2007), Influence of the Arctic circumpolar vortex on the mass balance of Canadian high Arctic glaciers, *J. Climate*, *20*(18), 4586-4598, doi: 10.1175/JCLI4268.1.

Gardner, A. S., G. Moholdt, B. Wouters, G. J. Wolken, D. O. Burgess, M. J. Sharp, J. G. Cogley, C. Braun, and C. Labine (2011), Sharply increased mass loss from glaciers and ice caps in the Canadian Arctic Archipelago, *Nature*, *473*(7347), 357-360, doi:10.1038/nature10089.

Gardner, A. S., et al. (2013), A reconciled estimate of glacier contributions to sea level rise: 2003 to 2009, *Science*, *340*(6134), 852-857, doi:10.1126/science.1234532.

Hall D. K., R. S. Williams Jr, K. A. Casey, N. E. DiGirolamo, and Z. Wan (2006), Satellite-derived, melt-season surface temperature of the Greenland Ice Sheet (2000–2005) and its relationship to mass balance, *Geophys. Res. Lett.*, *33*(11), L11501, doi:10.1029/2006GL026444.

Hall, D. K., R. S. Williams, S. B. Luthcke, and N. E. DiGirolamo (2008), Greenland ice sheet surface temperature, melt and mass loss: 2000–2006, *J. Glaciol.*, *54*(184), 81–93, doi:10.3189/002214308784409170.

He, T., S. L. Lian, and D. X. Song (2014), Analysis of global land surface albedo climatology and spatial-temporal variation during 1981-2010 from multiple satellite products, *J. Geophys. Res.-Atmos.*, *119*(17), 10281-10298, doi: 10.1002/2014/JD021667.

Kalnay, E., et al. (1996), The NCEP/NCAR 40 year reanalysis project, *Bull. Am. Meteorol. Soc.*, *77*(3), 437–471, doi:10.1175/1520-0477(1996) 077<0437:TNYRP>2.0.CO;2.

- King, M. D., S. Platnick, P. Yang, G. T. Arnold, M. A. Gray, J. C. Ridei, S. A. Ackerman, and K. N. Liu (2004), Remote Sensing of Liquid Water and Ice Cloud Optical Thickness and Effective Radius in the Arctic: Application of Airborne Multispectral MAS Data, *J. Atmos. Ocean. Technol.*, 21(6), 857–875, doi:10.1175/1520-0426(2004)021<0857:RSOLWA>2.0.CO;2.
- Koerner, R. M. (1977), Devon Island ice cap: core stratigraphy and paleoclimate, *Science*, 196(4285), 15-18, doi: 10.1126/science.196.4285.15.
- Koerner, R. M. (1979), Accumulation, ablation, and oxygen isotope variations on the Queen Elizabeth Islands ice caps, Canada, *J. Glaciol.*, 22(86), 25-41.
- Koerner, R. M. (2005), Mass balance of glaciers in the Queen Elizabeth Islands, Nunavut, Canada, *Ann. Glaciol.*, 42, 417–423, doi:10.3189/172756405781813122.
- Lenaerts, J. T. M., J. H. van Angelen, M. R. van den Broeke, A. S. Gardner, B. Wouters, and E. van Meijgaard (2013), Irreversible mass loss of Canadian Arctic Archipelago glaciers, *Geophys. Res. Lett.*, 40(5), 870–874, doi:10.1002/grl.50214.
- Lyapustin, A., Y. Wang, X. Xiong, G. Meister, S. Platnick, R. Levy, B. Franz, S. Korkin, T. Hilker, J. Tucker, F. Hall, P. Sellers, A. Wu, and A. Angal (2014), Scientific impact of MODIS C5 calibration degradation and C6+ improvements, *Atmos. Meas. Tech.*, 7(12), 4353-4365, doi:10.5194/amt-7-4353-2014.
- Millan, R., J. Mouginot, and E. Rignot (2017), Mass budget of the glaciers and ice caps of the Queen Elizabeth Islands, Canada, from 1991 to 2015, *Environ. Res. Lett.*, 12(02), 1-8, doi: 10.1088/1748-9326/aa5b04.
- Paden, J., et al. (2016), 3D Imaging and automated bottom tracking of Canadian Arctic Archipelago ice sounding data, AGU annual fall meeting, 12 December, C13C-0846.
- Polashenski, C. M., J. E. Dibb, M. G. Flanner, J. Y. Chen, Z. R. Courville, A. M. Lai, J. J. Schauer, M. M. Shafer and M. Bergin (2015), Neither dust nor black carbon causing apparent albedo decline in Greenland's dry snow zone: Implications for MODIS C5 surface reflectance, *Geophys. Res. Lett.*, 42(12), 9319-9327, doi: 10.1002/2015GL065912.

Schaaf, C., and Z. Wang (2015), MCD43A3 MODIS/Terra+Aqua BRDF/Albedo Daily L3 Global – 500m V006. NASA EOSDIS Land Processes DAAC, <https://doi.org/10.5067/MODIS/MCD43A3>.

Sharp, M., D. O. Burgess, J. G. Cogley, M. Ecclestone, C. Labine, and G. J. Wolken (2011), Extreme melt on Canada's Arctic ice caps in the 21st century, *Geophys. Res. Lett.*, 38(11), L11501, doi:10.1029/2011GL047381.

Shuai, Y., J. G. Masek, F. Gao, C. Schaaf, and T. He (2014), An approach for the long-term 20-m land surface snow-free albedo retrieval from historic Landsat surface reflectance and MODIS-based a priori anisotropy knowledge, *Remote Sens. Environ.*, 152(2014), 467-479, doi: 10.1016/j.rse.2014.07.009.

Strabala, K. I., S. A. Ackerman, and W. P. Menzel (1994), Cloud Properties inferred from 8–12- μm Data, *J. Appl. Meteor.*, 33(2), 212–229, doi:10.1175/15200450(1994)033<0212:CPIFD>2.0.CO;2.

von Salzen, K., J. F. Scinocca, N. A. McFarlane, J. Li, J. N. S. Cole, D. Plummer, D. Verseghy, M. C. Reader, X. Ma, M. Lazare, and L. Solheim (2013), The Canadian Fourth Generation Atmospheric Global Climate Model (CanAM4). Part I: representation of physical processes, *Atmosphere-Ocean*, 51(1), 104-125, doi: 10.1080/07055900.2012.755610.

Wang L., M. Sharp, B. Rivard, S. Marshall, and D. Burgess (2005), Melt season duration on Canadian Arctic ice caps, 2000-2004, *Geophys. Res. Lett.*, 32(19), L19502, doi: 10.1029/2005GL023962.

Wang, Z., C. B. Schaaf, M. J. Chopping, A. H. Strahler, J. Wang, M. O. Román, A. V. Rocha, C. E. Woodcock, and Y. Shuai (2012), Evaluation of Moderate-resolution Imaging Spectroradiometer (MODIS) snow albedo product (MCD43A) over tundra, *Remote Sens. Environ.*, 117, 264-280, doi: 10.1016/j.rse.2011.10.002.

Zadra, A., D. A. Caya, J. E. Cote, B. E. Dugas, C. Jones, R. E. Laprise, K. A. Winger, and L. P. Caron (2008), The next Canadian regional climate model, *Phys. Can.*, 64(2), 75-83.

Zwally, H. J., et al. (2011), GLAS/ICESat L1B Global Elevation Data V031, 20 February 2003 to 11 October. (National Snow and Ice Data Center, Boulder, CO. Digital media., 2011).

6.0 Thesis References

Abdalati, W., W. Krabill, E. Frederick, S. Manizade, C. Martin, J. Sonntag, R. Swift, R. Thomas, J. Yungel, and R. Koerner (2004), Elevation changes of ice caps in the Canadian Arctic Archipelago, *J. Geophys. Res.*, *109*(F04007), doi: 10.1029/2003JF000045.

Ackerman, S. A., K. I. Strabala, P. W. Menzel, R. A. Frey, C. C. Moeller, and L. E. Gumley (1998), Discriminating clear sky from clouds with MODIS, *J. Geophys. Res.*, *103*(D24), 32141–32157, doi:10.1029/1998JD200032.

Alexander, P. M., M. Tedesco, X. Fettweis, R. S. W. van de Wal, C. J. P. P. Smeets, and M. R. van den Broeke (2014), Assessing spatiotemporal variability and trends in modeled and measured Greenland Ice Sheet albedo (2000-2013), *The Cryosphere*, *8*(6), 2293-2312, doi: 10.5194/tc-8-2293-2014.

Alt, B. T. (1978), Synoptic climate controls of mass-balance variations on Devon Island Ice Cap, *Arct. Alp. Res.*, *10*(1), 61–80, doi:10.2307/1550657.

Alt, B. T. (1987), Developing synoptic analogs for extreme mass balance conditions on Queen Elizabeth Island ice caps, *Journal of Applied Climate*, *26*(12), 1605-1623, doi: 10.1175/1520-0450(1987)026<1605:DSAFEM>2.0.CO;2.

Arendt, A. A., K. A. Echelmeyer, W. D. Harrison, C. S. Lingle, and V. B. Valentine (2002), Rapid wastage of Alaska Glaciers and their contribution to rising sea level, *Science*, *297*(5580), 382-386, doi: 10.1126/science.1072497.

Arendt, A., K. Echelmeyer, W. Harrison, C. Lingle, S. Zirnheld, V. Valentine, B. Ritchie, and M. Druckenmiller (2006), Updated estimates of glacier volume changes in the western Chugach Mountains, Alaska, and a comparison of regional extrapolation methods, *J. Geophys. Res.: Earth Surf.*, *111*(F3), doi: 10.1029/2005JF000436.

Arendt, A., et al. (2012), Randolph Glacier Inventory Vers. 3.0: a dataset of Global Glacier Outlines. Global Land Ice Measurements from Space, Boulder, CO. Digital media: http://www.glims.org/RGI/rgi32_dl.html.

- Bamber, J. L., W. Krabill, W. Raper, J. A. Dowdeswell, and J. Oerlemans (2005), Elevation changes measured on Svalbard glaciers and ice caps from airborne laser data, *Ann. Glaciol.*, 42(1), 202-208, doi: 10.3189/172756405781813131.
- Bezeau, P., M. Sharp, D. Burgess, and G. Gascon (2013), Firn profile changes in response to extreme 21st-century melting at Devon Ice Cap, Nunavut, Canada, *J. Glaciol.*, 59(217), 981-991, doi:10.3189/2013JoG12J208.
- Bezeau, P., M. Sharp, and G. Gascon (2015), Variability in summer anticyclonic circulation over the Canadian Arctic Archipelago and west Greenland in the late 20th/early 21st centuries and its effects on glacier mass balance, *Int. J. Climatol.*, 35(4), 540-557, doi:10.1002/joc.4000.
- Box, J. E., X. Fetwweis, J. C. Stroeve, M. Tedesco, D.K. Hall, and K. Steffen (2012), Greenland ice sheet albedo feedback: thermodynamics and atmospheric drivers, *Cryosphere*, 6(4), 821-839, doi: 10.5194/tc-6-821-2012.
- Braithwaite, R. J. (2005), Mass balance characteristics of arctic glaciers, *Ann. Glaciol.*, 42, 225-229, doi: 10.3189/17275640578182899.
- Burgess, D., and M. J. Sharp (2008), Recent changes in thickness of the Devon Island ice cap, Canada, *J. Geophys. Res.*, 113(B07204), 1-18, doi: 10.1029/2007/JB005238.
- Casey, K. A., C. M. Polashenski, J. Chen, and M. Tedesco (2016), Impact of MODIS sensor calibration updates on Greenland Ice Sheet albedo trends, AGU annual fall meeting, 12 December, C13B-0813.
- Clarke, A. D., and K. J. Noone (1985), Soot in the Arctic snowpack: a cause for perturbations in radiative transfer, *Atmospheric Environment*, 19(12), 2045-2053, doi: 10.1016/0004-6981(85)90113-1.
- Cogley, J. G., R. Hock, L. A. Rasmussen, A. A. Arendt, A. Bauder, R. J. Braithwaite, P. Jansson, G. Kaser, M. Möller, L. Nicholson, and M. Zemp (2011), Glossary of Glacier Mass Balance and Related Terms, IHP-VII Technical Documents in Hydrology No. 86, IACS Contribution No. 2, UNESCO-IHP, Paris.
- Colbeck, S. C. (1982), An overview of seasonal snow metamorphism, *Rev. Geophys.*, 20(1), 45-61, doi: 10.1029/RG020i001p00045.

Colgan W., J. Davis, and M. Sharp (2008), Is the high-elevation region of Devon Ice Cap thickening?, *J. Glaciol.*, **54**(186), 428-436, doi: 10.3189/002214308785837084.

Conway, H., A. Gades, and C.F. Raymond (1996), Albedo of dirty snow during conditions of melt, *Water Resour. Res.*, **32**(6), 1716-1718, doi: 10.1029/96WR00712.

Copland, L., M. J. Sharp, and J. A. Dowdeswell (2003), The distribution and flow characteristics of surge-type glaciers in the Canadian High Arctic, *Ann. Glaciol.*, **36**(1), 73-81, doi:10.3189/172756403781816301.

Cuffey, K. M. and W. Paterson (2010), *The physics of glaciers*, 4th edn. Butterworth-Heinemann, Oxford.

Doherty, S. J., S. G. Warren, T. C. Grenfell, A. D. Clarke, and R. E. Brandt (2010), Light absorbing impurities in Arctic snow, *Atmos. Chem Phys*, **10**(23), 11647-11680, doi: 10.5194/acp-10-11647-2010.

Doherty, S. J., T. C. Grenfell, S. Forsstrom, D. L. Hegg, R. E. Brandt, and S. G. Warren (2013), Observed vertical redistribution of black carbon and other insoluble light-absorbing particles in melting snow, *J. Geophys. Res.-Atmos.*, **118**(11), 5553-5569, doi: 10.1002/jgrd.50235.

Flanner, M. G., C. S. Zender, J. T. Randerson, and P. J. Rasch PJ (2007), Present-day climate forcing and response from black carbon in snow, *J. Geophys. Res.*, **112**, D11202, doi:10.1029/2006JD008003.

Flato, G. M., G. J. Boer, W. G. Lee, N. A. McFarlane, D. Ramsden, M. C. Reader, and A. J. Weaver (2000), The Canadian Centre for Climate Modelling and Analysis global coupled model and its climate, *Climate Dynamics*, **16**(6), 451-467, doi: 10.1007/s003820050339.

Fountain, A.G., M. Tranter, T. H. Nylén, and D. R. Müller (2004), Evolution of cryoconite holes and their contribution to meltwater runoff from glaciers in the McMurdo Dry Valleys, Antarctica, *J. Glaciol.*, **50**(168), 35-45, doi: 10.3189/172756504781830312.

Gao, F., C. B. Schaaf, A. H. Strahler, A. Roesch, W. Lucht, and R. Dickenson (2005), MODIS bidirectional reflectance distribution function and albedo Climate Modelling Grid products and the variability of albedo for major vegetation types, *J. Geophys. Res.-Atmos.*, **110**, D01104, doi: 10.1029/2004JD005190.

- Gardner, A. S., and M. Sharp (2007), Influence of the Arctic circumpolar vortex on the mass balance of Canadian high Arctic glaciers, *J. Climate*, 20(18), 4586-4598, doi: 10.1175/JCLI4268.1.
- Gardner, A. S., G. Moholdt, B. Wouters, G. J. Wolken, D. O. Burgess, M. J. Sharp, J. G. Cogley, C. Braun, and C. Labine (2011), Sharply increased mass loss from glaciers and ice caps in the Canadian Arctic Archipelago, *Nature*, 473(7347), 357-360, doi:10.1038/nature10089.
- Gardner, A. S., G. Moholdt, A. Arendt, and B. Wouters (2012), Accelerated contributions of Canada's Baffin and Bylot Island glaciers to sea level rise over the past half century, *The Cryosphere*, 6, 1103-1125, doi: 10.5194/tc-6-1103-2012.
- Gardner, A. S., et al. (2013), A reconciled estimate of glacier contributions to sea level rise: 2003 to 2009, *Science*, 340(6134), 852-857, doi:10.1126/science.1234532.
- Gascon, G., M. Sharp, and A. Bush (2013a), Changes in melt season characteristics on Devon Ice Cap, Canada, and their association with the Arctic atmospheric circulation, *Ann. Glaciol.*, 54, 101–110, doi:10.3189/2013AoG63A601.
- Gascon, G., Sharp M., Burgess D., Bezeau P. and A. B. G. Bush (2013b), Changes in accumulation-area firn stratigraphy and meltwater flow during a period of climate warming: Devon Ice Cap, Nunavut, Canada, *J. Geophys. Res. Earth Surf.*, 118(4), 2380-2391, doi:10.1002/2013JF002838.
- Greuell, W., J. Kohler, F. Obleitner, P. Glowacki, K. Melvold, E. Bernsen, and J. Oerlemans (2007), Assessment of interannual variations in the surface mass balance of 18 Svalbard glaciers from the Moderate Resolution Imaging Spectroradiometer/Terra albedo product, *J. Geophys. Res.*, 112, D07105, doi: 10.1029/2006JD007245.
- Hall D. K., R. S. Williams Jr, K. A. Casey, N. E. DiGirolamo, and Z. Wan (2006), Satellite-derived, melt-season surface temperature of the Greenland Ice Sheet (2000–2005) and its relationship to mass balance, *Geophys. Res. Lett.*, 33(11), L11501, doi:10.1029/2006GL026444.
- Hall, D. K. J. E. Box, K. A. Casey, S. J. Hook, C. A. Shuman, and K. Steffen (2008a), Comparison of satellite-derived and in-situ observations of ice and snow surface temperatures over Greenland, *Remote Sens. Environ.*, 112(10), 3739-3749, doi: 10.1016/j.rse.2008.05.007.

Hall, D. K., R. S. Williams, S. B. Luthcke, and N. E. DiGirolamo (2008b), Greenland ice sheet surface temperature, melt and mass loss: 2000–2006, *J. Glaciol.*, *54*(184), 81–93, doi:10.3189/002214308784409170.

Hall, D. K., J. C. Comiso, N. E. DiGirolamo, C. A. Shuman, J. R. Key, and L. S. Koenig (2012), A satellite-derived climate-quality data record of the clear-sky surface temperature of the Greenland ice sheet, *J. Clim.*, *25*, 4785–4798, doi: 10.1175/JCLI-D-11-00365.1.

Hall, D. K., J. C. Comiso, N. E. DiGirolamo, C. A. Shuman, J. E. Box and L. S. Koenig (2013), Variability in the surface temperature and melt extent of the Greenland ice sheet from MODIS, *Geophys. Res. Lett.*, *40*(10), 2114–2120, doi:10.1002/grl.50240.

He, T., S. L. Lian, and D. X. Song (2014), Analysis of global land surface albedo climatology and spatial-temporal variation during 1981–2010 from multiple satellite products, *J. Geophys. Res.-Atmos.*, *119*(17), 10281–10298, doi: 10.1002/2014/JD021667.

Howat, I. M., B. E. Smith, I. Joughin, and T. A. Scambos (2008), Rates of southeast Greenland ice volume loss from combined ICESat and ASTER observations, *Geophys. Res. Lett.*, *35*(17), doi: 10.1029/2008GL034496.

Jin, Y., C. B. Schaaf, C. E. Woodcock, F. Gao, X. Li, and A. H. Strahler (2003), Consistency of MODIS surface BRDF/Albedo retrievals: 1. Algorithm performance, *J. Geophys. Res.* *108*(D5), 4158, doi: 10.1029/2002JD002803.

Kalnay, E., et al. (1996), The NCEP/NCAR 40 year reanalysis project, *Bull. Am. Meteorol. Soc.*, *77*(3), 437–471, doi:10.1175/1520-0477(1996)077<0437:TNYRP>2.0.CO;2.

King, M. D., S. Platnick, P. Yang, G. T. Arnold, M. A. Gray, J. C. Ridei, S. A. Ackerman, and K. N. Liu (2004), Remote Sensing of Liquid Water and Ice Cloud Optical Thickness and Effective Radius in the Arctic: Application of Airborne Multispectral MAS Data, *J. Atmos. Ocean. Technol.*, *21*(6), 857–875, doi:10.1175/1520-0426(2004)021<0857:RSOLWA>2.0.CO;2.

Koenig, L. S., and D. K. Hall (2010), Comparison of satellite, thermochron and station temperatures at Summit, Greenland, during the winter of 2008/09, *J. Glaciol.*, *56*(198), 735–741 doi: 10.3189/002214310793146269.

- Koerner, R. M. (1977), Devon Island ice cap: core stratigraphy and paleoclimate, *Science*, 196(4285), 15-18, doi: 10.1126/science.196.4285.15.
- Koerner, R. M. (1979), Accumulation, ablation, and oxygen isotope variations on the Queen Elizabeth Islands ice caps, Canada, *J. Glaciol.*, 22(86), 25-41.
- Koerner, R. M. (2005), Mass balance of glaciers in the Queen Elizabeth Islands, Nunavut, Canada, *Ann. Glaciol.*, 42, 417–423, doi:10.3189/172756405781813122.
- Koerner, R. M., and D. A. Fisher (1990), A record of Holocene summer climate from a Canadian high-Arctic ice core, *Nature*, 343(6259), 630-631, doi: 10.1038/343630a0.
- Krabill, W. B., W. Abdalati, E. B. Frederick, S. S. Manizade, C. F. Martin, J. G. Sonntag, R. N. Swift, R. H. Thomas, and J. G. Yungel (2002), Aircraft laser altimetry measurement of elevation changes of the Greenland Ice Sheet: Techniques and accuracy assessment, *J. Geodyn.*, 34, 357-376, doi: 10.1016/s0264-3707(02)00040-6.
- Krabill, W. B. (2010), updated 2016. *IceBridge ATM L2 Icessn Elevation, Slope, and Roughness. Version 2*. [Greenland 2011,2012,2014,2015]. Boulder, Colorado USA: NASA DAAC at the National Snow and Ice Data Center. <http://dx.doi.org/10.5067/CPRXXK3F39RV>, accessed July 2016.
- Krabill, W. B. (2012), *Pre-IceBridge ATM LIB Qfit Elevation and Return Strength, Version 1*. [Greenland and Arctic Canada 1995, 2000, 2005, 2006]. Boulder, Colorado USA. NASA National Snow and Ice Data Center Distributed Active Archive Center. doi: <http://dx.doi.org/10.5067/8Q93SAT2LG3Q>, accessed February – July 2014
- Krabill, W. B. (2014a), updated 2016, *IceBridge ATM L4 Surface elevation rate of change, Version 1* [Greenland and arctic Canada 1995-2015] Boulder, Colorado USA: NASA DAAC at the National Snow and Ice Data Center. <http://dx.doi.org/10.5067/BCW6CI3TXOCY>, accessed 6 July – 22 August 2016
- Krabill, W. B. (2014b), updated 30 June 2016, IceBridge ATM L4 Surface elevation rate of change Version 1 user guide, <http://nsidc.org/data/docs/daac/icebridge/idhdt4/index.html>.

Kwok, R., G. F. Cunningham, S. S. Manizade, and W. B. Krabill (2012), Arctic sea ice freeboard from IceBridge acquisitions in 2009: Estimates and comparisons with ICESat, *J. Geophys. Res.*, *117*(C2), doi: 10.1029/2011JC007654.

Land Processes Distributed Active Archive Center (LP DAAC) USGS EROS Data Center (2004) MODIS Land data operational product evaluation (LDOPE) tools, Release 1.4, 30 April 2001, LDOPE Tools User's Manual, 103 pages.

Land Processes Distributed Active Archive Center (LP DAAC), MODIS Albedo 16-day Level 3 Global 500 m Grid SIN Version 5 (MCD43A3v05). NASA EOSDIS Land Processes DAAC, USGS Earth Resources Observation and Science (EROS) Center, Sioux Falls, South Dakota (<https://lpdaac.usgs.gov>), accessed September 2014 - October 2016 at <http://e4ftl01.cr.usgs.gov>.

Land Processes Distributed Active Archive Center (LP DAAC), MODIS Level 3 Global 1 km Grid SIN Version 5. NASA EOSDIS Land Processes DAAC, USGS Earth Resources Observation and Science (EROS) Center, Sioux Falls, South Dakota (<https://lpdaac.usgs.gov>), accessed September 2014 - October 2015 at <http://e4ftl01.cr.usgs.gov>.

Lenaerts, J. T. M., J. H. van Angelen, M. R. van den Broeke, A. S. Gardner, B. Wouters, and E. van Meijgaard (2013), Irreversible mass loss of Canadian Arctic Archipelago glaciers, *Geophys. Res. Lett.*, *40*(5), 870–874, doi:10.1002/grl.50214.

Liu, J., C. B. Schaaf, A. H. Strahler, Z. Jiao, Y. Shuai, Q. Zhang, M. Román, J. A. Augustine, and E. G. Dutton (2009), Validation of Moderate Resolution Imaging Spectroradiometer (MODIS) albedo retrieval algorithm: Dependence of albedo on solar zenith angle, *J. Geophys. Res.-Atmos.*, *114*, D01106, doi:10.1029/2008JD009969.

Lucht, W., C. B. Schaaf, and A. H. Strahler (2000), An algorithm for the retrieval of albedo from space using semiempirical BRDF models, *IEEE Transactions on Geoscience and Remote Sensing*, *38*, 977-998.

Lyapustin, A., Y. Wang, X. Xiong, G. Meister, S. Platnick, R. Levy, B. Franz, S. Korkin, T. Hilker, J. Tucker, F. Hall, P. Sellers, A. Wu, and A. Angal (2014), Scientific impact of MODIS C5 calibration degradation and C6+ improvements, *Atmos. Meas. Tech.*, *7*(12), 4353-4365, doi:10.5194/amt-7-4353-2014.

Machguth H., M. MacFerrin, D. van As, J. E. Box, C. Charalampidis, W. Colgan, R. S. Fausto, H. A. J. Meijer, E. Mosley-Thompson, and R. S. W. van de Wal (2016), Greenland meltwater storage in firm limited by near-surface ice formation, *Nat. Clim. Change*, 6, 390-393, doi: 10.1038/NCLIMATE2899.

Martin, C. F., W. B. Krabill, S. S. Manizade, R. L. Russell, J. G. Sonntag, R. N. Swift, and J. K. Yungel (2012), Airborne topographic mapper calibration procedures and accuracy assessment. NASATM-2012-215891.

Millan, R., J. Mouginot, and E. Rignot (2017), Mass budget of the glaciers and ice caps of the Queen Elizabeth Islands, Canada, from 1991 to 2015, *Environ. Res. Lett.*, 12(02), 1-8, doi: 10.1088/1748-9326/aa5b04.

Mortimer, C. A., M. Sharp, and B. Wouters (2016), Glacier surface temperatures in the Canadian high arctic, 2000-2015, *J. Glaciol.*, 62(23), 963-975, doi: 10.1017/jog.2016.80.

Mortimer, C. A. and M. Sharp, Glacier albedo change in the Canadian High Arctic (2001-2015) and its relationship to recent climate warming, in review for *J. Geophys. Res.: Earth Surface*.

Namazi, M., K. Von Salzes, and J. N. S. Cole (2015), Simulation of black carbon in snow and its climate impact in the Canadian Global Climate Model, *Atmos. Chem. Phys.*, 15(18), 10887-10904, doi: 10.5194/acp-15-10887-2015.

Paden, J., et al. (2016), 3D Imaging and automated bottom tracking of Canadian Arctic Archipelago ice sounding data, AGU annual fall meeting, 12 December, C13C-0846.

Pfeffer, W. T., and N. F. Humphrey (1998) Formation of ice layers by infiltration and refreezing of meltwater, *Ann. Glaciol.*, 26, 83-91.

Pfeffer, W. T. et al. (2014), The Randolph Glacier Inventory: a globally complete inventory of glaciers, *J. Glaciol.*, 60(221), 537-552, doi:10.3189/2014JoG13J176.

Polashenski, C. M., J. E. Dibb, M. G. Flanner, J. Y. Chen, Z. R. Courville, A. M. Lai, J. J. Schauer, M. M. Shafer and M. Bergin (2015), Neither dust nor black carbon causing apparent albedo decline in Greenland's dry snow zone: Implications for MODIS C5 surface reflectance, *Geophys. Res. Lett.*, 42(12), 9319-9327, doi: 10.1002/2015GL065912.

Radić V., A. Bliss, A. C. Beedlow, R. Hock, E. Miles, J. G. and Cogley (2014), Regional and global projections of twenty-first century glacier mass change in response to climate scenarios from global climate models, *Clim. Dyn.*, 42(1-2), 37-58, doi:10.1007/s00382-013-1719-7.

Rajewicz, J., and S. J. Marshall SJ (2014), Variability and trends in anticyclonic circulation over the Greenland ice sheet, 1948-2013, *Geophys. Res. Lett.*, 41(8), 2842-2850, doi:10.1002/2014GL059255.

Román, M. O., C. B. Schaaf, P. Lewis, F. Gao, G. P. Anderson, J. L. Privette, A. H. Strahler, C. E. Woodcock, and M. Barnsley (2010), Assessing the coupling between surface albedo derived from MODIS and the fraction of diffuse skylight over spatially-characterized landscapes, *Remote Sens. Environ.*, 114(4), 738-760, doi: 10.1016/j.rse.2009.11.014.

Salomon, J. G., C. B. Schaaf, A. H. Strahler, F. Gao, and Y. Jin (2006), Validation of the MODIS Bidirectional Reflectance Distribution Function and Albedo retrievals using combined observations from the Aqua and Terra platforms, *IEEE Transactions on Geoscience and Remote Sensing*, 44(6), 1555-1565.

Schaaf, C. B., et al. (2002), First operational BRDF, albedo nadir reflectance products from MODIS, *Remote Sens. Environ.*, 83(1), 135-148, doi: 10.1016/S0034-4257(02)00091-3.

Schaaf, C. L. B., J. Liu, F. Gao, and A. H. Strahler (2011a), MODIS albedo and reflectance anisotropy products from Aqua and Terra. In B. Ramachandran Justice C and M Abrams (Eds), Land remote sensing and global environmental change: NASA's earth observing system and the science of ASTER and MODIS. Remote Sensing and Digital Image Processing Series, vol 11, Springer-Verlag (873 pp).

Schaaf, C. B., Z. Wang, and A. H. Strahler (2011b), Commentary on Wang and Zender – MODIS snow albedo bias at high solar zenith angles relative to theory and in situ observations in Greenland, *Remote Sens. Environ.*, 115(5), 1296-1300, doi: 10.1016/j.rse.2011.01.002.

Schaaf, C., and Z. Wang (2015), MCD43A3 MODIS/Terra+Aqua BRDF/Albedo Daily L3 Global – 500m V006. NASA EOSDIS Land Processes DAAC, <https://doi.org/10.5067/MODIS/MCD43A3>.

Sharp, M., D. O. Burgess, J. G. Cogley, M. Ecclestone, C. Labine, and G. J. Wolken (2011), Extreme melt on Canada's Arctic ice caps in the 21st century, *Geophys. Res. Lett.*, 38(11), L11501, doi:10.1029/2011GL047381.

Sharp, M., et al. (2015) [Arctic] Glaciers and ice caps (outside Greenland [in "State of the Climate 2014"], *Bull. Am. Meteorol. Soc.*, 96(7), 135-137.

Short, N. H., and A. L. Gray (2005), Glacier dynamics in the Canadian High Arctic from RADARSAT-1 speckle tracking, *Can. J. Remote Sens.*, 30(3), 504-509.

Shuai, Y., J. G. Masek, F. Gao, C. Schaaf, and T. He (2014), An approach for the long-term 20-m land surface snow-free albedo retrieval from historic Landsat surface reflectance and MODIS-based a priori anisotropy knowledge, *Remote Sens. Environ.*, 152(2014), 467-479, doi: 10.1016/j.rse.2014.07.009.

Shuman C. A., D. K. Hall, N. E. DiGirolamo, T. K. Mefford, and M. J. Schnaubelt (2014), Comparison of near-surface air temperatures and MODIS ice-surface temperatures at Summit, Greenland (2008-13), *J. Appl. Meteor. Climatol.*, 53(9), 2171 – 2180, doi:10.1175/JAMC-D-14-0023.1.

Strabala, K. I., S. A. Ackerman, and W. P. Menzel (1994), Cloud Properties inferred from 8–12- μm Data, *J. Appl. Meteor.*, 33(2), 212–229, doi:10.1175/15200450(1994)033<0212:CPIFD>2.0.CO;2.

Strahler, A. H., et al. (1999), MODIS BRDF/Albedo product: algorithm theoretical basis document version 5.0.

Stroeve, J. C., J. Box, F. Gao, S. Liang, A. Nolin, and C. Schaaf (2005), Accuracy assessment of the MODIS 16-day albedo product for snow: Comparison with Greenland in situ measurements, *Remote Sens. Environ.*, 94(1), 46-60, doi: 10.1016/j.rse.2004.09.001.

Stroeve, J. C., J. Box, and T. Haran (2006), Evaluation of the MODIS (MOD10A1) daily snow albedo product over the Greenland Ice Sheet, *Remote Sens. Environ.*, 105(2), 155-171, doi: 10.1016/j.rse.2006.06.009.

Stroeve, J., J. E. Box, Z. Wang, C. Schaaf, and A. Barret (2013), Re-evaluation of MODIS MCD43 Greenland albedo accuracy and trends, *Remote Sens. Environ.*, 138, 199-214, doi: 10.1016/j.rse.2013.07.023.

Strugnell, N., and W. Lucht (2001), Continental-scale albedo inferred from AVHRR data, land cover class and field observations of typical BRDFs, *J. Clim.*, 14(7), 1360-1376, doi: 10.1175/1520-0442(2001)014<1360:AATICS>2.0.CO;2.

Tedesco M., S. Doherty, X. Fettweis, P. Alexander, J. Jeyaratnam, and J. Stroeve (2016), The darkening of the Greenland ice sheet: trends, drivers, and projections (1981-2100), *The Cryosphere*, 10, 477-496, doi: 10.5194/tc-10-477-2016.

van den Broeke, M. R., C. J. P. P. Smeets, and R. S. W. van de Wal (2011), The seasonal cycle and interannual variability of surface energy balance and melt in the ablation zone of the west Greenland ice sheet, *The Cryosphere*, 5(2), 377-390, doi: 10.5194/tc-5-377-2011.

van Wychen, W., J. Davis, D. O. Burgess, L. Copland, L. Gray, M. Sharp, and C. Mortimer (2016), Characterizing interannual variability of glacier dynamics and dynamic discharge (1999-2015) for the ice masses of Ellesmere and Axel Heiberg Islands, Nunavut, Canada, *J. Geophys. Res.- Earth Surf.*, 121, 39-63, doi:10.1002/2015JF003708.

van Wychen, W., J. Davis, L. Copland, D. O. Burgess, L. Gray, M. Sharp, J. A. Dowdeswell, and T. J. Benham (2017), Variability in ice motion and dynamic discharge from the Devon Ice Cap, Nunavut, Canada, *J. Glaciol.*, 1-14, doi: 10.1017/jog.2017.

Vermote, E. F., S. Y. Kotchenova, and J. P. Ray (2011), MODIS surface reflectance user's guide. MODIS Land Surface Reflectance Science Computing Facility, version 1.

von Salzen, K., J. F. Scinocca, N. A. McFarlane, J. Li, J. N. S. Cole, D. Plummer, D. Versegny, M. C. Reader, X. Ma, M. Lazare, and L. Solheim (2013), The Canadian Fourth Generation Atmospheric Global Climate Model (CanAM4). Part I: representation of physical processes, *Atmosphere-Ocean*, 51(1), 104-125, doi: 10.1080/07055900.2012.755610.

Wan, Z., Y. Zhang, Q. Zhang, and Z. L. Li (2002), Validation of the land-surface temperature products retrieved from Terra Moderate Resolution Imaging Spectroradiometer data, *Remote Sens. Environ.*, 83(1-2), 163-180, doi:10.1016/S0034-4257(02)00093-7.

Wan Z., and Z. L. Li (1997), A physical-based algorithm for retrieving land-surface emissivity and temperature from EOS/MOSI data, *IEEE Transactions on Geoscience and Remote Sensing*, 35(4), 980-996.

Wan, Z. M. (2008), New refinements and validation of the MODIS Land-Surface Temperature/Emissivity products, *Remote Sens. Environ.*, 112(1), 59–74, doi:10.1016/j.rse.2006.06.026.

Wang L., M. Sharp, B. Rivard, S. Marshall, and D. Burgess (2005), Melt season duration on Canadian Arctic ice caps, 2000-2004, *Geophys. Res. Lett.*, 32(19), L19502, doi: 10.1029/2005GL023962.

Wang, Z., C. B. Schaaf, M. J. Chopping, A. H. Strahler, J. Wang, M. O. Román, A. V. Rocha, C. E. Woodcock, and Y. Shuai (2012), Evaluation of Moderate-resolution Imaging Spectroradiometer (MODIS) snow albedo product (MCD43A) over tundra, *Remote Sens. Environ.*, 117, 264-280, doi: 10.1016/j.rse.2011.10.002.

Wanner, W., A. H. Strahler, B. Hu, P. Lewis, J. P. Muller, X. Li, C. L. B. Schaaf, and M. J. Barnsley (1997), Global retrieval of bidirectional reflectance and albedo over than from EOS MODIS and MISR data: theory and algorithm, *J. Geophys. Res.* 102(D14), 17143-17162, doi: 10.1029/96JD03295.

Warren, S. G. (1982), Optical properties of snow, *Reviews of Geophysics*, 20(1), 67-89, doi: 10.1029/RG020i001p00067.

Warren, S. G., and W. J. Wiscombe (1980), A model for the spectral albedo of snow. II Snow containing atmospheric aerosols, *J. Atmos. Sci.*, 37(12), 2734-2745, doi: 10.1175/1520-0469(1980)037<2734:AMFTSA>2.0.CO;2.

Williamson, S., M. Sharp, J. Dowdeswell, and T. Benham (2008), Iceberg calving rates from northern Ellesmere Island ice caps, Canadian Arctic, 1999-2003, *J. Glaciol.*, 54(186), 391-400, doi: 10.3189/00221430878537048.

Wiscombe, W. J., and S. G. Warren (1980), A model for the spectral albedo of snow. I: Pure snow, *J. Atmos. Sci.*, 37(12), 2712-2732, doi: 10.1175.1520-0469(1980)037<2712:AMFTSA>2.0.CO;2.

Wolken G. J., M. Sharp, and L. Wang (2009), Snow and ice facies variability and ice layer formation on Canadian Arctic ice caps, 1999– 2005, *J. Geophys. Res.*, *114*(F3), F03011, doi:10.1029/2008JF001173.

World Meteorological Organization (2015), Provisional Statement on the Status of Global Climate in 2011-2015, Press release No 13, 25 November 2015, <https://www.wmo.int>.

World Glacier Monitoring Service Fluctuations of Glaciers (2016), Devon Ice Cap NW, Canada (WGMS_ID: 39), *Fluctuations of Glaciers Database*, version 2016-08-16, doi: 10.5904/wgms-fog-2016-08.

Zadra, A., D. A. Caya, J. E. Cote, B. E. Dugas, C. Jones, R. E. Laprise, K. A. Winger, and L. P. Caron (2008), The next Canadian regional climate model, *Phys. Can.*, *64*(2), 75-83.

Zdanowicz, C., A. Smetny-Sowa, D. Fisher, N. Schaffer, L. Copland, J. Eley, and F. Dupont (2012), Summer melt rates on Penny Ice Cap, Baffin Island: Past and recent trends and implications for regional climate, *J. Geophys. Res.*, *117*(F2), F02006, doi:10.1029/2011JF002248.

Zwally, H. J., et al. (2011), GLAS/ICESat L1B Global Elevation Data V031, 20 February 2003 to 11 October. (National Snow and Ice Data Center, Boulder, CO. Digital media., 2011).

Appendix 1

Canadian Digital Elevation Model (CDED DEM) 1:50k metadata

The CDED DEM edition 3.0 1:50k data (geogratis.gc.ca, downloaded December 2013) were used for baseline elevation data throughout this thesis. Horizontal and vertical coordinates for this dataset are referenced to the North American Datum 1983 (NAD83) and the Canadian Vertical Geodetic Datum 1928 (CVGD28), respectively (NRCAN, 2007). North-south and east-west resolutions are 23 m and 17-18 m, respectively. Post spacing is 0.75° by $1.5\text{-}3^\circ$.

The lower resolution 1:250k CDED DEM dataset has been found to be highly accurate with good horizontal control (Beaulieu and Clavet 2009; Gardner and others, 2012). Validation of surface elevations from 21 high arctic CDED 1:250k map sheets with ICESat-derived surface elevations returned a mean offset of +0.1 m above ICESat postings and a standard deviation of 6.2 m (Beaulieu and Clavet, 2009). Assessment of surface elevations from 340 CDED 1:250k map sheets over the Barnes and Penny Ice Caps against plane-fitted ICESat surface elevations found a mean offset of 1.1 m above ICESAT posting and a standard deviation of 5.1 m (Gardner and others, 2012). The spatial resolution of the 1:250k data were too coarse for the work presented in this thesis, instead the 1:50k data were used.

The 1:50k CDED DEM was produced mainly from historic stereo aerial photograph pairs (1958, 1959, and 1982), but also include vector data sourced from digitized topographic maps (1958, 1959, 1982, 1988, 2007), as well as modern DEMs created from satellite stereoscopic imagery (SPOT5 2007-2011) and radar interferometry (ERS-1: 1996, RADARSAT-2: 2010-2011) (NRCAN, 2007). The modern DEMs were used mainly in regions that previously had incomplete

or insufficient air photo coverage, primarily over snow and ice (NRCAN, 2007). Given the range of data types listed as source data for the CDED DEM 1:50k, an inventory of all tiles was performed.

A total of 561 individual map sheets, which, together provides complete coverage of the QEI, were inventoried. For each map sheet, the input data source, collection date, CDED edition number, Geobase issue, and production date were retrieved from the metadata files (geogratis.gc.ca). Input data source varies from recent SAR data, to aerial photographs, to topographic maps (vector data). The oldest data dates from 1959 and the most recent is from 2011. Given the observed mass loss in the region, the ~52 year differences in dates of input data means that even relative surface elevations (i.e. within the QEI) are only approximate.

An updated Digital Elevation dataset is being released (2016 to 2017) (NRCAN, 2016) and the CDED DEM used in this thesis is now considered a legacy product. However, inspection of these data finds that elevations for NTS sheets 120 and 340 (northwest Ellesmere Island) are mainly produced from the older aerial photographs. A detailed inventory of the newer data is recommended.

The following tables, organized by NTS map sheet, include the NTS map sheet number, the input data source, collection date, CDED edition number ('Edition'), Geobase issue ('Issue'), and production date. Where multiple data from several different dates were used, the start/end date shows the earliest and latest dates of these input data. Processing date ('Proc. Date) refers to the date the DEM was produced.

List of acronyms

- SPOT: SPOT5/HRS, Satellites Pour l'Observation de la Terre, High Resolution Stereoscopic
- R2: RADARSAT-2
- ERS-1: European Remote Sensing (ERS) satellite 1
- ASDB: Aerial Survey Database [followed by series (e.g. T) and number]
- NTDB: National Topographic Data Base
- BNDT: la Base de donnees topographiques
- BDG: la Base de donnees geographiques
- NRCAN ESS CCMEQ: Natural Resources Canada, Earth Sciences Sector, Canada Centre for Mapping and Earth Observation

List of Tables

Table A1: CDED 039
Table A1: CDED 039
Table A3: CDED 049
Table A4: CDED 059
Table A5: CDED 120
Table A6: CDED 340
Table A6: CDED 560

References

Beaulieu, A., and Clavet D. (2009), Accuracy assessment of Canadian digital elevation data using ICESat, *Photogrammetric Engineering and Remote Sensing*, 75(1), 81-86.

Government of Canada, Natural Resources Canada, Canada Centre for Mapping and Earth Observations (2007), Canada Digital Elevation Data, Level 1, Product Specifications. Edition 3.0, 2007-06-01. Geomatics Client Services.

Government of Canada, Natural Resources Canada, Map Information Branch (2016), Canadian Digital Elevation Model Product Specifications. Edition 1.1, 2016-10-21. Geomatics Client Services, Sherbrooke, Quebec, Canada.

Gardner, A., G. Moholdt, A. Arendt, and B. Wouters (2012), Accelerated contribution of Canada's Baffin and Bylot Island glaciers to sea level rise over the past half century, *The Cryosphere*, 6, 1103-1125, doi: 10.5194/tc-6-1103-2012.

Table A1: CDED 039

NTS sheet	Data	Start/end	Edition	Issue	Proc. date
1. 039b03	SPOT: 2008-06-17	2008-06-17 2008-06-17	1.0	3.0	2011-03-22
2. 039b04	SPOT: 2008-06-17	2008-06-17 2008-06-17	1.0	3.0	2011-03-18
3. 039b05	SPOT: 008-06-17; 2010-07-01	2008-06-17 2010-07-01	1.0	3.0	2011-04-19
4. 039b06	SPOT: 2010-07-01	2010-07-01 2010-07-01	1.0	3.0	2011-04-15
5. 039b10	SPOT: 2008-06-17	2008-06-17 2008-06-17	1.0	3.0	2012-01-17
6. 039b11	SPOT: 2008-06-17	2008-06-17 2008-06-17	1.0	3.0	2012-01-17
7. 039b12	SPOT: 2007-08-20; 2008-06-17	2007-08-20 2008-06-17	1.0	3.0	2012-01-17
8. 039b13	SPOT: 2008-06-17; 2010-06-09 R2: 2011-11-20; 2011-11-11	2008-06-17 2011-11-20	1.0	3.0	2012-02-01
9. 039b14	SPOT:2008-06-17;2011-07-04	2008-06-17 2011-07-04	1.0	3.0	2012-01-19
10. 039b15	SPOT: 2008-06-17;2011-07-04	2008-06-17 2011-07-04	1.0	3.0	2012-01-19
11. 039c03	R2: 2011-11-03 (x2); 2011-11-25; 2011-11-18 (x2); 2011-11-20	2011-11-03 2011-11-25	1.0	3.0	2012-01-19
12. 039c04	R2: 2011-11-03; 2011-11-18 (x2); 2011-11-20 (x2); 2011-11-11	2011-11-03 2011-11-20	1.0	3.0	2012-02-01
13. 039c05	SPOT: 2010-06-09	2010-06-09 2010-06-09	1.0	3.0	2011-04-21
14. 039c06	R2: 2011-11-03; 2011-11-25; 2011-11-27; 2011-11-18	2011-11-03 2011-11-27	1.0	3.0	2012-02-01
15. 039c07	R2: 2011-11-03; 2011-11-25; 2011-11-27; 2011-11-18	2011-11-03 2011-11-27	1.0	3.0	2012-01-09
16. 039c10	R2: 2011-11-18; 2011-11-20;	2011-11-18 2011-11-20	1.0	3.0	2012-01-11
17. 039c11	R2: 2011-11-18; 2011-11-20;	2011-11-18 2011-11-20	1.0	3.0	2012-01-27
18. 039c12	SPOT: 2010-06-09; 2008-06-05	2008-05-05 2010-06-09	1.0	3.0	2012-02-07
19. 039c13	SPOT : 2009-06-14	2009-06-14 2009-06-14	1.0	3.0	2011-04-21
20. 039c14	SPOT:2010-06-09	2010-06-09 2010-06-09	1.0	3.0	2011-05-04
21. 039c15	SPOT: 2010-06-09; 2008-06-05; 2010-08-10	2008-06-05 2010-08-10	1.0	3.0	2011-11-18
22. 039c16	SPOT: 2008-06-05; 2010-08-10	2008-06-05 2010-08-10	1.0	3.0	2011-11-18
23. 039d13	SPOT: 2010-06-09	2010-06-09 2010-06-09	1.0	3.0	2011-11-21
24. 039e04	SPOT: 2008-06-05; 2010-08-10 (x2)	2008-06-05 2010-08-10	1.0	3.0	2011-11-18
25. 039e05	SPOT: 2010-08-10	2010-08-10 2010-08-10	1.0	3.0	2011-11-18
26. 039e11	R2: 2011-11-08; 2011-11-10; 2011-11-15	2011-11-08 2011-11-15	1.0	3.0	2012-01-11
27. 039e12	SPOT: 2010-08-10	2010-08-10 2010-08-10	1.0	3.0	2011-11-22
28. 039e13	R2: 2011-11-08; 2011-11-10; 2011-11-15	2011-11-08 2011-11-15	1.0	3.0	2012-01-09
29. 039e14	R2: 2011-11-08; 2011-11-10; 2011-11-15	2011-11-08 2011-11-15	1.0	3.0	2012-01-09
30. 039f01	SPOT: 2008-06-05	2008-06-05 2008-06-05	1.0	3.0	2011-05-03
31. 039f02	SPOT: 2008-06-05; 2010-08-10	2008-06-05	1.0	3.0	2011-04-15

		2010-08-10			
32. 039f03	SPOT: 2008-06-05; 2010-06-09; 2010-08-10	2008-06-05 2010-08-10	1.0	3.0	2012-02-07
33. 039f04	SPOT: 2008-06-05;	2008-06-05	1.0	3.0	2012-02-07
34. 039f05	SPOT: 2008-08-26; 2008-06-05 (x2)	2008-06-05 2008-08-26	1.0	3.0	2012-01-24
35. 039f06	SPOT: 2008-06-05;	2008-06-05	1.0	3.0	2011-04-21
36. 039f07	SPOT: 2008-06-05;	2008-06-05	1.0	3.0	2011-04-21
37. 039f08	SPOT: 2008-06-05; 2009-06-14	2008-06-05 2009-06-14	1.0	3.0	2011-04-21
38. 039f09	SPOT: 2009-06-14	2009-06-14 2009-06-14	1.0	3.0	2011-05-03
39. 039f10	SPOT: 2008-06-05; 2009-06-14	2008-06-05 2009-06-14	1.0	3.0	2011-05-03
40. 039f11	SPOT: 2008-06-05;	2008-06-05	2.0	3.0	2011-06-14
41. 039f12	SPOT: 2008-05-14	2008-05-14	1.0	3.0	2011-06-04
42. 039f13	SPOT: 2008-08-26	2008-08-26	1.0	3.0	2011-06-04
43. 039f14	SPOT: 2008-08-26	2008-08-26	1.0	3.0	2011-06-04
44. 039f15	SPOT: 2009-06-14	2009-06-14	1.0	3.0	2011-06-08
45. 039f16	SPOT: 2008-08-26; 2009-06-14	2008-08-26 2009-06-14	1.0	3.0	2011-06-10
46. 039g01	SPOT: 2008-08-26	2008-08-26	2.0	3.0	2012-01-12
47. 039g02	SPOT: 2008-08-26; 2009-06-14	2008-08-26 2009-06-14	2.0	3.0	2012-01-13
48. 039g03	SPOT: 2008-08-26 (x2)	2008-08-26	2.0	3.0	2012-01-18
49. 039g04	SPOT: 2008-08-26	2008-08-26	2.0	3.0	2012-01-17
50. 039g05	SPOT: 2008-05-18; 2008-08-30	2008-05-18 2008-08-30	1.0	3.0	2011-07-20
51. 039g06	SPOT: 2008-08-26 (x2)	2008-08-26	1.0	3.0	2011-07-20
52. 039g07	SPOT: 2008-08-26	2008-08-26	1.0	3.0	2011-04-02
53. 039g08	SPOT: 2008-08-26 (x2)	2008-08-26	1.0	3.0	2011-04-02
54. 039g09	SPOT: 2008-08-26 (x2)	2008-08-26	1.0	3.0	2011-04-02
55. 039g10	SPOT: 2008-08-26; 2008-08-30	2008-08-26 2008-08-30	1.0	3.0	2011-04-02
56. 039g11	SPOT: 2008-08-30	2008-08-30	1.0	3.0	2011-03-26
57. 039g12	SPOT: 2008-08-30	2008-08-30	1.0	3.0	2011-05-13
58. 039g13	SPOT: 2008-08-30	2008-08-30	1.0	3.0	2011-06-14
59. 039g14	SPOT: 2008-08-30 (x2)	2008-08-30	1.0	3.0	2011-03-22
60. 039g15	SPOT: 2008-08-30 (x2)	2008-08-30	1.0	3.0	2011-03-22
61. 039g16	SPOT: 2008-08-30	2008-08-30	1.0	3.0	2011-04-14
62. 039h03	ASDB-TA09	1959-06-05 1959-06-05	1.0	3.0	2011-09-14
63. 039h04	ASDB-TA09	1959-06-05 1959-06-05	1.0	3.0	2011-09-14
64. 039h05	ASDB-T010	1959-07-05 1959-07-05	1.0	3.0	2011-09-22
65. 039h06	ASDB-T010	1959-06-05 1959-06-05	1.0	3.0	2011-09-22
66. 039h07	ASDB-T010	1959-06-05 1959-06-05	1.0	3.0	2011-09-22
67. 039h09	SPOT: 2008-08-26	2008-08-26	1.0	3.0	2011-05-11
68. 039h10	SPOT: 2008-08-26	2008-08-26	1.0	3.0	2011-06-02
69. 039h11	SPOT: 2008-08-26	2008-08-26	1.0	3.0	2011-06-02
70. 039h12	SPOT: 2008-08-26	2008-08-26	1.0	3.0	2011-06-02
71. 039h13	SPOT: 2008-08-30	2008-08-30	1.0	3.0	2011-04-21
72. 039h14	SPOT: 2008-08-26	2008-08-26	1.0	3.0	2011-04-22
73. 039h15	SPOT: 2008-08-26	2008-08-26	1.0	3.0	2011-06-03
74. 039h16	SPOT: 2008-08-26	2008-08-26	1.0	3.0	2011-05-12

Table A1: CDED 039

NTS sheet	Data	Start/end	Edition	Issue	Proc. date
1. 048a01 (BRUCE HEAD)	Vector digital data; NTDB tile 048A01 ed 4.0; NRCAN ESS, CCMEQ	1958 1958	1.0	2.1	2008-12-03
2. 048a02	ASDB-P031-0.0	1982-07-01	2.0	3.0	2009-03-05
3. 048a03 (MUCKPA MOUNTAIN)	ASDB-P031-0.0	1982-07-01	2.0	3.0	2009-03-18
4. 048a04	ASDB-P031-0.0	1982-07-01	1.0	3.0	2009-03-06
5. 048a05	ASDB-P031-0.0	1982-07-01	1.0	3.0	2009-03-10
6. 048a06	Vector data: BNDT-048A06-3.0	1982	1.0	2.1	2008-08-27
7. 048a07 (BELLVUE MOUNTAIN)	ASDB-P031-0.0	1982-07-01	1.0	3.0	2009-03-06
8. 048a08 (MILNE INLET)	Vector data: BNDT-048A08-4.1	1958, publ date: 2007-10- 03	1.0	2.1	2008-12-11
9. 048a09 (ALFRED POINT)	Vector data: BNDT-048A09-3.0	1958, publ date: 2007-10- 03	1.0	2.1	2008-12-11
10. 048a10	ASDB-P031-0.0	1982-07-01	1.0	3.0	2009-03-26
11. 048a11 (ALPHA RIVER)	Vector data: BNDT-048A11-3.0	1982, pub date: 2007-05-18	1.0	2.1	2008-08-26
12. 048a12 (FLEMING RIVER)	ASDB-P031-0.0	1982-07-01	1.0	3.0	2009-03-25
13. 048a13	Vector data: BNDT-048A13-0.0	1982, pub date: 2006-03-28	1.0	2.1	2008-12-11
14. 048a14	ASDB-P031-0.0	1982-07-01	1.0	3.0	2009-03-25
15. 048a15	ASDB-P031-0.0	1982-07-01	1.0	3.0	2009-03-26
16. 048a16	ASDB-P026-0.0	1982-07-01	1.0	3.0	2009-03-26
17. 048b01 (IKPIKITTUARJUK BAY)	ASDB-P031-0.0	1982-07-01	1.0	2.1	2007-11-08
18. 048b02 (UMIARTALIK COVE)	ASDB-P031-0.0	1982-07-01	1.0	2.1	2008-03-06
19. 048b03 (PUSINGNAJOJAQ HILL)	ASDB-P029-0.0	1982-07-01	1.0	2.1	2008-03-06
20. 048b04	ASDB-P029-0.0	1982-07-01	1.0	2.1	2008-02-28
21. 048b05	ASDB-P029-0.0	1982-07-01	1.0	2.1	2008-02-28
22. 048b06 (YELLOW VALLEY)	ASDB-P029-0.0	1982-07-01	1.0	2.1	2008-03-06
23. 048b07 (RED VALLEY)	Vector data: BNDT-048B07-4.0	1982	1.0	2.1	2008-12-11
24. 048b08 (FABRICIUS FIORD)	Vector data: BNDT-048B03-3.1	1982	1.0	2.1	2008-12-11
25. 048b09 (MOUNT PODOLSKY)	Vector data: BNDT-048B09-3.0	1982	1.0	2.1	2008-12-11
26. 048b10 (LEVASSEUR INLET)	Vector data: BNDT-048B10-3.3	1982	1.0	2.1	2008-12-11
27. 048b11 (KAKIAK POINT)	ASDB-P029-0.0	1982-07-02	1.0	2.1	2008-01-31
28. 048b12	ASDB-P029-0.0	1982-07-02	1.0	2.1	2008-02-14
29. 048b13	ASDB-P029-0.0	1982-07-02	1.0	2.1	2007-11-09
30. 048b14 (GIANTS CASTLE)	ASDB-P029-0.0	1982-07-02	1.0	2.1	2008-03-06
31. 048b15 (CAPE CUNNINGHAM)	Vector data: BNDT-048B15-2.1	1982	1.0	2.1	2008-12-11
32. 048b16 (ADAMS SOUND)	Vector data: BNDT-048B16-2.6	1982	1.0	2.1	2008-12-11
33. 048c01 (SILT POINT)	Compilation of vector data: tile 048C01 edition 10.0, pub date 2012-03-05	1982 2010-07-31	1.0	3.0	2012-05-02
34. 048c02 (ULUKSAN PENINSULA)	Vector data: BNDT-048C02-1.0	1982	1.0	1.0	2004-09-23
35. 048c03	Vector data: BNDT-048C03-3.0	1958	1.0	2.1	2009-02-17

36. 048c04 (ST JOSEPH PLATEAU)	Vector data: BNDT-048C04-3.1	1958	1.0	2.1	2009-02-17
37. 048c05	Vector data: BNDT-048C05-4.1	1958	1.0	2.1	2009-02-17
38. 048c06	Vector data: BNDT-048C06-2.6	1958	1.0	2.1	2009-02-17
39. 048c07	Vector data: BNDT-048C07-4.0	1958	1.0	2.1	2009-02-17
40. 048c08 (SHIP POINT)	Vector data: BNDT-048C08-2.6	1982	1.0	2.1	2009-02-18
41. 048c09 (CAPE CRAUFORD)	Vector data: BNDT-048C09-4.0	1958	1.0	2.1	2009-02-17
42. 048c10	Vector data: BNDT-048C10-2.7	1958	1.0	2.1	2009-02-17
43. 048c11	Vector data: BNDT-048C11-2.0	1958	1.0	2.1	2009-02-17
44. 048c12 (PEAK VALLEY)	Vector data: BNDT-048C12-3.2	1958	1.0	2.1	2009-02-18
45. 048c13 (CAPE YORK)	Vector data: BNDT-048C13-3.1	1958	1.0	2.1	2009-02-18
46. 048c14 (SARGENT POINT)	Vector data: BNDT-048C14-2.2	1958	1.0	2.1	2009-02-17
47. 048c15	Vector data: BNDT-048C15-2.1	1958	1.0	2.1	2009-02-17
48. 048c16	Vector data: BNDT-048C16-3.0	1958	1.0	2.1	2009-02-19
49. 048d01 (TULURIA MOUNTAIN)	Vector data: BNDT-048D01-1.4	1959	1.0	2.1	2008-12-11
50. 048d02 (IKKARLAK GLACIER)	Vector data: BNDT-048D02-2.0	1982	1.0	2.1	2008-12-11
51. 048d03 (MILITARY SURVEY MOUNTAIN)	Vector data: BNDT-048D03-1.1	1982	1.0	2.1	2008-12-11
52. 048d04	Compilation of vector data: tile 04DC04 edition 10.0, pub date 2012-02-22	1982 2006-08-02	1.0	3.0	2012-05-02
53. 048d05 ELWIN INLET	Compilation of vector data: tile 04DC05 edition 10.0, pub date 2012-02-22	1982 2010-07-25	1.0	3.0	2012-05-02
54. 048d06	Vector data: BNDT-048D06-1.0	1982	1.0	2.1	2008-12-11
55. 048d07 (KILUTEA RIVER)	Vector data: BNDT-048D07-1.3	1982	1.0	2.1	2008-12-11
56. 048d08 (CANADA POINT)	Vector data: BNDT-048D08-1.4	1982	1.0	2.1	2008-12-11
57. 048d09 (WOLLASTON ISLANDS)	Vector data: BNDT-048D09-2.1	1982	1.0	2.1	2008-12-11
58. 048d10 (BLUFF HEAD)	Vector data: BNDT-048D10-1.1	1982	1.0	2.1	2008-12-11
59. 048d11 (CAPE CHARLES YORKE)	Vector data: BNDT-048D11-1.2	1982	1.0	2.1	2008-12-11
60. 048d12 (CAPE JOY)	Vector data: BNDT-048D12-1.4	1982	1.0	2.1	2008-12-11
61. 048d16	Vector data: BNDT-048D16-3.0	1982	1.0	2.1	2008-12-15
62. 048e06	Vector data: BNDT-048E06-3.0	1959	1.0	2.1	2008-12-11
63. 048e07 (PHOENIX HEAD)	Vector data: BNDT-048E07-3.2	1959	1.0	2.1	2008-12-11
64. 048e09	Vector data: BNDT-048E09-2.2	1959	1.0	2.1	2008-12-15
65. 048e10 (PHOENIX HEAD)	Vector data: BNDT-048E10-3.0	1959	1.0	2.1	2008-12-15
66. 048e11 (DUNDAS HARBOUR)	Vector data: BNDT-048E11-2.4	1959	1.0	2.1	2008-12-15
67. 048e12 (CAPE ROSAMOND)	Vector data: BNDT-048E12-2.1	1959	1.0	2.1	2009-02-23
68. 048e13	Vector data: BNDT-048E13-3.0	1959	1.0	2.1	2009-02-23
69. 048e14	Vector data: BNDT-048E14-3.1	1959	1.0	2.1	2008-12-15
70. 048e15	SPOT: 2010-07-01; 2010-06-21	2010-06-21 2010-07-01	1.0	3.0	2011-04-22
71. 048e16 (BETHUNE INLET)	Vector data: BNDT-048E16-2.0	1959	1.0	2.1	2008-12-15
72. 048f05	Vector data: BNDT-048F05-1.1	1959	1.0	2.0	2005-09-01
73. 048f06	Vector data: BNDT-048F06-1.1	1959	1.0	2.0	2005-10-03

(CAPE PYRAMID)					
74. 048f07	Vector data: BNDT-048F07-2.1	1959	1.0	2.1	2009-02-23
75. 048f08 (CAPE BULLEN)	Complicated vector data: BDG-REGION_HYDRI-048F08-2.0 (waterbody geodatabase)	2009-07-23; publ date 2012-02-08	1.0	3.0	2012-04-03
76. 048f09 (CAPE BULLEN)	Vector data: BNDT-048F09-1.2	1959	1.0	2.1	2009-02-19
77. 048f10	Vector data: BNDT-048F10-1.2	1959	1.0	2.1	2009-02-19
78. 048f11	Vector data: BNDT-048F11-1.0	1959	1.0	2.1	2009-02-19
79. 048f12	Vector data: BNDT-048F12-1.2	1959	1.0	2.1	2009-02-19
80. 048f13	SPOT: 2007-08-20; 2010-08-26	2007-08-20 2010-08-26	1.0	3.0	2011-08-12
81. 048f14	SPOT: 2007-08-20	2007-08-20	1.0	3.0	2011-02-12
82. 048f15	SPOT: 2007-08-20 (x2)	2007-08-20	1.0	3.0	2011-02-12
83. 048f16	SPOT: 2007-08-20	2007-08-20	1.0	3.0	2011-02-25
84. 048g01	SPOT: 2007-08-20 (x2)	2007-08-20	1.0	3.0	2011-02-16
85. 048g02	SPOT: 2007-08-20	2007-08-20	1.0	3.0	2011-02-15
86. 048g03	SPOT: 2007-08-20 (x2)	2007-08-20	1.0	3.0	2011-02-15
87. 048g04	ASDB-T012	1959-07-17	1.0	3.0	2011-03-10
88. 048g05	ASDB-T012	1959-07-17	1.0	3.0	2011-03-05
89. 048g06	ASDB-T012	1959-07-17	1.0	3.0	2011-03-09
90. 048g07	SPOT: 2007-08-20 (x2)	2007-08-20	1.0	3.0	2011-02-15
91. 048g08	SPOT: 2007-08-20 (x2)	2007-08-20	1.0	3.0	2011-04-01
92. 048g09 (TRUELOVE INLET)	Vector data: BNDT-048G09-1.0	1959-07-17 1959-08-24	1.0	2.1	2007-02-23
93. 048g10	ASDB-T012	1959-07-17	1.0	3.0	2011-03-09
94. 048g11	ASDB-T012	1959-07-17	1.0	3.0	2011-03-09
95. 048g12	ASDB-T012	1959-07-17	1.0	3.0	2011-03-09
96. 048g16	ASDB-T012	1959-07-17	1.0	3.0	2011-03-23
97. 048h01	SPOT: 2010-07-01	2010-07-01	1.0	3.0	2011-10-19
98. 048h02	SPOT: 2010-07-01 (x2)	2010-07-01	1.0	3.0	2011-10-13
99. 048h03	SPOT: 2007-08-20; 2010-07-01 (x2)	2007-08-20 2010-07-01	1.0	3.0	2011-10-13
100. 048h04	SPOT: 2007-08-20 (x2)	2007-08-20	1.0	3.0	2011-04-01
101. 048h05	SPOT: 2007-08-20	2007-08-20	1.0	3.0	2011-04-01
102. 048h06	SPOT: 2007-08-20 (x2)	2007-08-20	1.0	3.0	2011-03-27
103. 048h07	SPOT: 2007-08-20; 2011-06-30; 2010-06-15	2007-08-20 2011-06-30	1.0	3.0	2012-01-05
104. 048h08	SPOT: 2010-07-01 (x2); 2010-06-21	2010-06-21 2010-07-01	1.0	3.0	2011-10-07
105. 048h09	SPOT: 2010-07-01	2010-07-01	1.0	3.0	2011-04-28
106. 048h10	SPOT: 2010-06-15	2010-06-15	1.0	3.0	2011-04-28
107. 048h11	SPOT: 2007-08-20 (x2)	2007-08-20	1.0	3.0	2011-03-27
108. 048h12	SPOT: 2007-08-20 (x2)	2007-08-20	1.0	3.0	2011-04-01
109. 048h13	ASDB-T012	1959-07-17	1.0	3.0	2011-03-09
110. 048h14	SPOT: 2007-08-20	2007-08-20	1.0	3.0	2011-03-29
111. 048h15	SPOT: 2007-08-20 (x2)	2007-08-20	1.0	3.0	2011-03-29

Table A3: CDED 049

NTS sheet	Data	Start/end	Edition	Issue	Proc. date
1. 049a01	SPOT: 2007-08-20	2007-08-20	1.0	3.0	2011-04-20
2. 049a02	SPOT: 2007-08-20 (x2); 2008-06-17	2007-08-20 2008-06-17	1.0	3.0	2011-04-20
3. 049a05 (SKERRIES)	Vector data: BNDT-049A05-3.1	1959	1.0	2.1	2008-11-05
4. 049a06	Vector data: BNDT-049A06-4.1	1959	1.0	2.1	2008-11-05
5. 049a07	SPOT: 2007-08-20	2007-08-20	1.0	3.0	2011-04-21
6. 049a08	SPOT: 2008-06-17	2008-06-17	1.0	3.0	2011-04-22
7. 049a09	SPOT: 2007-08-20	2007-08-20	1.0	3.0	2012-01-17
8. 049a10	SPOT: 2010-08-26	2010-08-26	1.0	3.0	2011-04-21
9. 049a11	Vector data: BNDT-049A11-3.0	1959	1.0	2.1	2008-11-05

(FIELDER POINT)					
10. 049a12	Vector data: BNDT-049A12-4.0	1959	1.0	2.1	2008-11-05
11. 049a13	SPOT: 2008-06-05	2008-06-05	1.0	2.1	2011-05-14
12. 049a14	SPOT: 2010-08-26	2010-08-26	1.0	3.0	2011-05-04
13. 049a15	R2: 2011-11-12; 2011-11-13; 2011-11-20; 2011-11-28 (x2); 2011-11-29; 2011-11-20; 2011-11-11 (x2)	2011-11-11 2011-11-29	1.0	3.0	2012-02-02
14. 049a16	R2: 2011-11-12; 2011-11-13; 2011-11-20; 2011-11-28 (x2); 2011-11-29; 2011-11-20; 2011-11-11 (x2)	2011-11-11 2011-11-29	1.0	3.0	2012-02-01
15. 049b05 (CAPE STORM)	SPOT: 2008-06-05	2008-06-05	1.0	3.0	2011-02-02
16. 049b06	SPOT: 2008-06-05; 2009-06-04	2008-06-05 2009-06-04	1.0	3.0	2011-02-03
17. 049b07	SPOT: 2009-06-04	2009-06-04	1.0	3.0	2011-03-09
18. 049b08	SPOT: 2008-06-05; 2007-08-20	2007-08-20 2008-06-05	1.0	3.0	2011-03-22
19. 049b09 (HEIM PENINSULA)	SPOT: 2008-06-05; 2009-06-04	2008-06-05 2009-06-04	1.0	3.0	2011-01-05
20. 049b10	SPOT: 2008-06-05; 2009-06-04	2008-06-05 2009-06-04	1.0	3.0	2011-01-05
21. 049b11	SPOT: 2009-06-04	2009-06-04	1.0	3.0	2011-02-02
22. 049b12 (MUSKOX FIORD)	SPOT: 2008-06-05; 2009-06-04	2008-06-05 2009-06-04	1.0	3.0	2011-02-03
23. 049b13	SPOT: 2010-06-23	2010-06-23	1.0	3.0	2011-05-11
24. 049b14	SPOT: 2010-06-23; 2008-06-05	2008-06-05 2010-06-23	1.0	3.0	2011-10-01
25. 049b15	SPOT: 2009-06-04; 2008-06-05	2008-06-05 2009-06-04	1.0	3.0	2011-03-17
26. 049b16	SPOT: 2008-06-05	2008-06-05	2.0	3.0	2011-05-18
27. 049c01	ASDB-TB09-0.0	1959-07-17	1.0	2.1	2008-03-06
28. 049c02	ASDB-TB09-0.0	1959-07-17	1.0	2.1	2008-02-28
29. 049c03 (BIRD FIORD)	ASDB-TB09-0.0	1959-07-24	1.0	2.1	2008-02-14
30. 049c04 (BIRD ISLAND)	ASDB-TB09-0.0	1959-07-24	1.0	2.1	2008-02-14
31. 049c05	ASDB-TB09-0.0	1959-07-22	1.0	2.1	2008-02-28
32. 049c06	ASDB-TB09-0.0	1959-07-22	1.0	2.1	2008-02-14
33. 049c07 (GUNNARS ISLAND)	ASDB-TB09-0.0	1959-07-17	1.0	2.1	2008-02-28
34. 049c08 (SOR FIORD)	ASDB-TB09-0.0	1959-07-17	1.0	2.1	2008-02-28
35. 049c09	ASDB-TB09-0.0	1959-07-08	1.0	3.0	2010-12-22
36. 049c10	ASDB-TB09-0.0	1959-07-17	1.0	3.0	2010-12-22
37. 049c11	ASDB-TB09-0.0	1958-07-22	1.0	2.1	2008-02-14
38. 049c12	ASDB-TB09-0.0	1958-07-22	1.0	2.1	2008-02-14
39. 049c13	ASDB-TB09-0.0	1958-07-22	1.0	2.1	2007-10-20
40. 049c14 (SCHEI POINT)	ASDB-TB09-0.0	1958-07-22	1.0	2.1	2007-10-20
41. 049c15	ASDB-TB09-0.0	1959-07-17	1.0	3.0	2010-12-23
42. 049c16	SPOT: 2008-08-26	2008-08-26	1.0	3.0	2011-05-27
43. 049d01	R2: 2011-11-12; 2011-11-13; 2011-11-20; 2011-11-28 (x2); 2011-11-29; 2011-11-20 (x2); 2011-11-11	2011-11-11 2011-11-29	1.0	3.0	2012-02-02
44. 049d02	SPOT: 2008-06-05 (x2)	2008-06-05	1.0	3.0	2011-05-21
45. 049d03	SPOT: 2008-06-05	2008-06-05	1.0	3.0	2011-05-21
46. 049d04	SPOT: 2008-06-05 (x2)	2008-06-05	1.0	3.0	2011-05-21
47. 049d05	ASDB-TB09-0.0	1959-06-07	1.0	3.0	2011-05-26
48. 049d06	ASDB-TB09-0.0	1959-06-07	1.0	3.0	2011-05-25
49. 049d07	SPOT: 2008-06-05 (x2)	2008-06-05	1.0	3.0	2011-04-02
50. 049d08	SPOT: 2008-06-05	2008-06-05	1.0	3.0	2011-04-02
51. 049d09	SPOT: 2008-06-05	2008-06-05	1.0	3.0	2011-04-05
52. 049d10	SPOT: 2008-06-05	2008-06-05	1.0	3.0	2011-05-20
53. 049d11	SPOT: 2008-06-05 (x2)	2008-06-05	1.0	3.0	2011-05-27
54. 049d12	ASDB-TB09-0.0	1959-06-07	1.0	3.0	2011-05-25
55. 049d13	ASDB-TB09-0.0	1959-07-08	2.0	3.0	2011-09-20

56. 049d14	ASDB-TB09-0.0	1959-06-07	1.0	3.0	2011-01-28
57. 049d15	SPOT: 2008-06-05; 2009-06-14	2008-06-05 2009-06-14	1.0	3.0	2011-05-20
58. 049d16	SPOT: 2009-06-14	2009-06-14	1.0	3.0	2011-05-20
59. 049e01	SPOT: 2009-06-14	2009-06-14	1.0	3.0	2011-05-19
60. 049e02 (YATES LAKE)	SPOT: 2009-06-14	2009-06-14	1.0	3.0	2011-02-15
61. 049e03 (MULLA RIVER)	SPOT: 2008-08-26; 2008-06-05; 2009-06-14	2008-06-05 2009-06-14	1.0	3.0	2011-02-25
62. 049e04	ASDB-TB09-0.0	1959-07-08	1.0	3.0	2011-01-15
63. 049e05	SPOT: 2008-08-26	2008-08-26	1.0	3.0	2011-05-27
64. 049e06	ASDB-TB09-0.0	1959-06-07	1.0	3.0	2011-06-10
65. 049e07	SPOT: 2009-06-14; 2008-08-26	2008-08-26 2009-06-14	1.0	3.0	2011-05-27
66. 049e08	SPOT: 2009-06-14; 2008-08-26	2008-08-26 2009-06-14	1.0	3.0	2011-05-19
67. 049e09	SPOT: 2008-08-26	2008-08-26	1.0	3.0	2011-05-19
68. 049e10	SPOT: 2008-08-26	2008-08-26	1.0	3.0	2011-05-27
69. 049e11	ASDB-TB09-0.0	1959-06-07	1.0	3.0	2011-06-10
70. 049e12	SPOT: 2008-08-26 (x2)	2008-08-26	1.0	3.0	2011-05-27
71. 049e13	ASDB-TB09-0.0	1959-07-08	1.0	3.0	2011-05-27
72. 049e14	ASDB-T007-0.0; ASDB-TB09-0.0	1959-06-07	1.0	3.0	2011-05-31
73. 049e15	SPOT: 2008-08-26 (x2)	2008-08-26	1.0	3.0	2011-06-03
74. 049e16	SPOT: 2008-05-14	2008-05-14	1.0	3.0	2011-05-19
75. 049f01	SPOT: 2008-08-26 (x2)	2008-08-26	1.0	3.0	2011-05-27
76. 049f02	SPOT: 2008-08-26	2008-08-26	1.0	3.0	2011-05-12
77. 049f03	ASDB-TB09-0.0	1958-07-28	1.0	2.1	2007-10-20
78. 049f04 (BEAR CORNER)	ASDB-TB09-0.0	1958-07-28	1.0	2.1	2007-10-20
79. 049f05	ASDB-T006; ASDB-TB09	1958-07-28	1.0	3.0	2011-03-23
80. 049f06	ASDB-TB09-0.0	1958-07-28	1.0	3.0	2011-03-18
81. 049f07	SPOT: 2008-08-26 (x2)	2008-08-26	1.0	3.0	2011-05-12
82. 049f08	SPOT: 2008-08-26 (x2)	2008-08-26	1.0	3.0	2011-05-27
83. 049f09	ASDB-TB09-0.0	1959-07-08	1.0	3.0	2011-03-29
84. 049f10	SPOT: 2008-05-18 (x2)	2008-05-18	1.0	3.0	2011-05-12
85. 049f11	ASDB-TB09-0.0	1959-06-07	1.0	3.0	2011-03-16
86. 049f12	SPOT: 2008-05-18	2008-05-18	1.0	3.0	2011-04-19
87. 049f13	ASDB-T006	1959-07-28	1.0	3.0	2011-03-17
88. 049f14	ASDB-T006; ASDB-TB09	1959-06-07	1.0	3.0	2011-03-17
89. 049f15	ASDB-T006; ASDB-TB09	1959-06-07	1.0	3.0	2011-03-24
90. 049f16	ASDB-T007; ASDB-TB09	1959-07-08	1.0	3.0	2011-03-26
91. 049g01 (VESLE FIORD)	ASDB-T007	1959-07-08	1.0	3.0	2011-03-24
92. 049g02 (FULMAR CHANNEL)	ASDB-T006	1959-06-07	1.0	3.0	2011-04-28
93. 049g03	ASDB-T006	1959-06-07	1.0	3.0	2011-04-21
94. 049g04	ASDB-T006	1959-07-28	2.0	3.0	2011-04-20
95. 049g05 (BUCHANAN GLACIER)	SPOT: 2010-06-25 (x2)	2010-06-25	1.0	3.0	2011-11-16
96. 049g06	ASDB-T006	1959-06-07	1.0	3.0	2011-04-28
97. 049g07	ASDB-T006	1959-06-07	1.0	3.0	2011-04-28
98. 049g08 (MAY POINT)	ASDB-T006; ASDB-T007	1959-07-08	1.0	3.0	2011-03-31
99. 049g09	ASDB-T007	1959-07-08	1.0	3.0	2011-03-31
100. 049g10 (DEPOT POINT)	ASDB-T006; ASDB-T007	1959-06-07	1.0	3.0	2011-03-31
101. 049g11	ASDB-T006; ASDB-T007	1959-06-07	1.0	3.0	2011-04-05
102. 049g12 (MOKKA FIORD)	ASDB-T006	1959-07-28	1.0	3.0	2011-04-05
103. 049g13 (GIBS FIORD)	Vector data: BNDT-049G13-4.0	1959	1.0	2.1	2011-04-28
104. 049g14 (HARE CAPE)	Vector data: BNDT-049G14-4.0	1959	1.0	2.1	2009-04-29

105. 049g15 (EUREKA)	Vector data: BNDT-049G15-1.7	1959	1.0	2.1	2009-04-28
106. 049g16 (SLIDRE RIVER)	Vector data: BNDT-049G16-2.3	1959	1.0	2.1	2009-04-28
107. 049h01	SPOT: 2008-08-26	2008-08-26	1.0	3.0	2011-06-03
108. 049h02	SPOT: 2008-08-26; 2008-05-14	2008-05-14 2008-08-26	1.0	3.0	2011-06-03
109. 049h03	SPOT: 2008-05-18	2008-05-18	1.0	3.0	2011-06-03
110. 049h04	SPOT: 2008-05-18; 2008-08-26	2008-05-18 2008-08-26	1.0	3.0	2011-09-07
111. 049h05	SPOT: 2008-05-18	2008-05-18	1.0	3.0	2011-08-30
112. 049h06	SPOT: 2008-05-18 (x2)	2008-05-18	1.0	3.0	2011-09-09
113. 049h07	SPOT: 2008-05-18 (x2)	2008-05-18	1.0	3.0	2011-07-20
114. 049h08	SPOT: 2008-08-26; 2008-05-14	2008-05-14 2008-08-26	1.0	3.0	2011-07-20
115. 049h09	SPOT: 2008-05-18; 2008-08-30	2008-05-18 2008-08-30	1.0	3.0	2011-05-05
116. 049h10	ASDB-T007	1959-06-07	1.0	3.0	2011-05-31
117. 049h11	SPOT: 2008-05-18 (x2)	2008-05-18	1.0	3.0	2011-05-11
118. 049h12	SPOT: 2008-05-18 (x2)	2008-05-18	1.0	3.0	2011-05-05
119. 049h13	SPOT: 2011-07-20	2011-07-20	1.0	3.0	2012-01-05
120. 049h14	SPOT: 2008-05-18	2008-05-18	1.0	3.0	2011-05-11
121. 049h15	SPOT: 2008-05-18; 2008-08-30	2008-05-18 2008-08-30	1.0	3.0	2011-05-13
122. 049h16	SPOT: 2008-05-18; 2008-08-30	2008-05-18 2008-08-30	1.0	3.0	2011-05-05

Table A4: CDED 059

NTS sheet	Data	Start/end	Edition	Issue	Proc. date
1. 059a02 (CAPE VERA)	SPOT: 2010-05-23; 2010-06-13	2010-06-13 2010-06-23	1.0	3.0	2011-05-03
2. 059a03 (WEST FIORD)	SPOT: 2010-05-23; 2010-06-13	2010-06-13 2010-06-23	1.0	3.0	2011-05-13
3. 059a04 (EIDSBOTN)	SPOT: 2010-08-08; 2010-06-23	2010-06-23 2010-08-08	1.0	3.0	2011-10-08
4. 059a05 (NORFOLK INLET)	SPOT: 2010-08-08; 2010-06-23; 2010-06-13	2010-06-13 2010-08-08	1.0	3.0	2011-10-08
5. 059a06 (CAPE ARUNDEL)	Vector data: BNDT-059A06-3.0	1958	1.0	2.1	2009-04-14
6. 059a07 (BAY OF WOE)	Vector data: BNDT-059A07-3.0	1959	1.0	2.1	2009-04-14
7. 059a08 (OLSEN ISLAND)	Vector data: BNDT-059A08-4.0	1959	1.0	2.1	2009-04-14
8. 059a09 (GOOSE FIORD)	SPOT: 2010-05-23 (x2)	2010-06-23	1.0	3.0	2012-01-05
9. 059a10 (HELL GATE)	Vector data: BNDT-059A10-3.0	1959	1.0	2.1	2009-04-14
10. 059a11 (CARDIGAN STRAIT)	Vector data: BNDT-059A11-3.1	1958	1.0	2.1	2009-04-14
11. 059a12 (BLANCHE MOUNTAIN)	ASDB-T004-0.0	1958-08-10	1.0	3.0	2011-03-24
12. 059a14 (CAPE BURGOYNE)	Vector data: BNDT-059A14-3.2	1958	1.0	2.1	2009-04-14
13. 059a15 (LANDS END)	Vector data: BNDT-059A15-4.0	1959	1.0	2.1	2009-04-14
14. 059a16 (NORDSTRAND POINT)	ASDB-TB09-0.0	1959-06-07	1.0	3.0	2011-03-18
15. 059b01 (POINT HOGARTH)	ASDB-T004-0.0	1959-07-16	1.0	3.0	2011-03-23
16. 059b02	SPOT: 2006-07-30 (x10) 2007-07-27(x10)	2006-07-30 2007-07-27	1.0	3.0	2011-03-23

17. 059b03 (MARGARET ISLAND)	Vector data: BNDT-059B03-3.0	1958	1.0	2.1	2009-04-15
18. 059b04 (PIONEER CHANNEL)	Vector data: BNDT-059B04-3.1	1958	1.0	2.1	2009-04-15
19. 059b05 (INGLIS BAY)	Vector data: BNDT-059B05-4.0	1959	1.0	2.1	2009-04-15
20. 059b06 (PORT REFUGE)	ASDB-T004-0.0	1959-07-17	1.0	3.0	2011-04-01
21. 059b07 (PRINCE ALFRED BAY)	ASDB-T004-0.0	1959-07-1723	1.0	3.0	2011-03-26
22. 059b08	SPOT: 2010-08-18; 2010-08-08; 2010-06-23	2010-06-23 2010-08-18	1.0	3.0	2011-03-23
23. 059b09 (TRITON BAY)	ASDB-T004-0.0	1958-08-10	1.0	3.0	2011-04-21
24. 059b10 (DISCOVERY MOUNTAIN)	ASDB-T004-0.0	1959-07-23	1.0	3.0	2011-05-12
25. 059b11	SPOT: 2010-07-07; 2010-08-18	2010-07-07 2010-08-18	1.0	3.0	2011-09-29
26. 059b12 (BARROW HARBOUR)	SPOT: 010-08-08	2010-08-08	1.0	3.0	2011-05-03
27. 059b13 (WHITMORE POINT)	SPOT: 2010-07-07; 2010-08-08	2010-07-07 2010-08-08	1.0	3.0	2011-05-03
28. 059b14 (PRINCESS ROYAL ISLAND)	ASDB-T004-0.0	1959-07-17	1.0	3.0	2011-04-14
29. 059b15 (MOUNT PARKER)	ASDB-T004-0.0	1959-07-23	1.0	3.0	2011-03-26
30. 059c04 (TABLE ISLAND)	ASDB-T004-0.0	1959-07-23	1.0	3.0	2011-03-15
31. 059c05 (CAPE O'BRIEN)	ASDB-T002-0.0	1958-07-25	1.0	3.0	2011-03-02
32. 059c06 (PELL POINT)	ASDB-T002-0.0	1959-07-23	1.0	3.0	2011-03-02
33. 059c07 (CAPE AVERDEEN)	ASDB-T002-0.0	1959-07-23	1.0	3.0	2011-03-17
34. 059c10 (GORDON HEAD)	ASDB-T002-0.0	1959-07-23	1.0	3.0	2011-03-02
35. 059c11 (JAEGER RIVER)	ASDB-T002-0.0	1959-07-23	1.0	3.0	2011-03-05
36. 059c12	ASDB-T002-0.0	1958-07-25	1.0	3.0	2011-03-19
37. 059c13 (HENDRIKSEN STRAIT)	ASDB-T003-0.0	1958-07-25	1.0	3.0	2011-05-14
38. 059c14 (MOUNT NICOLAY)	ASDB-T002-0.0	1958-07-25	1.0	3.0	2011-05-13
39. 059c15	ASDB-T002-0.0	1959-07-23	1.0	3.0	2011-03-03
40. 059d01	ASDB-TB09-0.0	1959-07-24	1.0	2.1	2008-02-14
41. 059d02	Vector data: BNDT-059D02-2.4	1959	1.0	2.1	2008-04-15
42. 059d03 (MOUNT WINDSOR)	Vector data: BNDT-059D03-2.2	1959	1.0	2.1	2008-04-15
43. 059d04	Vector data: BNDT-059D04-2.1	1959	1.0	2.1	2008-04-15
44. 059d05	Vector data: BNDT-059D05-2.0	1959	1.0	2.1	2009-04-29
45. 059d06	Compilation of vector data: Hydrographic and Ground: 059D06-4.0	1959 2007-07-27	1.0	3.0	2012-04-12
46. 059d07	Compilation of vector data: Hydrographic and Ground: 059D06-4.0	1959 2007-07-27	1.0	3.0	2012-03-20
47. 059d09	ASDB-TB09-0.0	1958-07-22	1.0	2.1	2008-02-14
48. 059d10	Vector data: BNDT-059D10-2.1	1959	1.0	2.1	2008-04-29
49. 059d11	Compilation of vector data: Hydrographic and Ground: 059D06-4.0	1959 2007-07-27	1.0	3.0	2012-04-12
50. 059d12	Vector data: BNDT-059D12-2.1		1.0	2.1	2009-05-01
51. 059d16	ASDB-TB09-0.0	1958-07-22	1.0	2.1	2007-10-20
52. 059e01 (HYPERITE POINT)	ASDB-T006-0.0	1959-07-29	1.0	3.0	2011-02-04

53. 059e02 (SHERWOOD HEAD)	ASDB-T006-0.0	1959-07-28	1.0	3.0	2011-02-04
54. 059e03	ASDB-T006-0.0	1959-07-28	1.0	3.0	2011-02-04
55. 059e04	ASDB-T006-0.0	1958-07-22	1.0	3.0	2011-02-16
56. 059e05	SPOT: 2008-09-19 (x2)	2008-09-19	1.0	3.0	2011-03-30
57. 059e06 (SURPRISE FIORD)	SPOT: 2008-09-19 (x2)	2008-09-19	1.0	3.0	2011-03-24
58. 059e07 (GLACIER FIORD)	SPOT: 2008-09-19; 2010-08-18; 2010-07-07	2008-09-19 2010-08-18	1.0	3.0	2011-07-23
59. 059e08 (WOLF FIORD)	SPOT: 2008-09-19; 2010-08-18; 2010-07-07	2008-09-19 2010-08-18	1.0	3.0	2011-07-27
60. 059e09	SPOT: 2008-09-19(x2); 2008-05-18	2008-05-18 2008-09-19	1.0	3.0	2011-04-21
61. 059e10	SPOT: 2008-09-19 (x2)	2008-09-19	1.0	3.0	2011-04-19
62. 059e11	SPOT: 2008-09-19	2008-09-19	1.0	3.0	2011-03-25
63. 059e12	SPOT: 2008-09-19 (x2)	2008-09-19	1.0	3.0	2011-01-05
64. 059e13	SPOT: 2008-09-19	2008-09-19	1.0	3.0	2011-05-04
65. 059e14	SPOT: 2008-09-19; 2008-05-18	2008-05-18 2008-09-19	1.0	3.0	2011-05-13
66. 059e15	SPOT: 2008-09-19 (x2)	2008-09-19	1.0	3.0	2011-05-07
67. 059e16 (SKAARE FIORD)	SPOT: 2008-05-18	2008-05-18	1.0	3.0	2011-04-21
68. 059f01 (CAPE SOUTHWEST)	ASDB-T006-0.0	1958-07-22	1.0	3.0	2011-02-03
69. 059f03 (HAIG-THOMAS ISLAND)	ASDB-T003-0.0	1958-07-25	1.0	3.0	2011-05-31
70. 059f04	ASDB-T003-0.0	1958-07-25	1.0	3.0	2011-05-31
71. 059f05 (STRUCTURAL RIVER)	ASDB-T003-0.0	1958-07-25	1.0	3.0	2011-02-26
72. 059f06	ASDB-T003-0.0	1958-07-25	1.0	3.0	2011-05-14
73. 059f08 (CAPE MAUNDY THURSDAY)	ASDB-T006-0.0	1958-07-22	1.0	3.0	2011-02-03
74. 059f09 (GOOD FRIDAY BAY)	SPOT: 2008-09-19 (x2)	2008-09-19	1.0	3.0	2011-01-05
75. 059f10	ASDB-T006-0.0	1958-07-22	1.0	3.0	2011-02-11
76. 059f12	ASDB-T003-0.0	1958-07-25	1.0	3.0	2011-02-26
77. 059f14 (CAPE LEVVEL)	ASDB-T006-0.0	1958-07-22	1.0	3.0	2011-05-14
78. 059f15 (SAND BAY)	SPOT: 2008-09-19 (x2)	2008-09-19	1.0	3.0	2011-04-22
79. 059f16	SPOT: 2008-09-19 (x2)	2008-09-19	1.0	3.0	2011-04-27
80. 059g01 (AMAROK RIVER)	ASDB-T006-0.0	1959-07-25	1.0	3.0	2011-06-01
81. 059g02 (VANTAGE HILL)	ASDB-T006-0.0	1958-07-22	1.0	3.0	2011-06-01
82. 059g03	ASDB-T005-0.0 ASDB-T006-0.0	1958-07-22	1.0	3.0	2011-05-19
83. 059g05	ASDB-T005-0.0	1958-07-24	1.0	3.0	2011-05-26
84. 059g06 (SOUTH FIORD)	SPOT: 2011-07-24	2011-07-24	1.0	3.0	2011-12-06
85. 059g07 (EAST FIORD)	SPOT: 2011-07-24 (x2)	2011-07-24	1.0	3.0	2012-01-26
86. 059g08 (ICEGERG BAY)	SPOT: 2010-06-25	2010-06-25	1.0	3.0	2011-11-09
87. 059g09 (ICEBERG GLACIER)	SPOT: 2011-07-24 (x2)	2011-07-24	1.0	3.0	2011-12-06
88. 059g10 (PLATEAU LAKE)	SPOT: 2011-07-24	2011-07-24	1.0	3.0	2011-12-06
89. 059g11 (GOSLING INLET)	SPOT: 2011-07-24 (x2)	2011-07-24	1.0	3.0	2011-12-07
90. 059g12 (MIDDLE FIORD)	SPOT: 2011-07-24; 2009-06-18; 2011-07-24	2009-06-18 2011-07-24	1.0	3.0	2011-12-06

91. 059g13	SPOT: 2009-06-18	2009-06-18	1.0	3.0	2011-04-09
92. 059g14 (MIDDLE RIVER)	SPOT: 2011-07-24	2011-07-24	1.0	3.0	2011-12-10
93. 059g15 (SCAIFE GLACIER)	SPOT: 2011-07-24	2011-07-24	1.0	3.0	2011-12-06
94. 059g16 (WHITE CROWN MOUNTAIN)	SPOT: 2011-07-24 (x2)	2011-07-24	1.0	3.0	2011-12-02
95. 059h01	SPOT: 2008-09-19	2008-09-19	1.0	3.0	2011-06-03
96. 059h02	SPOT: 2008-09-19	2008-09-19	1.0	3.0	2011-06-01
97. 059h03	SPOT: 2008-09-19 (x2)	2008-09-19	1.0	3.0	2011-04-30
98. 059h04 (STRAND FIORD)	SPOT: 2008-09-19 (x2)	2008-09-19	1.0	3.0	2011-05-13
99. 059h05 (EXPEDETION FIORD)	SPOT: 2010-06-25	2010-06-25	1.0	3.0	2011-11-09
100. 059h06 (MONKHEAD MOUNTAIN)	SPOT: 2008-09-19	2008-09-19	1.0	3.0	2011-06-01
101. 059h07	SPOT: 2008-09-19	2008-09-19	1.0	3.0	2011-06-01
102. 059h08 (STRAND FIORD PASS)	SPOT: 2010-06-25	2010-06-25	1.0	3.0	2011-11-10
103. 059h09	ASDB-T006-0.0	1959-07-29	1.0	3.0	2011-04-22
104. 059h10 (EUREKA PASS)	SPOT: 2010-06-25	2010-06-25	1.0	3.0	2011-11-22
105. 059h11 (PHANTOM LAKE)	SPOT: 2010-06-25 (x2)	2010-06-25	1.0	3.0	2011-11-22
106. 059h12 (PYRAMID PEAK)	SPOT: 2010-06-25 (x2)	2010-06-25	1.0	3.0	2011-11-11
107. 059h13	SPOT: 2011-07-24	2011-07-24	1.0	3.0	2011-12-08
108. 059h14	SPOT: 2011-07-24	2011-07-24	1.0	3.0	2012-01-10
109. 059h15 (GEODETIC HILLS)	SPOT: 2010-06-25 (x2)	2010-06-25	1.0	3.0	2011-11-22
110. 059h16	ASDB-T005-0.0	1959-07-28	1.0	3.0	2011-05-11

Table A5: CDED 120

NTS sheet	Data	Start/end	Edition	Issue	Proc. date
1. 120b03	ASDB-T010-0.0	1959-07-06	1.0	3.0	2011-09-12
2. 120b04	SPOT: 2008-08-26; 2010-07-27; 2008-05-14	2008-05-14 2010-07-27	1.0	3.0	2011-09-10
3. 120b05	SPOT: 2008-05-14; 2008-05-28	2008-05-14 2008-05-28	1.0	3.0	2011-04-12
4. 120b06	SPOT: 2008-05-28	2008-05-28	1.0	3.0	2011-04-07
5. 120b11	SPOT: 2008-05-28	2008-05-28	1.0	3.0	2011-04-09
6. 120b12	SPOT: 2010-07-27; 2008-05-14; 2010-07-27	2008-05-14 2010-07-27	1.0	3.0	2011-11-15
7. 120b13	SPOT: 2010-07-27; 2008-05-28; 2010-07-27	2008-05-28 2010-07-27	1.0	3.0	2011-11-23
8. 120b14	SPOT: 2008-05-28; 2010-07-27; 2008-05-28	2008-05-28 2010-07-27	1.0	3.0	2012-02-15
9. 120b15 (CAPE BLACK)	ASDB-T010-0.0; ASDB-TA10-0.0	1959-06-06	2.0	3.0	2009-11-03
10. 120c01	ASDB-T010-0.0	1959-07-25	1.0	3.0	2011-10-07
11. 120c02	ASDB-T010-0.0	1959-06-06	1.0	3.0	2012-02-15
12. 120c03 (RECORD POINT)	Vector data: BNDT-120C03-2.0	1959	1.0	2.1	2009-05-01
13. 120c04 (MOUNT NEVILLE)	Vector data: land (BDG-FILAMENTAIRE-120C04-3.0) and Waster Body GDB (BDG-REGION-HYDRI-120C04-3.0) SPOT: 2010-07-27	1959 2010-07-27	1.0	3.0	2012-06-01
14. 120c05 (CAROLYN LAKE)	Vector data: BNDT-120C05-2.1	1959	1.0	2.1	2009-04-29
15. 120c06 (SIMMONS ICE CAP)	Vector data: BNDT-120C06-2.7	1959	1.0	2.1	2009-04-29

16. 120c07 (HARE POINT)	Vector data: BNDT-120C07-5.0	1959	1.0	2.1	2009-04-29
17. 120c08	ASDB-T010-0.0	1959-06-06	1.0	3.0	2011-11-13
18. 120c09 (BELLOT ISLAND)	Vector data: BNDT-120C09-4.1	1959	1.0	2.1	2009-05-01
19. 120c10 (MILLER ISLAND)	Vector data: BNDT-120C10-4.6	1959	1.0	2.1	2009-05-01
20. 120c11 (IDA BAY)	Vector data: BNDT-120C11-3.1	1959	1.0	2.1	2009-05-01
21. 120c12 (DYAS ISLAND)	Vector data: BNDT-120C12-3.4	1959	1.0	2.1	2009-05-01
22. 120c13 (JOHNS ISLAND)	Compilation of vector data (land(1959) and water body(1999)): 120C13-3.0	1959 1999-07-21	1.0	3.0	2012-06-08
23. 120c14 (CRAIG LAKE)	Vector data: BNDT-120C14-2.5	1959	1.0	2.1	2009-05-19
24. 120c15 (BLACK ROCK VALE)	Vector data: BNDT-120C15-4.1	1959	1.0	2.1	2009-05-19
25. 120c16 (HOGBACK MOUNTAIN)	Vector data: BNDT-120C16-4.0	1959	1.0	2.1	2009-05-20
26. 120d13 (CAPE BEECHEY)	ASDB-TA11-0.0	1959-07-06	1.0	2.1	2006-08-04
27. 120e03 (LINCOLN BAY)	ASDB-TA11-0.0	1959-07-06	1.0	2.1	2006-08-03
28. 120e04 (MOUNT PARY)	ASDB-TA11-0.0	1959-06-06	1.0	2.1	2006-08-07
29. 120e05 (ALERT)	Vector data: BNDT-120E05-3.2	1988	1.0	2.1	2009-05-14
30. 120e06 (CAPE RAWSON)	Vector data: BNDT-120E06-3.0	1959	1.0	2.1	2009-05-14
31. 120e12 (PATTERSON BAY)	Vector data: BNDT-120E12-4.0	1959	1.0	2.1	2009-05-14
32. 120e13 (CAPE JOSEPH HENRY)	ASDB-TA11-0.0	1959-06-06	1.0	2.1	2006-08-07
33. 120f01	Vector data: BNDT-120F01-4.1	1959	1.0	2.1	2009-05-19
34. 120f02 (BOULDER HILLS)	Vector data: BNDT-120F02-5.1	1959	1.0	2.1	2009-05-19
35. 120f03 (TURNABOUT GLACIER)	Vector data: BNDT-120F03-2.6	1959	1.0	2.1	2009-05-20
36. 120f04 (MOUNT NUKAP)	Vector data: BNDT-120F04-3.0	1959	1.0	2.1	2009-05-14
37. 120f05 (FORK MOUNTAIN)	ASDB-TA11-0.0	1959-07-15	2.0	3.0	2010-07-07
38. 120f06 (BARRIER GLACIER)	Vector data: BNDT-120F06-3.1	1959	1.0	2.1	2009-05-20
39. 120f07 (MOUNT EUGENE)	ASDB-TA11-0.0	1959-06-05	1.0	2.1	2006-08-07
40. 120f08 (GRANT RIVER)	ASDB-TA11-0.0	1959-06-06	1.0	2.1	2006-08-07
41. 120f09	ASDB-TA11-0.0	1959-06-06	1.0	2.1	2006-08-07
42. 120f10	ASDB-TA11-0.0	1959-06-05	1.0	2.1	2006-08-04
43. 120f11 (CLEMENTS MARKHAM RIVER)	Vector data: BNDT-120F11-4.0	1959	1.0	2.1	2009-05-20
44. 120f12	ASDB-TA11-0.0	1959-07-07	1.0	2.1	2006-08-01
45. 120f13 (MOUNT HORNBY)	Compilation of vector data (land and water body): 120F13-6.2	1959	1.0	3.0	2012-06-01
46. 120f14 (GYPSUM RIVER)	Compilation of vector data (land and water body): 120F14-6.4	1959	1.0	3.0	2012-06-01
47. 120f15 (MOUNT DISRAELI)	Compilation of vector data (land and water body): 120F15-5.1	1959	1.0	3.0	2012-06-01
48. 120f16 (CAPE HECLA)	ASDB-TA11-0.0	1959-06-06	1.0	2.1	2006-08-07

49. 120g03 (PARR BAY)	Vector data: BNDT-120G03-2.0	1959	1.0	2.1	2009-05-19
50. 120g04 (MOUNT COOPER KEY)	Compilation of vector data (land and water body): 120G04-5.3	1959	1.0	3.0	2012-06-01

Table A6: CDED 340

NTS sheet	Data	Start/end	Edition	Issue	Proc. date
1. 340a01	SPOT: 2008-08-26; 2008-05-14	2008-05-14 2008-08-26	1.0	3.0	2011-10-13
2. 340a02	SPOT: 2008-09-03; 2008-05-14	2008-05-14 2008-09-03	2.0	3.0	2011-06-16
3. 340a03	SPOT: 2008-08-30	2008-08-30	1.0	3.0	2011-06-16
4. 340a04	SPOT: 2008-08-30 (x2)	2008-08-30	1.0	3.0	2011-06-16
5. 340a05	SPOT: 2008-08-30; 2008-06-25	2008-08-30 2008-06-25	1.0	3.0	2011-12-20
6. 340a06	SPOT: 2010-06-25; 2008-09-03	2008-09-03 2010-06-25	2.0	3.0	2011-06-15
7. 340a07	SPOT: 2010-06-25 (x2); 2008-09-03	2008-09-03 2010-06-25	1.0	3.0	2011-09-13
8. 340a08	SPOT: 2008-08-26; 2010-06-25; 2008-05-14	2008-05-14 2010-06-25	1.0	3.0	2011-09-13
9. 340a09	SPOT: 2010-06-25; 2010-07-27	2010-06-25 2010-07-27	1.0	3.0	2011-09-16
10. 340a10	SPOT: 2010-06-25 (x2)	2010-06-25	1.0	3.0	2011-09-13
11. 340a11	SPOT: 2010-06-25; 2008-09-03	2008-09-03 2010-06-25	1.0	3.0	2011-06-15
12. 340a12	SPOT: 2010-06-25	2010-06-25	1.0	3.0	2011-12-10
13. 340a13	SPOT: 2010-06-25(x2); 2008-09-03	2008-09-03 2010-06-25	1.0	3.0	2011-12-07
14. 340a14	SPOT: 2010-06-25(x2); 2008-09-03	2008-09-03 2010-06-25	2.0	3.0	2011-10-18
15. 340a15	SPOT: 2010-06-25 (x2)	2010-06-25	1.0	3.0	2011-10-19
16. 340a16	SPOT: 2010-06-25; 2010-07-27 (x2)	2010-06-25 2010-07-27	1.0	3.0	2011-09-13
17. 340b01 (GREENROCK RIVER)	SPOT: 2010-06-25	2010-06-25	1.0	3.0	2011-09-15
18. 340b02 (CANON FIORD)	Vector data: BNDT-340B02-2.4	1959	1.0	2.1	2009-05-19
19. 340b03 (BLACK TOP RIDGE)	Vector data: BNDT-340B03-4.0	1959	1.0	2.1	2009-05-19
20. 340b04 (SKRAELING POINT)	Vector data: BNDT-340B04-3.1	1959	1.0	2.1	2009-05-19
21. 340b05 (ICEBRG POINT)	ASDB-T005-0.0; ASDB-T007-0.0	1959-06-07	1.0	3.0	2011-03-27
22. 340b06 (MOUNT LOCKWOOD)	ASDB-T007-0.0	1959-06-07	1.0	3.0	2011-03-30
23. 340b07	ASDB-T007-0.0	1959-07-08	1.0	3.0	2011-02-11
24. 340b08	SPOT: 2010-06-25; 2010-06-23; 2010-06-25	2010-06-23 2010-06-25	1.0	3.0	2011-09-07
25. 340b09	SPOT: 2010-06-25; 2010-06-23; 2010-06-25	2010-06-23 2010-06-25	1.0	3.0	2011-09-07
26. 340b10 (BORUP FIORD)	SPOT: 2010-06-25; 2010-06-23; 2010-06-25	2010-06-23 2010-06-25	1.0	3.0	2011-11-26
27. 340b11 (BLACKWELDER MOUNTAINS)	SPOT: 2010-06-23 (x2)	2010-06-23	1.0	3.0	2011-11-30
28. 340b12 (CONFEDERATION POINT)	ASDB-T008-0.0	1959-06-07	1.0	3.0	2011-04-15
29. 340b13 (HARE FIORD)	ASDB-T008-0.0	1959-06-07	1.0	3.0	2011-03-23
30. 340b14 (MOUNT SCHECHERT)	SPOT: 2010-06-23	2010-06-23	1.0	3.0	2011-11-30

31. 340b15 (KRIEGER MOUNTAINS)	SPOT: 2010-06-23 (x2)	2010-06-23	1.0	3.0	2011-11-26
32. 340b16 (MOUNT BURRILL)	SPOT: 2010-06-25; 2010-06-23; 2010-06-25	2010-06-23 2010-06-25	1.0	3.0	2012-02-15
33. 340c01	R2: 2010-08-08 (x2); 2010-08-13; 2010-08-16 (x2); 2010-08-18 (x2); 2010-08-23 (x3); 2010-08-25 (x3); 2010-08-30 (x2)	2010-08-08 2010-08-30	1.0	3.0	2012-12-14
34. 340c02	R2: 2010-08-08; 2010-08-09 (x2); 2010-08-11 (x3); 2010-08-13; 2010-08-16 (x3); 2010-08-18 (x3); 2010-08-23 (x2); 2010-08-25 (x2); 2010-08-30	2010-08-08 2010-08-30	1.0	3.0	2012-12-16
35. 340c03 (VAN HAUEN PASS)	R2: 2010-08-02; 2010-08-04 (x2); 2010-08-09 (x3); 2010-08-11 (x3); 2010-08-19 (x2); 2010-08-21 (x2); 2010-08-26 (x2); 2010-08-28	2010-08-02 2010-08-28	1.0	3.0	2012-12-16
36. 340c04 (DEGERBLS ISLAND)	ASDB-T008-0.0	1959-06-07	1.0	3.0	2011-03-23
37. 340c05	R2: 2010-08-05 (x2); 2010-08-08; 2010-08-12 (x3); 2010-08-16; 2010-08-14 (x3); 2010-08-18; 2010-08-23 (x2); 2010-08-25; 2010-08-29; 2010-08-31 (x3)	2010-08-05 2010-08-31	1.0	3.0	2011-11-04
38. 340c06 (OTTO GLACIER)	R2: 2010-08-02; 2010-08-04 (x2); 2010-08-08 (x3); 2010-08-12 (x2); 2010-08-14 (x2); 2010-08-19 (x3); 2010-08-21 (x3); 2010-08-23; 2010-08-26 (x2); 2010-08-28; 2010-08-30 (x3)	2010-08-02 2010-08-30	1.0	3.0	2011-11-10
39. 340c07	R2: 2010-08-02 (x2); 2010-08-04 (x2); 2010-08-09 (x3); 2010-08-11 (x3); ; 2010-08-16 (x2); 2010-08-18 (x3); 2010-08-26 (x2); 2010-08-28	2010-08-02 2010-08-28	2.0	3.0	2011-11-10
40. 340c08	R2: 2010-08-06; 2010-08-08 (x2); 2010-08-10; 2010-08-12; 2010-08-16 (x4); 2010-08-17; 2010-08-18 (x3); 2010-08-19; 2010-08-23 (x3); 2010-08-25 (x3); 2010-08-30	2010-08-06 2010-08-30	1.0	3.0	2011-08-31
41. 340c09	R2: 2010-08-08 (x3); 2010-08-09 (x2); 010-08-16 (x3); 2010-08-17 (x2); 2010-08-18 (x2); 2010-08-19 (x2); 2010-08-23 (x4); 2010-08-25 (x2); 2010-08-26; 2010-08-30	2010-08-08 2010-08-30	1.0	3.0	2011-10-04
42. 340c10	R2: 2010-08-02; 2010-08-03; 2010-08-04 (x2); 2010-08-09 (x3); 2010-08-11 (x3); 2010-08-13; 2010-08-12; 2010-08-16; 2010-08-18 (x2); 2010-08-20; 2010-08-22; 2010-08-26 (x4); 2010-08-29	2010-08-02 2010-08-29	1.0	3.0	2011-09-30
43. 340c11	R2: 2010-08-02; 2010-08-06; 2010-08-04; 2010-08-08 (x2); 2010-08-13; 2010-08-12 (x3); 2010-08-14 (x2); 2010-08-15; 2010-08-19 (x3); 2010-08-21 (x3); 2010-08-22; 2010-08-26; 2010-08-29; 2010-08-30	2010-08-02 2010-08-30	2.0	3.0	2011-12-03
44. 340c12	R2: 2010-08-06; 2010-08-05; 2010-08-08 (x3); 2010-08-07; 2010-08-12; 2010-08-16; 2010-09-08; 2010-08-14 (x2); 2010-08-15; 2010-08-18; 2010-08-22 (x3); 2010-08-23 (x2); 2010-08-25; 2010-08-24 (x2); 2010-08-29; 2010-08-30 (x2); 2010-08-31 (x2)	2010-08-05 2010-09-08	1.0	3.0	2011-11-09
45. 340c13	R2: 2010-08-05; 2010-08-08; 2010-08-07; 2010-09-08 (x2); 2010-08-14 (x2); 2010-08-22 (x3); 2010-08-24 (x2); 2010-08-29; 2010-08-31 (x2)	2010-08-05 2010-09-08	1.0	3.0	2011-11-24
46. 340c14	R2: 2010-08-04; 2010-08-05 (x2); 2010-08-07; 2010-08-12 (x3); 2010-08-14 (x3); 2010-08-19; 2010-08-21 (x3); 2010-08-22; 2010-08-29	2010-08-04 2010-08-29	1.0	3.0	2011-12-02
47. 340c15	R2: 2010-08-02; 2010-08-03; 2010-08-04 (x3); 2010-08-09(x2); 2010-08-11 (x4); 2010-08-12 (x3); 2010-08-18 (x2); 2010-08-19 (x3); 2010-08-20; 2010-08-21; 2010-08-26 (x3); 2010-08-27; 2010-08-28; 2010-08-29 (x2);	2010-08-02 2010-08-29	1.0	3.0	2011-09-30
48. 340c16	R2: 2010-08-02; 2010-08-09 (x4); 2010-08-10; 2010-08-11 (x3); 2010-08-16 (x3); 2010-08-17; 2010-08-18 (x3); 2010-08-19 (x2); 2010-08-25 (x3); 2010-08-26 (x3)	2010-08-02 2010-08-26	1.0	3.0	2011-10-04
49. 340d01 (NAN LAKE)	Vector data: BNDT-340D01-2.3	1959	1.0	2.1	2009-05-20
50. 340d02 (MOUNT KOCH)	Vector data: BNDT-340D02-3.0	1959	1.0	2.1	2009-05-19
51. 340d03 (MOUNT NEBEL)	Vector data: BNDT-340D3-3.1	1959	1.0	2.1	2009-05-19

52. 340d04 (MCKINLEY BAY)	R2: 2010-08-06; 2010-08-08 (x2); 2010-08-13 (x3); 2010-08-15 (x3); 2010-08-20 (x2); 2010-08-22 (x2); 2010-08-29; 2010-08-30; 2010-08-27	2010-08-06 2010-08-30	1.0	3.0	2011-12-04
53. 340d05 (BENT GLACIER)	R2: 2010-08-06; 2010-08-08 (x3); 2010-08-09 (x3); 2010-08-31 (x3); 2010-08-13 (x2); 2010-08-15 (x3); 2010-08-17 (x2); 2010-08-19 (x2); 2010-08-20 (x2); 2010-08-22 (x2); 2010-08-23; 2010-08-26 (x2); 2010-08-24 (x2); 2010-08-30 (x2)	2010-08-06 2010-08-31	1.0	3.0	2011-09-02
54. 340d06 (TANQUARY CAMP)	Vector data: BNDT-340D06-3.0	1959	1.0	2.1	2009-05-21
55. 340d07 (MOUNT SHERWOOD)	Vector data: BNDT-340D07-2.3	1959	1.0	2.1	2009-05-21
56. 340d08 (MOUNT C.S. SMITH)	Vector data: BNDT-340D08-3.1	1959	1.0	2.1	2009-05-20
57. 340d09 (WHISLER ISLAND)	Vector data: BNDT-340D09-2.2	1959	1.0	2.1	2009-05-21
58. 340d10 (EKBLAW LAKE)	Vector data: BNDT-340D10-3.0	1959	1.0	2.1	2009-05-21
59. 340d11 (FIALA GLACIER)	Vector data: BNDT-340D11-3.1	1959	1.0	2.1	2009-05-21
60. 340d12 (YELVERTON LAKE)	ASDB-T008-0.0 (1959); ERS-1: 1996-01-28; 1995-02-20; 1995-01-29; 1995-02-21	1959-07-28 1996-02-21	2.0	2.1	2007-10-01
61. 340d13	R2: 2010-08-06; 2010-08-08 (x4); 2010-08-09; 2010-08-15 (x2); 2010-08-23 (x3); 2010-08-24; 2010-08-30	2010-08-06 2010-08-30	1.0	3.0	2011-07-20
62. 340d14	ASDB-TB11-0.0 (1959); ERS-1: 1996-01-28; 1996-02-20; 1996-01-29; 1996-02-21	1959-07-29 1996-02-21	2.0	2.1	2007-09-27
63. 340d15	ASDB-TB11-0.0 (1959); ERS-1: 1996-01-28; 1996-02-20; 1996-01-29; 1996-02-21	1959-07-15 1996-02-21	2.0	2.1	2007-09-27
64. 340d16 (HENRIETTA NESMITH GLACIER)	Complicated combo of vector data (land and hydro): 340D16-3.0	1999 1999-07-21	1.0	3.0	2012-06-08
65. 340e01	ASDB-TB11-0.0 (1959); ERS-1: 1996-01-28; 1996-02-20 (x2); 1996-01-29; 1996-02-21 (x2)	1959-07-07 1996-02-21	2.0	2.1	2007-09-27
66. 340e02 (MOUNT WHISLER)	ASDB-TB11-0.0 (1959); ERS-1: 1996-01-28; 1996-02-20 (x2); 1996-01-29; 1996-02-21 (x2)	1959-07-27 1996-02-21	2.0	2.1	2007-09-27
67. 340e03 (MOUNT VANIER)	ASDB-TB11-0.0 (1959); ERS-1: 1996-01-28; 1996-02-20; 1996-01-29; 1996-02-21	1959-07-29 1996-02-21	2.0	2.1	2007-09-27
68. 340e04	R2: 2010-08-08 (x3); 2010-08-09 (x2); 2010-08-31; 2010-08-15; 2010-09-07; 2010-08-16 (x6); 2010-08-23 (x2); 2010-08-25 (x3); 2010-08-24; 2010-08-30	2010-08-08 2010-09-07	1.0	3.0	2011-08-24
69. 340e05	R2: 2010-08-08 (x3); 2010-08-09 (x3); 2010-08-31 (x2); 2010-09-07 (x2); 2010-08-16 (x3); 2010-08-23 (x2); 2010-08-25 (x3); 2010-08-26; 2010-08-30 (x2)	2010-08-08 2010-09-07	1.0	3.0	2011-08-25
70. 340e06 (COMMONWEALTH MOUNTAIN)	ASDB-TB11-0.0	1959-07-29	2.0	2.1	2006-07-31
71. 340e07 (HARLEY RIDGE)	ASDB-TB11-0.0	1959-07-27	2.0	2.1	2006-08-01
72. 340e08	ASDB-TB11-0.0 (1959); ERS-1: 1996-01-28; 1996-02-20; 1996-01-29; 1996-02-21	1959-07-15 1996-02-21	2.0	2.1	2007-09-27
73. 340e09 (LORIMER RIDGE)	Vector data: BNDT-340E09-4.2	1959	1.0	2.1	2009-05-21
74. 340e10 (HARLEY RIDGE)	Vector data: BNDT-340E10-5.0	1959	1.0	2.1	2009-05-21
75. 340e11 (MOUNT AYLES)	Vector data: BNDT-340E11-5.1	1959	1.0	2.1	2009-05-25
76. 340e12	R2: 2010-08-08 (x3); 2010-08-09 (x2); 2010-08-31 (x2); 2010-08-13 (x3); 2010-09-07 (x3); 2010-08-16; 2010-08-18 (x2); 2010-08-19 (x2); 2010-08-20 (x2); 2010-08-21 (x2); 2010-08-25 (x2); 2010-08-26 (x2); 2010-08-30 (x2)	2010-08-08 2010-09-07	1.0	3.0	2011-12-15
77. 340e13	R2: 2010-08-02; 2010-08-08 (x2); 2010-08-12; 2010-08-18; 2010-08-19 (x2); 2010-08-25 (x2); 2010-08-26 (x2)	2010-08-02 2010-08-26	1.0	3.0	2011-12-15

78. 340e14 (EGINGWAH BAY)	Complicated combo of vector data (land and hydro): 340E14-6.2	1959	1.0	3.0	2012-06-04
79. 340e15 (DISRAELI CREEK)	Vector data: BNDT-340E15-2.4	1959	1.0	2.1	2009-05-26
80. 340e16 (DISRAELI FIORD)	Complicated combo of vector data (land and hydro): 340E16-5.3		1.0	3.0	2012-06-01
81. 340f01	R2: 2010-08-02; 2010-08-09 (x3); 2010-08-11 (x2); 2010-08-16 (x2); 2010-08-17 (x2); 2010-08-18; 2010-08-19 (x2); 2010-08-24 (x2)	2010-08-02 2010-08-24	1.0	3.0	2011-08-24
82. 340f02	R2: 2010-08-03; 2010-08-04 (x2); 2010-08-05; 2010-08-10 (x3); 2010-08-11 (x3); 2010-08-12 (x4); 2010-08-19 (x6); 2010-08-20 (x2); 2010-08-21 (x2); 2010-08-26 (x3); 2010-08-27; 2010-08-28	2010-08-03 2010-08-28	1.0	3.0	2011-12-17
83. 340f03	R2: 2010-08-05 (x2); 2010-08-07 (x3); 2010-08-13 (x3); 2010-08-12 (x3); 2010-09-08 (x2); 2010-08-14 (x2); 2010-08-20 (x2); 2010-08-21 (x2); 2010-08-22 (x5); 2010-08-29; 2010-08-30; 2010-08-31; 2010-08-29 (x2)	2010-08-05 2010-09-08	1.0	3.0	2011-11-23
84. 340f04	R2: 2010-08-08 (x4); 2010-08-07 (x3); 2010-08-16; 2010-09-08 (x3); 2010-08-15 (x2); 2010-08-17 (x2); 2010-08-22; 2010-08-23 (x3); 2010-08-22 (x2); 2010-08-25 (x2); 2010-08-24 (x2); 2010-08-30 (x2); 2010-08-31	2010-08-07 2010-09-08	1.0	3.0	2011-11-23
85. 340f05	R2: 2010-08-07 (x2); 2010-09-08 (x2)	2010-08-07 2010-09-08	1.0	3.0	2011-12-23
86. 340f06	R2: 2010-08-05; 2010-08-07 (x2); 2010-09-08 (x4); 2010-08-14 (x3); 2010-08-21 (x3); 2010-08-22 (x3); 2010-08-31 (x2)	2010-08-05 2010-09-08	1.0	3.0	2011-12-24
87. 340f07	R2: 2010-08-04 (x2); 2010-08-05 (x2); 2010-08-09 (x2); 2010-08-10 (x2); 2010-08-11 (x2); 2010-08-12 (x3); 2010-08-17 (x2); 2010-08-19 (x2); 2010-08-21 (x2); 2010-08-26 (x2); 2010-08-27; 2010-08-28; 2010-08-29	2010-08-04 2010-08-29	1.0	3.0	2011-12-23
88. 340f08	R2: 2010-08-02 (x2); 2010-08-09 (x3); 2010-08-31; 2010-08-16; 2010-08-17 (x2); 2010-08-18 (x2); 2010-08-23 (x2); 2010-08-25; 2010-08-24	2010-08-02 2010-08-31	1.0	3.0	2011-09-02
89. 340f09	R2: 2010-08-05; 2010-08-31 (x2); 2010-08-11 (x2); 2010-08-12 (x4); 2010-08-16 (x2); 2010-08-17 (x2); 2010-08-18 (x3); 2010-08-19 (x2); 2010-08-23 (x3); 2010-08-24 (x3); 2010-08-28; 2010-08-30 (x2)	2010-08-05 2010-08-31	1.0	3.0	2011-12-24
90. 340f10	R2: 2010-08-05; 2010-08-09; 2010-08-10; 2010-08-11; 2010-08-12; 2010-08-17; 2010-08-26; 2010-08-28 (x3); 2010-08-29 (x2)	2010-08-05 2010-08-29	1.0	3.0	2011-12-15
91. 340f16	R2: 2010-08-04; 2010-08-05; 2010-08-12; 2010-08-18 (x2); 2010-08-28	2010-08-04 2010-08-28	1.0	3.0	2011-12-24
92. 340h01 (CAPE ALBERT EDWARD)	Complicated combo of vector data (land and hydro): 340H01-5.1	1959	1.0	3.0	2012-06-01
93. 340h02 (WARD HUNT ISLAND)	Vector data: BNDT-340H02-2.2	1959	1.0	2.1	2009-05-25
94. 340h03	Vector data: BNDT-340H03-2.2	1959	1.0	2.1	2009-05-25

Table A6: CDED 560

NTS sheet	Data	Start/end date	Edition	Issue	Proc. date
1. 560a01	ASBD-T005-0.0	1959-07-28	1.0	3.0	2011-05-13
2. 560a02	SPOT: 2011-08-23	2011-08-23	1.0	3.0	2012-01-11
3. 560a03	SPOT: 2011-07-24 (x2)	2011-07-24	1.0	3.0	2012-01-05
4. 560a04 (LI FIORD)	SPOT: 2011-07-22	2011-07-22	1.0	3.0	2012-01-05
5. 560a05 (BALS FIORD)	SPOT: 2011-08-23	2011-08-23	1.0	3.0	2011-12-21
6. 560a06 (BUNDLE RIVER)	SPOT: 2011-08-23 (x2)	2011-08-23	1.0	3.0	2012-01-05
7. 560a07	SPOT: 2011-07-24; 2011-07-08	2011-07-08 2011-07-24	1.0	3.0	2012-01-12
8. 560a08	ASBD-T005-0.0	1959-07-28	1.0	3.0	2011-05-07

(FLAT SOUND)					
9. 560a09 (WHITE MOUNTAIN)	ASBD-T005-0.0; ASBD-T008-0.0	1959-07-28	1.0	3.0	2011-05-31
10. 560a10 (LIGHTFOOT RIVER)	ASBD-T005-0.0	1959-07-28	1.0	3.0	2011-05-21
11. 560a11 (BLIZZARD RIVER)	SPOT: 2011-08-23 (x2)	2011-08-23	1.0	3.0	2012-01-12
12. 560a12 (BJARNASON ISLAND)	SPOT: 2011-07-22; 2011-08-23 (x2)	2011-07-22 2011-08-23	1.0	3.0	2011-12-15
13. 560a13	SPOT: 2011-07-22 (x2)	2011-07-22	1.0	3.0	2011-12-15
14. 560a14	SPOT: 2011-07-22; 2011-08-23	2011-07-22 2011-08-23	1.0	3.0	2011-12-21
15. 560a15	ASBD-T005-0.0	1959-08-13	1.0	3.0	2011-05-21
16. 560a16 (CAPE ST. ANDREW)	ASBD-T008-0.0	1959-07-28	1.0	3.0	2011-03-18
17. 560b01 (BAD WEATHER CAPE)	ASBD-T005-0.0	1958-07-24	1.0	3.0	2011-02-22
18. 560b02 (HOSE STRAIT)	Vector data: BNDT-560B02-3.2	1959	1.0	2.1	2009-05-21
19. 560b03	Vector data: BNDT-560B03-3.0	1959	1.0	2.1	2009-05-21
20. 560b08 (CAPE NORTHWEST)	ASBD-T005-0.0	1959-07-28	1.0	3.0	2011-02-22
21. 560b09	SPOT: 2008-07-29 (x15); 2008-08-05 (x15)	2008-07-29 2008-08-05	1.0	3.0	2011-03-23
22. 560d01 (LINDSTROM CREEK)	ASBD-T008-0.0	1959-07-28	1.0	3.0	2011-03-24
23. 560d02 (WHITE POINT)	ASBD-T005-0.0; ASBD-T008-0.0	1959-08-13	1.0	3.0	2011-03-17
24. 560d03 (RENDS FIORD)	ASBD-T005-0.0	1959-07-25	1.0	3.0	2011-06-09
25. 560d04 (AURLAND FIORD)	ASBD-T005-0.0	1959-07-28	1.0	3.0	2011-06-07
26. 560d05 (CAPE THOMAS HUBBARD)	ASBD-T005-0.0	1959-07-28	1.0	3.0	2011-05-06
27. 560d06 (CAPE STALLWORTHY)	ASBD-T005-0.0	1959-07-25	1.0	3.0	2011-05-12
28. 560d07 (FJELDHOLMEN ISLAND)	ASBD-T008-0.0	1959-07-28	1.0	3.0	2011-05-31
29. 560d08 (EMMA FIORD)	ASBD-T008-0.0	1959-07-28	1.0	3.0	2011-06-07
30. 560d09	R2: 2010-08-02 (x3); 2010-08-08 (x3); 2010-08-09 (x3); 2010-08-11 (x3); 2010-09-03 (x2); 2010-08-16 (x2); 2010-09-08 (x3) 2010-08-17 (x3); 2010-08-18 (x3); 2010-08-22; 2010-08-25 (x4)	2010-08-02 2010-09-08	1.0	3.0	2011-11-29
31. 560d10 (AUDHILD BAY)	R2: 2010-08-02 (x2); 2010-08-11 (x2); 2010-08-19 (x2); 2010-08-26; 2010-08-28 (x2); 2011-08-07 (x2); 2011-08-16 (x2); 2011-08-23; 2011-09-07 (x2)	2010-08-02 2011-09-07	1.0	3.0	2011-12-23
32. 560d15 (CAPE BOURNE)	R2: 2010-08-02; 2010-08-11 (x2); 2010-09-03 (x3); 2010-08-18 (x2); 2010-08-19 (x2); 2010-08-25 (x3); 2010-08-26; 2010-08-28	2010-08-02 2010-09-03	1.0	3.0	2011-12-23
33. 560d16 (HENSON BAY)	R2: 2010-08-02; 2010-08-08 (x3); 2010-08-09 (x3); 2010-08-11 (x2); 2010-09-03 (x2); 2010-08-16 (x2); 2010-09-08 (x2); 2010-08-17 (x3); 2010-08-18 (x3); 2010-08-25 (x2); 2010-08-26; 2010-08-25 (x2); 2010-08-24 (x2)	2010-08-02 2010-09-08	1.0	3.0	2011-12-07
34. 560e01	R2: 2010-08-08 (x4); 2010-08-09 (x2); 2010-09-03 (x2); 2010-08-16 (x3); 2010-08-17 (x3); 2010-08-18 (x4); 2010-08-25 (x5); 2010-08-24	2010-08-08 2010-09-03	1.0	3.0	2011-11-30